GL01022

A COMPREHENSIVE STUDY OF LASL WELL C/T-2 ROOSEVELT HOT SPRINGS KGRA, UTAH, AND APPLICATIONS TO GEOTHERMAL WELL LOGGING.

by

William E. Glenn

Jeffrey B. Hulen

Dennis L. Nielson

Preliminary Copy
of Los Alamos Sci. Lab
report LA-8686

—1980—

(9-1)

EARTH SCIENCE LABORATORY
UNIVERSITY OF UTAH RESEARCH INSTITUTE
420 Chipeta Way, Suite 120
Salt Lake City, Utah 84108

CONTENTS

PAGE

ABSTRACT . . . .

I. INTRODUCTION . . . .
A. Background . . . .
B. Location . . . .
C. Geology of the Roosevelt Hot Springs KGRA . . . .

II. LITHOLOGIC LOGGING AND ALTERATION STUDIES . . . .
A. Methods and Procedures . . . .
B. Lithology, Alteration, and Inferred Structure . . . .
1. Lithology . . . .
a. Biotite-Quartz-Feldspar Gneiss . . . .
b. Biotite-Pyroxene-Hornblende Diorite . . . .
c. Hornblende-Biotite Granodiorite to Quartz Monzonite . . . .
d. Hornblende-Biotite Quartz Monzonite . . . .
e. Hornblende-Biotite Granite . . . .
f. Microdiorite and Andesite . . . .
2. Alteration and Inferred Structure . . . .
a. Discussion . . . .
3. Intervals Selected for Detailed Geochemical and Isotopic Investigation . . . .

III. GEOCHEMISTRY . . . .
A. Introduction . . . .
B. Methods and Procedures . . . .
C. Geochemistry of Composite Samples . . . .
D. Geochemistry of Detailed Study Intervals . . . .
E. Rare Earth Element Analyses . . . .
F. Fluid Chemistry . . . .

IV. OXYGEN AND CARBON ISOTOPE ANALYSES . . . .
A. Introduction . . . .
B. Sample Preparation and Analysis . . . .
C. Results . . . .
D. Discussion . . . .
1. Frequency Distribution . . . .
2. Isotope Geothermometry . . . .
E. Identification of Fluid Entries . . . .

V. PHYSICAL PROPERTY MEASUREMENTS . . . .
A. Bulk Density and Magnetic Susceptibility . . . .
B. Thermal Conductivity . . . .

VI. GEOPHYSICAL INTERPRETATION . . . . . .
A. Introduction . . . . . .
B. Log Descriptions . . . . . .
1. Temperature Log . . . . . .
2. Caliper Log . . . . . .
3. Acoustic (Velocity) Logs . . . . . .
4. Neutron Logs . . . . . .
5. Density Logs . . . . . .
6. Electrical Conductivity and SP Logs . . . . . .
7. Gamma-Ray Logs . . . . . .
8. Summary of Log Evaluations . . . . . .
C. Cross Plots . . . . . .
1. Basis for Plots . . . . . .
2. Neutron-Density Cross Plots . . . . . .
3. Neutron-Velocity Cross Plots . . . . . .
4. Density-Velocity Cross Plots . . . . . .
5. MN, AK and Z Plots . . . . . .
6. Gamma-Ray Cross Plots . . . . . .
7. Log Data - Chemical Data Cross Plots . . . . . .
D. Summary of Lot Interpretations . . . . . .

VII. SUMMARY . . . . . .

VIII. ACKNOWLEDGEMENTS . . . . . .

IX. REFERENCES . . . . . .

TABLES

Table 2.1 Petrographic summary, selected samples from Well C/T-2 .

Table 2.2 Microprobe chemical analyses of selected rock-forming and alteration minerals from Well C/T-2 . . . .

Table 2.3 Mineralogy of clay separates, selected samples from Well C/T-2 as determined by X-ray diffraction . . .

Table 3.1 Chemical analyses of composite whole rock samples from Well C/T-2 . . . . . .

Table 3.2 Chemical analyses of selected whole rock samples from Well C/T-2 . . . . . .

Table 3.3 Neutron activation analyses of selected samples from Well C/T-2 . . . . . .

Table 3.4 Water analyses from Well C/T-2 . . . . . .

Table 4.1 Oxygen and carbon isotope data from Well C/T-2 . . . . .

Table 4.2 Estimates of carbon and oxygen isotopic temperatures Well C/T-2 . . . . . .

Table 5.1 Magnetic susceptibiities and densities of cuttings from Well C/T-2 . . . . . .

Table 5.2 Thermal conductivity measurements on chip samples in C/T-2 at 150C and well bore temperatures . . . . .

Table 6.1 Well logs available obtained in C/T-2 by LASL . . . . .

Table 6.2 Comparison of porosity values read from Dresser Atlas calibration curve and polynomial equation . . . .

Table 6.3 Comparison of depths to various distinct features as seen on the different logs . . . . . .

Table 6.4 Two arbitrary, generalized igneous/metamorphic rock compositions . . . . . .

Table 6.5 Average and range of log values for the two rock types in the open hole interval of C/T-2 . . . . . .

FIGURES

Figure 1.1 Location map . . . . . .

Figure 1.2 Geologic map of a portion of the Roosevelt Hot Springs KGRA showing Well C/T-2 and other geothermal wells and shallow diamond drill holes . . . . . .

Figure 1.3 Geologic cross-section of the Roosevelt Hot Springs geothermal area showing Well C/T-2 . . . . . .

Figure 3.1 Composite whole rock analyses of Well C/T-2 as a function of depth . . . . . .

Figure 4.1 Oxygen isotope values as a function of depth in Well C/T-2 . . . . . .

Figure 4.2 Carbon isotope values as a function of depth in Well C/T-2 . . . . . .

Figure 4.3 Oxygen versus carbon isotope values from Well C/T-2 . .

Figure 4.4 Frequency histograms of oxygen and carbon isotope values from Well C/T-2 . . . . . .

Figure 4.5 Frequency histograms of temperatures calculated from oxygen and carbon isotope values from Well C/T-2 . . . . . .

Figure 4.6 Calculated oxygen and carbon isotopic temperatures plotted against lead values of composite samples from Well C/T-2 . . . . . .

Figure 5.1 Plot of magnetic susceptibility and density of cuttings from LASL C/T-2 . . . . . .

Figure 6.1 Dresser Atlas versus Schlumberger Neutron; depth interval 1280.9 to 1462.3m (4202.5 to 4797.5 ft); 1.52m (5 ft) data averages . . . . . .

Figure 6.2 Dresser Atlas versus Schlumberger Neutron; depth interval 1585.7 to 1767.1m (5202.5 to 5797.5 ft); 1.52m (5 ft) data averages . . . . . .

Figure 6.3 Dresser Atlas versus Schlumberger Neutron; depth interval 1890.5 to 2071.9m (6202.5 to 6797.5 ft); 1.52m (5 ft) data averages . . . . . .

Figure 6.4 Dresser Atlas versus Schlumberger Gamma-Ray; depth interval 1158.5 to 1317.7m (3801 to 4323 ft); .61m (2 ft) data averages . . . . . .

Figure 6.5 Dresser Atlas versus Schlumberger Gamma-Ray; depth interval 1531.6 to 1744.3m (5025 to 5723 ft); .61m (2 ft) data averages . . . . . .

Figure 6.6 Dresser Atlas versus Schlumberger Gamma-Ray; depth interval 1958.3 to 2085.8m (6425 to 6843 ft); .61m (2 ft) data averages . . . . . .

Figure 6.7 Density versus neutron porosity cross plot grid for "rock 1" composition in Table 6.4 . . . . . .

Figure 6.8 Density versus neutron porosity cross plot grid for "rock 2" composition in Table 6.4 . . . . . .

Figure 6.9 Expanded scale version of Figure 6.7 and includes a demonstrated use of grid . . . . . .

Figure 6.10 Bulk density versus neutron porosity; depth interval 1752.9 to 1813.2m (5751 to 5949 ft); .61m (2 ft) data averages . . . . . .

Figure 6.11 Bulk density versus neutron porosity; depth interval 1924.2 to 1957.7m (6313 to 6423 ft); .61m (2 ft) data averages . . . . . .

Figure 6.12 Bulk density versus neutron porosity; depth interval 2012.0 to 2072.3m (6601 to 6799 ft); .61m (2 ft) data averages . . . . . .

Figure 6.13 Velocity versus neutro porosity; depth interval 1752.9 to 1813.2m (5751 to 5949 ft); .61m (2 ft) data averages . . . . . .

Figure 6.14 Velocity versus neutron porosity; depth interval 1924.2 to 1957.7m (6313-6428 ft); .61m (2 ft) data averages . . . . . .

Figure 6.15 Velocity versus neutron porosity; depth interval 2012 to 2072.3m (6601 to 6799 ft); .61m (2 ft) data averages . . . . . .

Figure 6.16 Velocity versus bulk density; depth interval 1752.9 to 1813.2m (5751 to 5949 ft); .61m (2 ft) data averages . . . . . .

Figure 6.17 Velocity versus bulk density; depth interval 1924.2 to 1957.7m (6313 to 6423 ft); .61 m (2 ft) data averages . . . . . .

Figure 6.18 Velocity versus bulk density; depth interval 2012 to 2072.3m (6601 to 6799 ft); .61m (2 ft) data averages . . . . . .

Figure 6.19 Z-plot, bulk density versus neutron porosity with gamma-ray in Z direction; depth interval 1752.9 to 1813.2m (5751 to 5949 ft); .61m (2 ft) data averages . . . . . .

Figure 6.20 Z-plot, bulk density versus neutron porosity with gamma-ray in Z direction; depth interval 1924.2 to 1957.7m (6313 to 6423 ft); .61m (2 ft) data averages . . . . . .

Figure 6.21 Z-plot, bulk density versus neutron porosity with gamma-ray in Z direction; depth interval 2012.0 to 2072.3m (6601 to 6799 ft); .61m (2 ft) data averages . . . . . .

Figure 6.22 Gamma-ray versus a) neutron porosity and b) bulk density; depth interval 1752.9 to 1813.3m (5751 to 5949 ft); .61m (2 ft) data averages . .

Figure 6.23 Gamma-ray versus a) neutron porosity and b) bulk density; depth interval 1924.2 to 1957.7m (6313 to 6423 ft); .61m (2 ft) data averages . . . . . .

Figure 6.24 Gamma-ray versus a) neutron porosity and b) bulk density; depth interval 2012.0 to 2072.3m (6601 to 6799 ft); .61m (2 ft) data averages . . . . . .

Figure 6.25 Gamma-ray versus K_2O; depth interval 1759.9 to 1804.4m (5770 to 5920 ft); 3.1m (10 ft) data averages . . . . . .

Figure 6.26 Gamma-ray versus K_2O; depth interval 1905.0 1935.5m (6250 to 6350 ft); 3.1m (10 ft) data averages. . . . . .

Figure 6.27 Gamma-ray versus K_2O; depth interval 2023.8 to 2057.4m (6640 to 6750 ft); 3.1m (10 ft) data averages . . . . . .

Figure 6.28 Fe_2O + MgO versus bulk density; depth interval 1761.7 to 1804.4m (5780 to 5920 ft); 3.1m (10 ft) data averages . . . . . .

Figure 6.29 Fe_2O_3 + MgO bulk density; depth interval 1908.0 to 1938.5m (6260 to 6370 ft); 3.1m (10 ft) data averages . . . . . .

Figure 6.30 Fe_2O_3 + MgO versus bulk density; depth interval 2023.9 to 2057.4m (6640 to 6750 ft); 3.1m (10 ft) data averages . . . . . .

Figure 6.31 Loss versus neutron porosity; depth interval 1761.7 to 1804.4m (5780 to 5920 ft), 3.1m (10 ft) data averages . . . . . .

Figure 6.32 Loss versus neutron porosity; depth interval 2023.9 to 2057.4m (6640 to 6750 ft); 3.1m (10 ft) data averages . . . . . .

PLATES

Plate I Log composite of LASL C/T-2 (Utah State Geothermal Well 9-1) Roosevelt Hot Springs KGRA, Beaver County Utah . . . . . .

Plate II Log composite of selected logs, LASL C/T-2 (Utah State Geothermal Well 9-1), Roosevelt Hot Springs KGRA, Beaver County, Utah . . . . . .

Plate III Chemical radiometric and X-ray fluorescence data for LASL C/T-2 . . . . . .

Plate IV Chemical analysis (Loss, MgO, Fe_2O_3 and Fe_2O_3 + MgO) for LASL Well C/T-2 (Utah State Geothermal Well 9-1) . . . . . .

I. INTRODUCTION

A. Background

The Earth Science Laboratory (ESL)/University of Utah Research Institute (UURI), on behalf of Los Alamos Scientific Laboratory (LASL) has completed a comprehensive study of cuttings and well logs from LASL Well C/T-2 (Utah State Geothermal Well 9-1) in the Roosevelt Hot Springs KGRA, Beaver County, Utah. (Figure 1.1 and 1.2). The study was undertaken as part of LASL's Geothermal Log Interpretation Development Program (Mathews, 1978), the objective of which is the establishment of an effective geothermal logging industry in the United States. In support of this objective, Phillips Petroleum Company has donated the use of Utah State Geothermal Well 9-1 to LASL for calibration and testing of well-logging equipment in the hot, corrosive, geothermal environment. LASL has renamed the well C/T-2.

Well C/T-2 was collared March 3, 1975 and completed April 18, 1975 at a total depth of 2099.0m (6885 ft). The well encountered anomalously high temperatures (maximum 227°C (440°F) at 2099.0m), but no significant thermal fluid production zones. Cuttings samples and well logs obtained by ESL for well C/T-2 have been studied by various methods as herein reported. The report is organized by specific tasks outlined in Contract No. 4-N29-4988H-1.

B. Location

Well C/T-2 is located in the Roosevelt Hot Springs KGRA in Beaver County, Utah. The nearest town is Milford, Utah which is served by regularly scheduled commuter flights. The nearest rental cars are in Cedar City, roughly 50 miles southeast of Milford. Well C/T-2 can be reached by traveling three miles north of Milford on Highway 257, then turning east onto a graded

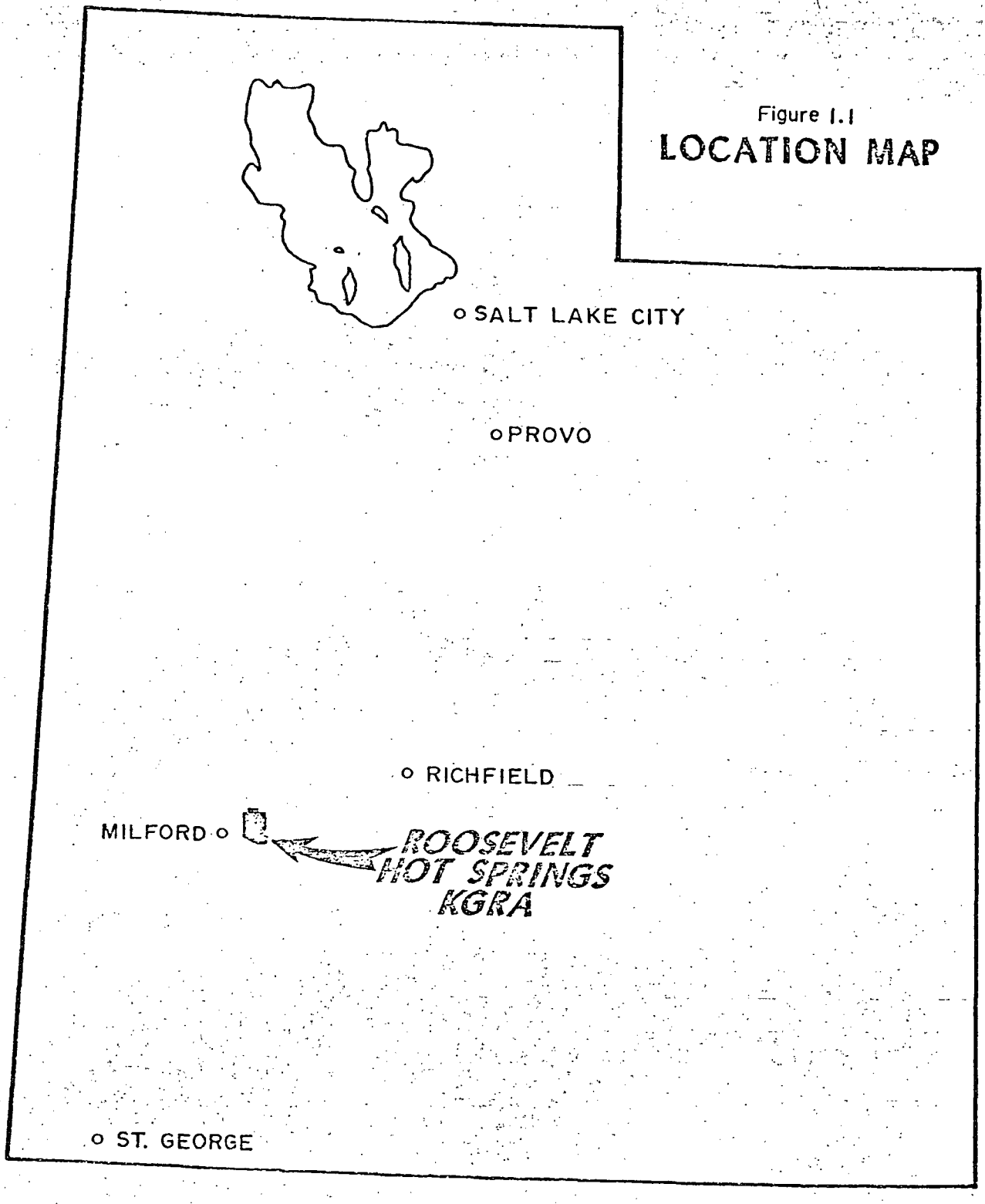

Figure 1.1
LOCATION MAP

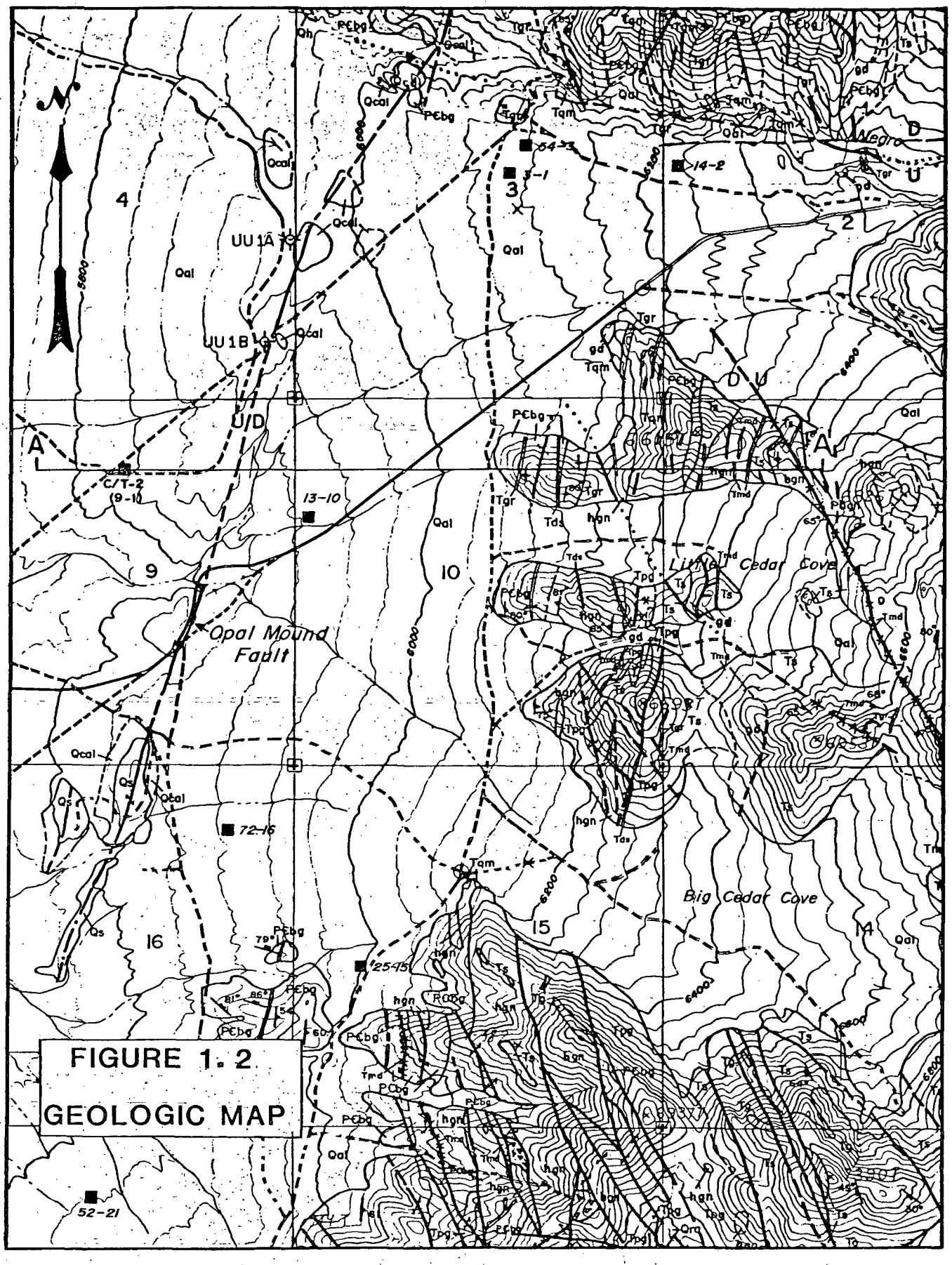

FIGURE 1.2

GEOLOGIC MAP

Explanation for Geologic Map and Cross Section (Figures 1.2 &1.3)

QUATERNARY	Qs	Opaline and chalcedonic sinter
	Qcal	Silica-cemented alluvium
	Qh	Hematite-cemented alluvium
	Qal	Alluvium
	Qra	Air-fall and non-welded ash-flow tuff
TERTIARY	Tds	Diabase dikes
	Tmd	Microdiorite dikes
	Tgr	Granite dikes; fine-grained
	Tg	Granite; medium- to coarse-grained
	Ts	Syenite; medium-grained
	Tpg	Biotite granite; medium- to coarse-grained
	Tqm	Quartz monzonite
AGE?	gd	Biotite granodiorite; fine- to medium-grained
	hgn	Hornblende gneiss; medium- to coarse-grained meta-quartz monzonite
PC	PCbg	Banded gneiss; conspicuously layered feldspar-quartz-biotite gneiss, schist and migmatite

Contact, dashed where uncertain

63 — Fault, intruded by microdiorite dike; arrow shows dip

50 — Fault, dashed where inferred, dotted where concealed; arrow shows dip

Brecciation

50 — Strike and dip of inclined and vertical joints

75 — Strike and dip of inclined and vertical foliation

Prospect

Shallow diamond drill hole

Geothermal well

From Sibbett & Nielson, 1980

county road and driving seven miles. The access road to the well takes off to the northeast. The county and access roads are marked with signs which point toward "LASL Well C/T-2".

C. Geology of the Roosevelt Hot Springs KGRA

The geology of Roosevelt Hot Springs KGRA has been described in detail by Nielson et al. (1978). In addition, a summary of the geology, geochemistry and geophysics has been published by Ward et al. (1978). Lithologic logs of available holes can be found in Hulen (1978) and Nielson et al. (1978). An evaluation of well logs from Utah State Geothermal Wells 72-16, 14-2, and 52-21 and temperature gradient hole GPC-15 can be found in Glenn and Hulen (1979a). A more regional picture of the geology of the central Mineral Mountains is presented in Sibbett and Nielson (1980).

The Roosevelt Hot Springs KGRA is located on the western edge of the Mineral Mountains in Beaver County, Utah. Exploration for geothermal resources at Roosevelt Hot Springs was initiated by Phillips Petroleum Company in 1975. The known geothermal resource is owned by Phillips and a joint venture of Thermal Power, AMAX, and O'Brien Mines. The geology of the presently known producing area is shown in Figure 1.2, which also shows the location of Well C/T-2 and ten producing test holes in the Roosevelt field. In general, the Roosevelt Hot Springs geothermal system is a hot-water dominated geothermal resource. Fluid temperatures in the producing region are in excess of 265°C (509°F). The geothermal reservoir is structurally controlled, occupying faults and fractures which cut plutonic and high-grade metamorphic rocks.

The lithologies which are present in the area are described in detail in

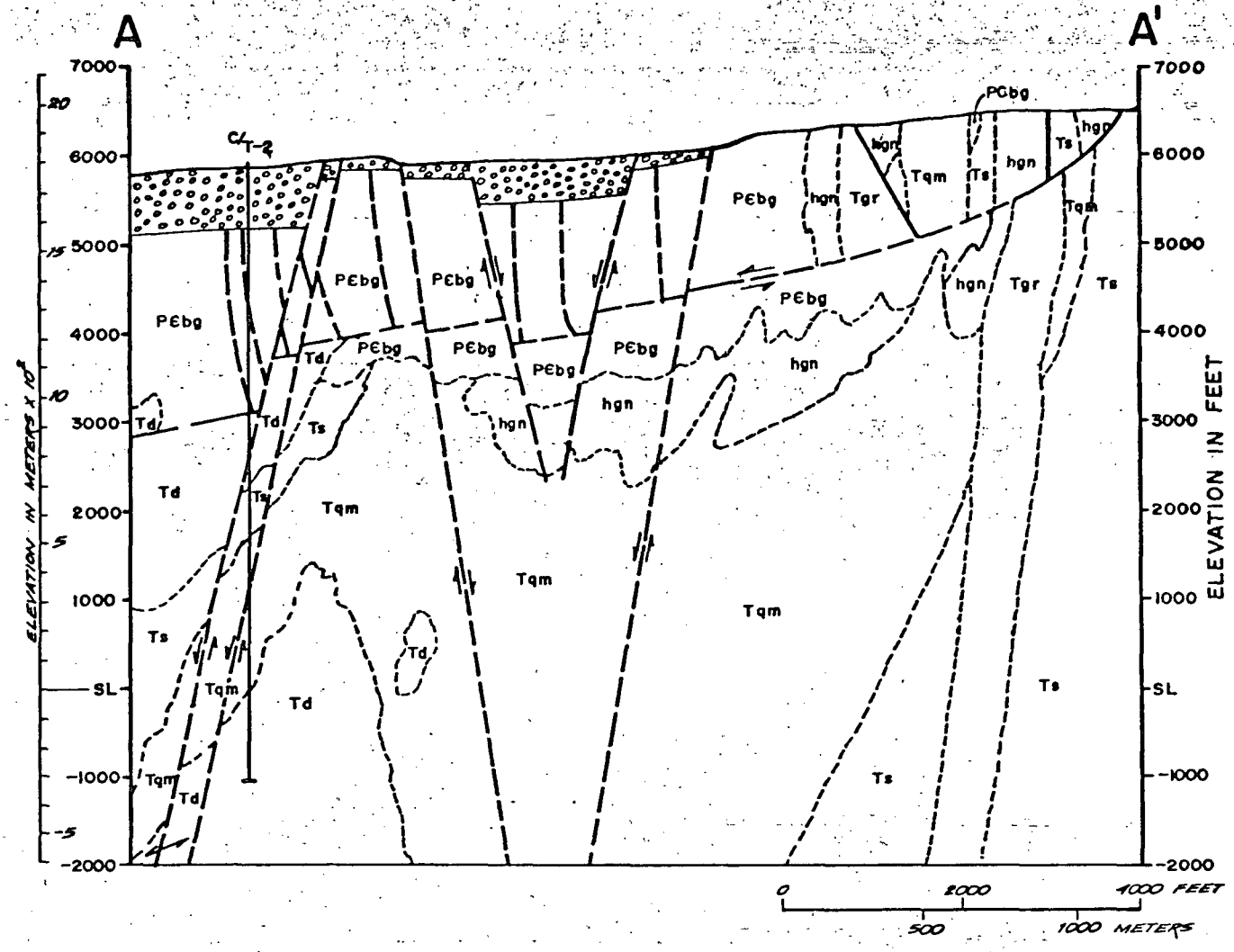

FIGURE 1.3 GEOLOGIC CROSS-SECTION OF THE ROOSEVELT HOT SPRINGS GEOTHERMAL AREA SHOWING WELL C/T-2.

Nielson et al. (1978) and Sibbett and Nielson (1980). The detailed logging of lithologies in hole C/T-2 will be related to the units observed in the Mineral Mountains.

The structure of Roosevelt Hot Springs KGRA is dominated by three principal fault directions. The oldest of these faults was developed during a period of low angle normal faulting. This activity has produced zones of cataclastic, silicified rock both along the low angle faults and along high angle faults in the hanging wall. A second series of faults, trending generally east-west, are high angle normal faults and are thought to be fairly long lived structures. The most recent faults in the area are north-south to northeast trending normal faults. These faults are represented in the geothermal area by the Opal Mound Fault (Figure 1.2) which has controlled the deposition of siliceous sinter in the recent past.

Nielson et al. (1978) proposed that the geothermal production is controlled by increased permeability developed at the zones of intersection of two or three of these principal fault directions. These zones of intersection are responsible for an upper level reservoir zone and the geothermal fluids have been channeled from depth along steeply dipping faults such as the Opal Mound fault.

Figure 1.3 is an east-west geologic cross section of the Roosevelt Hot Springs geothermal field through Well C/T-2. Note that the hole is located west of a horst which is bounded on the east by the Opal Mound Fault. A low angle normal fault passes through the hole at about 844.3m (2770 ft). The relationships which were mapped on the surface hold true within well C/T-2: the hanging wall of this fault is extensively brecciated while the footwall

has been intersected only by an occasional discrete fault. The rocks above 844.3m (2770 ft) have been extensively altered by hydrothermal fluids. No significant fluid entries have been reported and the entire hole intersects rocks with low permeability and is considered dry.

II. LITHOLOGIC LOGGING AND ALTERATION STUDIES

A. Methods and Procedures

Drill cuttings from well C/T-2 were collected by Phillips Petroleum Company generally at 4.6m (15 ft) intervals above a depth of 686.8m (2250 ft), and at 3.1m (10 ft) interval below this depth, to the bottom of the well. These cuttings were thoroughly washed to remove drilling mud and lost circulation material. Chipboards were prepared from small portions (roughly 1.5 g) of the cuttings.

Cuttings from well C/T-2 were first logged in detail by conventional binocular microscope at 8-40X magnification. Data logged include lithology, style and intensity of alteration and mineralization, and physical evidence of structural disruption, including amounts of fault gouge, microbreccia and mylonite present in each sample. This lithologic log is presented on Plate 1.

Petrographic study of selected cuttings samples from well C/T-2 resulted in more accurate characterization of rock types and alteration phases identified during binocular microscopic examination. Seventy-five grain-mount thin sections were examined. Half of each section was stained with sodium cobaltinitrite to aid identification of potassium feldspar. The sections were prepared from samples collected at roughly 30.5m (100 ft) intervals, except where lithologic complexity and/or alteration dictated closer sample spacing. For representative samples apparently consisting wholly or mostly of a single

rock type, modes were obtained (Table 2.1) by a combination of visual estimation and abbreviated point-count (200-300 points). Such point counts are not adequate for determination of trace and minor mineral percentages, but are believed to be more accurate than visual estimation for determination of major rock-forming mineral quantities.

Alteration mineralogy in well C/T-2 was further investigated by X-ray diffraction of clay separates (<2 μ) from representative cuttings samples. The clay fraction was prepared by pulverizing a 10g sample-split in a Spex shatterbox with tungsten carbide components, peptizing the pulverized sample with calgon, and centrifuging. X-ray diffraction patterns were obtained for oriented smears on glass slides following air-drying, and, if appropirate, vapor glycolation and heating to 250°C (482°F) and 550°C (1022°F).

Microprobe analyses of selected alteration and rock-forming minerals were obtained using a 3-channel ARL electron microprobe at an acceleration voltage of 15kV. X-rays were counted at an average of 5 spots on each grain for approximately 16 seconds. Clinopyroxene and kaersutite standards were used for most major and minor elements. A biotite standard was used for potassium, a barium oxide glass standard for barium, a fluorphlogopite standard for fluorine, and a scapolite standard for chlorine. Bence-Albee matrix corrections (Bence and Albee, 1968) were then calculated using a computer program developed by G. H. Ballantyne, J. M. Ballantyne and W. T. Parry, of the University of Utah Department of Geology and Geophysics. Input for this program requires an ideal water content for the mineral analyzed. The initial oxide data are corrected by an iterative routine which yields successively

more accurate approximations of actual bound water content (Ballantyne, J. M., 1978).

B. Lithology, Alteration and Inferred Structure

A major fault zone between depths of 835.1m (2740 ft) and 844.3m (2770 ft; Pl. I; Figure 1.3) divides well C/T-2 into two distinct structural, lithologic, and alteration regimes. Above this fault zone, lithology is complex, alteration is moderate to locally intense, and evidence of structural disruption is abundant. Below the fault zone, only a few rock types are present, and these are relatively unbroken and only weakly altered.

Lithologic units defined through logging well C/T-2 have been tentatively correlated with rock types mapped at the surface and identified in other wells and drill holes within and near the Roosevelt Hot Springs KGRA by Nielson et al. (1978) and Sibbett and Nielson (1980). Correlation was accomplished primarily through comparison of chip samples from well C/T-2 with representative surface samples crushed, screened, and washed to simulate drill cuttings.

Cuttings collected from well C/T-2 are extremely fine, averaging less than 0.5mm in diameter above 899.4m (2950 ft) and less than 0.3mm in diameter below this depth. The minuteness of these cuttings may hinder accurate characterization of certain parameters in the well, such as grain size and texture of coarser-grained rocks. Different minerals in a given rock may also have responded differently to fine-grinding at the drill bit in C/T-2. Feldspar and quartz, for instance, would pulverize readily, the original feldspar and quartz in a rock could be powdered and removed from cuttings along with drilling mud during sample collection and washing. This process

would yield a cuttings sample richer in biotite (and thus denser) than the rock penetrated.

References to grain size and texture of a given rock type in the discussions which follow apply only where drill chip size permits description of these parameters. In general, grain size can be determined with reliability only above a depth of 899.4m (2950 ft). Below this depth, drill chips average about 0.3mm in diameter, less than the average grain size of most of the rocks. Modes for 61 samples from C/T-2 as determined by point-counting and visual estimation, are presented in Table 2.1.

1. Lithology.

a. Biotite-Quartz-Feldspar Gneiss. Several zones of fine- to medium-grained biotite-bearing gneiss were penetrated in C/T-2, but only above the major fault zone centered on 838.2m (2750 ft) does this rock type occur in significant quantities. The gneiss is commonly foliated, even in drill cuttings. Identification of massive gneiss is based upon similarity to coexisting or nearby foliated varieties and upon comparision with surface samples of gneiss crushed to simulate drill cuttings.

Both foliated and massive (in cuttings) gneisses in the drill hole are typically xenomorphic to hypidiomorphic fine- to medium-grained aggregates of quartz, feldspar, biotite and hornblende, in highly variable ratios, with relatively high apatite content, minor sphene and magnetite-ilmenite, and local traces of zircon. Intergrain boundaries, where preserved, are highly irregular, and may show mortar texture. Quartz is generally strained and typically forms irregular aggregates--elongate in foliated varieties--of smaller interlocking irregular grains. Plagioclase (An_{20}-An_{30}) is commonly

DEPTH INTERVAL		VOLUME PER CENT:																
METERS	FEET	POTASSIUM FELDSPAR	PLAGIOCLASE	QUARTZ	BIOTITE	HORNBLENDE	CLINOPYROXENE	DARK OPAQUE MINERALS	COLOURLESS &/OR LEUCOXENE	APATITE	ZIRCON	EPIDOTE	ALLANITE	CHLORITE	CALCITE	SERICITE	CLAY	PYRITE	LIMONITE*	OTHER MINERALS	ROCK TYPE
213.9–222.5	700–730'	39	25	19	5			1	0.5	0.3 / Tr.		0.8 / Tr.		1.5 / Tr.	3 / 5		0.2				BIOTITE QUARTZ MONZONITE
231.6–236.2	760–775'	7	41	10	17	1.5		2	1	2 /		0.3 /		5 / Tr.	5 / 5		Tr. / 0.3				HBL–BTE : QTE–FSP. GNEISS
298.1–253.0	815–830'	48.5	19	25.5	2.5			0.3	0.4	0.8 / Tr.	Tr. / Tr.			1.5 / 0.7	3 / 3		Tr. / 0.3			MUS-COVITE	BIOTITE GRANITE
275.8–280.4	905–920'	47	20	25	2			0.5	0.5	0.5 / Tr.		0.3 /		1 / 0.5	2 / 0.5		Tr. / 0.4				BIOTITE GRANITE
298.7–303.3	980–995'	7.?	38	7.?	15	17		5		5 /		1 /		1 / 0.5	1 / 1.5				0.5% CARB. MUSC.		BIOTITE OXYHORNBL. MICRODIORITE
307.8–312.4	1010–1025'	46.5	25	22	3			0.5	0.5	0.8 / Tr.		0.3 /		Tr. / Tr.	1.5 / Tr.		Tr. / 0.2			MUS-COVITE	BIOTITE GRANITE
317.0–320.0	1040–1050'	22	35	17	15	Tr.		1.5	2.5	3 / Tr.		Tr. /		2 / 1	1.? / Tr.		0.1 / 0.2			MUS-COVITE	BTE–QTE–FELDSP. GNEISS.
332.2–336.9	1090–1105'	39.5	20	30	2			0.5	0.5	0.5 / Tr.		0.2 / Tr.		Tr. / Tr.	5 / 1		0.5 / 0.5			MUS-COVITE	BIOTITE GRANITE
423.7–428.2	1390–1405'	9% PLAGIOCLASE PHENOCRYSTS 11% OXYHORNBLENDE PHENOCRYSTS						5% DISSEMINATED MAGNETITE–ILMENITE REMAINDER CRYPTOKRY. GROUNDMASS													OXYHORNBLENDE ANDESITE PORPHYRY
496.5–451.1	1965–1980'	21	27	17	17			2	3	2 / Tr.		Tr. /		1.5 / 2	5 / 5		0.1 / 0.3				BTE.–QTE.–FELDSPAR GNEISS.
464.8–469.4	1525–1540'	15% BIOTITE PHENOCRYSTS 52 OXYHORNBLENDE PHENOCRYSTS						PLAG. PHENOCRYSTS 8% 5% APATITE REMAINDER FLOW-FOLDED CRYPTOKRY.													BTE. OXYHORNBLENDE ANDESITE PORPHYRY.
483.1–487.7	1585–1600'	7	36	5	11	5	11	5	3	1 / Tr.		3 /		5 / 3	3 / 1.3		0.5 / 0.8				PYROX–HBL.–BTE. DIORITE
506.0–510.5	1660–1675'	5	33.5	7	10	3	Tr.	5	3	1.4 / Tr.		3 /		11 / 7.5	3 / 1		0.5 / 0.1				ALTERED PYROX–HBL.–BTE. DIORITE
533.1–538.0	1750–1765'	7	31.5	5	9	11	7	4	2.5	1 /		5 /		5 / 8.5	5 / 1.5		0.3 / 0.5			TR. EPID.	PYROX–HBL.–BTE DIORITE
574.5–583.7	1005–1915'	9	32	7	9	3	3	4	3	2 /		3 /		11 / 5	5 / 3		0.5 / 0.5			TR. EPID.	PYROX.–HBL.–BTE DIORITE
611.1–615.7	2005–2020'	46	23	21	3			1	1.5	0.5 /		Tr. /		1.6 /	2 /		0.5 /			MUS-COVITE	BIOTITE GRANITE
638.6–643.1	2095–2110'	11	33	9	8	4	11	5	3	1.5 /		1.5 /		3 / 1.6	2.5 / 2		0.8 / 0.7			TR. MUS-COVITE	PYROX–HBL.–BTE PIORITE
762.0–765.0	2500–2510'	60	22	15	3	?*	?*	1	1.5	0.8 / 4		Tr. /		1.5 / 3	2 / 1		Tr. / 0.5			TR. MUS-COVITE	BIOTITE GRANITE.
816.9–819.9	2680–2690'	52	20	12	2.5	0.5*	?*	1.5	1.5	0.4 / 0.1		Tr. /		3 / 3	3 / Tr.		0.1 /				HORNBLENDE(?)–BIOTITE GRANITE
835.7–838.2	2740–2750'	15	15	12/6	7	1	0.5	5	2.5	2 /		Tr. /		12 / 5	12 / 7		0.3 / 0.1			TR. MUS-COVITE	MIXED ROCK TYPES PLUS MYLONITE.
883.9–887.0	2900–2910'	19	43	15	13	2	0.4	1.5	1.5	0.1 /		Tr. / 0.1		2 / 1.5	1 /		Tr. /			TR. MUS-COVITE	PYROX–HBL.–BTE. GRANODIORITE
914.4–917.4	3000–3010'	21	31	15	17	2.5	Tr.	2	1.5	1.4 /		1 / 0.1		3 / 2	2.5 / Tr.		Tr. /			MUS-COVITE	BIOTITE–HBL. QTZ. MONZONITE.
1018.0–1021.1	3340–3350'	21.5	30	12	15	4	0.5	2	1.5	1 /		0.4 / 0.1		3 / 2	1.6 /		Tr. / 0.5			TR. APATITE	PYROX–HBL–BTE GRANODIORITE
1098.5–1051.6	3440–3450'	7	40	3	9	15		5	1.3	0.8 /		1.5 /		3 / 1	1 /		0.1 / 0.1			TR. EPID. CALCITE	BIOTITE OXYHORNBL. MICRODIORITE
1094.2–1097.3	3590–3600'	45	27.5	13	6	1		2	0.5	0.4 /		Tr. /		1 / Tr.	3.5 / Tr.		0.1 / Tr.				HORNBLENDE–BTE. QUARTZ MONZONITE.
1124.7–1127.8	3690–3700'	50	29.5	11	7	1	Tr.	2	0.5	0.8 /		Tr. / 0.2		0.5 / Tr.	3 /		Tr. /				HORNBLENDE–BTE. GRANITE
1155.2–1158.2	3790–3800'	55	22.5	10	5	1		2	0.5	0.9 /		Tr. / 0.1		1 / Tr.	2 /		Tr. /				HORNBLENDE–BTE. GRANITE
1185.7–1188.7	3890–3900'	55	25.5	9	3	0.5		2	0.5	0.5 / Tr.		Tr. /		1 / Tr.	3 /		Tr. /				BIOTITE GRANITE
1219.2–1222.2	4000–4010'	54	26	11	3	0.5		2	0.5	0.5 /		Tr. /		1.5 /	2 /		Tr. /				BIOTITE GRANITE
1246.6–1250.0	4090–4100'	50	25	12	3	0.5		2	0.5	0.5 /		Tr. / Tr.		2 / 1.5	3 /		Tr. /				BIOTITE GRANITE
1277.1–1280.2	4190–4200'	35	25	12	15	3	0.5	2	1	0.5 /		0.5 /		3.5 / Tr.	2 /		Tr. /				HBL.–BTE. QUARTZ MONZONITE
1313.7–1316.7	4310–4320'	36	27	15	11	Tr.		2	1	0.5 / Tr.		Tr. /		3.6 / 2	2 /		Tr. /				HBL.–BTE QUARTZ MONZONITE
1338.1–1341.1	4390–4400'	36	27	15	12	2.5	Tr.	2.5	0.5	0.5 /		Tr. /		0.5 / 1.5	2 /		Tr. /			TR. CALCITE	HBL.–BTE QUARTZ MONZONITE
1368.6–1371.6	4490–4500'	35	29.5	15	12	1.5		2	1	0.5 /		Tr. /		1.5 / 0.8	1.5 /		Tr. /				HBL.–BTE. QUARTZ MONZONITE
1399.0–1402.1	4590–4600'	35	30	15	12	1.5	Tr.	2	1	0.5 /		Tr. /		1 / 0.5	1.5 /		Tr. /				HBL.–BTE. QUARTZ MONZONITE
1429.5–1432.6	4690–4700'	35	29	12	13	2		1.5	1.5	0.5 / Tr.		Tr. /		3 / 0.5	2 /		Tr. /				HBL.–BTE. QUARTZ MONZONITE
1450.8–1453.9	4760–4770'	22.5	13.?	30	5	0.5		2	2.?	0.8 / Tr.		0.4 /		T / 5	12 /		0.1 /				ALTERED BRECCIATED HBL–BTE QTE. MONZONITE
1460.0–1463.0	4790–4800'	39.5	28	15	5	0.5		1.5	2	0.8 /		0.8 /		5 / 1	1.8 /		Tr. /				HBL–BTE QUARTZ MONZONITE

TABLE 2.1 PETROGRAPHIC SUMMARY

SELECTED SAMPLES FROM WELL C/T-2

DEPTH INTERVAL		VOLUME PER CENT:																
METERS	FEET	POTASSIUM FELDSPAR	PLAGIOCLASE	QUARTZ	BIOTITE	HORNBLENDE	CLINOPYROXENE	OPAQUE MINERALS	SPHENE & OR LEUCOXENE	APATITE / ZIRCON	EPIDOTE / ALUNITE	CHLORITE	CALCITE	SERICITE	PYRITE / CLAY	KAOLINITE*	OTHER MINERALS	ROCK TYPE
1790.5–1793.5	9090–9100'	35	27	15	13	3		2	1.5	0.5 / Tr.	Tr. / 0.1	1 / 5	0.5 / 1	1.5 / 1.5	Tr. / 0.1			HORNBLENDE-BTE. QTZ. MONZONITE
1530.1–1533.1	5020–5030'	37	29.5	11	9	2		2	1	0.5 / Tr.	Tr. / 0.1	5 / 1	1.5 / 1.5	0.1				HBL.-BTE. QTZ. MONZONITE
1551.4–1554.5	5090–5100'	37	33	12	7	2		1.5	1	0.2 / Tr.	Tr. / 0.1	1.5 / 1	1.5					HBL.-BTE. QTZ. MONZONITE
1508.0–1508.0	5200–5210'	35	29	12	11	2		2	2	0.5 / Tr.	Tr. / 0.1	2 / 2.5	2					HBL.-BTE. QTZ. MONZONITE
1594.1–1577.2	5230–5240'	35	25	17	10	1		1.5	1	0.1 / Tr.	Tr. / 0.1	3 / 4	3		0.1			HBL.-BTE. QTZ. MONZONITE
1615.4–1618.5	5300–5310'	37	28	15	10	2	Tr.*	2	1.5	0.5 / Tr.	Tr. / 0.1	2 / 0.5	1.5				TR. ALT. PLAG. FELDSPAR	HBL.-BTE. QTZ. MONZONITE
1624.6–1627.6	5330–5340'	39	25.5	15	9	3	0.5*	2	1.5	0.3 / Tr.	Tr. / 0.1	0.2 / 0.5	3				TR. ALT. PLAG. FELDSPAR	HBL.-BTE. QTZ. MONZONITE
1642.9–1645.9	5370–5400'	37	31	15	7	2	Tr.*	2	1.5	0.8 / Tr.	Tr. / 0.1	0.5 / 0.5	3					HBL.-BTE. QTZ. MONZONITE
1673.4–1676.4	5490–5500'	39	31	17	9	2		2	1.5	0.5 / Tr.	Tr. / 0.1	1 / 0.5	1.5	Tr.			TR. ALT. PLAG. FELDSPAR	HBL.-BTE. QTZ. MONZONITE
1703.8–1706.9	5590–5600'	39	29	12	11	1		2	1	0.5 / 0.6	0.6 / 0.1	1 / 2	1	Tr.			TR. ALT. PLAG. FELDSPAR	HBL.-BTE QTZ. MONZONITE
1734.3–1737.4	5690–5700'	37		15	9	2	Tr.*	2	1.5	0.5 / Tr.	Tr. / 0.1	3 / 1.5	1.5	Tr.			TR. ALT. PLAG. FELDSPAR	HBL.-BTE. QTZ. MONZONITE
1764.8–1767.8	5790–5800'	35	19	15	5	Tr.		2	1.5	0.5 / 0.5	7 / 0.5	7					TR. ALT. PLAG. FELDSPAR	ALTERED PORPH. HBL.-BIOTITE QTZ. MONZONITE
1795.3–1798.3	5890–5900'	17	32.5	15	20	5	Tr.	2.5	1	1.5 / Tr.	0.3 / 0.1	0.7 / 3	2.5	Tr.				HBL.-BTE QTZ. MONZONITE
1823.8–1828.8	5990–6000'	21	31.5	17	17	5	Tr.	2	1.5	1 / Tr.	0.3 / Tr.	1.2 / 1	1.5	Tr.				HBL.-BTE QTZ. MONZONITE
1856.2–1859.3	6090–6100'	20	35	15	23	3	Tr.	1.5	1.5	1 / Tr.	0.5 / 0.1	0.7 / 1	1	Tr.			TR. ALT. PLAG. FELDSPAR	HBL.-BTE. QTZ. MONZONITE
1886.7–1889.8	6190–6200'	15	35	15	27	4	0.5	1.5	1	1 / Tr.	0.5 / Tr.	0.5 / Tr.	3	Tr.			TR. ALT. PLAG. FELDSPAR	HBL.-BTE QTZ. MONZONITE
1917.2–1920.2	6290–6300'	11	39	12	23	9	2	1	1.5	0.5 / Tr.	0.6 / Tr.	2 / Tr.	2.5	Tr.			TR. ALT. PLAG. FELDSPAR	PYROX-HBL.-BTE. GRANODIORITE
1947.7–1950.7	6390–6400'	13	37.5	12	25	4	0.5	2	1	1 / Tr.	0.5 / Tr.	1 / 1.5	1	Tr.			TR. ALT. PLAG. FELDSPAR	HBL.-BTE GRANODIORITE
1978.2–1981.2	6490–6500'	12.5	33	12	30	4	Tr.	1	1	1.5 / 0.1	0.1 / 0.1	Tr. / 0.5	0.5				TR. ALT. PLAG. FELDSPAR	HBL.-BTE. GRANODIORITE
2008.6–2011.7	6590–6600'	15	33.5	12	27	3	Tr.	1.5	1.5	1.5 / 0.3	0.3 / Tr.	1 / 2	1.5				TR. ALT. PLAG. FELDSPAR	HBL.-BTE GRANODIORITE
2039.1–2042.2	6690–6700'	13	38	10	23	5	3	3	1.4	1 / 0.3	0.3 / 0.1	1 / Tr.	1					PYROXENE-HBL.-BTE. GRANODIORITE
2069.6–2072.6	6790–6800'	13	37.5	12	31	4	Tr.	2	1.5	1 / 0.1	0.1 / Tr.	0.4 / Tr.	0.1			0.1%	TR. ALT. PLAG. FELDSPAR	HBL.-BTE. GRANODIORITE
2099.0–2093.5	6870–6875'	15	39	10	25	3	0.5	2.5	2	1.5 / Tr.	0.1 / 0.1	0.1 / 0.4	0.6				TR. ALT. PLAG. FELDSPAR	HBL.-BTE. GRANODIORITE

* PRESENCE MAY BE DUE TO CAVING

TABLE 2.1 CONTINUED

twinned, occasionally kink-banded, and may show vague gradational normal zoning. Biotite, also locally kink-banded, shows yellow-brown pleochroism and forms irregular grains with ragged terminations which may show sub-parallel alignment. These biotite grains are often riddled with inclusions of magnetite-ilmenite and/or apatite. Potassium feldspar, commonly with microcline twinning, occurs both as larger grains intergrown with other rock-forming minerals and as minute irregular interstitial grains. Hornblende typically forms rather stubby subhedral crystals which are pleochroic from medium brownish-green to deep bottle green.

Two varieties of apatite are usually present in the gneiss: 1) larger stubby crystals up to 0.2mm in length with 2:1 to 4:1 length:width ratios and 2) minute acicular needles less than 0.02mm in length. The former tend to be concentrated in mafic minerals whereas the latter are concentrated in plagioclase.

Sphene in the gneiss (up to 5%) forms irregular crystals up to 0.2mm in maximum dimension as well as aggregates of these crystals up to 0.7mm in maximum dimension. Sphene may also form discontinuous rims around magnetite-ilmenite grains.

Variation in composition, grain size, and foliation of the gneisses in C/T-2 causes them to resemble other rock types. Felsic varieties may resemble granitic intrusives. Mafic gneisses, if sufficiently fine-crystalline, may look like Tertiary microdiorite dikes. For example, between 826m (2710 ft) and 835.1m (2740 ft), a dense, dark greenish-gray rock originally identified as microdiorite was identified in thin-section as a very fine-grained gneiss.

All the gneisses in C/T-2 occur with coarser-grained granitic material.

This granitic rock, represents either felsic segregations, original compositional variations, or intrusions into the gneiss.

Comparison of the gneisses in C/T-2 with surface rock types described by Nielson et al. (1978) and Sibbett and Nielson (1980) strongly suggests correlation with the Precambrian banded gneiss (PEbg; Nielson et al., 1978, p. 8), the oldest rock exposed within the Roosevelt Hot Springs KGRA. In thin section, the granitic rocks associated with gneiss above 798.5m (2620 ft) in C/T-2 (213.3-222.5m (700-730 ft), 276.8-280.4m (905-920 ft), 307.8-312.4m (1010-1025 ft), 317.3-320m (1040-1050 ft), 332.2-336.8m (1019-1105 ft)) are observed to range in composition from granite to quartz monzonite. They are xenomorphic to hypidiomorphic-granular aggregates of quartz, potassium feldspar, plagioclase, and minor biotite with accessory apatite, magnetite-ilmenite, and sphene and traces of zircon. An absence of hornblende and relatively high quartz content, together with local foliation and development of strong undulatory extinction in quartz, distinguish these granitic rocks from others in the hole.

b. Biotite-Pyroxene-Hornblende Diorite. A very distinctive pyroxene-bearing diorite was penetrated in well C/T-2 in scattered intervals between 483.1m (1585 ft) and the major fault zone at 844.3m (2770 ft). With the exception of cataclasite, to be discussed in a subsequent section, the diorite is the most pervasively and strongly altered rock type encountered in the drill hole. The alteration commonly obscures original mineralogy and texture, so that the diorite may be mistaken for the mafic-rich gneiss with which it commonly occurs. The latter, however, is devoid of pyroxene,

relatively impoverished in hornblende and magnetite-ilmenite, and enriched in biotite and quartz. The diorite is also invariably massive and equigranular, while the gneiss is commonly well-foliated.

The diorite has no reported surface equivalent at Roosevelt. Of rock types mapped within and near the KGRA, only the hornblende gneiss (hgn), biotite granodiorite (gd), and biotite diorite (Td) (Sibbett and Nielson, 1980; Nielson, et al., 1978) are even vaguely similar to the diorite in C/T-2. Except for Tertiary microdiorite, the hornblende gneiss (hgn) and biotite diorite (Td) are the only surface rock types reported to contain pyroxene, but in much lower amounts (tr.-1%) than the diorite in C/T-2 (up to 13%). The diorite in the hole is also much richer in total mafic minerals. The biotite grandiorite (gd) is mafic-rich, but with no reported pyroxene. Nielson et al. (1978), however, describe this rock as "highly variable". Possibly the diorite of C/T-2, with its high mafic content and lack of schistosity, may be a pyroxene-rich variant of either the biotite diorite (Td) or biotite granodiorite (gd).

In thin-section, the diorite appears as a fine-grained equigranular aggregate of plagioclase, hornblende, biotite, and pyroxene with minor quartz, K-feldspar, magnetite-ilmenite, and sphene and traces of apatite and zircon. The rock typically shows a distinctive, well developed mosaic fabric, but may also be xenomorphic- to hypidiomorphic-granular.

Plagioclase (An_{32-36}), averaging about 30 volume percent of the diorite, typically occurs as equant to slightly elongate grains up to 1 mm in diameter or length which are very commonly twinned. The twinning is seldom parallel to grain boundaries and is often kink-banded. The plagioclase is invariably partially altered to various combinations of sericite, calcite, epidote and clay.

The three mafic components of the diorite--biotite, hornblende, and clinopyroxene--occur in highly variable ratios, depending largely on the extent to which pyroxene is replaced by hornblende and biotite and hornblende is replaced by biotite. All three minerals, which may reach at least 1 mm in maximum dimension, tend to be equant and irregular, or partially irregular and partially bound by straight margins not related to cleavage traces or crystallographic axes. Microprobe analyses of pyroxene, hornblende and biotite from the diorite at 483.1-487.7m (1585-1600 ft) are listed in Table 2.2. Pyroxene is colorless to very slightly brownish-tinged. In addition to being partially altered to hornblende and/or biotite, the pyroxene is also very commonly replaced by subsequent reticulating epidote (±chlorite) veinlets, which may occupy up to 50% of the original crystal volume. Hornblende is strongly pleochroic, from light brown or light brownish to yellowish-green to deep green or brownish green. Biotite is also pleochroic

Table 2.2. Microprobe Chemical Analyses of Selected Rock-Forming and Alteration Minerals from LASL C/T-2 (Utah State Geothermal Well 9-1)

	BIOTITE			HORNBLENDE		PYROXENE	CHLORITE	
	1	2	3	4	5	6	7	8
SAMPLE INTERVAL m.	483.1–487.7	1904.9–1908.0	2026.8–2029.9	483.1–487.7	1904.9–1908.0	483.1–487.7	1450.8–1453.8	2026.8–2029.9
SAMPLE INTERVAL ft.	1585–1600	6250–6260	6650–6660	1585–1600	6250–6260	1585–1600	4760–4770	6650–6660
SiO_2	36.98	36.89	37.28	45.47	44.68	52.18	29.24	26.69
TiO_2	3.71	4.02	3.65	0.98	1.61	0.19	0.02	0.18
Al_2O_3	14.21	14.21	14.32	8.42	9.51	1.16	19.37	20.51
FeO	17.74	17.95	18.11	16.22	15.48	8.74	27.39	22.47
MnO	0.21	0.15	0.34	0.33	0.30	0.47	0.56	0.28
MgO	13.29	12.72	13.36	12.19	12.58	12.86	13.84	17.58
CaO	0.27	0.18	0.07	12.29	12.19	23.26	0.14	0.13
K_2O	10.22	9.89	10.18	1.11	1.28	0.07	0.32	0.27
Na_2O	0.26	0.23	0.23	1.32	1.63	0.58	0.21	0.14
BaO	0.30	0.60	0.32	0.00	0.02	0.00	0.02	0.00
Cl	0.07	0.06	0.06	0.06	0.05	0.00	0.02	0.08
F	0.26	0.27	0.42	0.11	0.14	0.00	0.19	0.16
H_2O^*	3.70	3.70	3.63	1.94	1.93	0.00	11.33	11.52
O≡Cl	0.02	0.01	0.01	0.01	0.01	0.00	0.01	0.02
O≡F	0.11	0.11	0.18	0.05	0.06	0.00	0.08	0.07
TOTAL	101.09	100.75	101.78	100.38	101.39	99.51	102.56	99.92

NOTES:

(1) Biotite from biotite-pyroxene-hornblende diorite: 5 grains

(2) Biotite from hornblende-biotite granodiorite: 5 grains

(3) Biotite from hornblende-biotite granodiorite: 5 grains

(4) Hornblende from biotite-pyroxene-hornblende diorite: 5 grains

(5) Hornblende from hornblende-biotite granodiorite: 5 grains

(6) Pyroxene from biotite-pyroxene-hornblende diorite: 7 grains

(7) Chlorite intergrown with sericite in cataclasite: 2 grains

(8) Chlorite replacing biotite in hornblende-biotite granodiorite: 2 grains

* calculated H_2O

from light yellowish-brown to dark brown or greenish-brown. Alteration products of hornblende include biotite (earliest) and epidote, calcite, and chlorite in various combinations. Biotite is partially altered to chlorite, which may be accompanied by sagenitic rutile.

The diorite is relatively rich in magnetite-ilmenite (up to 5%) and sphene (3-4%). Magnetite-ilmenite forms irregular to subhedral grains up to 0.3mm in diameter which are invariably intergrown with and commonly rimmed by sphene. Sphene-magnetite-ilmenite intergrowths may reach 1mm in maximum dimension. Individual crystals of sphene are generally texturally similar to those of magnetite-ilmenite, although a few scattered sphene crystals are euhedral and reach 0.7mm in length (*contamination?*).

Quartz and K-feldspar in the diorite are commonly highly strained. K-feldspar is otherwise texturally similar to plagioclase. Quartz occurs as individual irregular grains up to 1mm. in diameter or as aggregates of the same size formed of smaller irregular grains as little as 0.05mm in diameter. Quartz is unaltered: K-feldspar may be lightly dusted with clay.

c. Hornblende-Biotite Granodiorite to Quartz Monzonite.[1*] Between 838.2m (2750 ft) and 1082m (3550 ft) and between 1776.9m (5830 ft) and 2095.4m (6875 ft), well C/T-2 encountered mafic-rich, possibly weakly metamorphosed intrusives varying in composition from granodiorite through plagioclase-rich quartz monzonite. The upper interval is generally impoverished in mafic minerals relative to the lower interval, but is otherwise very similar and

---

[1*] *For convenience of reference, this rock type will be referred to in the text as granodiorite.*

almost certainly part of the same intrusive sequence. Drill chips throughout most of the two intervals are too small for accurate characterization of the grain size and texture of the rock. A few larger chips indicate that the upper interval is medium-grained and the lower interval fine- to medium-grained, with both intervals hypidiomorphic-granular.

The upper contact of the upper granodiorite interval is apparently in fault contact with broken and altered gneiss between 838.2m (2750 ft) and 844.3m (2770 ft). The lower contact of this interval seems to be gradational between 1072.8m (3520 ft) and 1082m (3550 ft) (the three 3.1m (10 ft) intervals above 1082m, (3550 ft), contain about 20% granite each). The upper contact of the lower interval is sharp and may be fault-controlled.

The granodiorite encountered in C/T-2 correlates most readily with the biotite diorite (Td) mapped by Sibbett and Nielson (1980) in the northern Mineral Mountains. Samples of the diorite studied to date, however, are devoid of allanite, which is ubiquitous in the granodiorite of the drill hole. The granodiorite is also richer in clinopyroxene, which is present only in trace amounts in the diorite. The meta-granodiorite also closely resembles the biotite granodiorite (gd; Sibbett and Nielson, 1980), which, however, is apparently devoid of clinopyroxene.

Plagioclase (avg. 33% by volume) in the granodiorite ranges in composition from An_{30} to An_{35}. It occurs as anhedral to subhedral grains, up to 0.5mm in maximum dimension, as very rare myrmekitic intergrowths with quartz, and as exsolution blebs in perthite. It is invariably partially altered to one or more of the minerals sericite, epidote, and calcite. Potassium feldspar (avg. 15%) in the granodiorite is essentially unaltered and

is texturally similar to coexisting plagioclase.

Quartz accounts for an average 12% of the granodiorite It occurs as lightly strained to unstrained anhedral grains and grain aggregates up to 0.3mm in diameter.

Biotite (avg. 25%) is the dominant mafic constituent in the granodiorite. It is pleochroic from medium yellowish, greenish, or orange-brown to deeper values of the same hues. It occurs as subhedral-euhedral crystals up to 0.5mm in diameter or length, and may contain local traces of magnetite-ilmenite and apatite. A few crystals in both the upper and lower granodiorite intervals are sharply kink-banded. The biotite is generally partially altered to chlorite with very low first order or anomalous blue, red, and yellow-brown interference colors. Microprobe analyses of unaltered biotite from 1904.9-1908.0m (6250-6260 ft) and 2026.8-2029.9m (6650-6660 ft) are listed in Table 2.2.

Hornblende averages about 4.5% of the rock, but ranges from 1.5 to 9%. Subhedral crystals and fragments of hornblende, commonly enclosing small crystals of apatite and dark opaque minerals, reach 0.7mm in maximum dimension. The hornblende is pleochroic from medium, slightly brownish to yellowish-green to deeper values of the same hues or intense deep bottle green. Table 2.2 provides a microprobe analysis of hornblende from 1904.9-1908m (6250-6260 ft). The hornblende commonly partially replaces clinopyroxene, and is in turn partially replaced, generally along cleavage planes, by biotite. It may also be replaced by various combinations of chlorite, calcite, and epidote. The chlorite replacing hornblende is a different variety from that forming after biotite--it is yellowish- to

brownish-green with substantially higher birefringence.

Traces of clinopyroxene occur nearly in all samples of the granodiorite. The clinopyroxene locally accounts for 2% of the total rock volume. Subhedral crystals of the clinopyroxene tend to be stubby or equant, and apparently do not exceed 0.3mm in maximum dimension. They are colorless to very slightly brownish- to bluish-green, and are almost always partially replaced by hornblende and, to a lesser extent, by biotite, epidote, calcite, and chlorite.

Magnetite-ilmenite (avg. 2%), sphene (avg. 1.5%) and apatite (avg. 1%) in the granodiorite are texturally very similar to their occurrence in the mafic-rich diorite discussed previously. Sphene in the granodiorite, in particular, shows a strong tendency to form small rims around magnetite-ilmenite grains: Apatite may form larger euhedral crystals than in the diorite--up to 0.4 x 0.2 x 0.1mm.

The presence of allanite in all samples of the granodiorite examined distinguishes this rock type from all others in well C/T-2. The allanite occurs in anhedral, generally equant crystals and crystal fragments up to 0.05mm in diameter, but usually less than 0.01mm in diameter, which may rarely form irregular aggregates up to 0.3mm in diameter. The mineral may be intergrown with, or, more rarely, rimmed by colorless to pistachio-colored epidote.

Local traces of zircon and rutile are present in the granodiorite. Zircon is texturally similar to its occurrence in the previously discussed diorite higher in the well. The rutile is secondary, occurring with chlorite as an alteration product of biotite, and occurs as sagenitically arranged

acicular crystals less than 0.05mm in length.

d. Hornblende-Biotite Quartz Monzonite. Between 1249.6m (4100 ft) and 1776.9m (5830 ft), well C/T-2 penetrated hornblende biotite quartz monzonite. Drill cuttings from this interval average about 0.5mm in diameter and do not exceed 1.5 mm, so grain size and texture of the rock cannot be accurately determined. Larger chips, however, indicate the rock to be hypidiomorphic-granular and at least medium-grained.

The quartz monzonite is uniform in composition except where modified by hydrothermal alteration. Its upper contact with hornblende-biotite granite is gradational; its lower contact with mafic-rich granodiorite is sharp and may be fault-controlled.

Comparison of the quartz monzonite with surface rock types mapped by Nielson et al. (1978) and Sibbett and Nielson (1980) suggests it most closely correlates with their Tqm (Tertiary quartz monzonite). Drill chips of the quartz monzonite in C/T-2 may contain local traces of pyroxene, which could result from caving of pyroxene-bearing units higher in the hole. Average biotite content in the quartz monzonite of the drill hole (10%) is somewhat higher than that of Tqm (4%; Nielson, et al., 1978, Table 3). The higher biotite content probably reflects proximity to, and possible assimilation of, mafic-rich units such as the granodiorite in the lower portion of C/T-2.

Plagioclase forms 23-30% of the quartz monzonite in the drill hole and averages about 27%. It occurs as: 1) anhedral to subhedral, commonly twinned grains averaging at least 1mm in diameter, 2) irregular to subhedral, optically continuous patches, rods and spindles in perthite, and 3) rare myrmekitic intergrowths with quartz. Twin lamellae in the plagioclase are

undeformed. The plagioclase is invariably partially replaced by one or more of the minerals sericite, calcite, clay, and epidote, which will be discussed in a separate alteration section.

Potassium feldspar, texturally similar to coexisting plagioclase, accounts for 35-40% (avg. 37%) of the quartz monzonite. Both perthitic and non-perthitic varieties are present. The mineral is generally fresh, but a few crystals may contain a little sericite and/or calcite, which may actually be replacing cryptocrystalline patches of included plagioclase.

Quartz, mildly strained and nearly free of inclusions, forms an average 13% (11-17%) of the quartz monzonite. It occurs as individual anhedral crystals up to 0.5mm in diameter and as minute irregular grains as small as 0.05mm in diameter forming equally irregular aggregates up to 0.7mm in diameter. In larger drill chips, these aggregates are seen to occur interstially to the other main rock-forming minerals. Quartz also occurs as wormy intergrowths with plagioclase (myrmekite) and with hornblende.

Biotite, pleochroic from yellowish- or reddish-brown to deeper values of the same hues, accounts for 5-17% (avg. 10%) of the quartz monzonite. It occurs primarily as subhedral to euhedral crystals up to 0.7mm in length or diameter, but also locally as small patches partially replacing original rock hornblende. Rare wormy intergrowths of biotite and quartz may represent total replacement of similarly-textured hornblende-quartz intergrowths. Biotite commonly contains small inclusions of euhedral apatite and anhedral magnetite-ilmenite. It is rarely intergrown with apatite, sphene, and magnetite-ilmenite in irregular aggregates up to 0.7mm in diameter. A portion of the biotite in all samples of the quartz monzonite is partially replaced by

pleochroic green chlorite, locally accmpanied by sagenitic rutile.

Hornblende (avg. 1.5%) in the quartz monzonite is also pleochroic from slightly yellowish- or brownish-green to medium to deep bottle green. Its main occurrence is as subhedral to euhedral crystals with maximum dimensions of 0.7 x 0.3 x 0.2mm. A few hornblende grains throughout the quartz monzonite are riddled with wormy stringers and blebs of quartz. Many crystals contain small inclusions of apatite and dark opaque minerals. Throughout the quartz monzonite, but especially near probable fault zones, the hornblende is partially to completely replaced by various combinations of chlorite, epidote, and calcite.

Magnetite-ilmenite (avg. 2%), sphene (avg. 1.5%) and apatite (avg. 0.5%) are the dominant accessory minerals in the quartz monzonite. Magnetite-ilmenite occurs primarily as anhedral-subhedral equant grains up to 0.2mm in diameter and as inclusions less than 0.05mm in diameter in mafic minerals. It is commonly partially to completely replaced by red to maroon submetallic hematite. Sphene, usually partially replaced by leucoxene, forms subhedral grains up to 0.5mm in maximum dimension. Apatite typically occurs as euhedral prisms, up to 0.04 x 0.15mm in diameter, most commonly embedded in biotite but also in hornblende and plagioclase. Various combinations of these accessory minerals, commonly together with biotite and/or hornblende, form local irregular intergrowths up to at least 0.7mm in diameter.

Zircon and rutile are present in the quartz monzonite in local traces. Zircon occurs as euhedral prisms measuring less than 0.05 x 0.02mm and rutile occurs as sagenitic needles measuring up to 0.1 x <0.01mm in chlorite replacing biotite.

Pyroxene in the quartz monzonite is very rare, and may owe its presence to caving. It is very light, slightly brownish- to bluish green to colorless, and non-pleochroic and is identical to pyroxene occurring higher in the drill hole. It is commonly replaced by hornblende and/or biotite, and by chlorite, epidote, and calcite.

Alteration of the quartz monzonite and other rock types will be fully discussed in a separate section.

e. Hornblende-Biotite Granite. A distinctive quartz-poor granite was intersected in C/T-2 between 798.5m (2620 ft) and 826.0m (2710 ft) and in a major intercept between 1082.0m (3550 ft) and 1249.6m (4100 ft). Larger drill chips indicate this granite to be medium-grained and hypidiomorphic granular. The rock is distinguished from granitic material associated with gneiss above 798.5m (2620 ft) by its relatively low quartz content and by the ubiquitous presence of small amounts of hornblende. Among surface rocks mapped at Roosevelt, Tertiary syenite (Ts; Nielson, et al., 1978, p. 26, Table V) correlates most closely with the granite in C/T-2. The syenite, however, is even more impoverished in quartz, contains abundant microcline, which is not present in the granite, and is generally richer in mafic minerals and sphene.

Potassium feldspar (avg. 52%), plagioclase (avg. 23%) and quartz (avg. 11%) occur in the granite both as discrete crystals and as various types of intergrowths. Plagioclase and quartz in the granite commonly form myrmekite. Graphic intergrowths of potassium feldspar and quartz are rare. Quartz in the granite typically forms irregular aggregates of equally irregular interlocking grains, some of which are mildly to moderately strained.

Biotite, hornblende, sphene, magnetite-ilmenite and apatite also occur in the granite either as individual grains or in various combinations as irregular grain aggregates. Zircon is present in local traces. Biotite (2-5%) crystals are subhedral, pleochroic from light to dark orange-brown, and up to 1mm in length or diameter. Subhedral hornblende (Tr-1%) is also pleochroic, in various shades of brownish-green, and measures up to 1 x 0.5mm in longitudinal section. Sphene (0.5-1%) is honey yellow and anhedral to subhedral in crystals up to 0.3mm in length or diameter. Magnetite-ilmenite (1.5-2%) forms disseminated anhedral equant grains up to 0.2mm, but generally less than 0.05mm in diameter. Apatite (0.5%) may occur either as larger stubby crystals averaging about 0.1mm in length with 2:1 to 4:1 length:width ratios, or as minute acicular microlites less than 0.02mm in length. Zircon is euhedral in prisms less than 0.02mm in length with 2:1 to 3:1 length:width ratios.

The granite is weakly hydrothermally altered. Plagioclase may be partially altered to various combinations of sericite, calcite, and epidote; hornblende to chlorite, calcite and epidote; biotite to chlorite ± rutile; sphene to leucoxene, and magnetite-ilmenite to hematite and/or, more rarely, leucoxene. Alteration will be more fully discussed in a later section.

Relatively large grains of colorless to pale green muscovite, texturally similar to and commonly interlayered with biotite, occur in scattered traces throughout the granite. The muscovite may be primary in origin or it may be a hydrothermal or deuteric alteration product of biotite, although this relationship is not clearly demonstrated.

f. Microdiorite and Andesite. Dense gray microdiorites and andesites and their porphyritic equivalents occur in minor amounts in several short sample intervals in C/T-2 above 838.2m (2750 ft); 298.7-303.3m (980-995 ft); 423.7-428.3m (1390-1405 ft); 464.8-469.4m (1525-1540 ft); 758.9-762m (2490-2500 ft) and form the bulk of samples between 1045.4m (3430 ft) and 1063.7m (3490 ft). All are characterized by the presence of golden-brown to deep russet-brown oxyhornblende. Although compositionally similar, these rocks may be texturally disparate, even within a single chip sample. All gradations exist between sparsely porphyritic andesites with cryptocrystalline matrix and phaneritic-microcrystalline diorites. A given variety may be either flow-foliated or massive. Such variation probably reflects both multiple cogenetic intrusion as well as chilling and differential flowage within a single intrusion.

The microdiorites and andesites in C/T-2 are almost certainly correlative with the Tertiary microdiorite (Tmd) dikes mapped at the surface by Nielson et al. (1978, p. 29). A typical example of microdiorite in the drill hole intrudes granodiorite between 1045.4m (3430 ft) and 1063.7m (3490 ft). In thin-section, this rock is primarily a microcrystalline aggregate of plagioclase, oxyhornblende and biotite with lesser amounts of quartz, potassium feldspar, magnetite-ilmenite, tremolite, apatite and sphene.

Plagioclase and oxyhornblende are typically elongate, averaging about 0.07 x 0.2mm (up to 0.4 x 0.2mm) in longitudinal section, and are randomly oriented. Biotite (12%), pleochroic from light greenish-brown to medium greenish-brown, forms disseminated irregular shreddy crystals averaging about 0.07mm (up to 0.2mm) in length or diameter, as well as irregular aggregates of the crystals up to 0.5mm in maximum dimension. Quartz (7%) and potassium feldspar (7%), singly or intergrown, occur in irregular to polygonal masses up to 0.1mm in diameter interstitial to the main rock-forming minerals. Tremolite, conspicuously anomalous at 7% of the microdiorite, occurs as acicular slightly greenish transparent needles, up to 0.1 x 0.01mm in longitudinal section, which commonly form oriented clusters of 10 or more crystals. The mineral is most commonly embedded in plagioclase, but also to a lesser extent in other rock-forming minerals. Apatite (3%) is texturally identical to, and commonly difficult to distinguish from, tremolite, but the latter, by contrast, shows inclined extinction and generally higher birefringence. Magnetite-ilmenite, also abundant in the microdiorite (5%), occurs as disseminated anhedral to subhedral equant grains averaging less than 0.01mm in diameter. Sphene (0.7%) forms anhedral grains up to 0.2mm in length or diameter.

Microdiorites above 838.2m (2750 ft) in C/T-2 are mineralogically very similar to the microdiorite just described (though devoid of tremolite) but are generally porphyritic to seriate in texture. Plagioclase and oxyhornblende phenocrysts may form up to 10% and 17%, respectively, of the porphyritic variants. Plagioclase phenocrysts are euhedral, commonly twinned and/or vaguely zoned, may be either lath-shaped or roughly equant, and may reach 1mm (avg. 0.3mm) in maximum dimension. Lath-shaped euhedral

oxyhornblende phenocrysts may reach 0.2mm (avg. 0.1mm) in length. Groundmass in these microdiorite porphyries is nearly identical to, though more finely crystalline than, the microdiorite between 1045.4m (3430 ft) and 1063.7m (3490 ft). It may be locally prominently flow-foliated.

The sample interval between 423.7m (1390 ft) and 428.2m (1405 ft) contains, in addition to microdiorite, about 15% oxyhornblende andesite porphyry. The porphyry is formed of sharply euhedral oxyhornblende and plagioclase phenocrysts embedded in a dense, locally flow-foliated cryptocrystalline groundmass, which, like all microdiorites in the drill hole, is rich in disseminated magnetite-ilmenite.

2. Alteration and Inferred Structure. All rock types along the entire sampled length of Well C/T-2 have been more or less altered, particularly within and near probable fault or cataclasite zones. Alteration minerals documented to date in C/T-2 by petrographic examination and X-ray diffraction comprise quartz, sericite, mixed-layer illite-montmorillonite, chlorite, epidote, leucoxene, hematite, calcite, secondary potassium feldspar and anhydrite. These minerals, except potassium feldspar and anhydrite, are typical of propylitic alteration or lower greenschist-facies metamorphism. Alteration minerals identified petrographically and by X-ray diffraction are listed, respectively in Tables 2.1 and 2.3.

Alteration and inferred structural disruption are notably more intense above 844.3m (2770 ft) than below this depth. At least three major and numerous minor altered cataclasite zones were penetrated above this footage: only two such zones were encountered between 844.3m (2770 ft) and 2095.4m (6875 ft): 1450.8-1453.8m (4760-4770 ft) and 1764.7-1770.8m (5790-5810 ft).

Table 2.3. Mineralogy of Clay Separates, Selected Samples from Well C/T-2 as Determined by X-Ray Diffraction

SAMPLE INTERVAL		10 Å Mica: Biotite and/or Sericite	Mixed-Layer Illite-Montmorillonite	Chlorite	Contaminants: Hornblende	Contaminants: Plagioclase	Contaminants: Quartz
Meters	Feet						
213.4-222.5	700-730	X	X	X		X	X
329.2-332.2	1080-1090	X	X			X	X
364.2-368.8	1195-1210	X	X	X		X	X
464.8-469.4	1525-1540	X	X			X	X
492.3-496.8	1615-1630	X	X	X	X	X	X
592.8-897.4	1945-1960	X		X	X	X	X
835.2-838.2	2740-2750	X	X	X		X	X
914.8-944.9	3090-3100	X		X		X	X
1051.6-1054.6	3450-3460	X			X	X	X
1350.3-1353.3	4430-4440	X		X		X	X
1450.8-1453.9	4760-4770	X		X		X	X
1527.0-1530.1	5010-5020	X		X		X	X
1764.8-1767.8	5790-5800	X		X		X	X
1905.0-1908.0	6250-6260	X			X	X	X
2026.9-2030.0	6650-6660	X		X		X	X

Altered cataclasites in C/T-2 are typically dense, light to medium grayish-green, and aphanitic to very fine-crystalline. They locally display prominent streaky foliation. In thin section, the cataclasites are observed to consist of finely comminuted rock flour, with scattered larger clasts, microveined or cemented and partially replaced by one or more of the minerals quartz, chlorite, sericite and calcite with minor epidote, hematite, leucoxene, and pyrite.

Chlorite in the altered cataclasites is light yellowish- to brownish-green with moderately high birefringence. It occurs as a constituent of microveinlets and matrix and partially to completely replaces original mafic minerals, or rarely plagioclase. It may form fans and rosettes up to 0.3mm (but generally less than 0.05mm) in diameter. These textures are best developed in the cataclasite zone between 1450.8m (4760 ft) and 1453.8m (4770 ft). A microprobe analysis of chlorite from this zone is shown in Table 2.2.

Two varieties of secondary quartz occur in the altered cataclasites. The typical and most widespread variety consists of highly irregular grains averaging less than 0.02mm in diameter or length and forming, generally together with other alteration minerals, microveinlets and irregular mosaic matrix aggregates. Between 838.2m (2750 ft) and 844.3m (2770 ft) and in traces between 675.1m (2215 ft) to 679.7m (2230 ft) and 734.5m (2410 ft) and 740.6m (2430 ft), secondary quartz forms late-stage, terminated, clear euhedral crystals up to 2mm in length and 1mm in diameter.

Sericite in the cataclasite typically forms minute fibers less than 0.05mm in length replacing plagioclase and rock flour, or intergrown with other alteration minerals in microveinlets and matrix. It also forms rare

larger slightly greenish to transparent crystals (actually muscovite) apparently pseudomorphing original biotite.

Calcite and epidote in the cataclasites occur as minor microveinlet and matrix constituents and partially replace hornblende, pyroxene and plagioclase. Calcite may also locally partially replace sphene.

All the cataclasites contain minor magnetite-ilmenite and sphene. The former is invariably partially replaced by maroon- to brick-red submetallic hematite ± leucoxene; the latter by dense light gray to white leucoxene ± calcite. Magnetite-ilmenite apparently has a dual origin in the cataclasites. Most cataclasite is fragmental and obviously derived from the pre-existing rock. Vermiform blebs of magnetite-ilmenite in microveinlets and matrix, however, suggest addition to the cataclasites during hydrothermal alteration. Hematization of dark opaque minerals occurs along the entire length of C/T-2 and is clearly secondary in origin. Sphene is apparently all relict.

With few exceptions, alteration mineralogy away from cataclasite zones in C/T-2 is petrographically similar to, though much less intense than, alteration within these zones. Microveinlets and veinlet fragments of the principal alteration minerals in all combinations are ubiquitous, but rarely account for more than a fraction of a percent of a given sample. Chlorite and sericite as microveinlet constituents increase in frequency and volume with proximity to cataclasite zones.

Partial replacement of original rock-forming minerals is the dominant alteration mode away from the cataclasites. Plagioclase is replaced by sericite and epidote and, above 838.2m (2750 ft), by clay, presumably of supergene origin. X-ray diffraction of representative samples shows the clay

to be mixed-layer illite-montmorillonite (Table 2.3). Hornblende, and, to a lesser extent, pyroxene, are replaced by chlorite, calcite, epidote, and clay. The chlorite replacing these mafics is petrographically identical to the chlorite of the cataclasite zones. Biotite is also partially chloritized, but by a distinctive bright green chlorite with anomalous blue, red, and yellowish-brown birefringence. This chlorite locally contains sagenitically arranged rutile needles. Quartz and potassium feldspar are generally unaltered, although the local cloudy appearance and mottled extinction of the latter may be due to very weak argillization.

Pyrite, rarely accompanied by texturally similar chalcopyrite, occurs at least in traces throughout C/T-2. It is, however, concentrated within and adjacent to cataclasite zones and hornblende-rich units above 844.3m (2770 ft). The pyrite is found as disseminated, anhedral to subhedral grains up to 0.30mm, but typically less than 0.10mm in diameter, but it also occurs as similar grains with other alteration minerals in microeinlets and matrix aggregates. Among the rock forming minerals, magnetite-ilmenite, hornblende and plagioclase are the preferred hosts, in decreasing order of susceptibility, for sulfide replacement.

Anhydrite first appears in thin-section between 574.5m (1885 ft) and 583.7m (1915 ft) where it occurs as a single fragment, 0.15 x 0.1mm in size, cut by a chlorite microveinlet. It next occurs in plagioclase between 1018m (3340 ft) and 1021m (3350 ft) as a microveinlet and adjoining irregular replacement patch, measuring 0.1 x 0.03mm. Anhydrite is then absent until 1615.4m (5300 ft) below which it is present in nearly every sample. In all these lower samples, it occurs only as discrete drill-broken crystal

fragments, up to 0.2mm in diameter, almost certainly derived from veins.

Secondary potassium feldspar first appears in C/T-2 between 574.5m (1885 ft) and 583.7m (1915 ft). Here it is present in trace amounts as irregular discontinuous selvages on quartz and quartz-chlorite veinlets. Similar trace occurrences were documented in the following samples: 829m (2720 ft) to 832.1m (2730 ft), 838.2m (2750 ft) to 841.2m (2760 ft), 841.2m (2760 ft) to 844.3m (2770 ft). Secondary potassium feldspar is probably more abundant in the drill hole than reported here. In finely ground drill cuttings, secondary potassium feldspar is difficult to distinguish from primary potassium feldspar in perthite, antiperthite, or in granophyric intergrowths with quartz.

Calcite, an alteration production which can be readily separated from its host rock, was extracted from selected samples from C/T-2 for oxygen and carbon isotope analysis. The calcite partially replaces, in descending order of susceptibility to alteration, plagioclase, hornblende, pyroxene, and sphene. It also occurs as a common constituent of microveinlets and cataclasite. Calcite is ubiquitous in well C/T-2, but is concentrated in the upper portion of the well (above 838.2m (2750 ft)) and in fault and cataclasite zones, particularly those centered on 838.2m (2750 ft), 1453.8m (4770 ft) and 1767.8m (5800 ft). Paragenetic relationships for calcite relative to other alteration minerals in well C/T-2 are ambiguous, but cross-cutting veinlets indicate multiple periods of calcite deposition.

The small size of drill cuttings from C/T-2 hinders determination of paragenetic relationships among alteration minerals. Where larger chips and/or pervasive alteration permit such a determination, these relationships are generally ambiguous. In one sample, for instance, a given alteration

mineral may clearly pre-date another, whereas in a second sample the reverse may be true. In spite of these difficulties, a number of paragenetic relationships among alteration minerals in C/T-2 can be established with some confidence:

1) Hornblende and biotite after clinopyroxene, and biotite after hornblende are the earliest alteration products. They are consistently replaced by or cut by microveinlets of all other alteration minerals, and are probably magmatic, deuteric, or metamorphic in origin.

2) Microveinlets of chlorite ± quartz ± magnetite-ilmenite ± pyrite post-date all other alteration minerals except clay in the upper portion of the hole and quartz between 835.1m (2740 ft) and 838.2m (2750 ft). The chlorite in these microveinlets is petrographically identical to the chlorite of cataclasites mapped at the surface by Nielson and others (1978).

3) Small, clear euhedral quartz crystals in the altered fault zone between 835.1m (2740 ft) and 838.2m (2750 ft) apparently line open spaces in the veinlets described above, and therefore post-date these veinlets.

4) Veinlets and irregular patches of illite-montmorillonite are confined to the portion of the hole above 838.2m (2750 ft) and post-date all other alteration minerals. The clay may be largely of supergene origin.

a. Discussion. Hydrothermal alteration observed in well C/T-2 is texturally and mineralogically similar to that observed at intermediate to deep levels in other holes within the Roosevelt Hot Springs KGRA, including Utah State Geothermal Wells 72-16 (Rohrs and Parry, 1978), 14-2 (Parry, 1978;

Ballantyne and Parry, 1978; Ballantyne, J. M., 1978) and 52-21 (Ballantyne, G. H., 1978) (Figure 1.2). Near-surface alteration in C/T-2 could not be characterized due to an absence of cuttings between ground level and 121.9m (400 ft).

The age of alteration in C/T-2 relative to present geothermal activity is unknown. Sinter deposits and altered alluvium penetrated by shallow diamond drill holes along the Opal Mound Fault (DDH 1A, 1B and 76-1; Bryant and Parry, 1977; Parry, et al., 1980) (Figure 1.2) and altered alluvium in Utah State 72-16 (Rohrs and Parry, 1978) are clearly of recent geothermal origin. Other alteration at Roosevelt, however, may be partially paleohydrothermal. Cataclasites and mylonites and adjacent host rocks exposed in the west-central Mineral Mountains and within the KGRA, for instance, are typically altered to various combinations of chlorite, sericite, quartz, hematite and epidote (Nielson, et al., 1978). Epidote normally forms at temperatures greater than 220^{o}C (Zen and Thompson, 1964). Its present occurrence at the surface at Roosevelt suggests formation at deeper levels prior to present geothermal activity, then subsequent exposure by erosion. B. Sibbett (personal communication, 1980) has observed fresh glassy rhyolite flows, dated at 0.8 to 0.5 m.y. (Lipman, et al., 1978), resting on strongly chloritized, silicified and hematized cataclasite within the KGRA. This relationship strongly suggests a pre-geothermal origin for the alteration.

3. Intervals selected for Detailed Geochemical and Isotopic Investigation. Four intervals in well C/T-2 were selected for detailed geochemical and isotopic study: 1066.7-1097.2m (3500-3600 ft); 1758.6-1804.3m (5770-5920 ft); 1904.9-1935.4m (6250-6350 ft); and 2023.8-2057.3m (6660-6750

ft). The upper interval is in the cased portion of the hole and was chosen to provide calibration data for gamma-ray logging tools at moderate temperatures. The three lower intervals are all uncased, and were selected as potentially useful for calibrating gamma-ray and neutron logging equipment at high temperatures.

The interval 1066.7-1097.2m (3500-3600 ft) spans the contact at 1082.0m (3550 ft) between the upper hornblende biotite granodiorite and subjacent hornblende-biotite granite.

The interval 1758.6-1804.3m (5770-5920 ft) includes the contact at 1776.9m (5830 ft) between hornblende biotite quartz monzonite and the lower granodiorite. The interval also includes a fault zone between 1764.7m (5790 ft) and 1770.8m (5810 ft)

The two lower intervals, 1904.9-1935.4m (6250-6260 ft) and 2923.8-2057.3m (6650-6750 ft), are both in the lower hornblende-biotite granodiorite. Both intervals show strong gamma-ray and neutron log anomalies which do not correlate with readily apparent lithologic variations. Both intervals, however (especially 2023.8-2057.3m (6650-6750 ft)) are characterized by slightly more intense alteration and mineralization than is typical for the lower portion of C/T-2.

III. GEOCHEMISTRY

A. Introduction

Chemical analyses of cuttings from hole C/T-2 have been completed with two principal objectives in mind. First, various types of analyses can be useful in the interpretation of the genesis of geothermal systems and location of fluid entries within drill holes. Second, several of the geophysical logging techniques which will be discussed in a subsequent section measure chemical properties. The most obvious of these is the gamma log which measures the gamma radiation produced by the natural decay of uranium, thorium, and potassium. In addition, several elements have extremely large thermal neutron capture cross sections and are thus important in the evaluation of neutron logs.

B. Methods and Procedures

All cuttings samples for chemical analysis from well C/T-2 were initially thoroughly washed to remove drilling mud, lost circulation material and other contaminants. The samples were then cleaned of iron drill bit and drill rod shavings with a hand magnet. Composite samples were prepared at the rate of one gram of sample per foot of drill hole. Prior to analysis both individual and composite samples (except for closed-can gamma-ray spectrometry) were pulverized to a fine powder (<<270 mesh) in a Spex shatterbox.

Individual samples from the selected intervals of well C/T-2 were analyzed for Si, Ti, Al, Fe, Mn, Mg, Ca, P, Nb, Zr, Y, Sr, Rb, Th, Pb, Ba and U by X-ray fluorescence (XRF) using a Norelco (Phillips Electronics Instruments) X-ray fluorescence spectrograph. For each sample, two disks were prepared for analysis. Fused glass disks were used for Si, Ti, Al, Fe, Mn,

Mg, Ca and P. All other analyses were obtained from powder disks prepared by mixing one gram of chromatographic cellulose with one gram of sample and pressing the mixture into an aluminum cap with 20 tons pressure. XRF analytical techniques used for Si, Ti, Al, Fe, Mn, Mg, Ca and P are those of Norrish and Hutton (1969). U analyses required the methods of James (1977). All other XRF analyses were obtained by the methods of Jack and Carmichael (1969): For Ba, these methods were modified by F. Brown, of the University of Utah Department of Geology and Geophysics. Na and K analyses were obtained by lithium metaborate fusion and flame photometry using techniques outlined by Suhr and Ingamells (1966).

Sulfur analyses for the four selected intervals from well C/T-2 were completed with a LECO sulfur analyzer. For each analysis by this method, measured quantities of sample, Sn and Fe are inductively furnace-heated in a stream of oxygen, producing SO_2 which is then analyzed by titration with potassium iodide.

U in samples from the selected intervals was also determined by fluorometry, using a Jarrel-Ash fluorometer. In fluorometric analysis, each sample is digested in $HCLO_4$, HNO_3 and HF, then mixed with ethyl acetate. The resulting mixture is fused with a flux in a platinum disk, then excited by ultra-violet radiation, causing the sample to fluoresce. The fluorescence of the sample is compared with that of standards containing known quantities of U.

Closed-can gamma-ray spectrometry was used to determine K, Th, and U concentrations in samples from the selected intervals of well C/T-2. Analyses were obtained with a Tracor-Northern multichannel gamma-ray spectrometer.

Each cuttings sample was completely sealed in a can to prevent leakage of radon gas. The sealed sample was allowed to sit for four hours, then counted for 2000 seconds. A second reading of the same duration was obtained four days later, the results averaged, and the counts converted to K, Th and U values.

Arsenic concentrations in samples from the four selected intervals and in 100-foot composite samples were obtained by colorometric methods. Sample preparation for colorimetry begins with digestion in HF, $HClO_4$ and HCl. Arsenic in the acidified sample is reduced to a trivalent state by the addition of potassium iodide and stannous chloride solutions. Zinc is added and reacts with the acid, liberating hydrogen gas, which forms arsine from the arsenic in the sample. The arsine is bubbled into a solution of pyridine and silver diethyldithiocarbamate, with which the arsine forms a colored complex which is compared to standards.

Mercury analyses for composite samples and samples from the selected intervals of C/T-2 were obtained with a Jerome Instruments Model 301 gold-film detector. For this technique a weighed portion of each sample is heated in a closed tube to greater than 600°C to release Hg vapor. The vapor collects on a gold film, and concentration is measured by the resultant change in electrical resistance of the film.

Individual samples from the four selected intervals from well C/T-2 and 100-foot composite samples from the entire sampled length of the well were analyzed for the following elements by plasma spectrometry: Na, K, Ca, Mg, Fe, Al, Ti, P, Sr, Ba, V, Cr, Mn, Co, Ni, Cu, Mo, Pb, Zn, Cd, Au, Ag, Sb, Bi, Te, Sn, W, Li, Be, Zr, La, Ce, and Th. Analyses were obtained with a Model

137 Applied Research Laboratories Inductively Coupled Plasma Quantometer (ICPQ) with a 1080 line per millimeter grating and computer operating system which automatically performs calibration, matrix interference correction and background subtraction.

Sample preparation for analysis by ICPQ commences with oven-drying a one-gram portion for at least two hours at 120°C. This dried portion is then digested, in several stages, in HF, $HClO_4$, HCl, and HNO_3. This digestion yields for analysis an aqueous solution with approximate concentrations of 5% $HClO_4$, 10% HNO_3 and 1% total dissolved solid.

C. Geochemistry of Composite Samples

Numerous studies have drawn attention to the analogy between geothermal systems and the systems which have produced hydrothermal ore deposits (Ewers and Keays, 1977). The suite of metals which are concentrated in geothermal systems are similar to those which are found in epithermal ore deposits. Efforts are presently underway to understand the geochemical relationships in these systems and to adapt this understanding to the formulation of geochemical exploration methods (Bamford, 1968; Bamford, et al., 1980).

Several periods of hydrothermal activity can be documented in the Roosevelt geothermal area. The youngest period is the present one with alteration and mineral deposition being concentrated along the three major structural trends which have been discussed previously. Low angle normal faulting, the oldest fault episode recognized in the area was accompanied by hydrothermal activity. Numerous small exploration pits containing shows of malachite, chalcopyrite, and pitch limonite have been found along the mapped fault zones (Nielson, et al., 1978; Sibbett and Nielson, 1980). In addition,

small mineralized areas within the plutonic phases suggest that the intrusive episodes may have generated small hydrothermal systems, although age relationships are speculative at this time.

A geochemical reconnaissance study of C/T-2 was done to help evaluate the evolution of the geothermal system in this area and to allow comparison with data from the rest of the field. Whole rock samples were composited at 30.5 meter (100 ft) intervals and analyzed using an Induction Coupled Plasma Quantometer. These results are shown in Table 3.1 and selected elements are plotted as a function of depth in Figure 3.1. Bamford et al. (1980) have suggested that Li, As, Hg, Mn, Zn, and Sr, are important elements in evaluating the behavior of the geothermal system. In well C/T-2, Mn, Sr, and Zn show a strong correlation with rock type and are probably not geothermal indicators.

The hanging wall of the low angle fault (above 844.0m (2750 ft)) shows anomalous concentrations of Li, As, and Hg. An especially strong Hg anomaly is present in the 204.0-241.0m (670-790 ft) section. Detailed analysis of this interval shows 2800 ppb Hg in the 204.0-213.0m (670-700 ft) interval which is the location of the alluvium-bedrock contact. It is felt that this anomaly was produced by thermal waters which at one time leaked from the Opal Mound Fault or the western boundary fault of the Opal Mound horst (Figure 1.2). The entire hanging wall, however, shows a geochemical signature which is compatible with hydrothermal alteration. It will be seen in the next section that this area is characterized by $\delta^{18}O$ lows produced by equilibrium with thermal waters.

A zone of brecciation and alteration located between 1451.0m and 1454.0m

ELEMENT		121.9–149.1 m (400–490 ft)	149.1–176.8 m (490–580 ft)	176.8–204.2 m (580–670 ft)	204.2–240.8 m (670–790 ft)
NA	% OX.	4.15	4.02	4.37	4.06
K	% OX.	5.22	5.77	6.13	4.57
CA	% OX.	1.01	0.757	0.829	2.84
MG	% OX.	0.105	0.144	0.089	1.13
FE	% OX.	0.855	0.922	0.615	4.11
AL	% OX.	15.75	15.79	16.04	14.68
TI	% OX.	0.387	0.240	0.129	1.18
P	% OX.	0.049	0.055	0.042	0.430
SR	PPM	350	348	385	660
BA	% OX.	0.154	0.157	0.164	0.113
V	PPM	< 250	< 250	< 250	< 250
CR	PPM	4	5	< 2.00	< 2.00
MN	% OX.	0.013	0.009	0.010	0.064
CO	PPM	36	41	48	28
NI	PPM	< 5.00	< 5.00	< 5.00	8
CU	PPM	6	< 5.00	< 5.00	21
MO	PPM	< 50.0	< 50.0	< 50.0	< 50.0
PB	PPM	42	27	21	18
ZN	PPM	12	15	10	57
CD	PPM	< 5.00	< 5.00	< 5.00	< 5.00
AG	PPM	< 2.00	< 2.00	< 2.00	< 2.00
AU	PPM	< 4.00	< 4.00	< 4.00	< 4.00
AS	PPM	4.0	6.0	3.0	2.0
SB	PPM	< 30.0	< 30.0	< 30.0	< 30.0
BI	PPM	< 100	< 100	< 100	< 100
TE	PPM	< 50.0	< 50.0	< 50.0	< 50.0
SN	PPM	< 5.00	< 5.00	< 5.00	< 5.00
LI	PPM	4	4	3	21
BE	PPM	1.4	1.4	1.3	3.0
ZR	PPM	16	11	12	11
LA	PPM	26	22	18	34
CE	PPM	57	44	42	63
TH	PPM	< 150	< 150	< 150	< 150
HG	PPB	10	< 5	< 5	550

TABLE 3.1 CHEMICAL ANALYSIS OF COMPOSITE WHOLE ROCK SAMPLES FROM C/T-2

ELEMENT		240.8-271.3 m (790-890 ft)	271.3-303.3 m (890-995 ft)	303.3-332.2 m (995-1090 ft)	332.2-364.2 m (1090-1195 ft)
NA	% OX.	3.96	3.80	4.22	3.94
K	% OX.	4.56	4.52	3.31	3.17
CA	% OX.	2.15	2.19	2.38	2.27
MG	% OX.	0.594	0.987	0.815	0.624
FE	% OX.	2.51	2.92	3.09	3.33
AL	% OX.	14.12	13.96	15.18	13.56
TI	% OX.	0.573	0.629	0.840	0.823
P	% OX.	0.209	0.234	0.361	0.306
SR	PPM	471	439	599	497
BA	% OX.	0.102	0.083	0.115	0.098
V	PPM	< 250	< 250	< 250	< 250
CR	PPM	2	3	< 2.00	< 2.00
MN	% OX.	0.035	0.047	0.038	0.028
CO	PPM	39	41	51	39
NI	PPM	9	12	< 5.00	5
CU	PPM	24	21	13	10
MO	PPM	< 50.0	< 50.0	< 50.0	< 50.0
PB	PPM	65	19	23	29
ZN	PPM	72	44	34	26
CD	PPM	< 5.00	< 5.00	< 5.00	< 5.00
AG	PPM	< 2.00	< 2.00	< 2.00	< 2.00
AU	PPM	< 4.00	< 4.00	< 4.00	< 4.00
AS	PPM	2.0	1.0	4.0	6.0
SB	PPM	< 30.0	< 30.0	< 30.0	< 30.0
BI	PPM	< 100	< 100	< 100	< 100
TE	PPM	< 50.0	< 50.0	< 50.0	< 50.0
SN	PPM	< 5.00	< 5.00	< 5.00	< 5.00
LI	PPM	11	14	11	13
BE	PPM	3.1	2.5	3.2	3.3
ZR	PPM	9	14	11	9
LA	PPM	31	34	45	36
CE	PPM	54	57	79	63
TH	PPM	< 150	< 150	< 150	< 150
HG	PPB	15	15	15	10

TABLE 3.1 CONTINUED

ELEMENT		364.2–387.1 m (1195–1270 ft)	387.1–423.7 m (1270–1390 ft)	423.7–455.7 m (1390–1495 ft)	455.7–483.1 m (1495–1585 ft)
NA	% OX.	3.33	4.23	4.50	4.30
K	% OX.	3.99	3.72	3.02	4.00
CA	% OX.	3.24	3.63	3.98	3.58
MG	% OX.	0.866	1.25	1.22	1.33
FE	% OX.	3.76	4.04	4.51	4.78
AL	% OX.	14.89	16.34	15.59	15.71
TI	% OX.	0.729	1.05	1.12	1.16
P	% OX.	0.252	0.332	0.318	0.316
SR	PPM	520	712	613	574
BA	% OX.	0.123	0.128	0.117	0.119
V	PPM	< 250	< 250	< 250	< 250
CR	PPM	7	7	3	5
MN	% OX.	0.045	0.060	0.084	0.083
CO	PPM	29	34	30	30
NI	PPM	9	14	11	8
CU	PPM	15	23	89	50
MO	PPM	< 50.0	< 50.0	< 50.0	< 50.0
PB	PPM	21	22	19	28
ZN	PPM	35	46	54	56
CD	PPM	< 5.00	< 5.00	< 5.00	< 5.00
AG	PPM	< 2.00	< 2.00	< 2.00	< 2.00
AU	PPM	< 4.00	< 4.00	< 4.00	< 4.00
AS	PPM	< 4.0	< 2.0	< 3.0	< 2.0
SB	PPM	< 30.0	< 30.0	< 30.0	< 30.0
BI	PPM	< 100	< 100	< 100	< 100
TE	PPM	< 50.0	< 50.0	< 50.0	< 50.0
SN	PPM	< 5.00	< 5.00	< 5.00	< 5.00
LI	PPM	14	12	10	11
BE	PPM	2.6	2.5	2.4	1.8
ZR	PPM	8	10	10	15
LA	PPM	62	58	50	54
CE	PPM	105	104	92	103
TH	PPM	< 150	< 150	< 150	< 150
HG	PPB	10	20	20	25

TABLE 3.1 CONTINUED

ELEMENT		183.1–515.1 m (1585–1690 ft)	515.1–547.1 m (1690–1795 ft)	547.1–574.5 m (1795–1885 ft)	574.5–606.6 m (1885–1990 ft)
NA	% OX.	3.87	3.88	4.23	4.25
K	% OX.	3.04	3.11	2.91	2.76
CA	% OX.	6.56	6.61	6.69	6.43
MG	% OX.	2.66	3.03	3.12	2.35
FE	% OX.	8.50	8.76	8.68	8.95
AL	% OX.	15.65	16.43	17.03	16.60
TI	% OX.	2.03	2.12	2.14	2.54
P	% OX.	0.374	0.387	0.319	0.572
SR	PPM	724	957	860	784
BA	% OX.	0.071	0.125	0.085	0.083
V	PPM	< 250	< 250	< 250	< 250
CR	PPM	4	20	13	13
MN	% OX.	0.137	0.141	0.151	0.155
CO	PPM	45	36	42	39
NI	PPM	19	17	20	19
CU	PPM	106	59	69	78
MO	PPM	< 50.0	< 50.0	< 50.0	< 50.0
PB	PPM	38	41	24	17
ZN	PPM	71	102	114	116
CD	PPM	< 5.00	< 5.00	< 5.00	< 5.00
AG	PPM	< 2.00	< 2.00	< 2.00	< 2.00
AU	PPM	< 4.00	< 4.00	< 4.00	< 4.00
AS	PPM	2.0	3.0	7.0	4.0
SB	PPM	< 30.0	< 30.0	< 30.0	< 30.0
BI	PPM	< 100	< 100	< 100	< 100
TE	PPM	< 50.0	< 50.0	< 50.0	< 50.0
SN	PPM	< 5.00	< 5.00	< 5.00	< 5.00
LI	PPM	15	16	22	27
BE	PPM	2.5	2.4	2.6	2.7
ZR	PPM	21	16	32	32
LA	PPM	44	49	52	64
CE	PPM	87	95	109	132
TH	PPM	< 150	< 150	< 150	< 150
HG	PPB	15	10	10	15

TABLE 3.1 CONTINUED

ELEMENT		606.6-638.6 m (1990-2095 ft)	638.6-669.0 m (2095-2195 ft)	669.0-701.0 m (2195-2300 ft)	701.0-731.5 m (2300-2400 ft)
NA	% OX.	4.68	4.40	3.85	4.18
K	% OX.	4.17	3.10	3.17	2.64
CA	% OX.	4.93	6.31	7.13	7.42
MG	% OX.	1.75	2.04	3.03	3.06
FE	% OX.	5.88	7.21	8.66	8.49
AL	% OX.	17.07	16.70	15.96	16.48
TI	% OX.	1.50	1.88	2.13	2.09
P	% OX.	0.360	0.451	0.366	0.399
SR	PPM	583	796	757	830
BA	% OX.	0.074	0.078	0.077	0.078
V	PPM	< 250	< 250	< 250	< 250
CR	PPM	20	32	29	37
MN	% OX.	0.098	0.127	0.128	0.129
CO	PPM	31	45	43	38
NI	PPM	12	21	23	22
CU	PPM	60	80	84	90
MO	PPM	< 50.0	< 50.0	< 50.0	< 50.0
PB	PPM	99	44	25	43
ZN	PPM	83	92	92	95
CD	PPM	< 5.00	< 5.00	< 5.00	< 5.00
AG	PPM	< 2.00	< 2.00	< 2.00	< 2.00
AU	PPM	< 4.00	< 4.00	< 4.00	< 4.00
AS	PPM	8.0	2.0	4.0	25.0
SB	PPM	< 30.0	< 30.0	< 30.0	< 30.0
BI	PPM	< 100	< 100	< 100	< 100
TE	PPM	< 50.0	< 50.0	< 50.0	< 50.0
SN	PPM	< 5.00	< 5.00	< 5.00	< 5.00
LI	PPM	12	15	15	14
BE	PPM	2.2	2.5	2.4	2.4
ZR	PPM	17	21	25	23
LA	PPM	77	50	42	46
CE	PPM	138	102	84	90
TH	PPM	< 150	< 150	< 150	< 150
HG	PPB	10	15	15	15

TABLE 3.1 CONTINUED

ELEMENT		731.5-762.0m (2400-2500 ft)	762.0-792.5m (2500-2600 ft)	792.5-823.0m (2600-2700 ft)	823.0-850.4m (2700-2790 ft)
NA	% OX.	3.88	4.70	5.13	4.45
K	% OX.	3.52	1.84	4.37	2.51
CA	% OX.	4.21	4.80	1.91	5.65
MG	% OX.	1.61	1.97	0.442	2.57
FE	% OX.	5.37	6.83	3.20	6.82
AL	% OX.	15.84	16.26	14.53	17.35
TI	% OX.	1.27	1.72	0.756	1.63
P	% OX.	0.378	0.423	0.126	0.488
SR	PPM	602	652	277	918
BA	% OX.	0.112	0.096	0.058	0.137
V	PPM	250	< 250	< 250	< 250
CR	PPM	36	31	20	40
MN	% OX.	0.083	0.123	0.059	0.113
CO	PPM	30	33	26	30
NI	PPM	10	14	< 5.00	24
CU	PPM	44	49	15	50
MO	PPM	50.0	< 50.0	< 50.0	< 50.0
PB	PPM	372	26	27	71
ZN	PPM	93	106	44	89
CD	PPM	< 5.00	< 5.00	< 5.00	< 5.00
AG	PPM	< 2.00	< 2.00	< 2.00	< 2.00
AU	PPM	< 4.00	< 4.00	< 4.00	< 4.00
AS	PPM	7.0	3.0	3.0	7.0
SB	PPM	< 30.0	< 30.0	< 30.0	< 30.0
BI	PPM	< 100	< 100	< 100	< 100
TE	PPM	< 50.0	< 50.0	< 50.0	< 50.0
SN	PPM	< 5.00	< 5.00	< 5.00	< 5.00
LI	PPM	14	17	8	22
BE	PPM	2.7	2.1	1.3	2.1
ZR	PPM	14	18	23	16
LA	PPM	60	62	78	59
CE	PPM	110	117	148	112
TH	PPM	< 150	< 150	< 150	< 150
HG	PPB	15	10	5	10

TABLE 3.1 CONTINUED

ELEMENT		850.4-880.9m (2790-2890 ft)	883.9-908.3m (2900-2980 ft)	908.3-941.8m (2980-3090 ft)	941.8-972.3m (3090-3190 ft)
NA	% OX.	4.54	5.04	4.95	4.89
K	% OX.	4.64	3.20	2.79	2.80
CA	% OX.	4.23	4.29	5.28	5.75
MG	% OX.	2.50	1.74	2.28	2.68
FE	% OX.	5.87	4.90	6.78	7.13
AL	% OX.	18.34	17.34	18.76	18.76
TI	% OX.	1.31	1.21	1.77	1.91
P	% OX.	0.342	0.338	0.489	0.509
SR	PPM	958	988	1331	1512
BA	% OX.	0.212	0.223	0.244	0.238
V	PPM	< 250	< 250	< 250	< 250
CR	PPM	29	30	27	28
MN	% OX.	0.089	0.084	0.115	0.111
CO	PPM	23	22	21	20
NI	PPM	7	6	5	6
CU	PPM	34	20	19	17
MO	PPM	< 50.0	< 50.0	< 50.0	< 50.0
PB	PPM	275	71	92	29
ZN	PPM	104	81	96	107
CD	PPM	< 5.00	< 5.00	< 5.00	< 5.00
AG	PPM	< 2.00	< 2.00	< 2.00	< 2.00
AU	PPM	< 4.00	< 4.00	< 4.00	< 4.00
AS	PPM	3.0	2.0	2.0	1.0
SB	PPM	< 30.0	< 30.0	< 30.0	< 30.0
BI	PPM	< 100	< 100	< 100	< 100
TE	PPM	< 50.0	< 50.0	< 50.0	< 50.0
SN	PPM	< 5.00	< 5.00	< 5.00	< 5.00
W	PPM	< 1200	< 1200	< 1200	< 1200
LI	PPM	13	11	18	10
BE	PPM	2.0	1.9	1.7	1.7
ZR	PPM	8	10	10	10
LA	PPM	51	46	70	64
CE	PPM	88	83	128	122
TH	PPM	< 150	< 150	< 150	< 150
HG	PPB	10	10	10	5

TABLE 3.1 CONTINUED

ELEMENT		972.3-1005.8m (3190-3300 ft)	1005.8-1036.3m (3300-3400 ft)	1036.3-1066.8m (3400-3500 ft)	1066.8-1097.3m (3500-3600 ft)
NA	% OX.	5.15	5.47	4.99	5.36
K	% OX.	3.84	4.21	3.23	2.93
CA	% OX.	4.27	4.45	5.13	3.30
MG	% OX.	1.71	1.66	2.37	1.22
FE	% OX.	5.92	5.82	8.20	4.33
AL	% OX.	17.16	18.97	17.11	16.93
TI	% OX.	1.62	1.59	1.83	1.04
P	% OX.	0.349	0.367	0.545	0.214
SR	PPM	1253	1287	1155	711
BA	% OX.	0.356	0.328	0.254	0.164
V	PPM	< 250	< 250	< 250	< 250
CR	PPM	26	30	54	29
MN	% OX.	0.104	0.107	0.121	0.078
CO	PPM	18	23	25	20
NI	PPM	< 5.00	5	19	6
CU	PPM	13	18	25	15
MO	PPM	< 50.0	< 50.0	< 50.0	< 50.0
PB	PPM	35	37	43	33
ZN	PPM	81	86	103	70
CD	PPM	< 5.00	< 5.00	< 5.00	< 5.00
AG	PPM	< 2.00	< 2.00	< 2.00	2
AU	PPM	< 4.00	< 4.00	< 4.00	< 4.00
AS	PPM	3.0	2.0	2.0	1.0
SB	PPM	< 30.0	< 30.0	< 30.0	< 30.0
BI	PPM	< 100	< 100	< 100	< 100
TE	PPM	< 50.0	< 50.0	< 50.0	< 50.0
SN	PPM	< 5.00	< 5.00	< 5.00	< 5.00
LI	PPM	9	8	9	6
BE	PPM	1.4	1.4	1.9	1.2
ZR	PPM	11	11	40	12
LA	PPM	50	63	68	57
CE	PPM	93	111	127	98
TH	PPM	< 150	< 150	< 150	< 150
HG	PPB	< 5	< 5	5	< 5

TABLE 3.1 CONTINUED

ELEMENT		1097.3-1127.8 m (3600-3700 ft)	1127.8-1158.2 m (3700-3800 ft)	1158.2-1188.7 m (3800-3900 ft)	1188.7-1216.2 m (3900-3990 ft)
NA	% OX.	5.52	5.41	5.39	5.36
K	% OX.	3.82	3.65	5.21	4.47
CA	% OX.	1.88	1.91	1.78	1.81
MG	% OX.	0.524	0.552	0.578	0.676
FE	% OX.	2.13	3.37	2.26	2.80
AL	% OX.	16.56	15.99	16.62	16.74
TI	% OX.	0.539	0.877	0.607	0.691
P	PPM	0.087	0.133	0.094	0.115
SR	% OX.	292	260	244	302
BA	PPM	< 250	0.073 <	250	0.083
V	PPM	0.074 <	250	0.069 <	250
CR	% OX.	21	34	37	32
MN	PPM	0.049	0.065	0.057	0.064
CO	PPM	13	16	15	20
NI	PPM	< 5.00	5.00 <	5.00 <	5.00
CU	PPM	< 8	12	8	22
MO	PPM	< 50.0	50.0 <	50.0 <	50.0
PB	PPM	21	25	21	265
ZN	PPM	46	51	55	60
CD	PPM	< 5.00	< 5.00	< 5.00	< 5.00
AG	PPM	< 2.00	< 2.00	< 2.00	< 2.00
AU	PPM	< 4.00	< 4.00	< 4.00	< 4
AS	PPM	< 1.0	< 2.0	< 2.0	< 1.0
SB	PPM	< 30.0	< 30.0	< 30.0	< 30.0
BI	PPM	< 100	< 100	< 100	< 100
TE	PPM	< 50.0	< 50.0	< 50.0	< 50.0
SN	PPM	< 5.00	< 5.00	< 5.00	< 5.00
LI	PPM	5	5	6	6
BE	PPM	0.8	0.9	0.9	0.9
ZR	PPM	11	19	9	11
LA	PPM	48	89	40	50
CE	PPM	79	150	67	82
TH	PPM	< 150	< 150	< 150	< 150
HG	PPB	5	5	< 5	< 5

TABLE 3.1 CONTINUED

ELEMENT		1216.2–1246.6 m (3990–4090 ft)	1246.6–1277.1 m (4090–4190 ft)	1277.1–1307.6 m (4190–4290 ft)	1307.6–1338.1 m (4290–4390 ft)
NA	% OX.	5.19	5.08	5.18	5.47
K	% OX.	4.76	2.44	3.16	2.85
CA	% OX.	1.94	3.75	3.46	4.01
MG	% OX.	0.633	1.57	1.35	1.51
FE	% OX.	2.71	4.58	4.33	4.41
AL	% OX.	16.32	16.08	16.64	18.40
TI	% OX.	0.713	1.18	1.17	1.15
P	% OX.	0.115	0.273	0.255	0.297
SR	PPM	348	1077	1054	1157
BA	% OX.	0.108	0.273	0.293	0.298
V	PPM	< 250	< 250	< 250	< 250
CR	PPM	32	48	37	31
MN	% OX.	0.062	0.090	0.085	0.090
CO	PPM	17	15	18	22
NI	PPM	< 5.00	< 5.00	< 5.00	< 5.00
CU	PPM	9	10	10	10
MO	PPM	< 50.0	< 50.0	< 50.0	< 50.0
PB	PPM	28	19	20	22
ZN	PPM	60	89	77	98
CD	PPM	< 5.00	< 5.00	< 5.00	< 5.00
AG	PPM	< 2.00	< 2.00	< 2.00	< 2.00
AU	PPM	< 4.00	< 4.00	< 4.00	< 4.00
AS	PPM	2.0	1.0	1.0	1.0
SB	PPM	< 30.0	< 30.0	< 30.0	< 30.0
BI	PPM	< 100	< 100	< 100	< 100
TE	PPM	< 50.0	< 50.0	< 50.0	< 50.0
SN	PPM	< 5.00	< 5.00	< 5.00	< 5.00
LI	PPM	6	9	7	10
BE	PPM	1.0	1.4	1.3	1.6
ZR	PPM	11	8	10	9
LA	PPM	61	46	42	50
CE	PPM	102	77	71	84
TH	PPM	< 150	< 150	< 150	< 150
HG	PPB	< 5	< 5	< 5	< 5

TABLE 3.1 CONTINUED

ELEMENT		1338.1-1368.6m (4390-4490 ft)	1368.6-1399m (4490-4590 ft)	1399.0-1429.5m (4590-4690 ft)	1429.5-1460.0m (4690-4790 ft)
NA	% OX.	5.39	5.50	5.34	5.07
K	% OX.	2.89	4.15	3.02	3.18
CA	% OX.	3.73	4.16	3.66	3.38
MG	% OX.	1.27	1.63	1.72	1.35
FE	% OX.	4.48	4.88	4.44	4.12
AL	% OX.	17.09	18.10	18.27	16.74
TI	% OX.	1.25	1.28	1.07	1.08
P	% OX.	0.303	0.335	0.209	0.221
SR	PPM	1143	1130	1180	1044
BA	% OX.	0.324	0.289	0.330	0.323
V	PPM	< 250	< 250	< 250	< 250
CR	PPM	34	32	28	34
MN	% OX.	0.091	0.093	0.092	0.086
CO	PPM	30	21	23	19
NI	PPM	< 5.00	< 5.00	5	5
CU	PPM	10	12	10	10
MO	PPM	< 50.0	< 50.0	< 50.0	< 50.0
PB	PPM	22	258	115	45
ZN	PPM	73	83	85	68
CD	PPM	< 5.00	< 5.00	< 5.00	< 5.00
AG	PPM	< 2.00	< 2.00	< 2.00	< 2.00
AU	PPM	< 4.00	< 4.00	< 4.00	< 4.00
AS	PPM	5.0	< 1.0	1.0	< 1.0
SB	PPM	< 30.0	< 30.0	< 30.0	< 30.0
BI	PPM	< 100	< 100	< 100	< 100
TE	PPM	< 50.0	< 50.0	< 50.0	< 50.0
SN	PPM	< 5.00	< 5.00	< 5.00	< 5.00
W	PPM	< 1200	< 1200	< 1200	< 1200
LI	PPM	9	9	10	16
BE	PPM	1.5	1.4	1.4	1.4
ZR	PPM	10	10	9	9
LA	PPM	44	56	38	39
CE	PPM	75	92	61	65
TH	PPM	< 150	< 150	< 150	< 150
HG	PPB	5	5	5	10

TABLE 3.1 CONTINUED

ELEMENT		1460.0-1490.5m (4790-4890 ft)	1490.5-1521.0m (4890-4990 ft)	1521.0-1551.4m (4990-5090 ft)	1551.4-1581.9m (5090-5190 ft)
NA	% OX.	5.29	5.33	5.21	5.30
K	% OX.	5.24	3.21	3.08	3.40
CA	% OX.	3.30	3.28	3.05	2.83
MG	% OX.	1.28	1.25	1.15	1.06
FE	% OX.	4.41	4.22	3.58	3.82
AL	% OX.	17.58	17.84	16.86	15.93
TI	% OX.	1.16	1.21	0.989	0.971
P	% OX.	0.265	0.262	0.231	0.205
SR	PPM	989	965	868	852
BA	% OX.	0.331	0.339	0.314	0.324
V	PPM	< 250	< 250	< 250	< 250
CR	PPM	31	34	27	31
MN	% OX.	0.090	0.091	0.081	0.082
CO	PPM	18	20	20	25
NI	PPM	< 5.00	< 5.00	< 5.00	< 5.00
CU	PPM	9	9	9	8
MO	PPM	< 50.0	< 50.0	< 50.0	< 50.0
PB	PPM	31	25	60	40
ZN	PPM	70	66	61	66
CD	PPM	< 5.00	< 5.00	< 5.00	< 5.00
AG	PPM	< 2.00	< 2.00	< 2.00	< 2.00
AU	PPM	< 4.00	< 4.00	< 4.00	< 4.00
AS	PPM	< 1.0	< 1.0	< 1.0	< 1.0
SB	PPM	< 30.0	< 30.0	< 30.0	< 30.0
BI	PPM	< 100	< 100	< 100	< 100
TE	PPM	< 50.0	< 50.0	< 50.0	< 50.0
SN	PPM	< 5.00	< 5.00	< 5.00	< 5.00
LI	PPM	8	7	7	6
BE	PPM	1.3	1.2	1.3	1.2
ZR	PPM	12	13	11	12
LA	PPM	47	49	39	29
CE	PPM	78	81	65	50
TH	PPM	< 150	< 150	< 150	< 150
HG	PPB	5	5	10	5

TABLE 3.1 CONTINUED

ELEMENT		1581.9-1612.4m (5190-5290 ft)	1612.4-1642.9m (5290-5390 ft)	1642.9-1673.4m (5390-5490 ft)	1673.4-1703.8m (5490-5590 ft)
NA	% OX.	5.30	5.03	5.11	5.13
K	% OX.	3.85	3.99	3.91	4.03
CA	% OX.	3.35	2.95	2.72	2.88
MG	% OX.	1.21	1.10	1.12	1.27
FE	% OX.	4.92	4.82	4.10	4.13
AL	% OX.	16.78	15.93	16.26	17.07
TI	% OX.	1.31	1.23	1.10	1.11
P	% OX.	0.322	0.264	0.229	0.228
SR	PPM	886	807	734	789
BA	% OX.	0.306	0.294	0.285	0.283
V	PPM	< 250	< 250	< 250	< 250
CR	PPM	26	30	27	44
MN	% OX.	0.093	0.088	0.080	0.082
CO	PPM	18	21	20	24
NI	PPM	< 5.00	6	< 5.00	< 5.00
CU	PPM	11	12	9	8
MO	PPM	< 50.0	< 50.0	< 50.0	< 50.0
PB	PPM	35	45	38	26
ZN	PPM	65	66	68	74
CD	PPM	< 5.00	< 5.00	< 5.00	< 5.00
AG	PPM	< 2.00	< 2.00	< 2.00	< 2.00
AU	PPM	< 4.00	< 4.00	< 4.00	< 4.00
AS	PPM	< 1.0	< 1.0	1.0	< 1.0
SB	PPM	< 30.0	< 30.0	< 30.0	< 30.0
BI	PPM	< 100	< 100	< 100	< 100
TE	PPM	< 50.0	< 50.0	< 50.0	< 50.0
SN	PPM	< 5.00	< 5.00	< 5.00	< 5.00
LI	PPM	7	7	7	7
BE	PPM	1.3	1.3	1.2	1.2
ZR	PPM	16	16	14	15
LA	PPM	51	53	39	38
CE	PPM	84	86	62	63
TH	PPM	< 150	< 150	< 150	< 150
HG	PPB	10	10	5	5

TABLE 3.1 CONTINUED

ELEMENT		1703.8-1734.3m (5590-5690 ft)	1734.3-1764.8m (5690-5790 ft)	1764.8-1795.3m (5790-5890 ft)	1795.3-1825.8m (5890-5990 ft)	1825.8-1856.2m (5990-6090 ft)
NA	% OX.	5.15	4.73	4.99	5.04	5.25
K	% OX.	3.47	3.47	3.49	4.72	3.00
CA	% OX.	2.91	3.10	3.91	3.88	4.30
MG	% OX.	1.16	1.01	1.95	2.00	2.38
FE	% OX.	4.20	4.88	5.33	5.50	5.93
AL	% OX.	17.11	16.77	17.81	17.12	19.21
TI	% OX.	1.11	1.10	1.44	1.46	1.54
P	% OX.	0.242	0.229	0.340	0.348	0.336
SR	PPM	769	863	1016	925	1141
BA	% OX.	0.297	0.335	0.323	0.287	0.378
V	PPM	< 250	< 250	< 250	< 250	< 250
CR	PPM	36	72	48	69	61
MN	% OX.	0.082	0.083	0.102	0.102	0.109
CO	PPM	26	27	19	24	32
NI	PPM	< 5.00	9	< 5.00	< 5.00	< 5.00
CU	PPM	10	20	10	10	11
MO	PPM	< 50.0	< 50.0	< 50.0	< 50.0	< 50.0
PB	PPM	25	244	33	26	22
ZN	PPM	69	72	99	114	119
CD	PPM	< 5.00	< 5.00	< 5.00	< 5.00	< 5.00
AG	PPM	< 2.00	< 2.00	< 2.00	< 2.00	< 2.00
AU	PPM	< 4.00	< 4.00	< 4.00	< 4.00	< 4.00
AS	PPM	< 1.0	1.0	< 1.0	1.0	1.0
SB	PPM	< 30.0	< 30.0	< 30.0	< 30.0	< 30.0
BI	PPM	< 100	< 100	< 100	< 100	< 100
TE	PPM	< 50.0	< 50.0	< 50.0	< 50.0	< 50.0
SN	PPM	< 5.00	< 5.00	< 5.00	< 5.00	< 5.00
LI	PPM	7	9	10	9	9
BE	PPM	1.2	1.3	1.3	1.3	1.4
ZR	PPM	15	16	9	10	9
LA	PPM	45	48	47	39	47
CE	PPM	71	75	79	68	69
TH	PPM	< 150	< 150	< 150	< 150	< 150
HG	PPB	5	5	5	< 5	5

TABLE 3.1 CONTINUED

ELEMENT		1856.2-1886.7 m (6090-6190 ft)	1886.7-1917.2 m (6190-6290 ft)	1917.2-1947.7 m (6290-6390 ft)	1947.7 1978.2 m (6390-6490 ft)
NA	% OX.	5.01	4.44	4.81	4.70
K	% OX.	3.09	3.07	2.35	2.38
CA	% OX.	4.43	6.35	4.96	5.49
MG	% OX.	2.89	4.15	2.98	3.55
FE	% OX.	6.99	9.16	7.31	8.14
AL	% OX.	18.51	18.48	18.67	19.75
TI	% OX.	1.60	1.93	1.53	1.87
P	% OX.	0.303	0.336	0.399	0.531
SR	PPM	1197	1192	1178	465
BA	% OX.	0.334	0.197	0.313	0.296
V	PPM	< 250	< 250	< 250	< 250
CR	PPM	81	102	75	64
MN	% OX.	0.117	0.117	0.122	0.122
CO	PPM	44	52	62	23
NI	PPM	8	57	16	6
CU	PPM	13	35	21	14
MO	PPM	< 50.0	< 50.0	< 50.0	< 50.0
PB	PPM	20	21	51	23
ZN	PPM	137	127	143	154
CD	PPM	< 5.00	< 5.00	< 5.00	< 5.00
AG	PPM	< 2.00	< 2.00	< 2.00	< 2.00
AU	PPM	< 4.00	< 4.00	< 4.00	< 4.00
AS	PPM	1.0	1.0	1.0	1.0
SB	PPM	< 30.0	< 30.0	< 30.0	< 30.0
BI	PPM	< 100	< 100	< 100	< 100
TE	PPM	< 50.0	< 50.0	< 50.0	< 50.0
SN	PPM	< 5.00	< 5.00	< 5.00	< 5.00
LI	PPM	11	13	11	10
BE	PPM	1.6	2.0	1.6	1.7
ZR	PPM	8	15	12	8
LA	PPM	47	39	56	62
CE	PPM	76	70	92	104
TH	PPM	< 150	< 150	< 150	< 150
HG	PPB	5	5	< 5	< 5

TABLE 3.1 CONTINUED

ELEMENT		1978.2-2008.6m (6490-6590 ft)	2008.6-2039.1m (6590-6690 ft)	2039.1-2069.6m (6690-6790 ft)	2069.6-2095.8m (6790-6885 ft)
NA	% OX.	4.37	4.74	4.32	4.31
K	% OX.	3.97	3.63	2.85	4.16
CA	% OX.	5.33	4.37	5.79	4.81
MG	% OX.	3.41	2.77	3.39	3.14
FE	% OX.	8.36	6.96	8.62	7.60
AL	% OX.	18.61	18.73	18.73	18.07
TI	% OX.	1.94	1.59	2.11	1.72
P	% OX.	0.573	0.407	0.666	0.523
SR	PPM	1355	1096	1464	1147
BA	% OX.	0.259	0.248	0.249	0.256
V	PPM	< 250	< 250	< 250	< 250
CR	PPM	71	58	57	60
MN	% OX.	0.126	0.116	0.123	0.118
CO	PPM	32	23	24	25
NI	PPM	7	7	6	7
CU	PPM	17	15	19	16
MO	PPM	< 50.0	< 50.0	< 50.0	< 50.0
PB	PPM	38	27	22	39
ZN	PPM	147	122	125	125
CD	PPM	< 5.00	< 5.00	< 5.00	< 5.00
AG	PPM	< 2.00	< 2.00	< 2.00	< 2.00
AU	PPM	< 4.00	< 4.00	< 4.00	< 4.00
AS	PPM	2.0	2.0	1.0	2.0
SB	PPM	< 30.0	< 30.0	< 30.0	< 30.0
BI	PPM	< 100	< 100	< 100	< 100
TE	PPM	< 50.0	< 50.0	< 50.0	< 50.0
SN	PPM	< 5.00	< 5.00	< 5.00	< 5.00
LI	PPM	11	13	12	13
BE	PPM	1.7	1.4	1.8	1.8
ZR	PPM	10	11	9	10
LA	PPM	62	55	68	60
CE	PPM	107	93	118	102
TH	PPM	< 150	< 150	< 150	< 150
HG	PPB	< 5	< 5	5	< 5

TABLE 3.1 CONTINUED

(4760-4770 ft) contains a Li and As anomaly in the composite geochemistry. This zone does not show an associated Hg anomaly, but Hg is probably not stable at the temperatures which exist in this area (J. N. Moore, personal communication). No other zones which are beneath the casing show evidence of hot water entries using reconnaissance geochemical techniques.

D. Geochemistry of Detailed Study Intervals

The intervals selected for detailed log interpretation have been analyzed chemically at ten foot intervals. These analyses are presented in Table 3.2. In addition, Table 3.2 contains several spot analyses from the upper portion of the drill hole.

E. Rare Earth Element Analyses

The thermal neutron capture cross sections of several of the Rare Earth Elements is quite large. In particular gadolinium, samarium, and europium have capture cross sections of 46,000, 5,600, and 1,400 Barns respectively. In order to evaluate the influence of these elements on the neutron logs, several spot samples were analyzed by neutron activation techniques. These results are shown in Table 3.3.

F. Fluid Chemistry

Table 3.4 gives two analyses of water from well C/T-2. The first analysis is from Parry et al. (1976). The second analysis is of water collected in 1979 (Newman, 1979). Since water in the well is stagnant, some change in chemistry may be expected. In addition, chemical gradients may exist or develop in the fluid in the borehole.

Table 3.2. Chemical analyses of composite whole rock samples from Well C/T-2.

PHILLIPS 4-1

DATA	2005.00	2170.00	2260.00	2360.00	2460.00	FT
	611.1	661.4	688.8	719.3	749.8	METERS
SIO2	63.00	53.51	48.87	56.22	62.47	WT %
TIO2	0.81	2.14	2.52	1.92	1.11	WT %
AL2O3	17.28	16.97	14.57	15.65	15.50	WT %
FE2O3	3.12	8.29	11.01	8.49	4.93	WT %
MNO	0.13	0.16	0.15	0.12	0.07	WT %
MGO	0.65	1.77	3.47	3.08	1.42	WT %
CAO	1.89	5.71	7.52	6.39	3.11	WT %
K2O	6.52	3.15	2.50	3.28	5.36	WT %
NA2O	4.83	4.52	4.29	4.47	4.55	WT %
P2O5	0.15	0.67	0.48	0.37	0.33	WT %
SO3	0.03	0.21	0.26	0.18	0.04	WT %
LOSS	1.12	1.08	1.90	1.90	1.17	WT %
TOTAL	99.53	98.18	97.54	102.07	100.06	
NB	25.00	40.00	35.00	30.00	30.00	PPM
ZR	440.00	180.00	170.00	150.00	240.00	PPM
Y	20.00	30.00	20.00	25.00	25.00	PPM
SR	350.00	815.00	760.00	790.00	600.00	PPM
RB	90.00	45.00	65.00	70.00	125.00	PPM
PB	25.00	10.00	10.00	15.00	80.00	PPM
BA	700.00	700.00	400.00	800.00	1550.00	PPM
V	< 150.00	< 150.00	164.00	< 150.00	< 150.00	PPM
CR	24.00	26.00	46.00	35.00	36.00	PPM
CO	23.00	39.00	38.00	33.00	26.00	PPM
NI	< 5.00	17.00	27.00	17.00	8.00	PPM
CU	10.00	56.00	93.00	60.00	19.00	PPM
MO	< 50.00	< 50.00	< 50.00	< 50.00	< 50.00	PPM
ZN	44.00	124.00	104.00	82.00	65.00	PPM
CD	< 5.00	< 5.00	< 5.00	< 5.00	< 5.00	PPM
AG	< 2.00	< 2.00	< 2.00	< 2.00	< 2.00	PPM
AU	< 4.00	< 4.00	< 4.00	< 4.00	< 4.00	PPM
AS	< 1.00	18.00	2.00	3.00	4.00	PPM
SB	< 30.00	< 30.00	< 30.00	< 30.00	< 30.00	PPM
BI	< 100.00	< 100.00	< 100.00	< 100.00	< 100.00	PPM
TE	< 50.00	< 50.00	< 50.00	< 50.00	< 50.00	PPM
SN	< 5.00	7.00	7.00	7.00	5.00	PPM
LI	8.00	17.00	22.00	10.00	14.00	PPM
BE	1.20	2.20	2.30	2.30	2.60	PPM
LA	92.00	64.00	40.00	44.00	54.00	PPM
CE	157.00	130.00	72.00	77.00	93.00	PPM
HG	5.00	25.00	20.00	15.00	10.00	PPB
U (XRF)	< 2.00	< 2.00	< 2.00	< 2.00	< 2.00	PPM
U (F)	1.69	2.12	3.39	2.12	3.39	PPM
U (R)						PPM
TH (R)						PPM
TH (XRF)	15.00	< 5.00	10.00	5.00	10.00	PPM
K (R)						PPM

Table 3.2 continued

PHILLIPS 9-1

DATA	2560.00	2720.00	2810.00	3500.00	3510.00	FT
	780.3	829.2	856.5	1066.8	1069.8	METERS
SIO2	55.36	54.49	55.09		53.30	WT %
TIO2	1.91	1.64	1.41		1.74	WT %
AL2O3	17.50	15.68	19.10		18.39	WT %
FE2O3	7.42	8.29	5.89		8.22	WT %
MNO	0.14	0.11	0.08		0.11	WT %
MGO	2.43	3.69	2.58		2.16	WT %
CAO	5.82	5.61	4.76		5.16	WT %
K2O	3.80	3.35	3.77		3.04	WT %
NA2O	4.64	4.62	4.93		4.70	WT %
P2O5	0.48	0.42	0.40		0.46	WT %
SO3	0.15	0.11	0.06		0.12	WT %
LOSS	1.06	0.79	1.26		1.17	WT %
TOTAL	100.71	99.00	99.33	0.00	98.57	
NB	30.00	30.00	20.00		30.00	PPM
ZR	270.00	225.00	70.00		450.00	PPM
Y	25.00	25.00	15.00		25.00	PPM
SR	780.00	900.00	1220.00		1210.00	PPM
RB	60.00	90.00	70.00		50.00	PPM
PB	30.00	40.00	45.00		30.00	PPM
BA	1000.00	1450.00	2900.00		2200.00	PPM
V	< 150.00	< 150.00	< 150.00		< 150.00	PPM
CR	37.00	102.00	29.00		54.00	PPM
CO	34.00	31.00	36.00		19.00	PPM
NI	13.00	53.00	5.00		12.00	PPM
CU	47.00	54.00	18.00		39.00	PPM
MO	< 50.00	< 50.00	< 50.00		< 50.00	PPM
ZN	103.00	89.00	81.00		94.00	PPM
CD	< 5.00	< 5.00	< 5.00		< 5.00	PPM
AG	< 2.00	< 2.00	< 2.00		< 2.00	PPM
AU	< 4.00	< 4.00	< 4.00		< 4.00	PPM
AS	4.00	< 1.00	< 1.00		1.00	PPM
SB	< 30.00	< 30.00	< 30.00		< 30.00	PPM
BI	< 100.00	< 100.00	< 100.00		< 100.00	PPM
TE	< 50.00	< 50.00	< 50.00		< 50.00	PPM
SN	7.00	< 5.00	< 5.00		< 5.00	PPM
LI	11.00	17.00	9.00		11.00	PPM
BE	2.00	2.30	1.60		3.00	PPM
LA	60.00	68.00	35.00		114.00	PPM
CE	106.00	116.00	54.00		141.00	PPM
HG	15.00	15.00	10.00		5.00	PPB
U (XRF)	< 2.00	< 2.00	< 2.00		5.00	PPM
U (F)	1.27	1.27	0.85		0.85	PPM
U (R)				33.88	33.88	PPM
TH (R)				< 10.00	< 10.00	PPM
TH (XRF)	10.00	15.00	5.00		5.00	PPM
K (R)				4.00	3.60	PPM

Table 3.2 continued

PHILLIPS 9-1

DATA	3520.00	3540.00	3550.00	3560.00	3570.00	FT
	1072.9	1079.0	1082.0	1085.1	1088.1	METERS
SIO2	54.27	54.06	55.43	59.90	60.72	WT %
TIO2	1.44	1.47	1.36	1.08	0.93	WT %
AL2O3	19.09	19.39	19.46	19.03	19.24	WT %
FE2O3	7.50	6.81	6.36	4.82	4.03	WT %
MNO	0.11	0.10	0.09	0.08	0.06	WT %
MGO	2.28	2.01	1.86	1.19	1.04	WT %
CAO	5.11	4.52	4.57	3.10	2.73	WT %
K2O	3.19	3.65	3.91	5.86	6.39	WT %
NA2O	4.99	5.04	5.30	4.81	4.90	WT %
P2O5	0.44	0.36	0.37	0.26	0.21	WT %
SO3	0.11	0.11	0.11	0.08	0.06	WT %
LOSS	0.99	0.96	1.07	0.86	0.84	WT %
TOTAL	99.52	98.48	99.89	101.07	101.15	
NB	20.00	25.00	25.00	15.00	15.00	PPM
ZR	205.00	430.00	345.00	465.00	465.00	PPM
Y	20.00	20.00	20.00	15.00	15.00	PPM
SR	1240.00	1300.00	1250.00	665.00	580.00	PPM
RB	55.00	55.00	55.00	65.00	70.00	PPM
PB	75.00	35.00	25.00	45.00	50.00	PPM
BA	2150.00	2600.00	2450.00	1250.00	1200.00	PPM
V	< 150.00	< 150.00	< 150.00	< 150.00	< 150.00	PPM
CR	53.00	29.00	41.00	39.00	37.00	PPM
CO	22.00	19.00	17.00	20.00	15.00	PPM
NI	13.00	6.00	6.00	6.00	< 5.00	PPM
CU	37.00	21.00	22.00	20.00	14.00	PPM
MO	< 50.00	< 50.00	< 50.00	< 50.00	< 50.00	PPM
ZN	97.00	80.00	80.00	56.00	48.00	PPM
CD	< 5.00	< 5.00	< 5.00	< 5.00	< 5.00	PPM
AG	< 2.00	< 2.00	< 2.00	< 2.00	< 2.00	PPM
AU	< 4.00	< 4.00	< 4.00	< 4.00	< 4.00	PPM
AS	1.00	< 1.00	1.00	1.00	< 1.00	PPM
SB	< 30.00	< 30.00	< 30.00	< 30.00	< 30.00	PPM
BI	< 100.00	< 100.00	< 100.00	< 100.00	< 100.00	PPM
TE	< 50.00	< 50.00	< 50.00	< 50.00	< 50.00	PPM
SN	< 5.00	< 5.00	< 5.00	< 5.00	< 5.00	PPM
LI	12.00	10.00	8.00	7.00	5.00	PPM
BE	2.70	2.50	2.30	2.00	1.70	PPM
LA	89.00	97.00	91.00	78.00	71.00	PPM
CE	108.00	113.00	100.00	83.00	67.00	PPM
HG	5.00	< 5.00	5.00	5.00	< 5.00	PPB
U (XRF)	< 2.00	< 2.00	4.00	< 2.00	< 2.00	PPM
U (F)	1.69	1.27	1.27	1.69	1.27	PPM
U (R)	< 8.47	< 8.47	< 8.47	< 8.47	< 8.47	PPM
TH (R)	< 10.00	< 10.00	< 10.00	< 10.00	< 10.00	PPM
TH (XRF)	< 5.00	< 5.00	< 5.00	5.00	25.00	PPM
K (R)	3.80	3.80	4.30	6.50	6.20	PPM

Table 3.2 continued

PHILLIPS 9-1

DATA	3580.00	3590.00	3600.00	5780.00	5790.00	FT
	1091.2	1094.2	1097.3	1761.7	1764.8	METERS
SIO2	60.90	60.18	62.40	57.07	57.71	WT %
TIO2	0.86	0.80	0.68	1.06	1.01	WT %
AL2O3	18.85	18.40	19.22	18.78	18.72	WT %
FE2O3	3.79	3.85	2.86	4.59	4.07	WT %
MNO	0.07	0.07	0.06	0.09	0.09	WT %
MGO	0.69	0.88	0.85	1.41	1.38	WT %
CAO	2.45	2.03	2.08	3.14	3.34	WT %
K2O	6.67	6.57	7.08	5.80	5.90	WT %
NA2O	5.22	5.08	5.47	4.86	4.63	WT %
P2O5	0.18	0.15	0.14	0.24	0.24	WT %
SO3	0.04	0.03	0.03	0.07	0.04	WT %
LOSS	0.85	0.53	0.73	1.49	2.30	WT %
TOTAL	100.57	98.57	101.60	98.60	99.43	
NB	15.00	15.00	15.00	15.00	20.00	PPM
ZR	620.00	835.00	420.00	410.00	215.00	PPM
Y	15.00	15.00	15.00	15.00	15.00	PPM
SR	435.00	445.00	355.00	1085.00	1035.00	PPM
RB	70.00	60.00	60.00	70.00	65.00	PPM
PB	35.00	40.00	40.00	55.00	35.00	PPM
BA	900.00	850.00	700.00	3550.00	3650.00	PPM
V	220.00	< 150.00	< 150.00	< 150.00	< 150.00	PPM
CR	50.00	39.00	39.00	55.00	61.00	PPM
CO	20.00	17.00	17.00	38.00	35.00	PPM
NI	7.00	< 5.00	< 5.00	5.00	< 5.00	PPM
CU	19.00	14.00	12.00	13.00	8.00	PPM
MO	< 50.00	< 50.00	< 50.00	< 50.00	< 50.00	PPM
ZN	72.00	47.00	47.00	73.00	65.00	PPM
CD	5.00	< 5.00	< 5.00	< 5.00	< 5.00	PPM
AG	8.00	< 2.00	< 2.00	< 2.00	< 2.00	PPM
AU	10.00	< 4.00	< 4.00	< 4.00	< 4.00	PPM
AS	< 1.00	1.00	1.00	< 1.00	< 1.00	PPM
SB	52.00	< 30.00	< 30.00	41.00	< 30.00	PPM
BI	< 100.00	< 100.00	< 100.00	< 100.00	< 100.00	PPM
TE	< 50.00	< 50.00	< 50.00	< 50.00	< 50.00	PPM
SN	< 5.00	< 5.00	< 5.00	< 5.00	< 5.00	PPM
LI	13.00	6.00	6.00	18.00	25.00	PPM
BE	1.70	1.30	1.20	1.90	1.70	PPM
LA	88.00	109.00	116.00	69.00	58.00	PPM
CE	127.00	119.00	121.00	92.00	63.00	PPM
HG	< 5.00	< 5.00	< 5.00	5.00	5.00	PPB
U (XRF)	3.00	< 2.00	< 2.00	< 2.00	< 2.00	PPM
U (F)	1.27	0.85	1.69	1.27	1.27	PPM
U (R)	< 8.47	< 8.47	< 8.47			PPM
TH (R)	< 10.00	< 10.00	< 10.00			PPM
TH (XRF)	15.00	< 5.00	5.00	< 5.00	< 5.00	PPM
K (R)	7.20	7.40	7.40			PPM

Table 3.2 continued

PHILLIPS 9-1

DATA	5800.00	5810.00	5820.00	5830.00	5840.00	FT
	1767.8	1770.9	1773.9	1777.0	1780.0	METERS
SIO2	56.46	58.76	58.15	57.17	54.60	WT %
TIO2	1.14	1.20	1.05	1.07	1.75	WT %
AL2O3	18.28	19.11	19.34	19.28	19.07	WT %
FE2O3	4.88	5.10	4.24	4.32	7.42	WT %
MNO	0.09	0.09	0.09	0.08	0.12	WT %
MGO	1.35	1.31	1.41	1.27	2.23	WT %
CAO	2.83	2.91	3.13	3.21	4.31	WT %
K2O	5.98	6.14	6.04	5.71	4.65	WT %
NA2O	4.11	4.70	4.81	4.90	5.01	WT %
P2O5	0.31	0.32	0.25	0.26	0.44	WT %
SO3	0.09	0.10	0.04	0.03	0.11	WT %
LOSS	2.40	2.48	1.55	1.54	1.17	WT %
TOTAL	97.92	102.22	100.10	99.04	100.88	
NB	20.00	15.00	15.00	20.00	25.00	PPM
ZR	445.00	510.00	175.00	200.00	350.00	PPM
Y	15.00	15.00	15.00	15.00	15.00	PPM
SR	905.00	910.00	1205.00	1215.00	1050.00	PPM
RB	70.00	75.00	60.00	60.00	65.00	PPM
PB	40.00	30.00	25.00	30.00	30.00	PPM
BA	3650.00	3700.00	4000.00	3750.00	2900.00	PPM
V	< 150.00	332.00	< 150.00	< 150.00	< 150.00	PPM
CR	70.00	69.00	61.00	60.00	66.00	PPM
CO	19.00	17.00	18.00	17.00	18.00	PPM
NI	< 5.00	7.00	< 5.00	< 5.00	8.00	PPM
CU	11.00	17.00	8.00	9.00	16.00	PPM
MO	< 50.00	72.00	< 50.00	< 50.00	< 50.00	PPM
ZN	97.00	103.00	75.00	74.00	99.00	PPM
CD	< 5.00	6.00	< 5.00	< 5.00	< 5.00	PPM
AG	< 2.00	10.00	< 2.00	< 2.00	< 2.00	PPM
AU	< 4.00	8.00	< 4.00	< 4.00	< 4.00	PPM
AS	3.00	3.00	< 1.00	1.00	1.00	PPM
SB	< 30.00	63.00	< 30.00	< 30.00	< 30.00	PPM
BI	< 100.00	< 100.00	< 100.00	< 100.00	< 100.00	PPM
TE	< 50.00	51.00	< 50.00	< 50.00	< 50.00	PPM
SN	< 5.00	< 5.00	< 5.00	< 5.00	< 5.00	PPM
LI	24.00	28.00	16.00	15.00	13.00	PPM
BE	2.00	2.10	1.60	1.70	2.30	PPM
LA	64.00	90.00	54.00	66.00	98.00	PPM
CE	75.00	141.00	58.00	70.00	113.00	PPM
HG	10.00	5.00	5.00	< 5.00	10.00	PPB
U (XRF)	< 2.00	< 2.00	< 2.00	< 2.00	< 2.00	PPM
U (F)	1.69	1.69	1.27	1.27	1.27	PPM
U (R)	< 8.47	< 8.47	< 8.47	< 8.47	< 8.47	PPM
TH (R)	< 10.00	< 10.00	< 10.00	< 10.00	< 10.00	PPM
TH (XRF)	5.00	< 5.00	< 5.00	10.00	5.00	PPM
K (R)	6.30	6.50	5.40	6.50	4.90	PPM

Table 3.2 continued

PHILLIPS 9-1

DATA	5850.00	5860.00	5870.00	5880.00	5870.00	FT
	1783.1	1786.1	1789.2	1792.2	1795.3	METERS
SIO2	53.90	54.03	53.05	55.25	55.38	WT %
TIO2	1.57	1.57	1.68	1.59	1.45	WT %
AL2O3	18.66	18.89	19.16	19.84	19.40	WT %
FE2O3	6.86	6.79	7.97	7.37	6.65	WT %
MNO	0.11	0.12	0.12	0.13	0.11	WT %
MGO	2.02	1.94	2.17	2.42	2.35	WT %
CAO	4.20	4.19	4.37	4.36	4.39	WT %
K2O	4.58	4.72	4.60	4.75	4.60	WT %
NA2O	4.74	4.87	4.79	4.80	5.19	WT %
P2O5	0.41	0.40	0.50	0.41	0.43	WT %
SO3	0.10	0.08	0.14	0.13	0.06	WT %
LOSS	1.19	1.17	0.95	0.87	0.80	WT %
TOTAL	98.34	98.77	100.50	101.92	100.81	
NB	20.00	25.00	30.00	20.00	20.00	PPM
ZR	335.00	310.00	475.00	355.00	180.00	PPM
Y	15.00	15.00	20.00	15.00	15.00	PPM
SR	1070.00	1085.00	1055.00	1070.00	1085.00	PPM
RB	60.00	65.00	60.00	60.00	60.00	PPM
PB	20.00	20.00	40.00	30.00	20.00	PPM
BA	2950.00	2900.00	2850.00	2900.00	3000.00	PPM
V	< 150.00	< 150.00	< 150.00	< 150.00	< 150.00	PPM
CR	66.00	67.00	64.00	58.00	47.00	PPM
CO	16.00	16.00	15.00	14.00	13.00	PPM
NI	< 5.00	< 5.00	< 5.00	< 5.00	< 5.00	PPM
CU	15.00	9.00	13.00	9.00	7.00	PPM
MO	< 50.00	< 50.00	< 50.00	< 50.00	< 50.00	PPM
ZN	94.00	92.00	94.00	87.00	81.00	PPM
CD	< 5.00	< 5.00	< 5.00	< 5.00	< 5.00	PPM
AG	< 2.00	< 2.00	< 2.00	< 2.00	< 2.00	PPM
AU	< 4.00	< 4.00	< 4.00	< 4.00	< 4.00	PPM
AS	1.00	< 1.00	< 1.00	< 1.00	< 1.00	PPM
SB	31.00	< 30.00	< 30.00	< 30.00	< 50.00	PPM
BI	< 100.00	< 100.00	< 100.00	< 100.00	< 100.00	PPM
TE	< 50.00	< 50.00	< 50.00	< 50.00	< 50.00	PPM
SN	< 5.00	< 5.00	< 5.00	< 5.00	< 5.00	PPM
LI	15.00	9.00	9.00	8.00	8.00	PPM
BE	2.20	1.40	1.50	1.30	1.20	PPM
LA	86.00	61.00	74.00	48.00	39.00	PPM
CE	101.00	90.00	115.00	71.00	57.00	PPM
HG	5.00	10.00	5.00	< 5.00	< 5.00	PPB
U (XRF)	< 2.00	< 2.00	< 2.00	< 2.00	< 2.00	PPM
U (F)	1.27	0.85	0.85	1.27	1.27	PPM
U (R)	< 8.47	< 8.47	< 8.47			PPM
TH (R)	< 10.00	< 10.00	< 10.00			PPM
TH (XRF)	< 5.00	< 5.00	< 5.00	< 5.00	< 5.00	PPM
K (R)	5.50	5.70	5.30			PPM

Table 3.2 continued

PHILLIPS 9-1

DATA	5900.00	5910.00	5920.00	6060.00	6270.00	FT
	1798.3	1801.4	1804.4	1908.0	1911.1	METERS
SIO2	54.51	52.65	52.87	47.56	49.66	WT %
TIO2	1.46	2.34	2.08	2.31	1.89	WT %
AL2O3	18.94	18.26	18.24	16.26	15.76	WT %
FE2O3	6.35	9.32	8.50	12.45	11.56	WT %
MNO	0.11	0.15	0.14	0.16	0.17	WT %
MGO	2.50	2.55	2.62	5.60	6.06	WT %
CAO	4.30	4.46	4.16	8.03	7.98	WT %
K2O	4.51	4.28	4.34	2.34	2.58	WT %
NA2O	4.80	4.51	4.38	3.83	3.49	WT %
P2O5	0.42	0.48	0.42	0.50	0.42	WT %
SO3	0.09	0.22	0.19	0.26	0.20	WT %
LOSS	0.79	0.63	0.67	0.62	0.74	WT %
TOTAL	98.78	99.85	98.66	99.92	100.51	
NB	15.00	30.00	30.00	25.00	25.00	PPM
ZR	185.00	510.00	435.00	285.00	285.00	PPM
Y	20.00	20.00	20.00	25.00	25.00	PPM
SR	1060.00	1000.00	1025.00	945.00	890.00	PPM
RB	65.00	60.00	65.00	45.00	55.00	PPM
PB	15.00	35.00	40.00	15.00	25.00	PPM
BA	2800.00	2600.00	2700.00	1150.00	1150.00	PPM
V	< 150.00	< 150.00	< 150.00	< 150.00	< 150.00	PPM
CR	38.00	90.00	89.00	176.00	218.00	PPM
CO	14.00	15.00	15.00	66.00	62.00	PPM
NI	< 5.00	6.00	5.00	115.00	187.00	PPM
CU	13.00	16.00	13.00	72.00	68.00	PPM
MO	< 50.00	< 50.00	< 50.00	< 50.00	< 50.00	PPM
ZN	87.00	136.00	135.00	120.00	111.00	PPM
CD	< 5.00	< 5.00	< 5.00	< 5.00	< 5.00	PPM
AG	< 2.00	< 2.00	< 2.00	< 2.00	< 2.00	PPM
AU	< 4.00	< 4.00	< 4.00	< 4.00	< 4.00	PPM
AS	< 1.00	< 1.00	< 1.00	< 1.00	< 1.00	PPM
SB	< 50.00	< 50.00	< 30.00	< 30.00	< 30.00	PPM
BI	< 100.00	< 100.00	< 100.00	< 100.00	< 100.00	PPM
TE	< 50.00	< 50.00	< 50.00	< 50.00	< 50.00	PPM
SN	< 5.00	< 5.00	< 5.00	< 5.00	< 5.00	PPM
LI	8.00	8.00	8.00	10.00	9.00	PPM
BE	1.20	1.60	1.50	2.20	2.20	PPM
LA	25.00	71.00	51.00	50.00	48.00	PPM
CE	40.00	111.00	77.00	89.00	83.00	PPM
HG	5.00	10.00	5.00	10.00	5.00	PPB
U (XRF)	< 2.00	< 2.00	< 2.00	< 2.00	< 2.00	PPM
U (F)	0.85	1.27	1.27	1.27	1.69	PPM
U (R)				< 8.47	< 8.47	PPM
TH (R)				< 10.00	< 10.00	PPM
TH (XRF)	< 5.00	< 5.00	15.00	< 5.00	< 5.00	PPM
K (R)				2.50	2.80	PPM

Table 3.2 continued

PHILLIPS 9-1

DATA	6280.00	6290.00	6300.00	6310.00	6320.00	FT
	1914.1	1917.2	1920.2	1923.3	1926.3	METERS
SIO2	51.81	52.06	57.54	57.19	49.86	WT %
TIO2	1.73	1.82	1.12	1.16	1.74	WT %
AL2O3	15.82	15.96	14.46	15.12	16.27	WT %
FE2O3	10.59	10.80	7.44	7.99	10.29	WT %
MNO	0.15	0.15	0.11	0.11	0.15	WT %
MGO	4.09	4.82	3.93	4.32	4.50	WT %
CAO	7.19	6.75	5.00	5.58	6.74	WT %
K2O	2.81	2.89	3.55	3.42	3.02	WT %
NA2O	4.04	3.52	3.43	3.55	3.67	WT %
P2O5	0.42	0.41	0.28	0.28	0.56	WT %
SO3	0.20	0.19	0.14	0.13	0.23	WT %
LOSS	0.72	0.86	0.83	0.89	0.85	WT %
TOTAL	100.37	100.23	97.83	99.74	97.88	
NB	25.00	25.00	25.00	25.00	30.00	PPM
ZR	275.00	330.00	240.00	205.00	230.00	PPM
Y	25.00	20.00	25.00	25.00	30.00	PPM
SR	915.00	910.00	625.00	670.00	805.00	PPM
RB	50.00	55.00	85.00	85.00	75.00	PPM
PB	275.00	230.00	125.00	75.00	60.00	PPM
BA	1450.00	1250.00	800.00	750.00	850.00	PPM
V	< 150.00	< 150.00	< 150.00	< 150.00	< 150.00	PPM
CR	249.00	226.00	177.00	176.00	130.00	PPM
CO	61.00	71.00	40.00	43.00	51.00	PPM
NI	115.00	113.00	91.00	93.00	74.00	PPM
CU	65.00	61.00	39.00	40.00	53.00	PPM
MO	< 50.00	< 50.00	< 50.00	< 50.00	< 50.00	PPM
ZN	236.00	180.00	113.00	110.00	126.00	PPM
CD	< 5.00	< 5.00	< 5.00	< 5.00	< 5.00	PPM
AG	< 2.00	< 2.00	< 2.00	3.00	3.00	PPM
AU	< 4.00	< 4.00	< 4.00	< 4.00	< 4.00	PPM
AS	2.00	2.00	< 1.00	< 1.00	1.00	PPM
SB	< 30.00	< 30.00	< 30.00	< 30.00	< 30.00	PPM
BI	< 100.00	< 100.00	< 100.00	< 100.00	< 100.00	PPM
TE	< 50.00	< 50.00	< 50.00	< 50.00	< 50.00	PPM
SN	< 5.00	< 5.00	< 5.00	< 5.00	< 5.00	PPM
LI	9.00	9.00	9.00	9.00	9.00	PPM
BE	2.20	2.20	2.20	2.30	2.50	PPM
LA	57.00	56.00	78.00	70.00	65.00	PPM
CE	96.00	93.00	112.00	107.00	116.00	PPM
HG	5.00	10.00	5.00	< 5.00	10.00	PPB
U (XRF)	< 2.00	< 2.00	< 2.00	< 2.00	< 2.00	PPM
U (F)	1.69	1.69	1.69	1.69	1.69	PPM
U (R)	< 8.47	< 8.47	< 8.47	< 8.47	84.70	PPM
TH (R)	< 10.00	< 10.00	< 10.00	< 10.00	< 10.00	PPM
TH (XRF)	5.00	10.00	15.00	10.00	< 5.00	PPM
K (R)	2.70	3.10	3.50	3.70	5.40	PPM

Table 3.2 continued

PHILLIPS 9-1

DATA	6330.00	6340.00	6350.00	6650.00	6660.00	FT
	1929.4	1932.4	1935.5	2027.0	2030.0	METERS
SIO2	49.38	50.54	52.43	51.88	52.75	WT %
TIO2	2.01	1.94	1.72	1.80	1.63	WT %
AL2O3	16.51	17.03	18.61	17.63	17.68	WT %
FE2O3	10.97	10.67	9.26	8.44	7.41	WT %
MNO	0.15	0.16	0.15	0.13	0.11	WT %
MGO	4.49	3.75	3.27	3.21	2.75	WT %
CAO	7.25	6.28	5.66	4.76	4.30	WT %
K2O	3.05	3.71	4.03	4.17	4.52	WT %
NA2O	3.59	4.00	4.17	4.51	3.46	WT %
P2O5	0.76	0.65	0.55	0.54	0.45	WT %
SO3	0.25	0.25	0.24	0.16	0.13	WT %
LOSS	0.78	0.74	0.78	2.71	2.16	WT %
TOTAL	99.19	99.72	100.87	99.94	97.35	
NB	30.00	20.00	20.00	20.00	15.00	PPM
ZR	195.00	145.00	120.00	375.00	440.00	PPM
Y	30.00	25.00	20.00	20.00	20.00	PPM
SR	855.00	915.00	1010.00	1140.00	1125.00	PPM
RB	70.00	65.00	65.00	65.00	65.00	PPM
PB	45.00	55.00	55.00	20.00	30.00	PPM
BA	850.00	1750.00	2200.00	3250.00	3600.00	PPM
V	< 150.00	< 150.00	< 150.00	< 150.00	< 150.00	PPM
CR	117.00	104.00	109.00	78.00	84.00	PPM
CO	43.00	37.00	31.00	22.00	23.00	PPM
NI	46.00	18.00	13.00	6.00	6.00	PPM
CU	41.00	29.00	23.00	14.00	14.00	PPM
MO	< 50.00	< 50.00	< 50.00	< 50.00	< 50.00	PPM
ZN	122.00	144.00	147.00	123.00	114.00	PPM
CD	< 5.00	< 5.00	< 5.00	< 5.00	< 5.00	PPM
AG	< 2.00	< 2.00	< 2.00	< 2.00	< 2.00	PPM
AU	< 4.00	< 4.00	< 4.00	< 4.00	< 4.00	PPM
AS	1.00	< 1.00	1.00	< 1.00	< 1.00	PPM
SB	< 30.00	< 30.00	< 30.00	< 30.00	< 30.00	PPM
BI	< 100.00	< 100.00	< 100.00	< 100.00	< 100.00	PPM
TE	< 50.00	< 50.00	< 50.00	< 50.00	< 50.00	PPM
SN	< 5.00	< 5.00	< 5.00	5.00	5.00	PPM
LI	8.00	9.00	9.00	10.00	11.00	PPM
BE	2.20	1.90	1.70	1.20	1.10	PPM
LA	63.00	60.00	51.00	57.00	38.00	PPM
CE	106.00	98.00	79.00	95.00	62.00	PPM
HG	5.00	5.00	10.00	5.00	5.00	PPB
U (XRF)	< 2.00	< 2.00	< 2.00	< 2.00	< 2.00	PPM
U (F)	1.27	1.27	1.69	1.27	1.27	PPM
U (R)	< 8.47	< 8.47	< 8.47			PPM
TH (R)	< 10.00	< 10.00	< 10.00			PPM
TH (XRF)	5.00	5.00	< 5.00	< 5.00	5.00	PPM
K (R)	3.40	3.80	5.00			PPM

Table 3.2 continued

PHILLIPS 9-1

DATA	6670.00	6680.00	6690.00	6700.00	6710.00	FT
	2033.0	2036.1	2039.1	2042.2	2045.2	METERS
SIO2	53.69	50.90	52.49	51.64	51.49	WT %
TIO2	1.62	1.78	1.81	1.98	1.88	WT %
AL2O3	17.75	18.48	18.87	17.69	18.97	WT %
FE2O3	7.08	8.89	8.67	9.22	9.24	WT %
MNO	0.11	0.13	0.12	0.14	0.13	WT %
MGO	2.43	3.85	3.59	3.49	3.04	WT %
CAO	4.24	4.71	5.00	5.24	5.17	WT %
K2O	4.84	4.12	4.00	3.81	3.75	WT %
NA2O	3.68	3.41	4.63	3.85	4.24	WT %
P2O5	0.48	0.45	0.51	0.59	0.54	WT %
SO3	0.13	0.16	0.16	0.20	0.19	WT %
LOSS	1.68	2.35	1.58	1.67	0.73	WT %
TOTAL	97.73	99.23	101.43	99.52	99.37	
NB	15.00	15.00	15.00	20.00	20.00	PPM
ZR	495.00	225.00	270.00	290.00	295.00	PPM
Y	20.00	15.00	15.00	20.00	25.00	PPM
SR	1155.00	1020.00	1055.00	1035.00	1050.00	PPM
RB	65.00	65.00	60.00	60.00	65.00	PPM
PB	25.00	25.00	30.00	15.00	25.00	PPM
BA	4000.00	2450.00	2550.00	2260.00	1650.00	PPM
V	< 150.00	< 150.00	< 150.00	< 150.00	< 150.00	PPM
CR	80.00	85.00	84.00	81.00	73.00	PPM
CO	26.00	24.00	22.00	24.00	20.00	PPM
NI	7.00	8.00	8.00	9.00	9.00	PPM
CU	15.00	14.00	15.00	20.00	19.00	PPM
MO	< 50.00	< 50.00	< 50.00	< 50.00	< 50.00	PPM
ZN	107.00	138.00	120.00	125.00	112.00	PPM
CD	< 5.00	< 5.00	< 5.00	< 5.00	< 5.00	PPM
AG	< 2.00	< 2.00	< 2.00	< 2.00	< 2.00	PPM
AU	< 4.00	< 4.00	< 4.00	< 4.00	< 4.00	PPM
AS	< 1.00	< 1.00	< 1.00	< 1.00	1.00	PPM
SB	< 30.00	< 30.00	< 30.00	32.00	< 30.00	PPM
BI	< 100.00	< 100.00	< 100.00	< 100.00	< 100.00	PPM
TE	< 50.00	< 50.00	< 50.00	< 50.00	< 50.00	PPM
SN	6.00	7.00	< 5.00	< 5.00	< 5.00	PPM
LI	10.00	14.00	11.00	12.00	12.00	PPM
BE	1.10	1.20	1.40	1.50	1.60	PPM
LA	50.00	42.00	53.00	68.00	63.00	PPM
CE	86.00	73.00	88.00	123.00	95.00	PPM
HG	5.00	10.00	5.00	5.00	< 5.00	PPB
U (XRF)	< 2.00	< 2.00	< 2.00	< 2.00	< 2.00	PPM
U (F)	1.27	< 0.85	1.27	< 0.85	< 0.85	PPM
U (R)				16.94	25.41	PPM
TH (R)				< 10.00	< 10.00	PPM
TH (XRF)	5.00	5.00	5.00	5.00	5.00	PPM
K (R)				6.10	4.70	PPM

Table 3.2 continued

PHILLIPS 9-1

DATA	6720.00	6730.00	6750.00	F1
	2048.3	2051.3	2057.4	METERS
SIO2	55.06	59.65	48.83	WT %
TIO2	1.60	1.55	1.77	WT %
AL2O3	17.20	15.19	18.66	WT %
FE2O3	8.34	7.57	9.78	WT %
MNO	0.12	0.12	0.13	WT %
MGO	2.58	2.34	3.86	WT %
CAO	4.52	4.36	5.69	WT %
K2O	3.68	3.35	3.59	WT %
NA2O	4.64	3.92	4.35	WT %
P2O5	0.50	0.54	0.63	WT %
SO3	0.21	0.24	0.31	WT %
LOSS	0.84	1.23	1.01	WT %
TOTAL	99.29	100.06	99.01	
NB	20.00	15.00	20.00	PPM
ZR	275.00	240.00	165.00	PPM
Y	20.00	20.00	20.00	PPM
SR	990.00	955.00	1470.00	PPM
RB	70.00	70.00	75.00	PPM
PB	35.00	20.00	15.00	PPM
BA	1650.00	1650.00	2700.00	PPM
V	< 150.00	< 150.00		PPM
CR	82.00	79.00	72.00	PPM
CO	21.00	24.00	20.00	PPM
NI	7.00	7.00	6.00	PPM
CU	17.00	14.00	15.00	PPM
MO	< 50.00	< 50.00	< 50.00	PPM
ZN	103.00	99.00	136.00	PPM
CD	< 5.00	< 5.00	< 5.00	PPM
AG	< 2.00	< 2.00	< 2.00	PPM
AU	< 4.00	< 4.00	< 4.00	PPM
AS	1.00	1.00	1.00	PPM
SB	< 30.00	< 30.00	< 30.00	PPM
BI	< 100.00	< 100.00	< 100.00	PPM
TE	< 50.00	< 50.00	< 50.00	PPM
SN	< 5.00	< 5.00	< 5.00	PPM
LI	11.00	11.00	11.00	PPM
BE	1.70	1.60	1.70	PPM
LA	54.00	55.00	48.00	PPM
CE	80.00	85.00	79.00	PPM
HG	5.00	5.00	5.00	PPB
U (XRF)	< 2.00	< 2.00	< 2.00	PPM
U (F)	2.12	2.54	1.69	PPM
U (R)	8.47	< 8.47	< 8.47	PPM
TH (R)	< 10.00	< 10.00	< 10.00	PPM
TH (XRF)	5.00	< 5.00	< 5.00	PPM
K (R)	3.70	3.30	3.70	PPM

Table 3.3 Neutron activation analyses of selected samples from Well C/T-2

(data not available yet)

C/T-2

ROOSEVELT KGRA
BEAVER COUNTY, UTAH

SAMPLE TYPE: WHOLE ROCK
VERT. SCALE: 1000.0 FT./IN.
(DEPTH SHOWN IN 1000 FT UNITS)

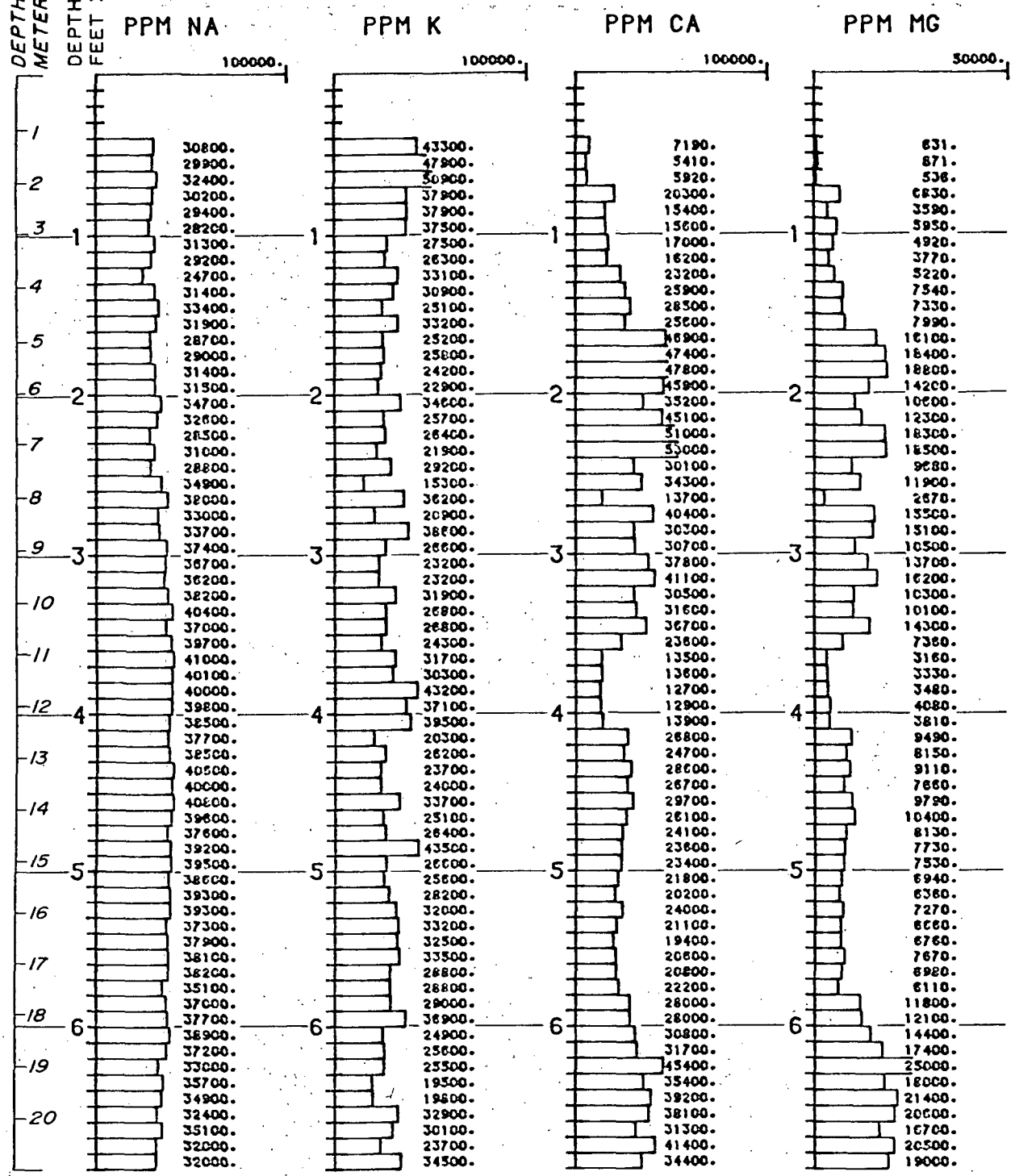

FIGURE 3.1 COMPOSITE WHOLE ROCK ANALYSES OF WELL C/T-2 AS A FUNCTION OF DEPTH.

C/T-2

ROOSEVELT KGRA
BEAVER COUNTY, UTAH

SAMPLE TYPE: WHOLE ROCK
VERT. SCALE: 1000.0 FT./IN
(DEPTH SHOWN IN 1000 FT UNITS)

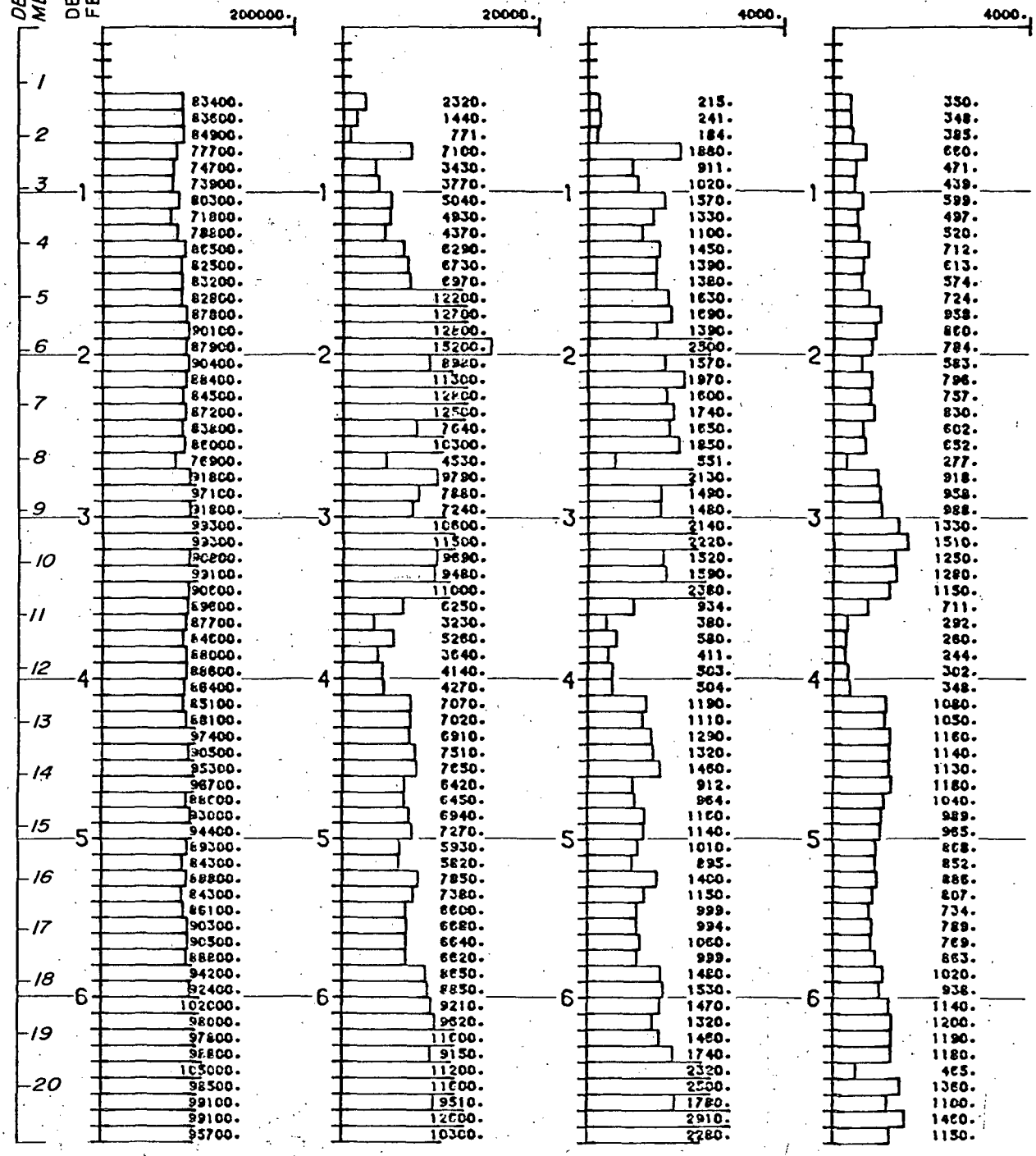

FIGURE 3.1 CONTINUED.

C/T-2

ROOSEVELT KGRA
BEAVER COUNTY, UTAH

SAMPLE TYPE: WHOLE ROCK
VERT. SCALE: 1000.0 FT./IN.
(DEPTH SHOWN IN 1000 FT UNITS)

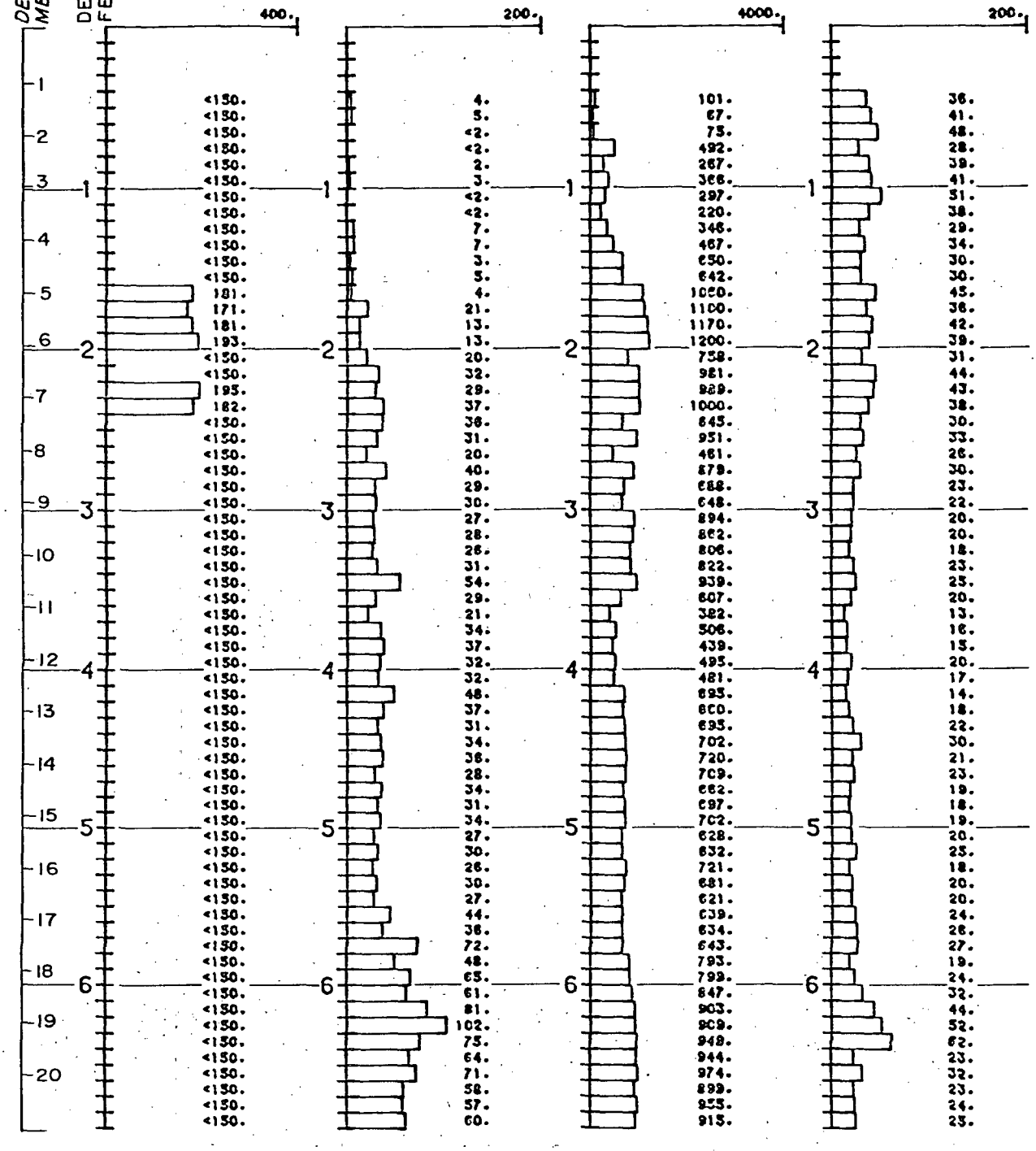

FIGURE 3.1 CONTINUED.

C/T-2

ROOSEVELT KGRA
BEAVER COUNTY, UTAH

SAMPLE TYPE: WHOLE ROCK
VERT. SCALE: 1000.0 FT./IN.
(DEPTH SHOWN IN 1000 FT UNITS)

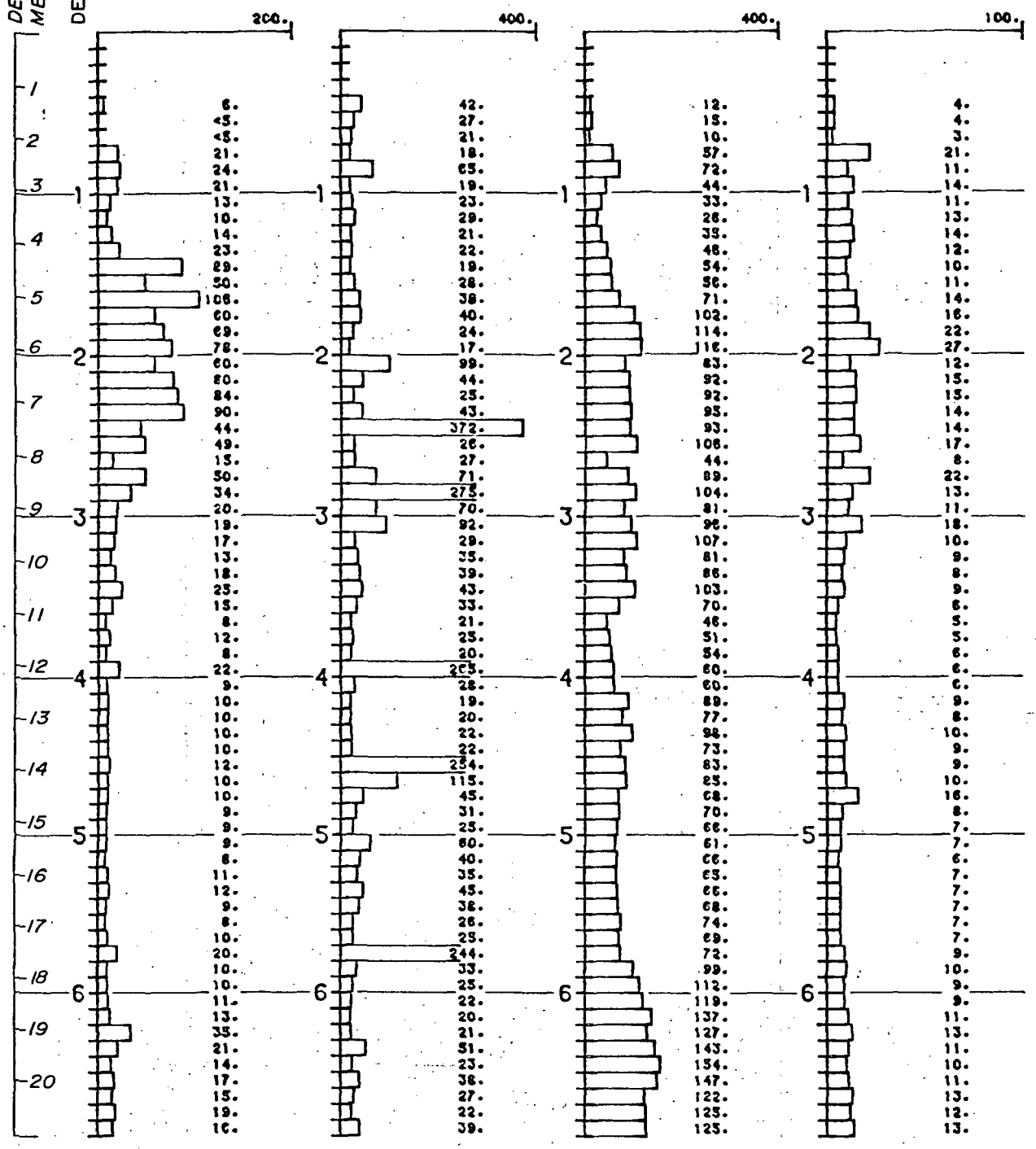

FIGURE 3. 1. CONTINUED.

C/T-2

ROOSEVELT KGRA
BEAVER COUNTY, UTAH

SAMPLE TYPE: WHOLE ROCK
VERT. SCALE: 1000.00 FT./IN.
(DEPTH SHOWN IN 1000 FT UNITS)

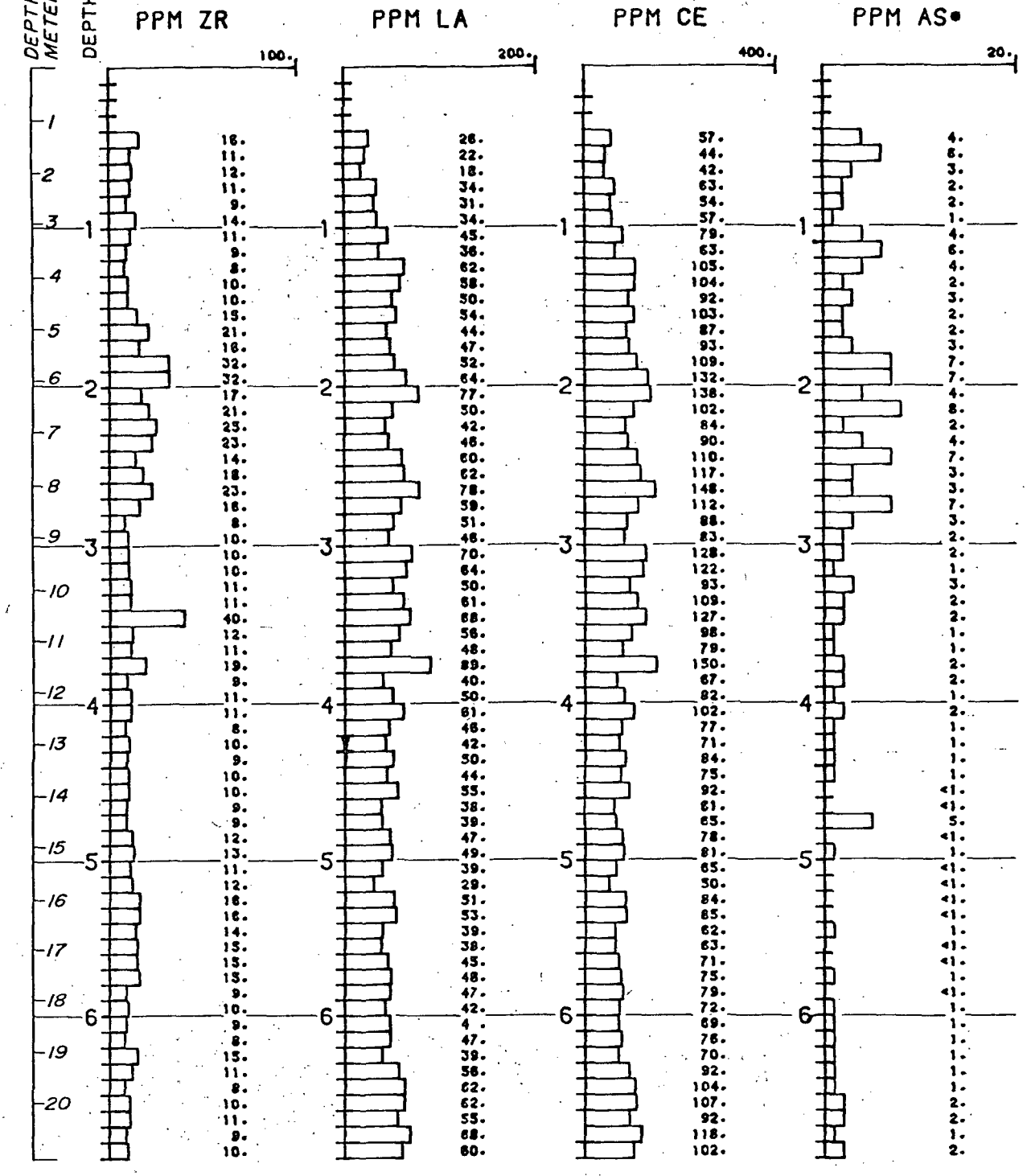

FIGURE 3-1. CONTINUED.

C/T-2

ROOSEVELT KGRA
BEAVER COUNTY, UTAH

SAMPLE TYPE: WHOLE ROCK
VERT. SCALE: 1000.0 FT./IN
(DEPTH SHOWN IN 1000 FT UNITS)

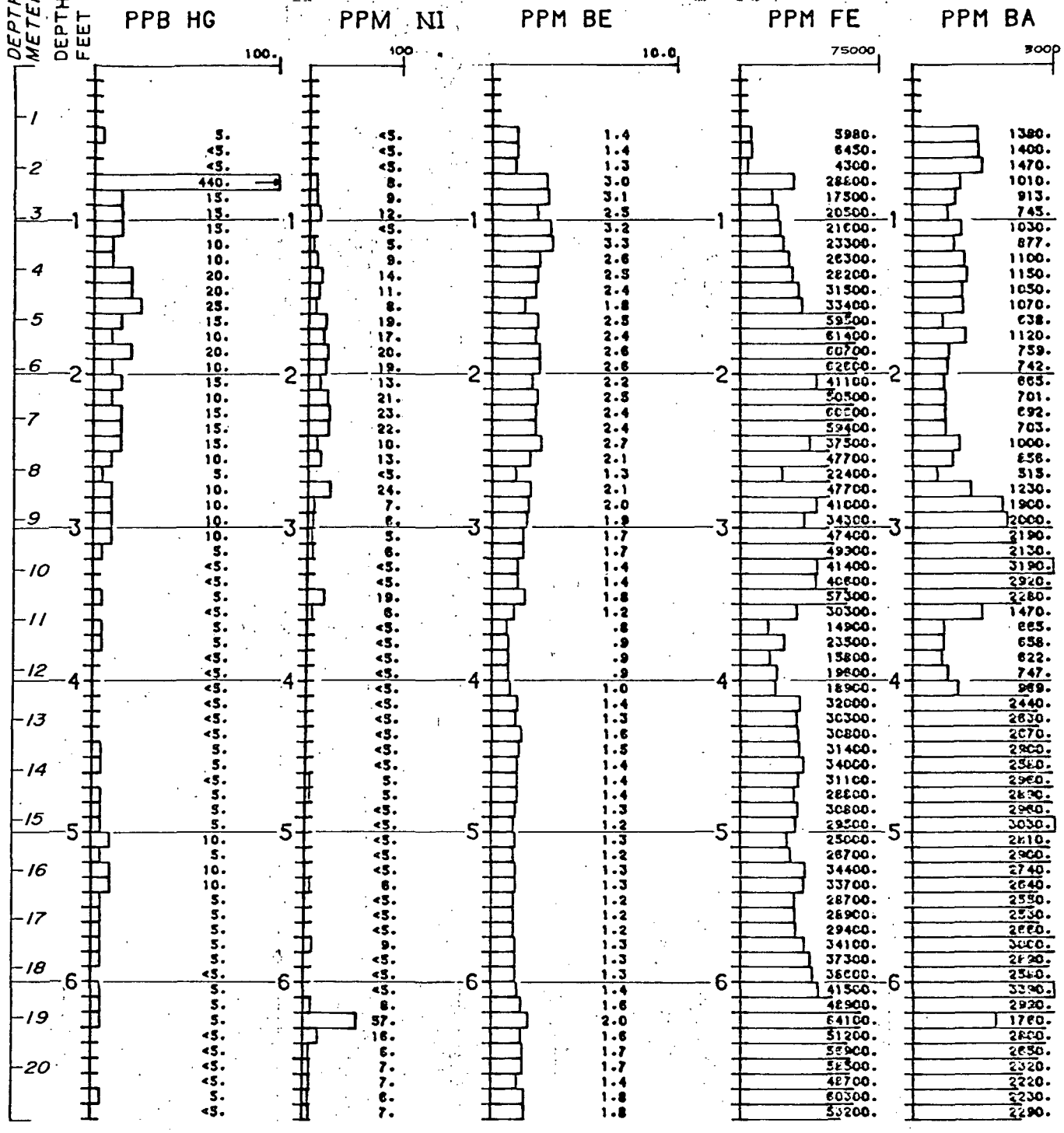

FIGURE 3.1 CONTINUED.

Table 3.4. Water Analyses from Well C/T-2

	1	2
Na	2210	2000.0
Ca	83	41.0
K	425	374.0
SiO_2	364	169
Mg	-	0.4
Cl	3800	2140.0
$SO_4^=$	122	67.0
HCO_3^-		394.0
$CO_3^=$		0.0
Fe		5.1
Mn		0.41
Sr		4.7
Ba		.41
B		28.0
Li		19.0
NH_4		24.0
TDS		6520.0
pH		5.9

NOTES:

1 - Analysis from Parry et al, 1976

2 - Analysis from Newman, 1979

IV. OXYGEN AND CARBON ISOTOPES

A. Introduction

Stable isotopes of carbon and oxygen have been used effectively to estimate the temperatures of deposition of hydrothermal minerals (Ohmoto and Rye, 1979; Taylor, 1979). This estimate is accomplished by measurement of the isotopic compositions of minerals and either a measurement or an estimation of the isotopic compositions of fluids with which the minerals are in equilibrium. Carbon and oxygen isotopic analyses of alteration phases such as calcite have been useful in predicting fluid entries in some geothermal systems (Kendall, 1976, Elders, et al., 1978).

In order to document and quantify the hydrothermal processes effecting hole C/T-2, twenty-six samples were selected for stable isotope analysis of carbonate minerals. Analyses of carbon and oxygen isotopes in calcite will provide a base from which temperatures may be estimated and trends of isotopic enrichment or depletion which can be correlated with entries identified by logging or geochemical signatures such as mercury or arsenic anomalies.

Calcite is a common alteration phase in the Roosevelt Hot Springs geothermal system and is particularly abundant in highly altered zones which are related to fault structures (see section on lithologic logging). Carbonate veins cross-cutting older carbonate veins have been observed in thin section, along with carbonate replacements in plagioclase. In addition, altered zones frequently contain veinlets of fine grained quartz which are also related to the hydrothermal process. However, efforts to sample these veins for isotopic analysis were unsuccessful because of their fine-grain size.

B. Sample Preparation and Analyses

The samples analyzed were from drill cuttings collected at 3.1 and 4.6m (10 and 15 ft) intervals. Thus, the analyses presented are average values for these intervals and no distinction is made fo separate carbonates of different ages. Cuttings from selected 3.1 or 4.6m (10 or 15 ft) intervals were crushed to less than 200 mesh. For several intervals, the samples of 80 to 150 mesh were analyzed to test the influence of grain size on the isotopic values. Approximately 500 mg of sample was reacted with 100% distilled phosphoric acid for 12 to 15 hours at 25°C (McCrea, 1950). The liberated CO_2 gas was then extracted and purified for carbon ad oxygen isotopic analysis. The gas was analyzed on a Micromass Model 602D, twin-collecting, 90° mass spectrometer.

The isotope data are reported as $\delta\,^{18}O$ or $\delta\,^{13}C$ where:

$$\delta = \left(\frac{R_{sample}}{R_{standard}} - 1 \right) \quad 1000$$

and R_{sample} is the $^{18}O/^{16}O$ or $^{13}C/^{12}/C$ ratio in the sample and $R_{standard}$ is the corresponding ratio for the standard. The standards used are Standard Mean Ocean Water (SMOW) for oxygen (Craig, 1961) and the Chicago PDB Standard for carbon (Craig, 1957). A δ-value = +5 would mean that the sample is 5 per mil (5 parts per thousand) or 0.5 percent richer in ^{18}O than SMOW or ^{13}C than PDB. Negative numbers signify relative depletion in the heavy isotopes.

C. Results

The oxygen and carbon isotopic analyses for hole C/T-2 are listed in Table 4.1 and plotted as a function of depth in Figures 4.1 and 4.2. In addition, the $\delta\,^{18}O$ and $\delta\,^{13}C$ values are plotted against each other in Figure

Table 4.1. Oxygen and Cargon Isotope Data from Well C/T-2

INTERVAL		ALTERATION			POWDERED		COARSE	
Meters	Feet	W	M	S	$\delta^{18}O^{o}/oo$	$\delta^{13}C^{o}/oo$	$\delta^{18}O^{o}/oo$	$\delta^{13}C^{o}/oo$
236.2-240.8	775-790		X		+6.7	-3.6		
275.8-280.4	905-920	X			+9.3	-2.4		
359.7-364.2	1180-1195			X	+0.4	-3.1		
368.8-378.0	1210-1240		X		+0.4	-1.8		
446.5-451.1	1465-1480		X		+0.8	-0.7	-0.3	-0.9
492.3-496.8	1615-1630			X	+1.8	-3.5	+0.7	-2.6
515.1-519.7	1690-1705		X		+2.2	-3.8		
592.8-597.4	1945-1960			X	+0.7	-3.3	-0.7	-3.2
611.1-615.7	2005-2020		X		+2.6	-4.7		
615.7-620.3	2020-2035		X		+2.5	-4.1		
734.6-737.6	2410-2420		X		+4.7	-5.0		
835.2-838.2	2740-2750			X	-0.3	-4.5	-1.1	-4.3
862.6-865.6	2830-2840	X			+5.2	-5.5		
1002.8-1005.8	3290-3300		X		+1.3	-4.1		
1063.8-1066.8	3490-3500	X			+7.0	-3.4		
1185.7-1188.7	3890-3900	X			+3.5	-3.5		
1292.4-1295.4	4240-4250	X			+7.3	-7.3		
1450.8-1362.5	4760-4770			X	-0.4	-5.0	-1.0	-4.8
1505.7-1508.8	4940-4950	X			+7.2	-3.8		
1734.3-1737.4	5690-5700	X			+6.6	-5.4		
1764.8-1767.8	5790-5800		X		-0.2	-5.1		
1795.3-1798.3	5890-5900	X			+5.3	-4.5		
1895.9-1898.9	6220-6230	X			+7.6	-6.5		
1914.1-1917.2	6280-6290	X			+5.7	-5.4		
1941.6-1944.6	6370-6380	X			+9.7	-8.2		
2026.9-2030.0	6650-6660	X			+4.8	-4.0		

Analyst: DAVID ROHRS

Alteration: W(weak); M(moderate); S(strong)

Powdered Samples = 200

Coarse Samples = +80 to +150 mesh

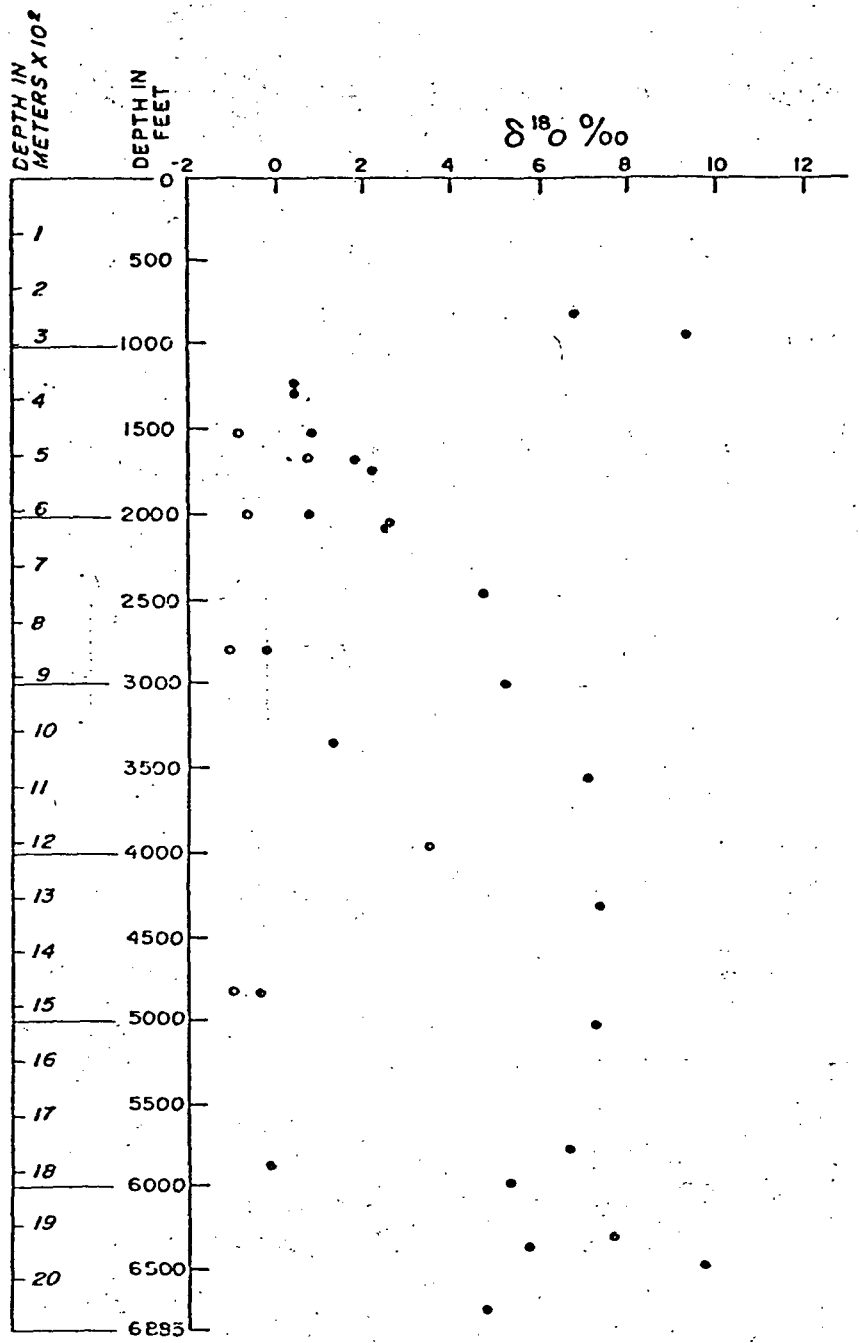

FIGURE 4.1 OXYGEN ISOTOPE VALUES AS A FUNCTION OF DEPTH IN WELL C/T-2. OPEN CIRCLES ARE COARSE SAMPLES AND CLOSED CIRCLES ARE POWDERED SAMPLES.

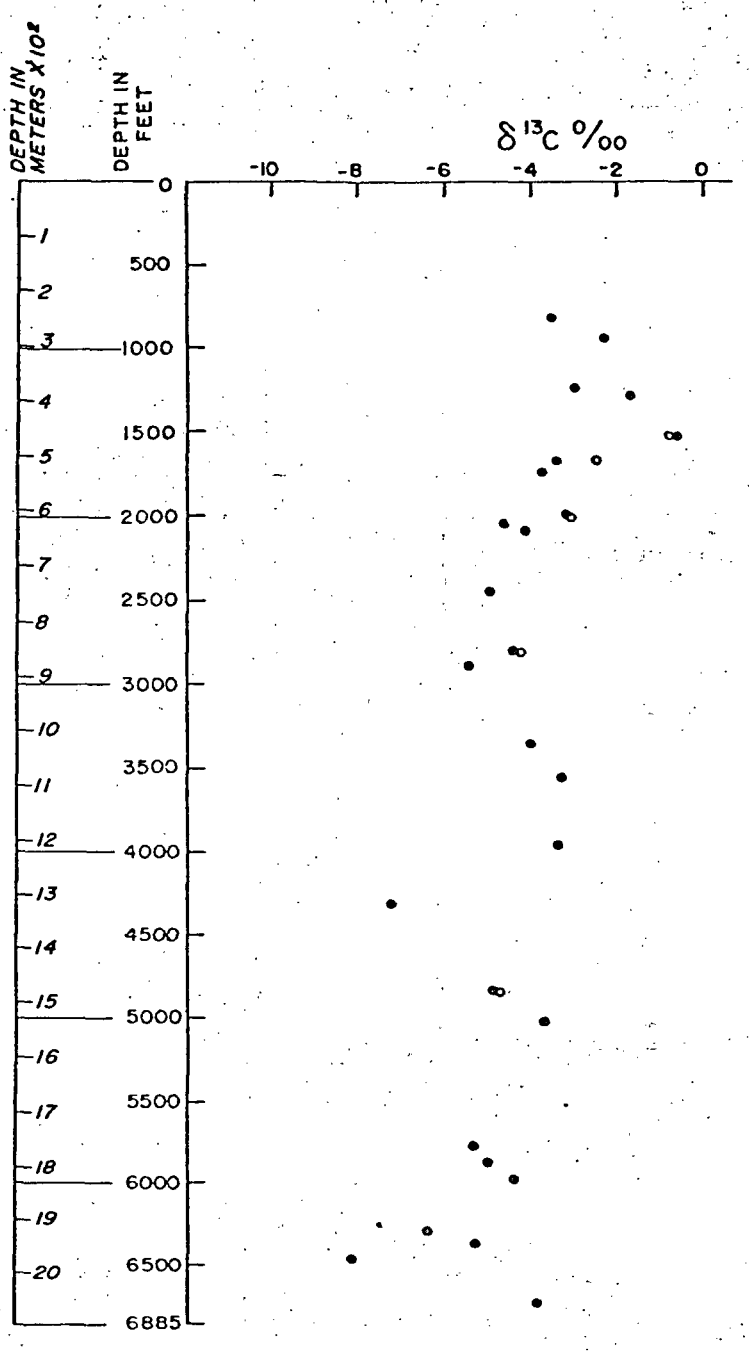

FIGURE 4.2 CARBON ISOTOPE VALUES AS A FUNCTION OF DEPTH IN WELL C/T-2. OPEN CIRCLES ARE COARSE SAMPLES AND CLOSED CIRCLES ARE POWDERED SAMPLES.

4.3. The $\delta^{18}O$ values range from -0.4 to +9.7o/oo and exhibit no systematic variation with depth except for a gross trend of increasing $\delta^{18}O$ with depth. Conversely, the $\delta^{13}C$ values show less scatter and a pronounced decrease with increasing depth, with values ranging from -0.7 to 8.2o/oo. The $\delta^{18}O$ values of the coarse grained samples are isotopically lighter than their fine grained equivalents, while similar $\delta^{13}C$ values were obtained for both the coarse and the fine grained fractions.

The $\delta^{13}C$ and $\delta^{18}O$ data shown in Figure 4.3 exhibit a general trend of decreasing $\delta^{13}C$ with increasing $\delta^{18}O$ in the calcites. This trend is opposite that typically observed in hydrothermal carbonates. For example, carbonates associated with felsic extrusives at the Tui Mine, New Zealand (Robinson, 1974) and the Sunnyside Mine, Colorado (Casadevall and Ohmoto, 1977) display a trend of increasing $\delta^{13}C$ with increasing $\delta^{18}O$. This trend has been correlated with a decrease in the temperature of formation. The range in $\delta^{18}O$ and $\delta^{13}C$ values from these deposits is however similar to the range observed in C/T-2, and is typical of many hydrothermal carbonate minerals which occur in ore deposits in various types of host rock, regardless of whether or not carbonate rocks are known, or inferred, to be in the area (Bethke and Rye, 1979).

In general, the left-hand portion of the $\delta^{13}C$- $\delta^{18}O$ trend is composed of carbonates found in strongly altered zones (Zone A, Figure 4.3). The central portion of the plot is comprised of carbonates from moderate-to-weakly altered rocks (Zone B), while the right-hand segment is characterized by carbonates from weakly altered lithologies (Zone C).

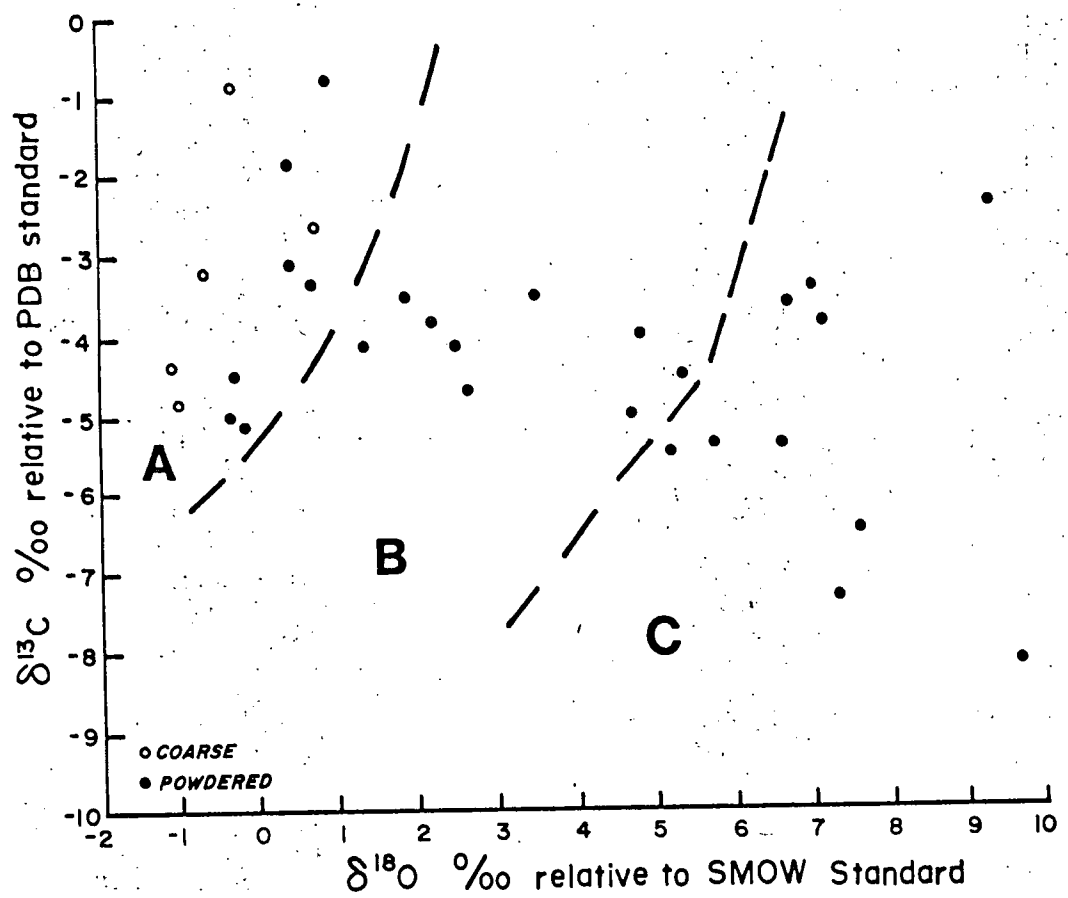

FIGURE 4.3 OXYGEN VERSUS CARBON ISOTOPE VALUES FROM WELL C/T-2.

D. Discussion

The interpretation of data given in Table 4.1 and plotted in Figures 4.1, 4.2, and 4.3 is hindered by several factors which include: (1) our inability at present to evaluate isotopically various generations of calcite, (2) lack of fluid inclusions which could be analyzed to ascertain the isotopic composition of fluids in equilibrium with the alteration phases, and (3) our poor understanding of the temporal relationship between the present-day fluid and the alteration assemblages. Although these obstacles cannot be immediately overcome, the evaluation of the data distribution, application of geothermometers, and correlation of calculated temperatures with measured temperatures and trace element distribution patterns may aid in quantifying the hydrothermal processes which effected C/T-2.

1. Frequency Distribution. The oxygen and carbon isotopic data given in Table 4.1 are graphically depicted in the form of frequency histograms in Figure 4.4. This plot shows that the oxygen isotopic data are composed of two distinct populations, while the carbon isotopic data are confined to one population. The oxygen isotope population I contains carbonates which occur above about 915.0m (3000 ft) in the zone of moderate to strong alteration. Population II consists of carbonates from below 915.0m in the zone of weak alteration.

Vastly different temperature regimes could explain the split of $\delta^{18}O$ values into two populations. However, one might also expect a similar split in the $\delta^{13}C$ values. A more plausible alternative might be the presence of different types of water, where $\delta^{18}O$ fluid values varied, but the $\delta^{13}C$ fluid composition remained essentially constant. Superimposed on this behavior

FIGURE 4.4 FREQUENCY HISTOGRAMS OF OXYGEN AND CARBON ISOTOPE VALUES FROM WELL C/T-2

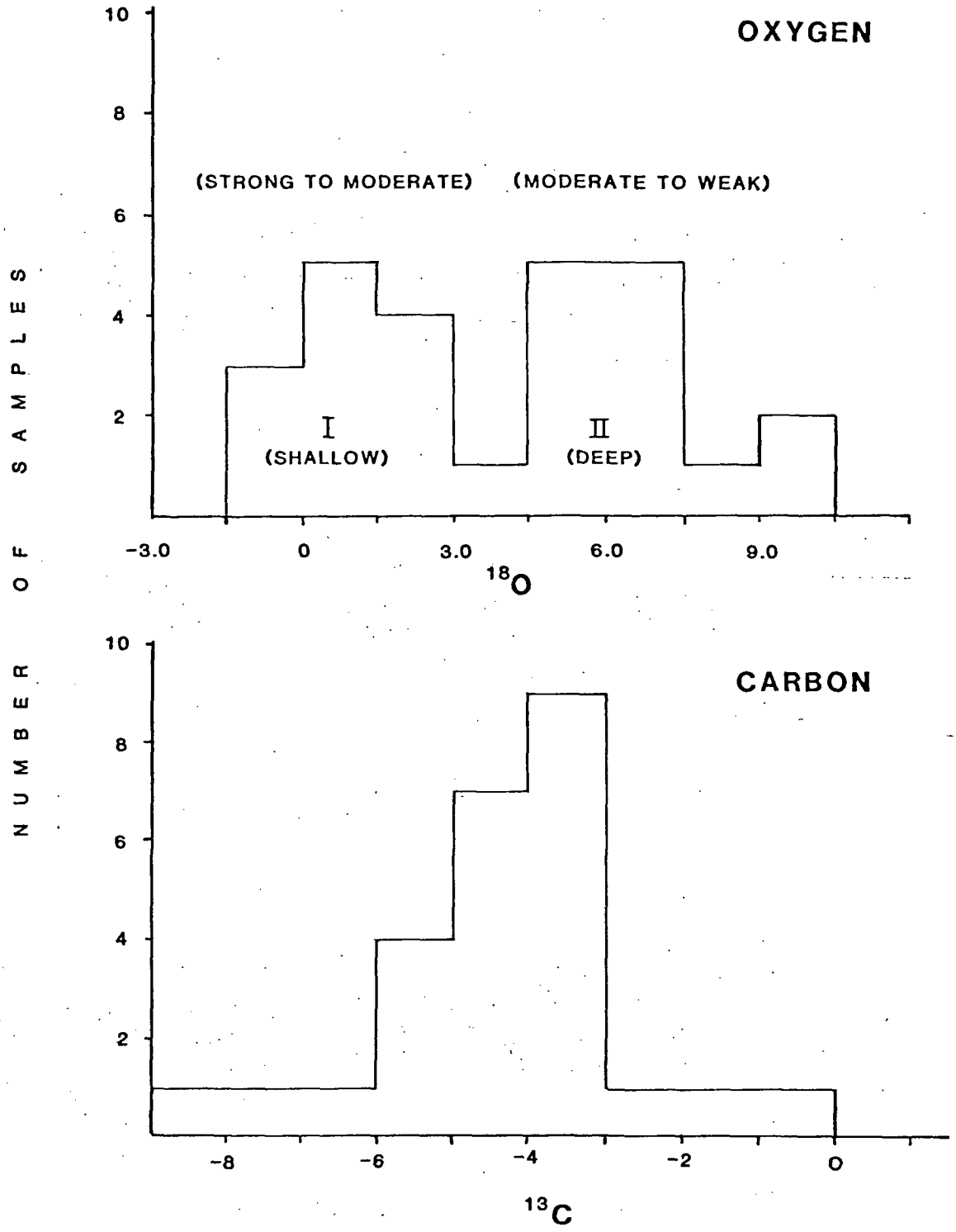

could be slightly different temperatures not nearly so drastic as those required to produce the split in the populations. The break between these two $\delta^{18}O$ groups appears to coincide with the position of the low-angle fault which cuts the hole at about 838.0m. The upper plate is badly brecciated and more permeable than the lower plate thereby permitting greater access by downward percolating groundwaters.

Application of the chloride-enthalpy mixing model (Fournier, 1979) to the C/T-2 fluid (analysis 1, Table 3.4) indicates that approximately 33% mixing with a cold water component is likely. If we assume that the bulk of this mixing occurs above the fault, and that a $\delta^{18}O$ value of -12.6 observed in hole 14-2 (unmixed) a few miles away is typical of the deep fluid and -15.7°/oo is representative of cold groundwater, a mixed fluid $\delta^{18}O$ of about -13.7°/oo is computed. We might conclude from this that below the fault, a ^{18}O fluid value of about -12.6°/oo dominates, while above the fault, a value of -13.7°/oo prevails. The presence of one $\delta^{13}C$ population for the carbonates suggests that the $\delta^{13}C$ value of the fluid varied little and probably averaged around -7°/00, typical of many groundwaters (Ohmoto and Rye, 1979)

2. Isotope Geothermometry. If we assume that these $\delta^{18}O$ and $\delta^{13}C$ fluid values are reasonable, then temperatures of formation for the carbonates can be computed using isotope geothermometry. The application of isotope geothermometry depends on the establishment of equilibrium between the fluid and the phase being deposited. Thus, in the system calcite-water, the oxygen and carbon isotopic fractionation factors can be defined as:

$$\alpha^{o}_{cc-w} = \frac{(^{18}O/^{16}O)cc}{(^{18}O/^{16}O)w} \qquad \text{and}$$

$$\alpha^{o}_{cc\text{-}w} = \frac{(^{13}C/^{12}C)cc}{(^{13}C/^{12}C)w}$$, respectively.

The fractionation factor (α) is related to the equilibrium constant (K) of the appropriate isotopic exchange reaction in the following way,

$$\alpha = K^{1/n}$$

where n is the number of exchanged atoms.

Note that from the definition of given previously, that

$$\ln\alpha_{cc\text{-}w} = \ln(1 + \frac{\delta_{cc}}{1000}) - \ln(1 - \frac{\delta_{w}}{1000})$$

which simplifies to: $1000\ln\alpha_{cc\text{-}w}$, with δ_{cc} and δ_{w} representing either $\delta^{18}O$ or $\delta^{13}C$ values. The fractionation factor (α) has been shown to be a function of $1/T^2$ and relationships have been derived from the experimental calibration of calcite-water isotopic exchange to give:

$$1000\ln\alpha_{cc\text{-}w} = 2.78(10^6)/T^2 - 2.89$$

for oxygen (Friedman and O'Neil, 1976) and from theoretical work by Bottinga (1968) for carbon:

$$1000\ln\alpha_{c\text{-}w} = -8.914(10^8)/T^3+8.557(10^6)/T^2+-18.11(10^3)/T+8.2)$$

taken from Ohmoto and Rye (1979). Temperature in these equations is in Kelvin. Therefore, by relating the difference between $\delta^{18}O$ or $\delta^{13}C$ values of carbonates and water in C/T-2 with these expressions, the temperatures of formation can be determined.

Temperatures estimated in this manner are given in Table 4.2 and plotted

Table 4.2. Estimates of Carbon and Oxygen Isotopic Temperatures in Well C/T-2

Interval (feet)	$1000\ln\alpha^{o}_{cc-w}$	T^{oxy}_{calc} (°C)	$1000\ln\alpha^{c}_{cc-w}$	T^{carb}_{calc} (°C)
775 - 790	20.4	70	3.4	111
905 - 920	23.0	55	4.6	90
1180 - 1195	14.1	132	3.9	103
1210 - 1240	14.1	132	5.2	82
1465 - 1480	14.5	127	6.3	67
1615 - 1630	15.5	117	3.5	110
1690 - 1705	15.9	110	3.2	115
1945 - 1960	14.4	130	3.7	107
2005 - 2020	16.3	105	2.3	133
2020 - 2035	16.2	107	2.9	120
2410 - 1420	18.4	90	2.0	140
2740 - 2750	13.4	140	2.5	130
2830 - 2840	18.9	85	1.5	150
3290 - 3300	13.5	140	2.9	120
3490 - 3500	19.2	83	3.6	108
3890 - 3900	15.7	112	3.5	110
4240 - 4250	19.5	80	-0.3	200
4760 - 4770	11.8	160	2.0	140
4940 - 4950	19.4	82	3.2	115
5690 - 5700	18.8	86	1.6	148
5790 - 5800	12.0	160	1.9	142
5890 - 5900	17.5	98	2.5	130
6220 - 6230	19.8	78	0.5	175
6280 - 6290	17.9	94	1.6	148
6370 - 6380	21.9	64	-1.2	240
6650 - 6660	17.0	102	3.0	119

NOTE:

Assumed a $\delta^{18}O_w$ = -13.7 above 3000'

a $\delta^{18}O_w$ = -12.6 below 3000'

in frequency histogram form in Figure 4.5. The two distinct populations present in the $\delta^{18}O$ raw data (Figure 4.4) are now replaced by one population with a mean temperature somewhat less than the mean predicted for the carbon isotopic temperature distribution. The oxygen isotopic temperatures never exceed about 170°C, while carbon isotopic temperatures reach as high as 240°C in the deeper part of the hole. Little can be said about the validity of these temperatures because the fluid isotopic data is assumed and not measured. In a very general way, carbon isotopic temperatures increase with depth, while oxygen isotopic temperatures exhibit distinctive highs and lows which seem to alternate back and forth with depth. The oxygen isotopic temperatures are generally less than the measured temperatures except in the upper part of the hole, 304.8-594.4m (1000-1950 ft).

E. Identification of Fluid Entries

A graphical comparision of the oxygen and carbon isotopic temperature profiles with Pb distribution is shown in Figure 4.6. The enrichments of Pb, As or Hg over some background concentration have generally been correlated with permeable, fluid entries in the rock. Many of the oxygen isotopic temperature spikes correlated quite closely with the highs observed in these trace elements. This is particularly true for oxygen and Pb below about 1200m (4000 ft). Typically, carbon isotopic temperatures do not correlate with trace element highs. Rather, they mimic, in a gross way, the present temperature distribution in the system.

These data suggest that the oxygen isotopic compositions of carbonates may have continually re-equilibrated with fluids moving through the system. Carbon isotopes, on the other hand, have retained their initial values fixed

FIGURE 4.5 FREQUENCY HISTOGRAMS OF TEMPERATURES CALCULATED FROM OXYGEN AND CARBON ISOTOPE VALUES FROM WELL C/T-2

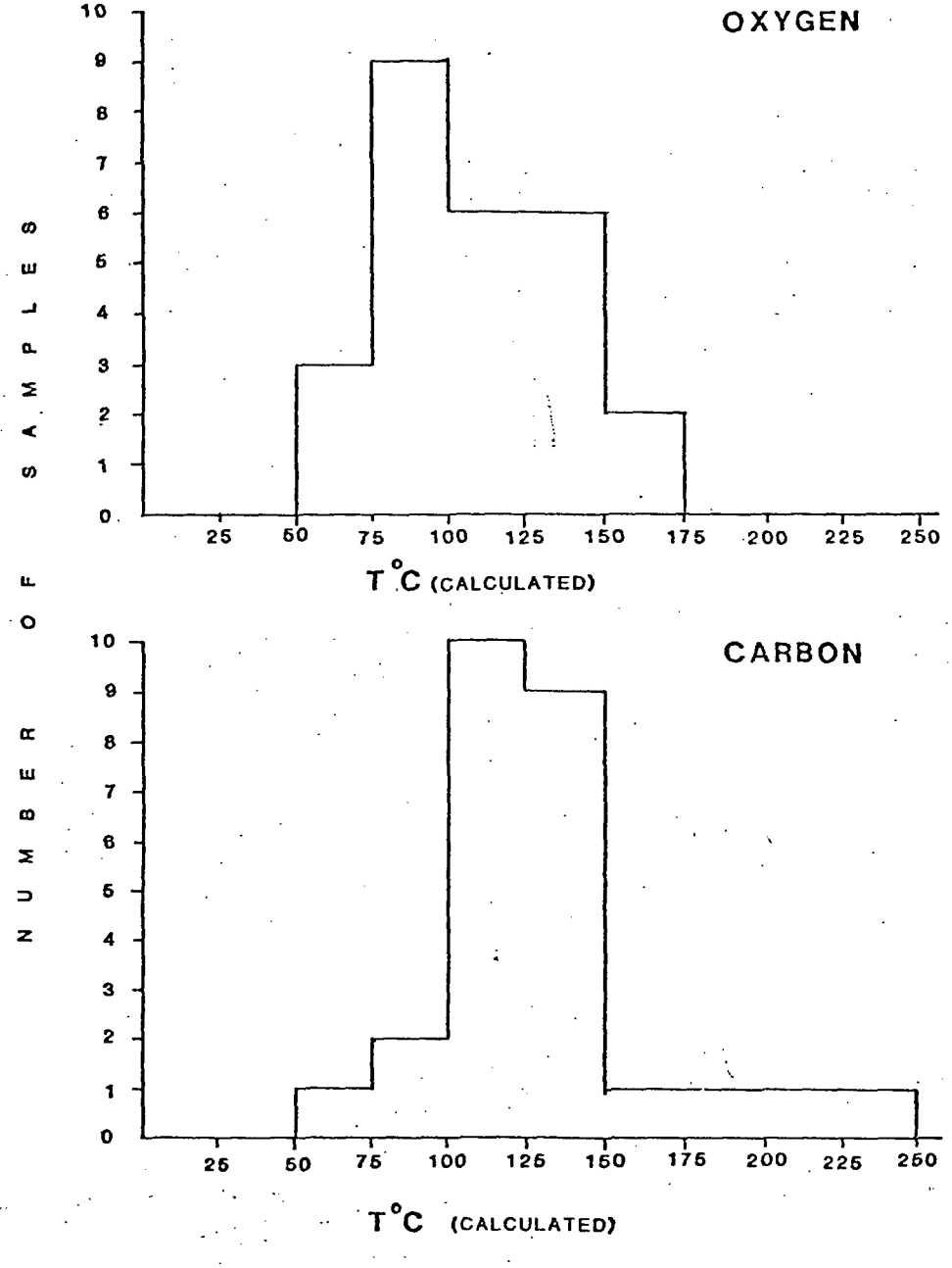

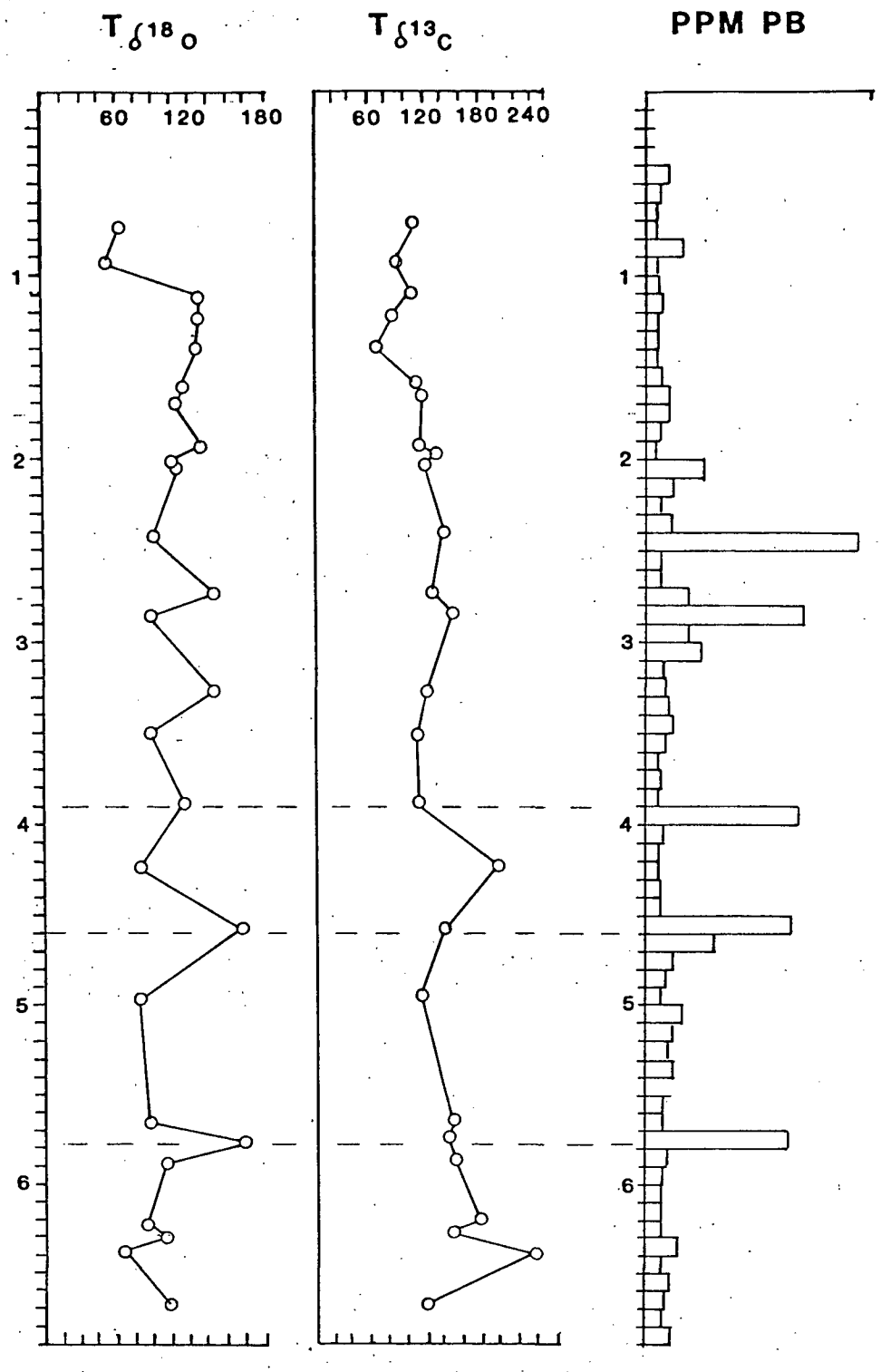

FIGURE 4.6 CACULATED OXYGEN AND CARBON ISOTOPIC TEMPERATURES PLOTTED AGAINST LEAD VALUES FROM WELL C/T-2

at the time of deposition. This hypothesis fits in well with experimental isotopic exchange rate data which predict much faster rates of exchange for oxygen than carbon. This trend coupled with the possibility that the CO_2 concentration in the fluid may have decreased significantly since the deposition of the carbonates would result in a case where the $\delta^{13}C$ values remain essentially unchanged. This conclusion is substantiated to a certain degree by the fact that coarse and fine grained carbonates have essentially the same $\delta^{13}C$ values, indicating the presence, through time, of a uniform $\delta^{13}C$ value in the fluid and absence of re-equilibration in response to variations in temperature.

V. PHYSICAL PROPERTY MEASUREMENTS

A. Bulk Density and Magnitude Susceptibility Measurements

Bulk density and magnetic susceptibility measurements were obtained for 335 cuttings samples between 122m (400 ft) and 2092m (6885 ft) in LASL C/T-2 (Table 5.1). Magnetic susceptibility was measured using a Bison Susceptibility Bridge (Model 3101) and bulk density was determined by fluid displacement and sample weight. The latter measurement was quite difficult because the chips' size was very small. The small size made it difficult to saturate the volume of grains with water. Trapped air would lower any density measurements. Every effort was made to eliminate this problem.

The magnetic susceptibility values ranged between 40 and 200 μ cgs in the alluvium and between 2000 and 600 μcgs in the crystalline rocks. No clear, general correlation is evident between lithology and magnetic susceptibility, although the highest values tend to be associated with the microdiorite and Precambrian gneisses which are rocks containing the highest amount of mafic minerals.

The bulk density values indicate a correlation with rock type. The more mafic rocks, primarily the biotite-pyroxene-hornblende diorite and hornblende microdiorite, are more dense than the felsic granitic rocks such as the hornblende, biotite granite.

Figure 5.1 is a plot of density versus magnetic susceptibility and indicates increasing density correlates with an increase in magnetic susceptibility. This result is due to the higher density of magnetite and the fact that the rocks containing more mafic minerals, which have higher densities, have higher magnetic susceptibilities.

Table 5.1 - Magnetic Susceptibilities and Densities of Cuttings from LASL C/T-2.

FOOTAGE (feet)	(meters)	DENSITY (gm/cc)	MAG SUSCEP ($x10^{-6}$ μcgs)
415.0	126.5	2.66	100.
475.0		2.52	90.
535.0		2.32	47.
595.0		2.62	42.
655.0		2.55	109.
685.0		2.58	57.
715.0	218.0	2.59	446.
737.5		2.73	2276.
752.5		2.76	3023.
767.5		2.74	2677.
782.5		2.74	2147.
795.0		2.64	1787.
822.5	250.7	2.47	487.
837.5		2.43	545.
852.5		2.85	1163.
882.5		2.57	868.
912.5	278.1	2.67	602.
927.5		2.68	758.
942.5		2.58	641.
957.5		2.80	2087.
972.5		2.83	2781.
987.5		2.73	2196.
1002.5	305.6	2.69	945.
1017.5		2.66	335.
1032.5		2.65	1208.
1045.0		2.65	1752.
1055.0		2.75	1136.
1065.0		2.66	847.
1075.0		2.63	164.
1085.0		2.55	158.
1097.5	334.5	2.65	107.
1112.5		2.58	74.
1127.5		2.62	151.
1142.5		2.65	1197.
1157.5		2.68	545.
1172.5		2.64	196.
1187.5		2.68	245.
1202.5	366.5	2.62	654.
1225.0		2.58	332.
1255.0		2.61	224.
1285.0		2.59	732.
1337.5		2.62	1416.
1352.5		2.70	1467.
1367.5		2.55	814.
1382.5		2.63	1979.
1397.5	426.0	2.68	1764.
1420.0		2.60	1155.
1442.5		2.65	1115.
1457.5		2.73	2184.
1472.5		2.63	2139.
1487.5		2.61	1484.
1502.5	458.0	2.56	2385.
1517.5		2.80	2922.
1532.5		2.68	2039.

(feet)	(meters)	DENSITY (gm/cc)	MAG SUSCEP ($x10^6$ µcgs)
1547.5		2.64	536.
1562.5		2.73	3975.
1575.0		2.60	1795.
1592.5		2.78	6365.
1607.5	490.0	2.95	7607.
1622.5		2.79	5964.
1637.5		2.84	6119.
1652.5		2.76	2247.
1667.5		2.82	4357.
1682.5		2.74	3080.
1697.5		2.80	2880.
1712.5		2.77	3096.
1727.5		2.75	3165.
1745.0		2.82	3407.
1757.5		2.92	3328.
1772.5		2.76	2689.
1787.5		2.72	2670.
1797.5		2.71	1221.
1805.0	550.2	2.75	3977.
1817.5		2.77	4283.
1832.5		2.63	2742.
1847.5		2.70	2435.
1862.5		2.68	4149.
1877.5		2.89	3856.
1900.0	579.1	2.74	4206.
1922.5		2.82	4597.
1937.5		2.76	4153.
1952.5		2.81	4469.
1967.5		2.77	3790.
1982.5		2.74	4246.
1995.0		2.66	884.
2002.5	610.4	2.65	818.
2012.5		2.61	488.
2027.5		2.73	3756.
2042.5		2.72	2854.
2057.5		2.85	3355.
2072.5		2.70	3618.
2087.5		2.81	4246.
2102.5	640.8	2.77	3533.
2117.5		2.69	2510.
2132.5		2.74	2565.
2147.5		2.70	3105.
2162.5		2.80	3835.
2177.5		2.81	3771.
2192.5		2.82	3969.
2207.5	672.9	2.79	3105.
2222.5		2.86	3192.
2237.5		2.65	1000.
2247.5		2.72	3243.
2255.0		2.77	4572.
2265.0		2.85	3987.
2275.0		2.82	3045.
2285.0		2.68	2508.
2295.0		2.82	3231.
2305.0	705.6	2.73	3002.
2315.0		2.88	3053.
2325.0		2.86	2766.

(feet)	(meters)	DENSITY (gm/cc)	MAG SUSCEP ($x10^6$ µcgs)
2335.0		2.79	2318.
2345.0		2.81	2086.
2355.0		2.78	3262.
2365.0		2.72	3180.
2375.0		2.76	3335.
2385.0		2.78	4487.
2410.0	734.6	2.70	2457.
2425.0		2.69	2324.
2435.0		2.66	2304.
2445.0		2.74	967.
2455.0		2.11	729.
2465.0		2.68	2259.
2495.0		2.71	1649.
2505.0	763.5	2.64	2554.
2525.0		2.75	4470.
2535.0		2.68	2005.
2545.0		2.66	3360.
2555.0		2.72	2761.
2565.0		2.66	2993.
2575.0		2.72	2925.
2585.0		2.65	3051.
2595.0		2.72	3364.
2605.0	794.0	2.77	4410.
2615.0		2.72	3564.
2625.0		2.70	1446.
2645.0		2.62	1409.
2665.0		2.62	1440.
2685.0		2.63	2994.
2705.0	824.5	2.61	3900.
2715.0		2.76	2718.
2725.0		2.80	2849.
2745.0		2.67	2400.
2755.0		2.71	2582.
2765.0		2.71	2374.
2780.0		2.61	1976.
2800.0	853.4	2.71	2210.
2825.0		2.67	946.
2845.0		2.69	787.
2865.0		2.52	787.
2915.0	888.5	2.56	891.
2935.0		2.56	1294.
2955.0		2.45	1414.
2975.0		2.52	2108.
3005.0	915.9	2.58	1616.
3045.0		2.53	1316.
3065.0		2.57	2074.
3085.0		2.61	1450.
3105.0	945.4	2.56	1413.
3165.0		2.64	3389.
3200.0	975.4	2.56	1520.
3215.0		2.67	1862.
3235.0		2.63	2134.
3255.0		2.62	3313.
3285.0		2.64	2938.
3305.0	1007.4	2.67	1678.
3330.0		2.68	1953.
3355.0		2.66	2144.

(feet)	(meters)	DENSITY (gm/cc)	MAG SUSCEP ($x10^6$ µcgs)
4505.0	1373.1	2.63	2366.
4525.0		2.68	1588.
4545.0		2.66	2452.
4565.0		2.64	1632.
4585.0		2.65	1270.
4605.0	1403.6	2.57	1484.
4625.0		2.60	1117.
4645.0		2.66	2081.
4665.0		2.64	2372.
4685.0		2.64	3464.
4715.0	1437.1	2.61	2521.
4735.0		2.67	2638.
4760.0		2.66	1530.
4785.0		2.60	1030.
4805.0	1464.6	2.66	1059.
4825.0		2.62	1668.
4845.0		2.64	2231.
4865.0		2.62	2057.
4885.0		2.65	1652.
4905.0	1495.0	2.65	1282.
4925.0		2.59	2110.
4945.0		2.68	2278.
4975.0		2.63	2121.
4995.0		2.75	1485.
5015.0	1528.6	2.59	1563.
5035.0		2.58	1045.
5055.0		2.63	1080.
5075.0		2.67	1601.
5095.0		2.63	1006.
5115.0	1559.1	2.65	2039.
5135.0		2.60	1773.
5155.0		2.58	2051.
5175.0		2.67	3448.
5200.0	1585.0	2.61	2160.
5225.0		2.64	1993.
5245.0		2.65	3213.
5275.0		2.60	1646.
5300.0	1615.4	2.63	1758.
5335.0		2.67	3185.
5360.0		2.66	1724.
5385.0		2.68	2337.
5405.0	1647.4	2.71	2547.
5425.0		2.74	1972.
5445.0		2.77	1881.
5465.0		2.67	2204.
5485.0		2.71	1707.
5520.0	1682.5	2.79	2117.
5545.0		2.80	1891.
5565.0		2.76	1806.
5585.0		2.70	2051.
5605.0	1708.4	2.70	1847.
5625.0		2.73	2280.
5645.0		2.69	2155.
5665.0		2.64	2630.
5685.0		2.68	2391.
5705.0	1738.9	2.70	1944.
5725.0		2.51	5478.

(feet)	(meters)	DENSITY (gm/cc)	MAG SUSCEP ($x10^6$ µcgs)
3375.0		2.68	2178.
3405.0	1037.8	2.57	3340.
3425.0		2.65	1701.
3455.0		2.68	5421.
3465.0		2.75	7050.
3485.0		2.77	3422.
3495.0		2.73	3249.
3515.0	1071.4	2.63	2614.
3530.0		2.64	2608.
3545.0		2.74	2406.
3555.0		2.62	2050.
3575.0		2.50	1315.
3595.0		2.61	897.
3615.0	1101.9	2.49	887.
3635.0		2.53	1277.
3655.0		2.49	1107.
3675.0		2.48	1267.
3695.0		2.51	1007.
3715.0	1132.3	2.49	1135.
3735.0		2.56	2264.
3755.0		2.61	2404.
3775.0		2.57	2333.
3795.0		2.60	2272.
3815.0	1162.8	2.52	1313.
3835.0		2.43	778.
3855.0		2.53	1817.
3875.0		2.60	1438.
3895.0	1187.2	2.63	918.
3925.0		2.62	2847.
3955.0		2.56	2060.
3975.0		2.61	731.
4000.0	1219.2	2.51	1777.
4025.0		2.52	2639.
4045.0		2.60	2201.
4065.0		2.61	1945.
4085.0		2.59	3182.
4095.0		2.58	1635.
4105.0	1251.2	2.63	1814.
4125.0		2.70	1521.
4145.0		2.70	1089.
4165.0		2.76	1275.
4185.0		2.63	2581.
4205.0	1281.7	2.57	1584.
4225.0		2.66	2622.
4245.0		2.66	2026.
4265.0		2.64	1813.
4285.0		2.63	1597.
4305.0	1312.2	2.61	827.
4325.0		2.60	927.
4345.0		2.55	1936.
4365.0		2.65	1561.
4385.0		2.69	1667.
4405.0	1342.6	2.61	1521.
4425.0		2.61	1631.
4445.0		2.62	1644.
4465.0		2.67	1770.
4485.0		2.65	3747.

(feet)	(meters)	DENSITY (gm/cc)	MAG SUSCEP ($x10^6$ µcgs)
5750.0		2.71	1188.
5775.0		2.65	1299.
5795.0	1772.4	2.68	1014.
5815.0		2.69	953.
5825.0		2.70	1046.
5835.0		2.72	2075.
5865.0		2.86	2673.
5885.0		2.67	1173.
5905.0	1799.8	2.77	3106.
5925.0		2.80	1754.
5945.0		2.84	1276.
5965.0		2.70	1037.
5985.0		2.73	1846.
6005.0	1830.3	2.79	968.
6025.0		2.84	1647.
6040.0		2.81	976.
6065.0		2.79	1697.
6090.0		2.84	1216.
6115.0	1863.9	2.79	2083.
6135.0		2.80	2403.
6155.0		2.79	1831.
6175.0		2.85	1331.
6195.0		2.80	2546.
6215.0	1894.3	2.87	1854.
6235.0		2.87	2461.
6255.0		2.86	2688.
6275.0		2.75	2537.
6295.0		2.70	958.
6315.0	1924.8	2.85	2005.
6335.0		2.78	3742.
6355.0		2.73	1623.
6375.0		2.78	1799.
6395.0		2.85	2222.
6415.0	1955.3	2.71	1368.
6435.0		2.62	1590.
6455.0		2.78	1181.
6475.0		2.74	1131.
6495.0		2.74	1263.
6515.0	1985.8	2.74	1521.
6535.0		2.64	2231.
6555.0		2.67	2009.
6580.0		2.67	1840.
6625.0	2019.3	2.70	2187.
6650.0		2.72	1517.
6665.0		2.67	1788.
6685.0		2.74	1792.
6705.0		2.81	2607.
6725.0		2.62	2616.
6755.0		2.73	2337.
6785.0		2.68	2116.
6835.0	2083.3	2.77	2098.
6855.0		2.54	2020.
6865.0		2.58	1888.

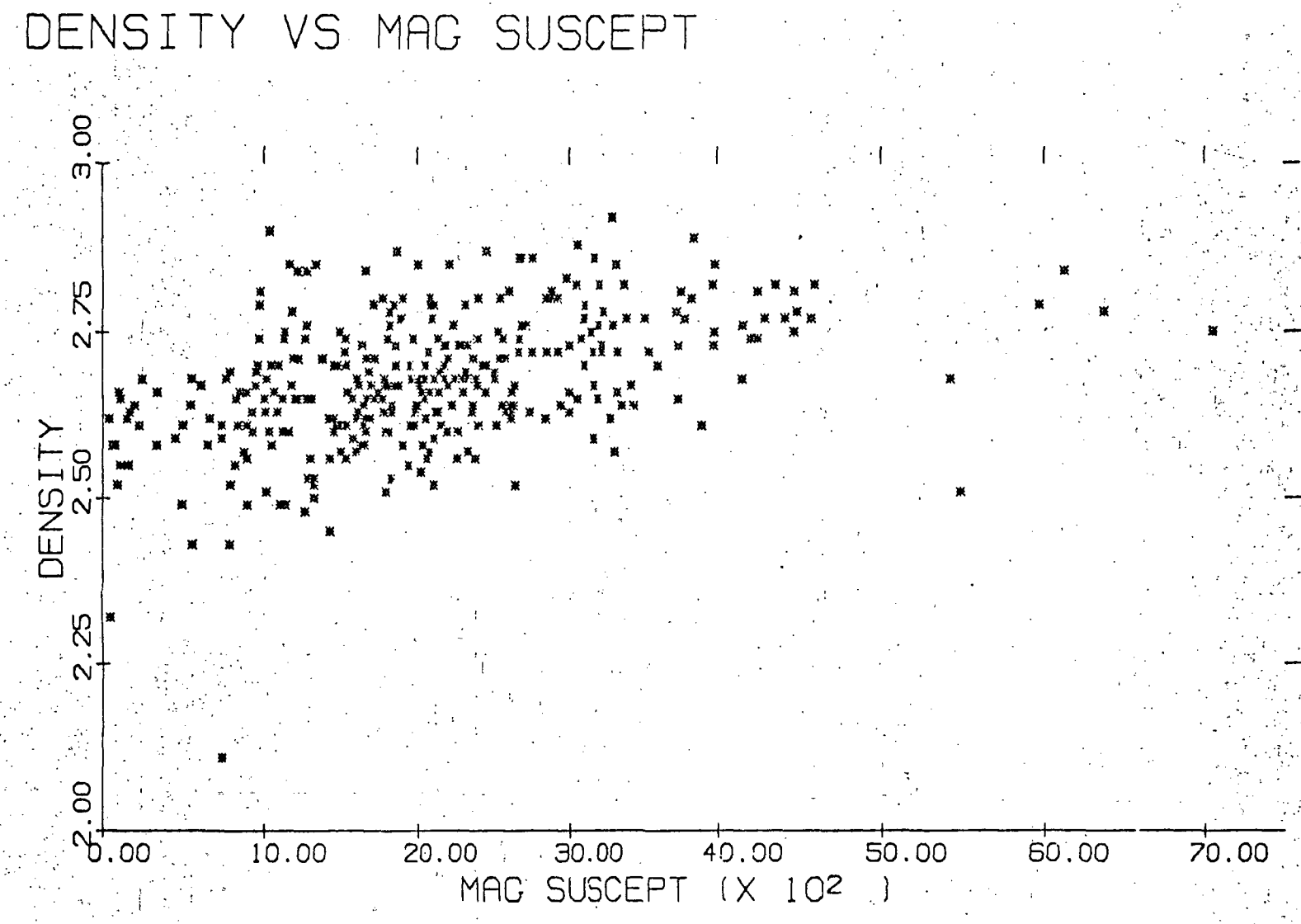

FIGURE 5.1 PLOT OF MAGNETIC SUSCEPTIBILITY AND DENSITY OF CUTTINGS FROM LASL C/T-2.

Table 5.2. Thermal Conductivity Measurements on Chip Samples in C/T-2 at 15 C and Well Bore Temperature. (Values are for dry, non-porous rock.)

DEPTH		K_s	T	K_s^*
Feet	Meters	($Wm^{-1}K^{-1}$)	(^oC)	($Wm^{-1}K^{-1}$)
700-730	213-223	2.90	56	2.83
760-775	232-236	1.87	60	1.82
815-830	248-253	2.79	70	2.70
920-935	280-285	2.52	77	2.43
935-950	285-290	2.69	77	2.59
950-965	290-294	2.07	78	1.99
965-980	294-299	1.94	79	1.87
980-995	299-303	2.07	79	1.99
995-1010	303-308	1.84	80	1.77
1010-1025	308-312	2.28	81	2.19
1025-1040	312-317	1.84	82	1.77
1150-1165	351-355	2.07	89	1.98
1240-1270	378-387	2.40	95	2.29
1345-1360	410-415	2.28	98	2.17
1450-1465	442-447	1.87	103	1.77
1660-1675	506-511	2.20	116	2.07
1705-1720	520-524	1.80	119	1.69
1750-1765	533-538	2.03	121	1.90
1855-1870	565-570	2.10	125	1.96
2000-2005	610-611	2.13	131	1.98
2155-2170	657-661	2.12	136	1.97
2250-2260	686-689	2.21	140	2.05
2350-2360	716-719	2.13	143	1.97
2450-2460	747-750	2.27	146	2.10
2550-2560	777-780	1.81	150	1.67
2710-2720	826-829	2.07	154	1.90
2800-2810	853-856	1.76	156	1.62
2850-2860	869-872	2.08	158	1.91
2900-2910	884-887	1.95	159	1.79
2950-2960	899-902	1.71	160	1.57
3000-3010	914-917	1.90	161	1.74
3050-3060	930-933	1.91	162	1.75
3100-3110	945-948	1.97	163	1.80
3150-3160	960-963	1.84	164	1.68
3200-3210	975-978	1.78	165	1.62
3360-3370	1024-1027	1.85	168	1.68
3390-3400	1033-1036	1.87	169	1.70
3450-3460	1052-1055	2.02	170	1.84
3500-3510	1067-1070	1.77	170	1.61
3560-3570	1085-1088	1.77	170	1.61
3600-3610	1097-1100	1.81	171	1.65
3650-3660	1113-1116	1.88	172	1.71
3700-3710	1128-1131	1.91	173	1.73
3800-3810	1158-1161	1.92	175	1.74
4000-4100	1219-1250	1.65	180	1.49
4200-4210	1280-1283	1.71	181	1.55
4400-4410	1341-1344	1.75	185	1.58

Table 5.2. Continued

DEPTH		K_s	T	K_s^*
Feet	Meters	($Wm^{-1}K^{-1}$)	(^oC)	($Wm^{-1}K^{-1}$)
4600-4610	1402-1405	1.76	190	1.58
4800-4810	1463-1466	1.80	192	1.62
5090-5100	1551-1554	1.78	195	1.59
5200-5210	1585-1588	1.80	197	1.61
5400-5410	1645-1649	1.77	201	1.58
5600-5610	1709-1710	1.95	203	1.74
5800-5810	1768-1771	1.86	207	1.65
6000-6010	1829-1832	1.62	210	1.44
6200-6210	1890-1893	1.92	211	1.70
6400-6410	1951-1954	1.76	215	1.56
6600-6610	2012-2015	2.01	218	1.78
6800-6810	2073-2076	1.94	223	1.71

B. Thermal Conductivity.

Thermal conductivity values were obtained on 59 cuttings samples from LASL C/T-2, between 213.4m (700 ft) and 2075.7m (6810 ft) and are listed in Table 5.2. These measurements were made on a divided bar apparatus (Sass, et al., 1971) which was calibrated with fused and crystalline quartz (Ratcliffe, 1959). Measurements were made at 15°C using the cell technique described by Sass et al. (1971) and adjusted for the appropriate borehole temperature using the method described by Wilson and Chapman (1980).

The temperature correction is computed using the following expression.

$$K_s^* = K_o \, e^{-\alpha T}$$

where $\alpha = 0.609 \times 10^{-3} \, {}^oC^{-1}$

and $K_o = K_s^* \, e^{15\alpha}$

K_s is the measured solid rock thermal conductivity at 15°C and K_s^* is the temperature corrected thermal conductivity at temperature T(°C). Borehole temperatures were taken from the Dresser Atlas log of C/T-2 obtained by LASL. The sample depths, K_s, T and K_s^* are listed in Table 5.2. The thermal conductivity data are given in SI units, Watts/m°K. To obtain cgs units, mcal/cm°C sec, simply multiply the data by 2.39.

The thermal conductivities appear to be lower than might be expected. Typical values for these rock types fall between 2 and 3.5 Watts/m°K (approximately). The measurements have a precision of 2% or better and an accuracy of 10% or better. However, measurements are made on chips and a mixing formula is used to convert these measurements to ones for solid material. The measurement system was checked using crushed quartz standards with good results. However, C/T-2 chips are quite small and difficulties may

arise from use of the mixing formula or from estimating solid material volume. The latter problem existed in the density measurements. Several experiments have been proposed and are scheduled to study the problems of estimating thermal conductivities from chip samples.

A further problem, noted earlier, is that the quartz and feldspar grains may have been crushed to such a size that these minerals were depleted in the chip samples at the time of collection and later during the washing process. The greater concentrations of mafic minerals, particularly biotite, would lower the thermal conductivity.

The data in Table 5.2 would represent zero porosity material. If porosity corrections were made, the thermal conductivities would be lowered (Plewa, 1976). However, porosity of these rocks is quite low (<2%, with few exceptions) and the correction would be small.

VI GEOPHYSICAL INTERPRETATIONS

A. Introduction

A number of well logs have been obtained in C/T-2 by Phillips Petroleum Company (PPC) and LASL. The PPC logs are confidential and were examined but not analyzed. The LASL logs have been digitized at 0.15m (0.5 ft) increments, plotted at 12 and 24m/cm (100 and 200 ft per inch) scales and interpreted in terms of geologic and geophysical properties. The logs have been correlated where possible to each other and to geologic rock types.

The well was cased to 1280.1m (4200 ft) and the casing cemented prior to logging by LASL. Hence the log data are not studied in detail above this depth. Unfortunately most of the interesting, varied geology occurs above 844.3m (2770 ft), as noted earlier, and lies behind casing. All logs available for study are listed in Table 6-1. The table lists the logging company, log type, log data, logged interval, cased interval and bottom hole temperature.

Both Schlumberger (Schl) and Dresser Atlas (DA) natural gamma logs were recorded with the neutron logs. The caliper log was recorded with the temperature log. The electric log was obtained with an induction tool. Each log will be discussed individually and interpretations of each log and log data cross plots will be presented and discussed.

The log data have been plotted in Plate I at a 24m/cm (200 ft/inch) scale and in the same units in which they were recorded. A lithology log and columns showing (1) altered cataclasite, gouge and microbreccia, (2) chlorite after mafic minerals, (3) estimated volume per cent sulfides and (4) estimated volume per cent "limonite" are included in Plate I. The magnetic

TABLE 6.1 Well Logs Obtained in C/T-2 by LASL[1]

LOG NAME	LOGGING COMPANY	LOG DATE	LOGGED INTERVAL meters (ft)	BOTTOM HOLE TEMP. °F (°C)
Diff. Temperature	Dresser Atlas	11/14/78	0-2079.6 (0-6823)	442 (227.8)
Gamma-Ray Neutron[2]	Dresser Atlas	11/16/78	234.7-2080.8 (770-6827)	446 (230.0)
Comp. Densilog[3]	Dresser Atlas	11/17/78	234.7-2080.2 (770-6825)	443 (228.3)
Acoustic CBL/VDL	Dresser Atlas	11/17/78	231.6-1767.8 (760-5800)	446 (230.0)
Borehole Comp. Sonic[4]	Schlumberger	2/5/79	1287.4-2087.8 (4224-6850)	440 (226.7)
Induction - SP[5]	Schlumberger	2/5/79	1297.8-2085.9 (4258-6844)	440 (226.7)
Gamma-Ray Neutron[6]	Schlumberger	2/5/79	243.8-2089.0 (800-6854)	440 (226.7)

NOTES: [1]Hole was cased to 1280.1m (4200 ft) for all logs.

[2]Thermal Neutron - NT = N, 130.

[3]Both long and short detector spacings recorded.

[4]No transmitter - receiver separation available to calculate interval travel time.

[5]Single Induction log - 6FF40.

[6]Thermal Neutron - GNT/N.

susceptibility and density measurements obtained from chip samples and discussed earlier are plotted in Plate I.

A second plot, at 12m/cm (100 ft/inch) scale and for the portion of the hole below casing, 1280.1-2099.4m (4200-6855 ft), has been created and is shown in Plate II. A few of the logs shown on Plate I have been excluded, new data added, thermal conductivity and temperature gradient, and the DA neutron and density logs are shown converted to porosity and density units, respectively.

Reference to Plates I and II will be made frequently in following sections. All data recording parameters were in English and/or Oil Field units. SI and the original units are both shown on Plates I and II as they will be throughout the rest of this report.

B. Log Descriptions.

1. Temperature Log. DA recorded their Differential Temperature Log in C/T-2 at 30.5m/min (100 ft/min). Both absolute temperature and a differential temperature log were recorded. Only the absolute temperature log has been digitized and it is plotted in Plate I. Temperature gradients have been computed from this log using 3.05 and 15.3m (10 and 50 ft) depth intervals, and are plotted in Plate II.

A curious feature of the temperature log is the several, quite smooth near zero gradient intervals throughout the log; examples can be noted between 472.4 and 499.9m (1550 and 1640 ft) and between 823.0 and 883.9m (2700 and 2900ft). Either these intervals reflect instrument malfunction or small convective cells in the borehole. Instrument problems (intermittent ones) would be the most probable cause of these features. An earlier PPC

temperature log does not exhibit any similar features and the DA tool did fail at the bottom of the hole before any post survey calibration could be made.

The temperature gradient exhibits larger variations in the 3.05m (10 ft) interval values than in the 15.3m (50 ft) interval values. These variations cannot be completely explained by thermal conductivity changes (see Plate II). Remember that the thermal conductivity measurements are for zero porosity rock and that thermal conductivity decreases with increasing porosity. Note that the low temperature gradient interval between 1630.7 and 1691.6m (5350 and 5550 ft) correlates with a low, near zero neutron porosity. Below 1706.9m (5600 ft) the neutron porosity correlates with a temperature gradient increase. The neutron porosity reflects the presence of both porosity and hydrous minerals and both would lower the thermal conductivity and increase the gradient.

2. Caliper Log. The DA caliper log was recorded simultaneously with the temperature log. Several abrupt, unexplained recording offsets occurred in the caliper log and these were removed before the data were plotted in Plate I. The log shows insignificant hole enlargement or caving which might indicate fracture intercepts in the well bore. Fault gouge was noted in drill chips in intervals centered at 1453.9m (4770 ft) and 1767.8m (5800 ft) and neither interval has generated any hole enlargement which suggests both fractured intervals are well sealed.

The caliper log shows a decreasing hole size with depth in casing and an increasing hole size with depth in the open hole. A temperature effect should result in only a single type of variation such as an increase in apparent hole diameter with depth. Note too, that the casing depth is clearly lower on the

caliper log than reported by PPC. This discrepancy appears on nearly all the logs and indicates a depth recording problem in the logging of C/T-2. This problem will be discussed further in a later section.

3. Acoustic (Velocity) Logs. LASL obtained a Schl. Borehole Compensated Sonic Log (BHC) and a DA Acoustic Cement Bond Log (VDL) in C/T-2. Little of particular interest for this study is contained in the VDL log and it is not shown in Plate I. This log is referenced where it contains information supporting an interpretation of another log. The Schl. log contains a Δt measurement using a single receiver, an amplitude measurement and a variable density (wave form peaks) measurement. The Δt and amplitude log data are reproduced in Plate I. Again the variable density log exhibits very little of interest and is not shown on Plate I. The Schl. log was recorded only in the open hole. The BHC log exhibits only minor problems of cycle skipping. However, the tool did experience a transmitter failure below 1944.6m (6380 ft) and data were lost between 1944.6 and 1966.0m (6380 and 6450 ft). A second transmitter in the tool was used successfully thereafter. Notes on the log indicate a switch was made to a different receiver at 1834.3m (6018 ft) and that the Δt data are invalid (no reason given) between 1318.3 and 1325.9m (4325 and 4350 ft). The Δt curve shifts to longer travel times between 1834.3 and 1925.7m (6018 and 6318 ft) due to a change in transmitter receiver separation.

The tool was centralized and pulled at 15.2m/min (50 ft/min). No transmiter-receiver separations were reported; therefore, the data cannot be converted to conventional units of μsec/m (μ sec/ft).

4. Neutron Logs. Both a DA thermal neutron log (N-TN) and a Schl.

thermal neutron log (GNT-N) were obtained in C/T-2. The DA log was obtained at 10.7/m/min (35 ft/min) and a time constant of two seconds and the Schl. log was obtained at 18.3m/min (60 ft/min) and time constant of one second. Both logs were recorded in API units although the DA log scale was calibrated for an air-filled hole and labeled as N-TN/ ϕ units. A simple multiplication of the DA neutron log scale by 12 converts it to the correct API units, as noted on Plate I. The corrected log is plotted in Plate II. Clearly the logs from the two companies do not compare favorably. First, there is a depth offset, which will be discussed later, between the two logs; second, the DA log exhibits a much greater variability than the Schl. log although changes in response are coincident (allowing for the depth offset) and three, the Schl. log response in the open hole is beyond the limit of the calibration curve (much less than 1% porosity) for this tool given in Schlumberger (1972) whereas the DA tool response is largely within the calibration range shown on their calibration graph (Dresser Atlas, 1980). Figures 6.1, 6.2, and 6.3 are cross plots of data from the two neutron logs for three arbitrarily selected intervals. The data have been averaged on 1.52m (5 ft) intervals. Since both logs are in API units they should be expected to show closer agreement. Of the three intervals plotted, only the one between 1866.9 and 1988.8m (6125 and 6525 ft) demonstrates any significant variability in the Schl. log. A linear relationship between the two logs was determined from data in this interval to be

$$DA = 10137 - 3.50\ Schl. \qquad (6\text{-}1)$$

A third degree polynomial was fit to the DA calibration curve and was used to convert the DA log to porosity units (Table 6.2). The polynominal

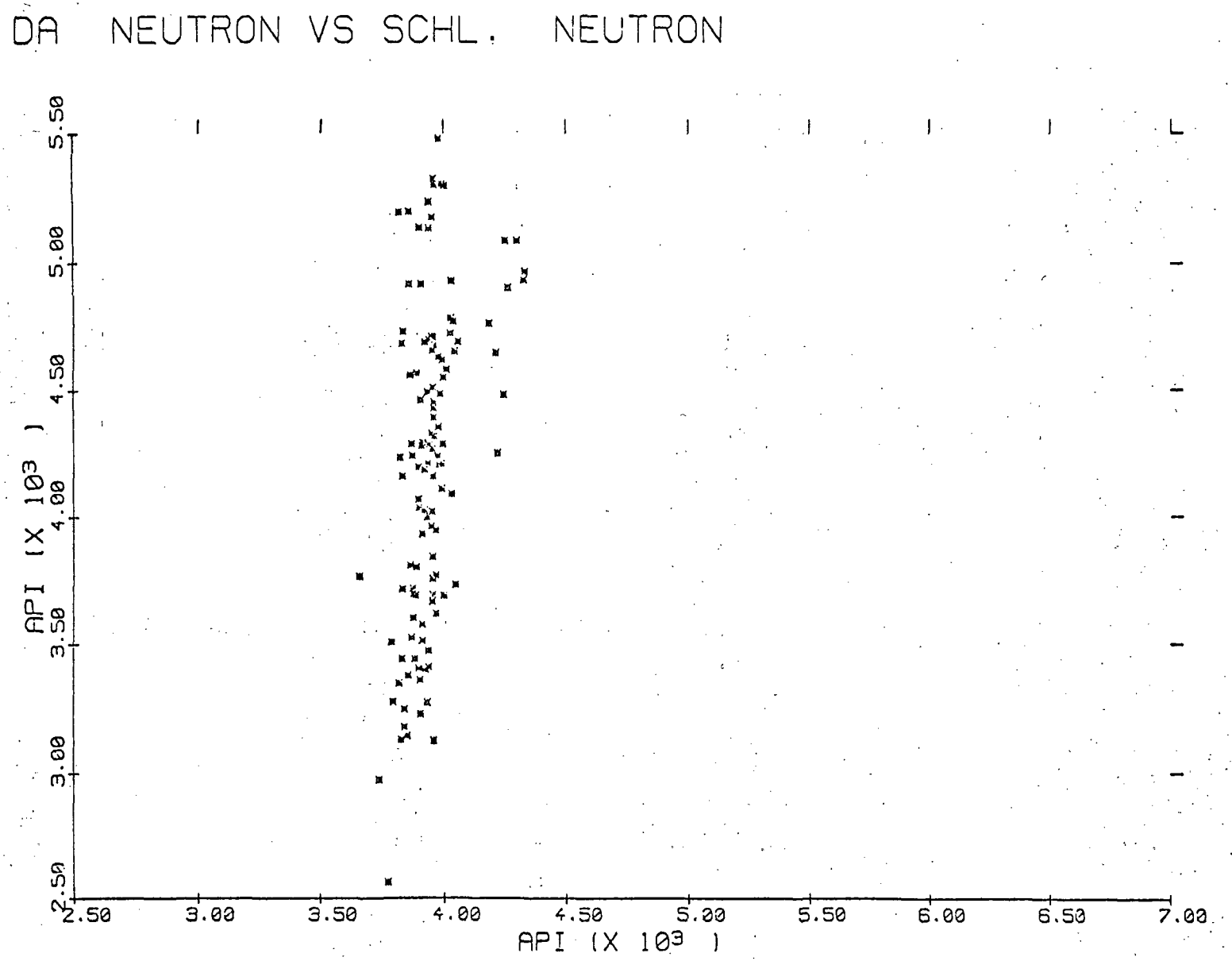

C/T-2 FIGURE 6.1

4202.50 - 4797.50 FEET, 1280.9 - 1462.3 METERS
AT 5.00 DEPTH UNIT INTERVALS, 1.82 METER INTERVALS

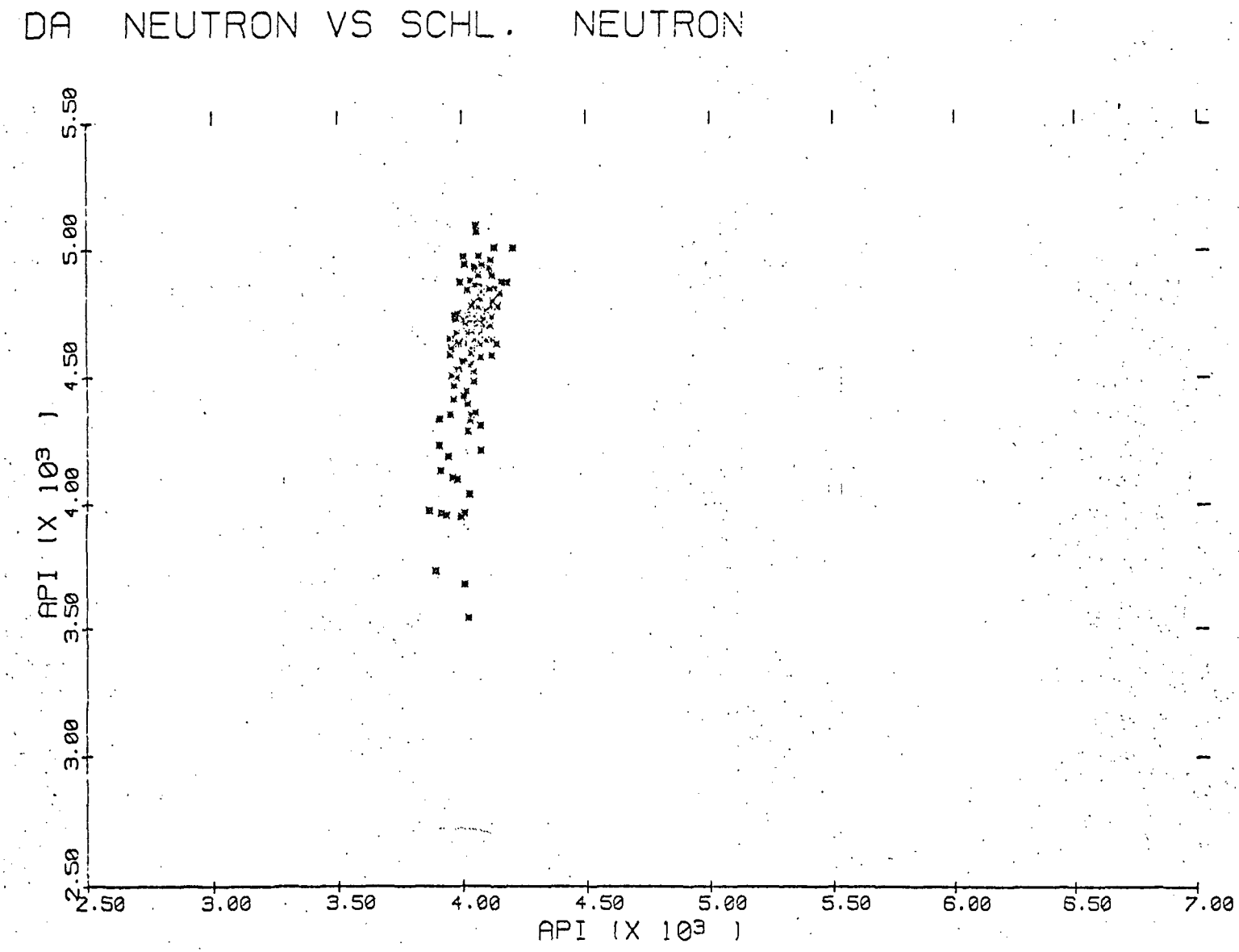

C/T-2 FIGURE 6.2

5202.50 - 5797.50 FEET, 1585.7 - 1767.1 METERS
AT 5.00 DEPTH UNIT INTERVALS, 1.52 METER INTERVALS

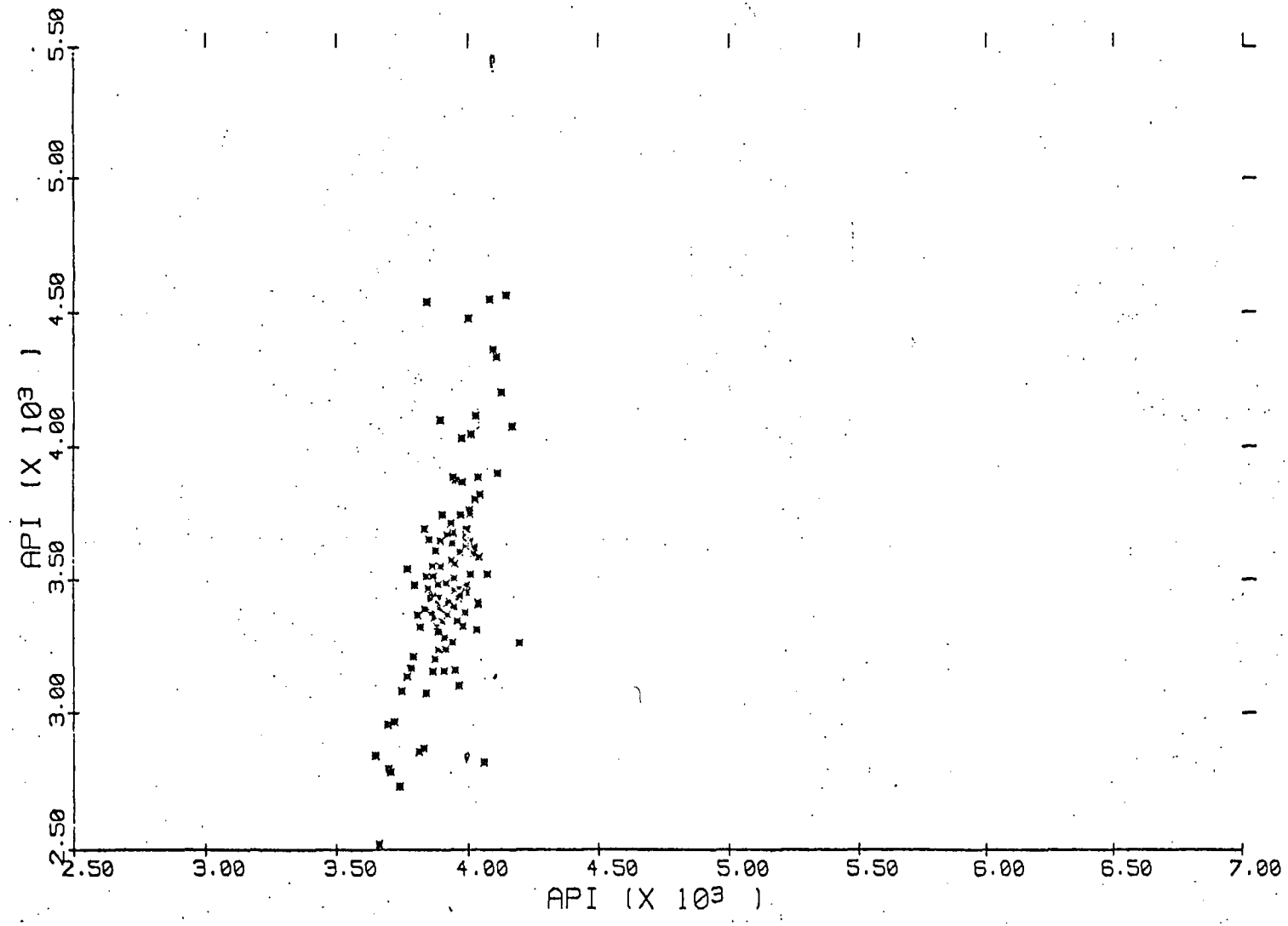

C/T-2 FIGURE 6.3

6202.50 - 6797.50 FEET, 1890.5 - 2071.9 METERS
AT 5.00 DEPTH UNIT INTERVALS, 1.52 METER INTERVALS

TABLE 6-2: COMPARISON OF POROSITY VALUES READ FROM DA CALIBRATION CURVE AND POLYNOMIAL EQUATION.

API	POROSITY (GRAPH)	POROSITY (CALC.)
300	40.5	37.5
600	26.5	26.3
900	19.2	19.2
1200	13.5	13.7
1500	9.6	9.8
1800	7.1	7.0
2100	5.2	5.0
2400	3.75	3.6
2700	2.75	2.6
3000	1.9	1.8
3300	1.3	1.3
3520	1.0	1.0
4000	---	.6
5000	---	.2

equation is:

$$\log \phi = 1.72-4.86X10^{-4}A-8.11X10^{-11}A^2, \quad (6\text{-}2)$$

where A is in API units.

The data in Table 6.2 indicate that the polynomial equation used to convert the DA neutron log from API to porosity units is quite good for the normal porosity range of rocks. The neutron porosity data are plotted in Plate II and indicate the porosity of rocks intersected by C/T-2 below 1280.2m (4200 ft) averages less than 4% and nowhere exceeds 8%. A component of the neutron porosity is due to hydrous numerals which will be demonstrated later.

5. Density Logs. LASL obtained a DA dual spacing DENSILOG in C/T-2. The log was run at 15.2m/min (50 ft/min) and a time constant of one second. The detector spacings were 19 cm (7.5 in), the long spacing, and 33 cm (13 in), the short spacing. The data were recorded in counts/min for both short and long spaced logs. These data are plotted in Plate I. The upper portion of the long spaced log varied widely and was not digitized. Therefore, it is not shown in Plate I. Apparently the scales shown on the original logs are reversed. To correct this error simply divide the long spaced data by two and multiply the short spaced data by two. These operations are noted on Plate I.

Based on calibration curves supplied by DA we determined the following equations to convert counts to bulk density.

Short Spaced: $X_D = 2.722-2.559 \log X_C$ (6-3)

(Aluminum calibrator counts: 7500)

Long Spaced: $X_D = 2.739-1.035 \log X_C$ (6-4)

(Aluminum calibrator counts: 11475)

where X_C is counts and X_D is bulk density. The log counts are first divided by the aluminum calibration counts and then used in the formula. Dennis Lynch of DA, Ventura, California informed us that the long spaced counts should yield the better density estimates. The bulk densities were computed using the above formulas and are plotted on Plate II. The short spaced values are consistently lower than would be expected for these rock types whereas the long spaced counts appear reasonable.

Note that the densities determined from chip samples are plotted by points along with the DA bulk densities. With few exceptions, the chip values are significantly greater than those calculated from the well logs below 1623.1m (5325 ft). Although the data do not agree, they do show the same variations. Above 1623.1m (5325 ft) the data show better agreement. The chip densities might reflect sampling problems. A greater amount of heavier minerals may have been concentrated in the chip samples below 1623.1m (5325 ft). The density log may be underestimating the density of rocks high in mafics; however, this error should not be greater than several tenths of a gm/cc. Assuming no error, the difference could be explained by approximately 8% porosity which seems too high and is not suported by the neturon porosity values. We suspect all three factors have contributed to the descrepancy between the two measurements.

6. Electrical Conductivity and SP Logs. The Schl. 6FF40 induction log was run in C/T-2 at a speed of 305m/min (1000 ft/min). The tool was not centered and a borehole correction of -25 millimhos was used. Both a conductivity and resistivity log were recorded and linear scales were used. An SP log was also obtained. No values of R_m, R_{mf}, or R_{mc} were recorded. The

logs were obtained long after the hole was completed and the borehole fluid at the time of the logging was water. The water samples analyses (Table 3.4) indicates the borehole fluid contains approximately 6200 ppm TDS. Using the temperature range 185 to 227°C (365 and 440°F), observed in the drill hole between 1280.1 and 2098.5m (4200 and 6885 ft), the borehole fluid resistivity ranges between 0.19 and 0.15 (Schlumberger, 1972a, p.9) ohm/m and little or no contrast should exist between the borehole and formation fluid resistivities.

Schlumberger (1972b, p.31 and 1974, p.3) notes that induction logs, including the 6FF40, yield poor resolution and accuracy where formation resistivities exceed 100 ohm-m, and there may be a 2mmho zero error as well. The induction log conductivity values in C/T-2 are almost entirely below 10 mmhos/m (greater than 100 ohm-m resistivity) and numerous intervals show a 2mmho/m or lower conductivity. Also Schlumberger (1974, p.3) notes that the 6FF40 tool requires standoff for best accuracy. The casing diameter being less than the open hole diameter precluded use of centralizers on the induction tool. Hence, the electrical resistivity (or conductivity) measurements in C/T-2 are probably inaccurate. This problem was observed in electrical logging of other Roosevelt Hot Srings' drill holes (Glenn and Hulen, 1979).

The SP log contains a few interesting variations. The fault at 1453.9m (4770 ft), and the 57.9m (190 ft) immediately above the fault, show a right deflection (shale direction) on the log. The right deflection may reflect the presence of clay minerals in the fault intercept at 1453.9m (4770 ft) and the probability that the fault either parallels the drill hole over a 61.0m (200 ft) interval or the fault zone is 61.0m (200 ft) thick. A similar, shorter

response occurs opposite the fault at 1767.8m (5800 ft) and again reflects the presence of clay minerals in the fault.

Several left deflections occur between the bottom of casing at 1280.1m (4200 ft) and 1399.0m (4590 ft). We offer no explanation for these events, although permeable fractures may be responsible.

7. Gamma-Ray Logs. Two gamma-ray logs were obtained in C/T-2, one by DA and one by Schl. Both logs were obtained simultaneously with the neutron logs and were recorded in API units. The Schl. log was run at 15.2m/min (50 ft/min) and a one second time constant, whereas the DA log was run at 10.7m/min and a two second time constant. Unlike the neutron logs, the two gamma-ray logs agree reasonably well. Both logs are shown in Plate I and for simplicity only the DA log is shown in Plate II. Note the depth offset between the two logs. Plots of the DA Gamma-Ray log data versus the Schl. Gamma-Ray log data are shown in Figures 6.4, 6.5, and 6.6 for three arbitrary depth intervals. The data are averages over .61m (2 ft). A forty-five degree line has been drawn in each figure for reference.

As expected, the more acidic rock units generate the highest and the more mafic rock units generate the lowest gamma-ray counts. In particular, the hornblende-biotite granite/syenite has a distinct high gamma-ray count, for example interval 1080.0 to 1249.7m (3540 to 4100 ft), and the hornblende-biotite granodiorite has a distinct low gamma-ray count, for example 804.6 to 1079.0m (2640 to 3540 ft).

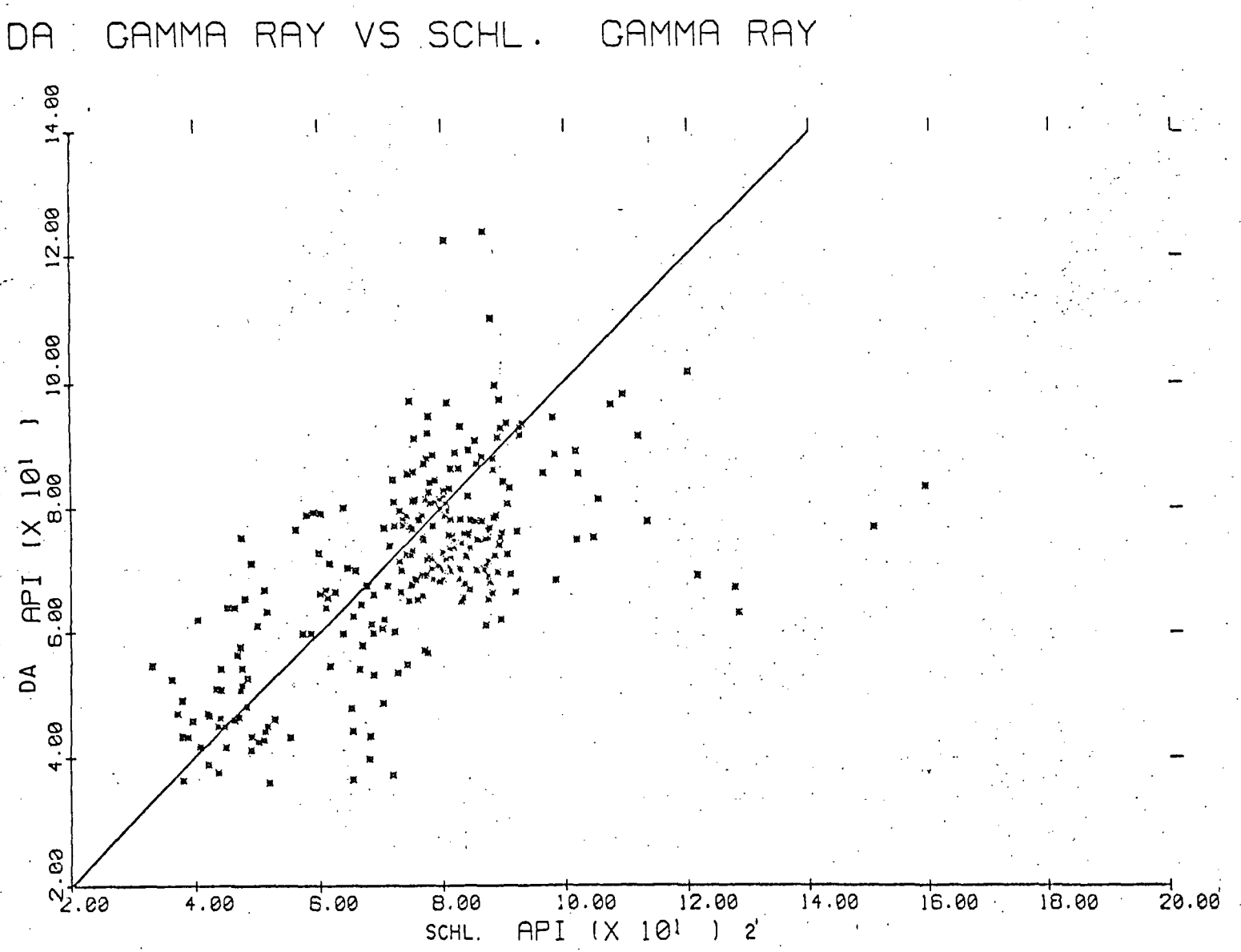

C/T-2 FIGURE 6.4

3801.00 - 4323.00 FEET, 1158.5 - 1317.7 METERS
AT 2.00 DEPTH UNIT INTERVALS, .61 METER INTERVALS

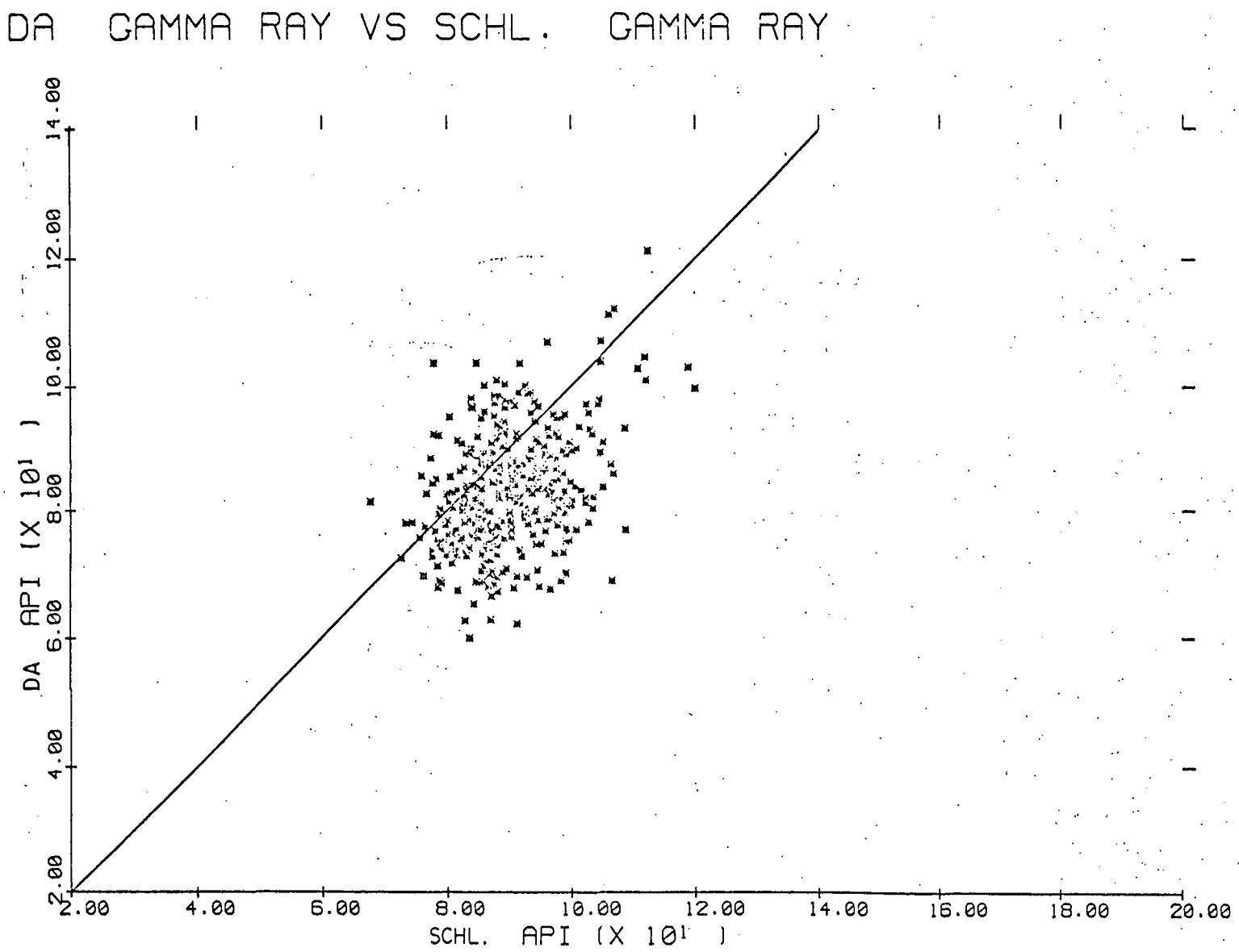

C/T-2 FIGURE 6.5

AT 5025.00 - 5723.00 FEET, 1531.6 - 1744.3 METERS
2.00 DEPTH UNIT INTERVALS, .61 METER INTERVAL

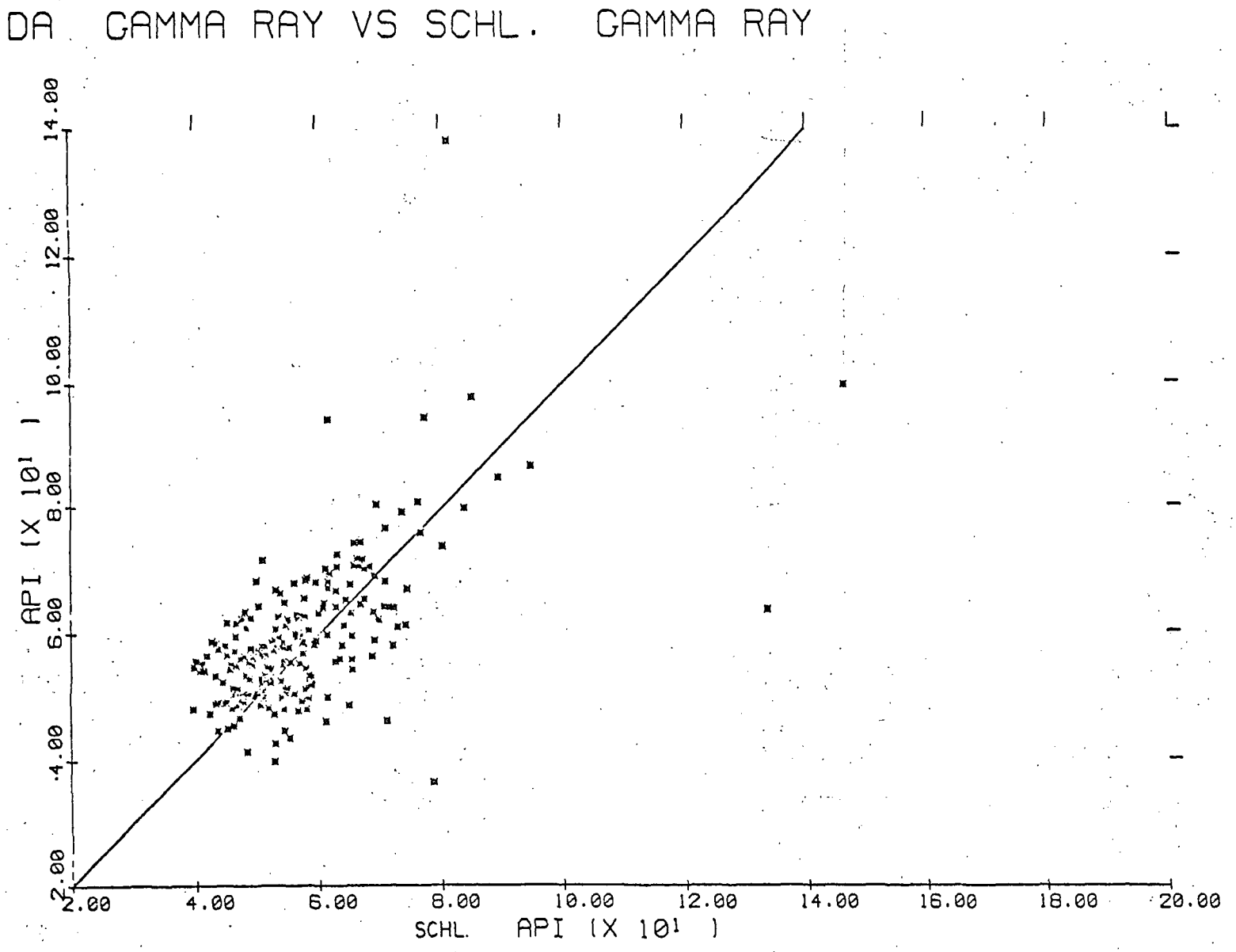

C/T-2 FIGURE 6.6

6425.00 - 6843.00 FEET, 1958.3 - 2085.8 METERS
AT 2.00 DEPTH UNIT INTERVALS, .61 METER INTERVAL

The high counts over short intervals, such as seen at 1920.2m (6300 ft), are attributed to anomalous values of uranium, thorium and/or their daughters in these intervals. Analyses presented earlier for 1920.2-1923.3m (6300-6310 ft) substantiates this conclusion. We noted earlier that the anomalous contributions at 1920.2m (6300 ft) were from thorium, and uranium and thorium daughters. The uranium has been largely depleted.

8. Summary Log Evaluations. The Dresser Atlas temperature and caliper logs exhibited characteristics attributed to tool malfunction. The temperature tool did fail shortly after reaching the bottom of the hole. The log contained several short intervals of near zero temperature variation with depth and a number of descrete offsets. Otherwise the log appears quite good and the bottom hole temperature agrees with the previously reported value. The caliper log displayed both an increasing, in casing, and decreasing, in the open hole, hole size with depth. One, but probably not both changes can be attributed to temperature affects.

Thermal conductivity measurements obtained from chip samples could not explain all the variations seen in the temperature gradient curve computed from the temperature log. The gradient curve correlated in many instances to the neutron porosity log.

The Schlumberger acoustic logs appear reasonably good. Tool malfunctions did occur with some loss of data. A single receiver measurement was made which may mean the data are less accurate than would have been possible with a two receiver measurement. Also, a transmitter receiver separation was not supplied and the travel times could not be converted to interval transit time or velocities. This separation was not constant for the entire log.

The two neutron logs were recorded in API units although the Dresser Atlas log was miscalibrated. The miscalibration was easily corrected. However, the Schlumberger log exhibitied very little variability and the data were all well beyond the calibration curve, implying porosities close to zero throughout the open hole interval. Our guess is that the Schlumberger tool lost sensitivity in the high temperature environment although an error by the equipment operator cannot be excluded.

The Dresser Atlas density log was recorded in counts/min for both the long and short spaced detectors. The scales were labelled in reverse and the correction was trivial. As predicted by Dresser Atlas, the long spaced measurement yielded the more reasonable density estimates. A significant descrepancy between the density log and the chip sample densities occurred in the lower portion of C/T-2. The differences can be attributed to one or more of the following: errors in the chip samples densities, larger than expected lower estimates of density in heavy mineral rocks by the density tool and an anomalous high porosity, up to 8%, which cannot be supported by the neutron log.

The electric log was Schlumberger's 6FF40 induction log and a SP log was recorded simultaneously. The rock resistivities, as might be anticipated, were greater than 100 ohm-m and not particularly suited for logging by an induction device. The tool could not be centralized because of casing size above 1280.1m (4200 ft). Therefore, the resistivity log yields probable minimum values and very little quantitative data. The SP log exhibited characteristic shale deflections opposite clay gouge and alteration mineral assemblages in fracture and fault zones. Several short sand type deflections

may indicate permeable fractures.

The Schlumberger and Dresser Atlas gamma-ray logs were both recorded in API units and agree reasonably well. The logs showed common characteristics; acidic rocks generated higher gamma-ray counts than did the more mafic rocks. Fractures corresponded to anomalously high gamma-ray counts. Analyses indicated this response could be attributed to presence of uranium and thorium and/or their daughters.

A problem mentioned earlier, but addressed now, is the one of disagreement in recording of depth among the logs. Commonly, logs can be aligned using a point of distinct response observed across a suite of logs. In C/T-2 several such features are available for comparing the logs. The most obvious feature is the bottom of casing which Phillips Petroleum Company reported to be at 1280m (4200 ft). We have listed in Table 6.3 the casing point as seen on the various logs. Three points of distinct log response have also been picked on the various logs and listed in Table 6.3. These points are the three fault or fracture intercepts at 1453.9m (4770 ft), 1767.8m (5800 ft) and 1920.2m (6300 ft). The only accurate depths appear to be found on Schl. neutron, gamma-ray and velocity logs. All but the DA neutron seems to remain a fixed distance off throughout the hole. The DA neutron depth error appears to increase with depth from about 4.6m (15 ft) near the top of the hole to about 9.1m (30 ft) at the bottom of the hole. In the next section, various data cross plots are studied and all logs were adjusted to common depths prior to making the cross plots.

C. Cross Plots

1. Basis for Plots. A common log interpretation technique utilized by

TABLE 6-3: COMPARISON OF DEPTHS TO VARIOUS DISTINCT FEATURES AS SEEN ON THE DIFFERENT LOGS. THE DATA ILLUSTRATES THE INCONSISTENT DEPTH RECORDING AMONG THE LOGS AND TO THE TRUE DEPTH OF THE FEATURES.

Log	Casing Depth	First Fault	Second Fault	Third Fault
Reported Depth	1280m (4200 ft)	1454m (4770 ft)	1768m (5800 ft)	1920m (6300 ft)
DA Caliper	1292m (4240 ft)	---	---	---
DA Velocity (CCL)	1289m (4255 ft)	---	---	---
Schl. Velocity	1297m (4255 ft)	1451 - 1463m (4760-4800 ft)	1768-1771m (5800-5810 ft)	1914 - 1923m (6280-6310 ft)
DA Neutron	1276m (4185 ft)	1446m (4744 ft)	1762m (5780 ft)	1913m (6275 ft)
Schl. Neutron	1281m (4203 ft)	1453m (4766 ft)	1768-1771m (5799-5810 ft)	1920m (6300 ft)
DA Density	1277m (4190 ft)	1448m (4750 ft)	1762m (5780 ft)	1917m (6290 ft)
Schl. Induction/SP	---	1452m (4765 ft)	1768m (5800 ft)	---
Schl. Gamma-Ray	1281m (4203 ft)	1453m (4766 ft)	---	1919-1922m (6295-6304 ft)
DA Gamma-Ray	---	---	---	1914m (6279 ft)

log analysts in the oil and gas industry is the cross plot (Savre, 1963; Burke, et al., 1969; Poupon, et al., 1970; Pickett, 1973). Two or more sets of log data are plotted versus each other for the purpose of identifying distinct lithologies and estimating better porosity values. Very few logs, and often only in particular instances, respond to a single rock property. Hence one log may produce one set of data but two or more unknowns. To illustrate we will examine the commonly accepted response equations for the three so-called "porosity" tools, the neutron, the density and the velocity tools.

The response equations are (ϕ is porosity in each case):

$$\text{neutron:} \quad ND(\text{counts}) = C + D \log \phi_N \tag{6-5}$$

where C and D are empirical constants,

$$\text{density} \quad \rho_b = \rho_g(1 - \phi_D) + \rho_f \phi_D \tag{6-6}$$

where ρ_b and ρ_g are the bulk and grain densities, respectively and ϕ_f is the fluid density, and

$$\text{velocity:} \quad \Delta t = \Delta t_m + B \phi_V \tag{6-7}$$

where Δt and Δt_m are the interval transit time from the log and the matrix travel time (assumed constant) and B is an empirical constant.

The porosity in each case is given a subscript to indicate which log was used to compute it, N for neutron, D for density and V for velocity. The practice is to eliminate porosity from each pair of equations and a plot of the one log versus the other should yield values for the matrix constants C, D, ρ_g and Δt_m. Note that any plot involving the neutron log will be a log-log plot unless the neutron log is in porosity units. In this instance equation 6-5 simply reduces to ϕ_N. The measurement of ϕ_N is dependent on

lithology and neutron logs are commonly calibrated in limestone, sandstone and dolomite units.

These three equations are often expanded to describe several matrix components, each having a different response on the various logs (Edmundson and Raymer, 1979). The paper by Glenn and Hulen (1979) describes this expansion in the way most suitable to a study of igneous and metamorphic rocks. The neutron porosity is assumed to be composed of three parts, the pore porosity, ϕ_p, the bound water "porosity", ϕ_b, and an error term, ϕ_e, due to any number of things including calibration error. The matrix density is assumed composed of lighter, non-hydrous minerals such as quartz and feldspars which constitute the bulk of most common igneous and metamorphic rocks, heavier, non-hydrous minerals, usually metallic minerals, and heavier hydrous minerals, usually the mafic minerals, the micas, the amphiboles and chlorite. Clays, if present may be considered as either heavy or light hydrous minerals and are difficult to handle. The bound water in hydrous minerals is used to obtain a value for ϕ_b. The contribution of the various matrix minerals to the velocity equation is more complex. The increased density of the mafic minerals may produce higher velocities but if present in significant amounts and if mostly platey minerals such as chlorite and the micas, the velocity may be reduced (Glenn and Hulen, 1979b).

In any case the previous equations can be rewritten as

$$\phi_N = \phi_p + \phi_b + \phi_e \qquad (6\text{-}8)$$

where ϕ_e may be assumed to be zero, a constant or unknown and ignored.

$$\rho_b = \rho_s(1 - \phi_D - X) + \rho_f \phi_D + \rho_m X \qquad (6\text{-}9)$$

where ρ_s is the density of the non-hydrous minerals and ρ_m and X are

the density and volume fraction, respectively, of the hydrous mafic minerals.

$$\Delta t = \Delta t_s(1-X) + \Delta t_m X + B\phi_v \qquad (6\text{-}10)$$

where Δt_s and Δt_m are the travel times of the non-hydrous and hydrous mineral components in the matrix. The assumption that these components do not appreciably affect B is somewhat tenuous.

To illustrate the cross plot technique we will use a model presented by Glenn and Hulen (1979b) and we will use the neutron density cross plot as an illustration.

Many of the hydrous mafic minerals in igneous and metamorphic rocks are denser than quartz and feldspar, which are commonly the predominant mineral constituent of the rock. Hence, these minerals should contribute to the response of both the neutron porosity and bulk density tools.

To illustrate, we will use two rock compositions shown in Table 6.4.

TABLE 6.4

MINERAL	ROCK 1		ROCK 2	
	Density(gm/cc)	Vol. $\%H_2O$	Density(gm/cc)	Vol. $\%H_2O$
Non-Hydrous Silicates	2.60	0.	2.60	0.
Hydrous Mafic Minerals	3.15	8.0	2.80	30.
Water (Porosity)	1.00	100.	1.00	100.

TABLE 6-4: Two arbitrary, generalized igneous/metamorphic rock compositions.

The grids shown in Figure 6.7, 6.8, and 6.9 were constructed using these compositions and the log response equations. The grid lines with negative slopes are the usual porosity trends and each line represents a constant grain density and bound water content. The grid lines with a positive slope represent expected trends produced by varying hydrous mineral content at a constant porosity. If both porosity and hydrous mineral variations occur simultaneously, the data may plot in a very scattered fashion, a not uncommon experience. Figures 6.7 and 6.8 illustrate the effect of changing both the density and bound water content of the hydrous mafic minerals. Figure 6.9 is an expanded version of Figure 6.7 and depicts the typical density and neutron porosity ranges that occur in igneous and metamorphic rocks. Figure 6.9 illustrates the determination of true porosity, true grain density and per cent hydrous mineral for some arbitrary data point P. Note that one does not extrapolate to zero porosity and the bulk density axis at zero neutron porosity to obtain the grain density, but to the zero mafic minerals line.

The plots shown in Figures 6.7, 6.8 and 6.9 ignore any calibration effects or non-linear effects known to exist at low porosities. Most logs are recorded using limestone or sandstone calibrations. No calibrations exist for any of the variety of igneous and metamorphic rocks encountered in C/T-2 but the authors' experience suggests that most of these rocks would exhibit data trends that would fall between the limestone and sandstone calibration lines. Matrix effects are often present in the neutron response and, for example, sandstone porosity using a limestone calibration, begins at -1.5% porosity for Schlumberger's compensated neutron log. Non-linear effects are also evident, particularly at low porosities. Glenn and Hulen (1979b) showed empirically

FIGURE 6.7 Density versus Neutron Porosity Cross Plot Grid for "Rock 1" Composition in table 6.4

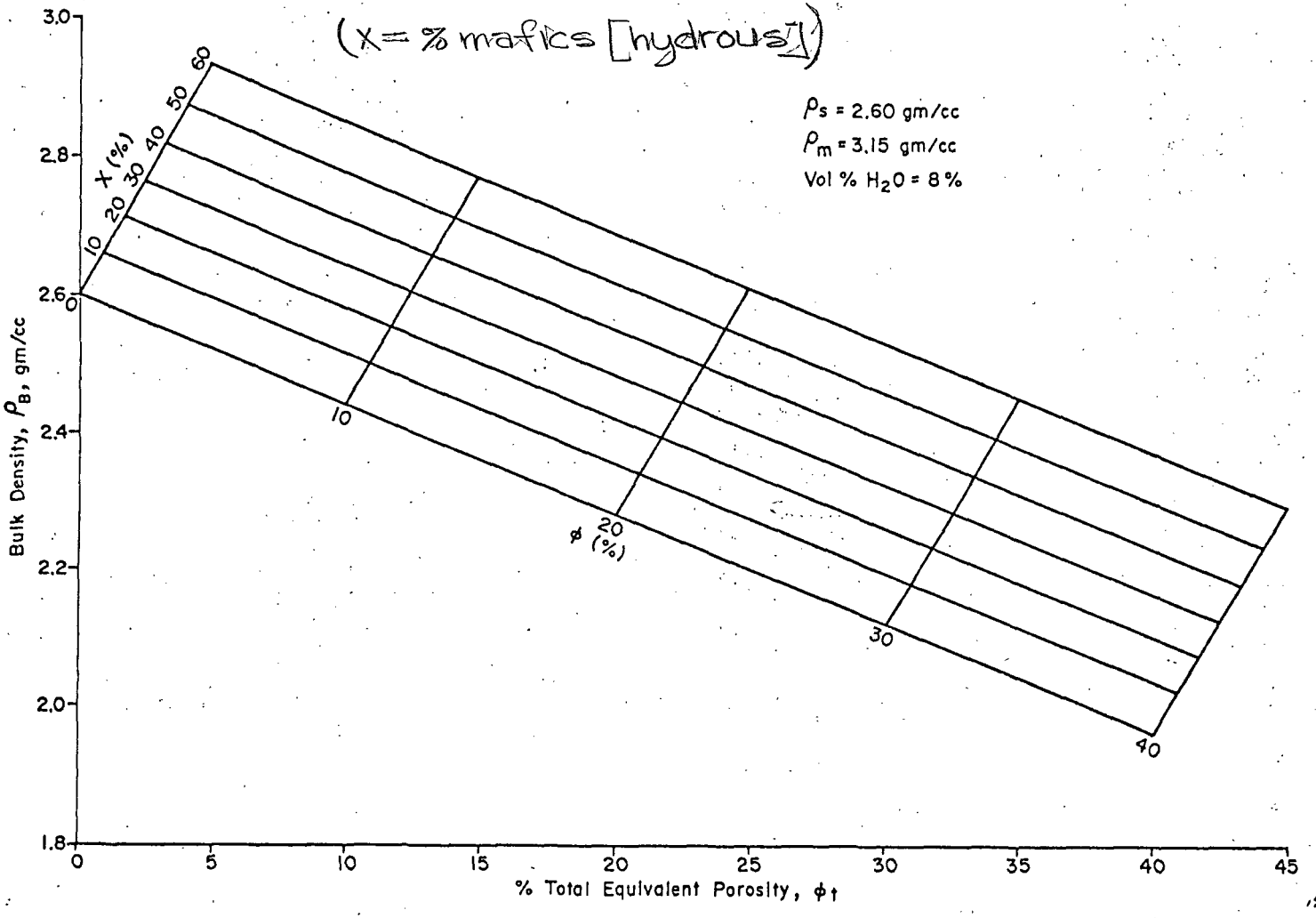

12.2

FIGURE 6.8 Density versus Neutron Porosity Cross Plot Grid for "Rock 2" Composition in Table 6.4

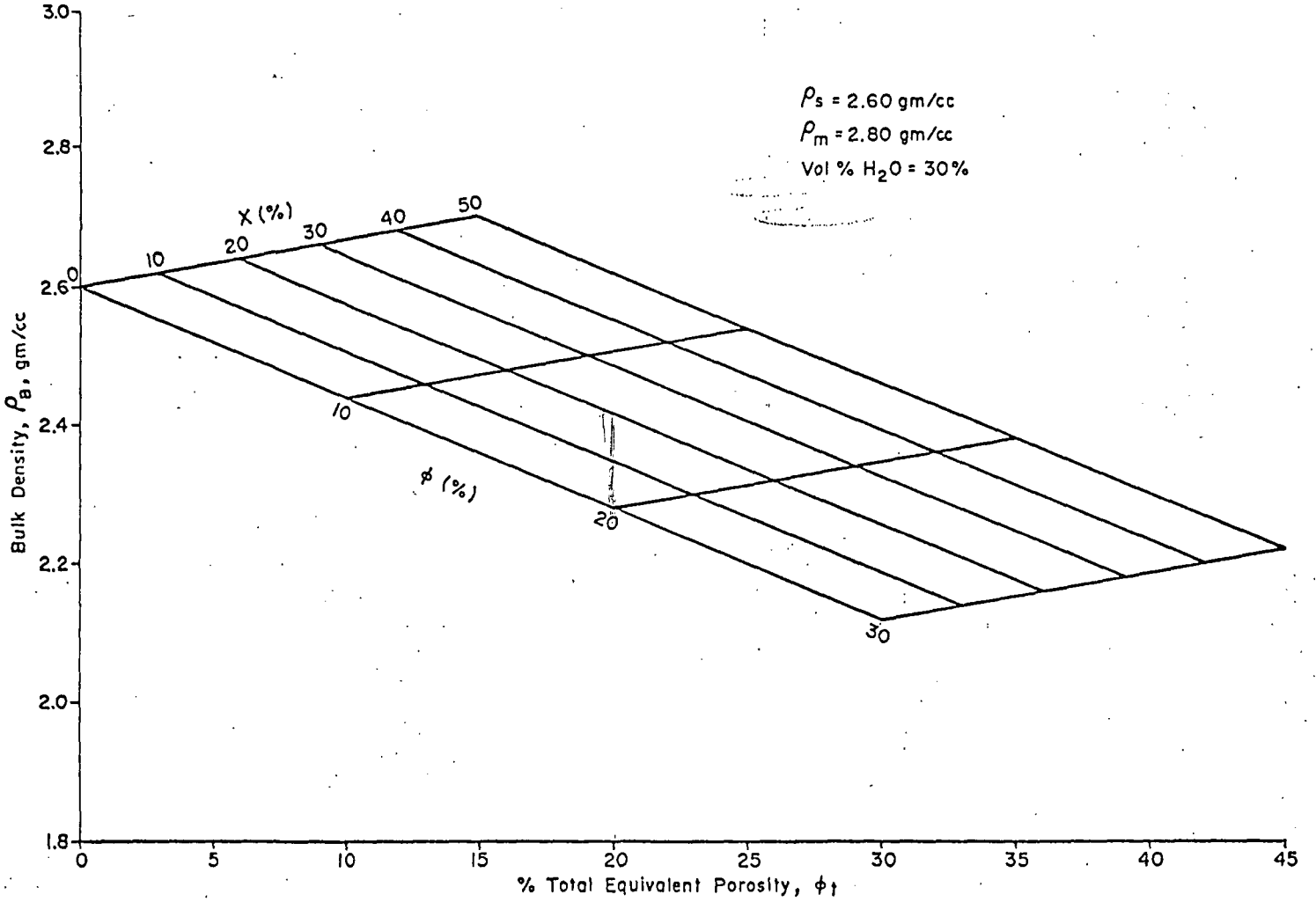

FIGURE 6.9 Expanded Scale Version of figure 6.7 (Includes a Demonstrated Use of Grid)

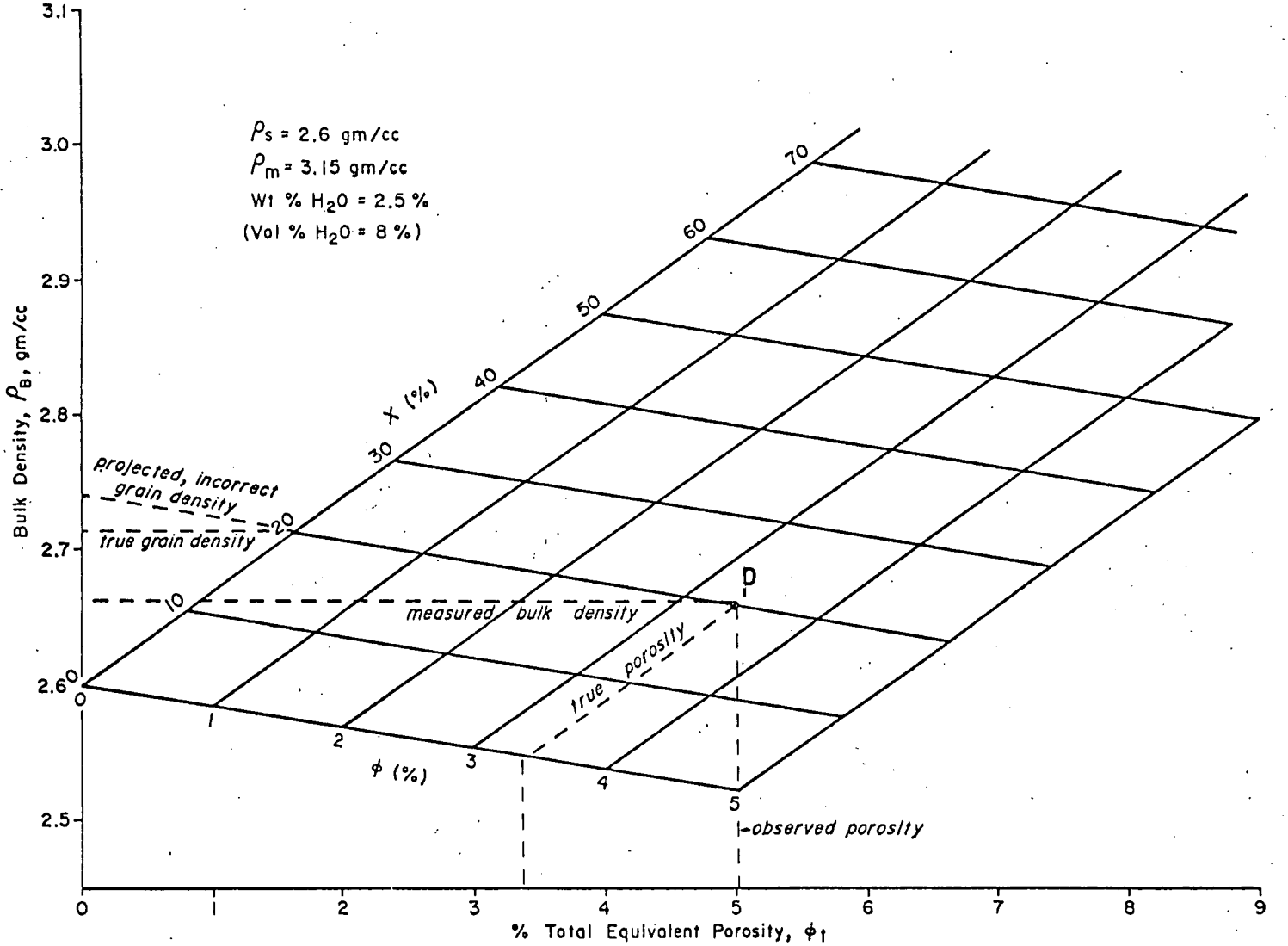

that matrix porosity for the Schlumberger CNL tool in Roosevelt Hot Springs rocks is minus one to two per cent. Edmundson and Raymer (1979) have calculated -1.0 to -2.0% porosity for feldspars and the Schlumberger neutron tools and a limestone calibration. The DA neutron tools' zeros may be -2 to -4 per cent (Dresser Atlas, 1979). Therefore, the porosity zero for C/T-2 rocks should be at least -1 to -2 per cent using a limestone calibration and approximately zero using a sandstone calibration. A limestone calibration curve was used to convert the DA neutron log data to porosity data. The densities of many heavy minerals may be underestimated 0.01 to 0.03 gm/cc by a density tool. A few minerals have errors outside this range or possibly an over estimate of density. These errors are not examined here.

Data analyses, primarily cross plots, have been made for selected open hole intervals. The intervals have been selected as representative of different log response characteristics. Only two rock types occur in the open hole interval of C/T-2 and it is not possible to study all the lithologies intersected by the drill hole.

2. Neutron-Density Cross Plots. The neutron log was shifted downhole by 6.7m (22 ft) and the density log by 3.7m (12 ft) to correct for the depth offset problem noted earlier. Three depth intervals are cross plotted in Figures 6.10, 6.11 and 6.12 and the intervals include the ones where chip samples were analyzed in detail. The values used to compute the grid in each case are included in the figures. The density and neutron porosity of water are assumed to be 1 gm/cc and 100% and the apparent neutron porosity of the non-hydrous minerals is assumed to be -2.0%.

BULK DENSITY VS NEUTRON POROSITY

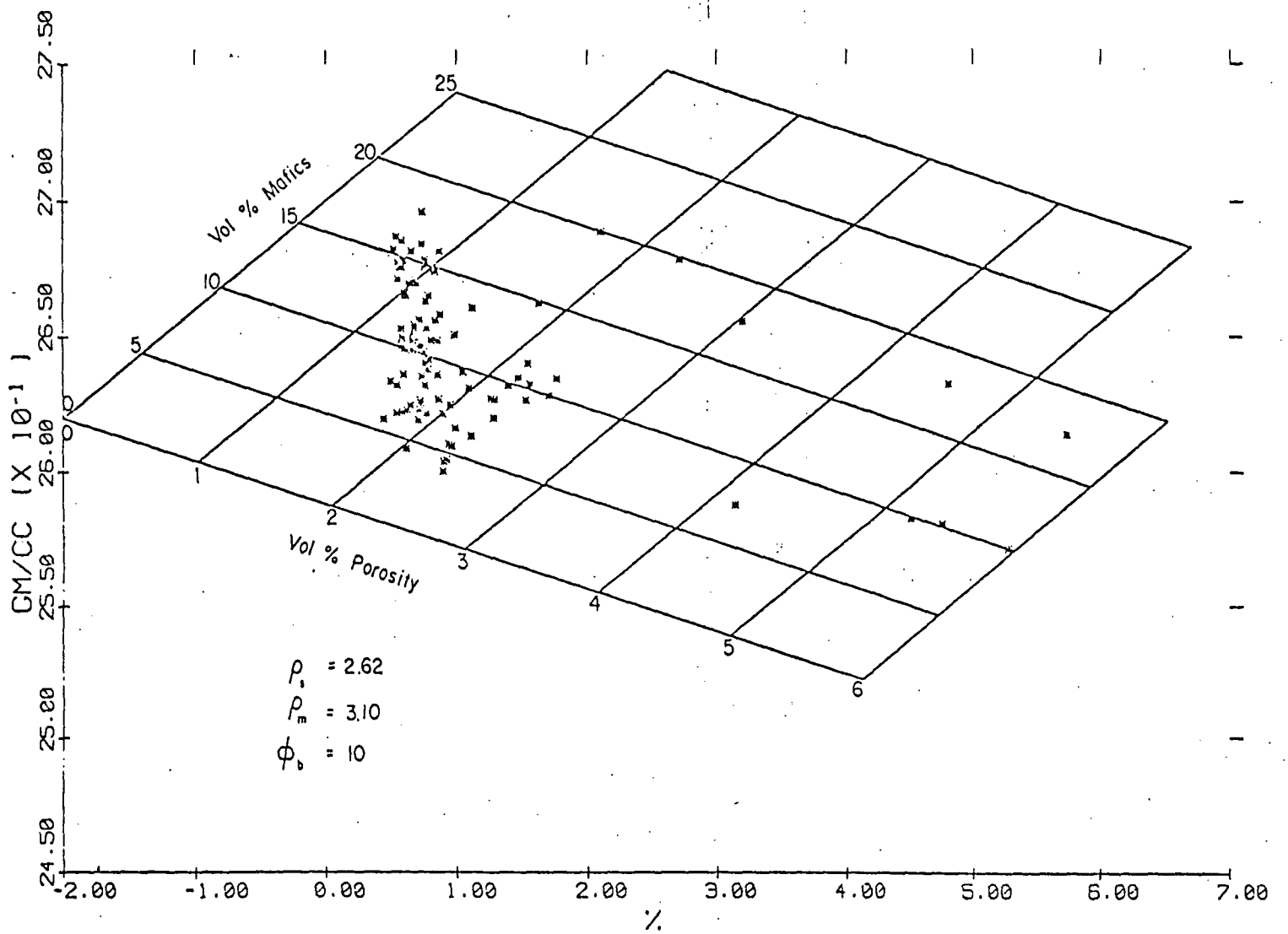

C/T-2 FIGURE 6.10

AT 5751.00 - 5949.00 FEET, 1753 - 1813 METERS
2.00 DEPTH UNIT INTERVALS, .61 METER INTERVALS

BULK DENSITY VS NEUTRON POROSITY

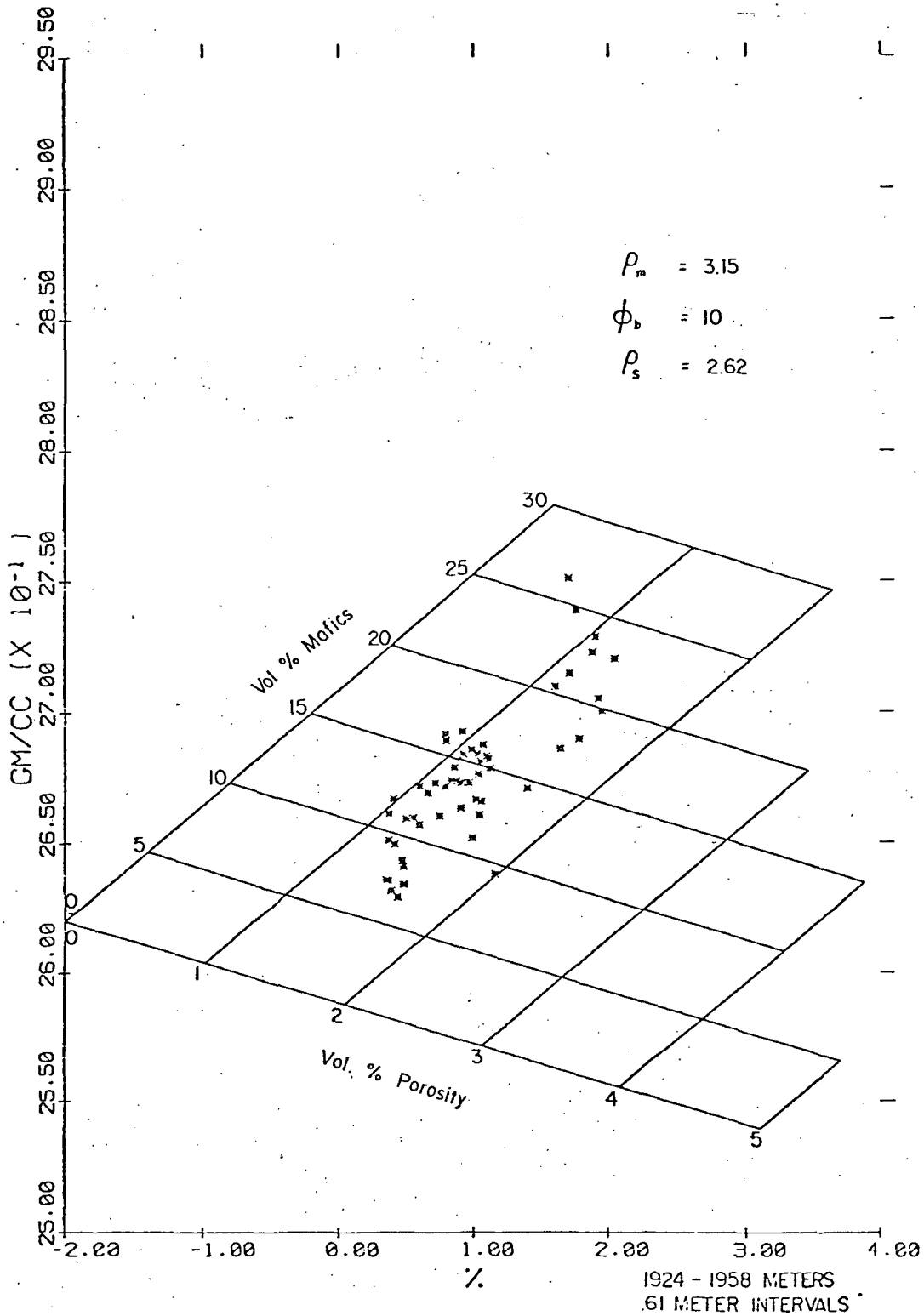

1924 - 1958 METERS
.61 METER INTERVALS
6313.00 - 6423.00 FEET
AT 2.00 DEPTH UNIT INTERVALS

C/T-2 FIGURE 6.11

BULK DENSITY VS NEUTRON POROSITY

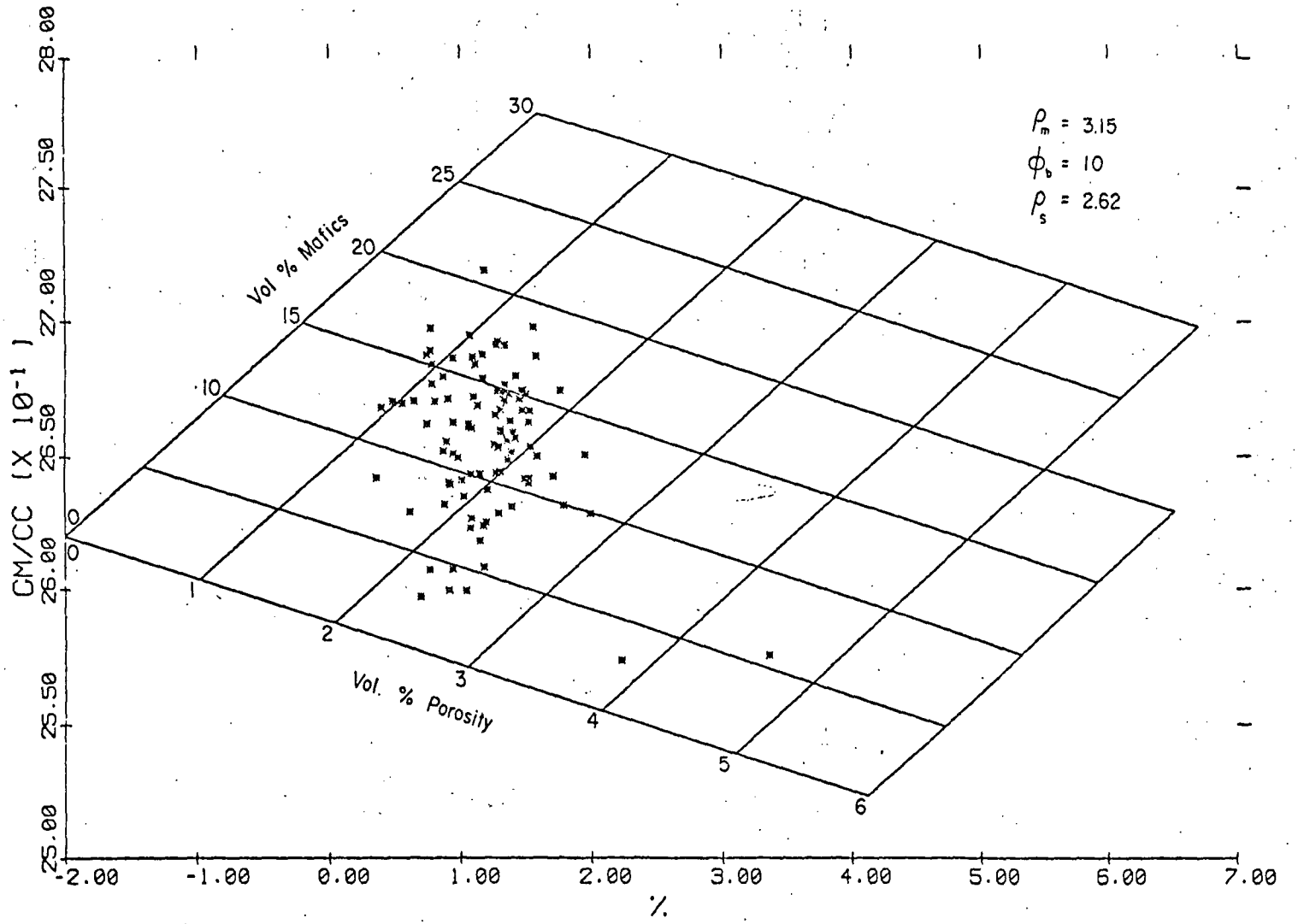

C/T-2 **FIGURE 6.12**

AT 6601.00 - 6799.00 FEET, 2012-2072 METERS
2.00 DEPTH UNIT INTERVALS, .61 METER INTERVALS

All three plots, particularly Figure 6.11, demonstrate the neutron and density measurement dependence on the mafic mineral content of the rock. The parameters used to construct the grids appear to be reasonable choices both in terms of the grids' fit the data and to the known composition of the rock. The data in Figure 6.10 follow a trend which exhibits a strong density variation and a very small neutron response. This trend arises in part, because the data interval crosses the quartz monzonite and granodiorite contact. The intervals plotted in Figure 6.11 and 6.12 are entirely within the granodiorite. The log interpretations verify the analyses shown in Table 2.1 and the differentiation of two distinct rock units. The granodiorite contains 5 to 10 percent more mafic minerals than the quartz monzonite. The data in Table 2.1 suggest a slightly higher mafic mineral content than does the log data. We have stated earlier that the chips may have been depleted in quartz and feldspar minerals due to the very fine grained state of the chip samples. The log data tend to support this conclusion.

3. Neutron-Velocity Cross Plots. The velocity log was not shifted in depth since we were not positive where true depth on this log occurred. Also, the absence of a transmitter-receiver separation precluded the construction of the commonly used neutron and velocity cross plots. Three plots, for the same intervals discussed above, are shown in Figures 6.13, 6.14, and 6.15. No clear trends are evident in the data, although both porosity and grain density affects can explain the scatter in the points. The main difference is the apparent average travel times observed between the quartz monzonite and the granodiorite, 260 microseconds for the former and 250 microseconds for the latter rock type.

TRAVEL TIME VS NEUTRON POROSITY

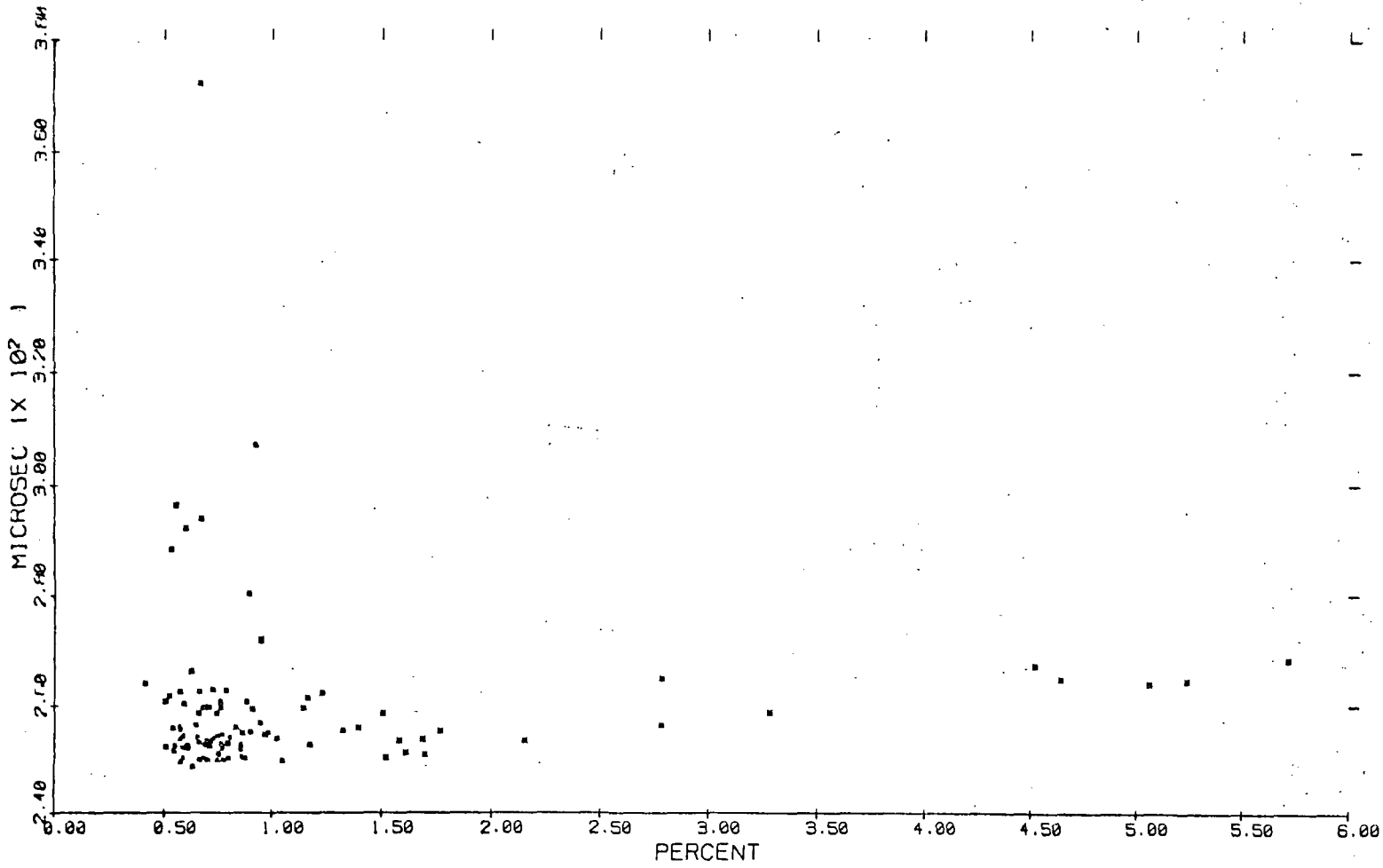

C/T 2 FIGURE 6.13

AT 5751.00 - 5949.00 FEET, 1752.9 - 1813.2 METERS
2.00 DEPTH UNIT INTERVALS, .61m INTERVALS

TRAVEL TIME VS NEUTRON POROSITY

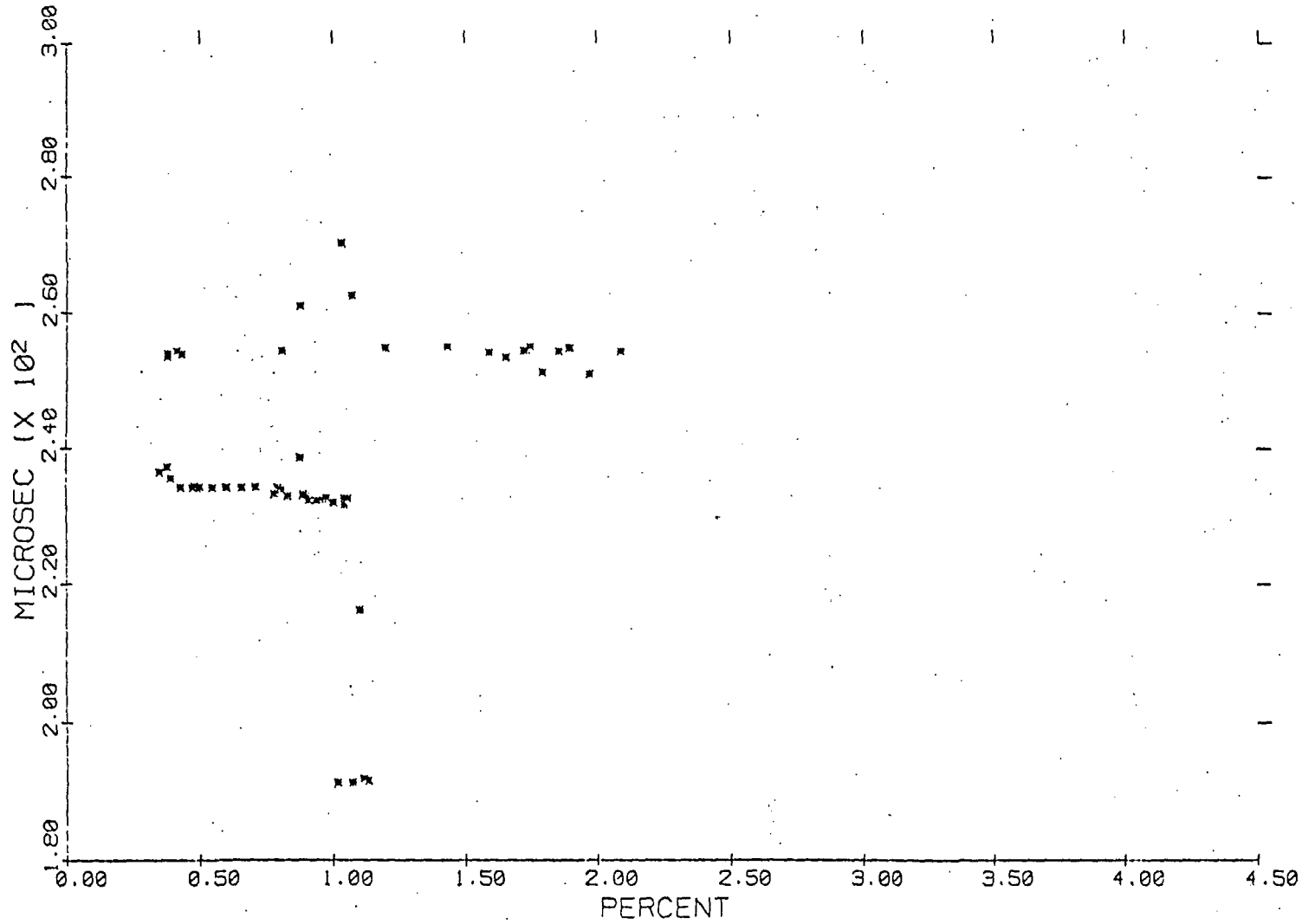

C/T FIGURE 6.14

6313.00 - 6423.00 FEET, 1924.2-1957.7 METERS
AT 2.00 DEPTH UNIT INTERVALS 1.61m INTERVALS

TRAVEL TIME VS NEUTRON POROSITY

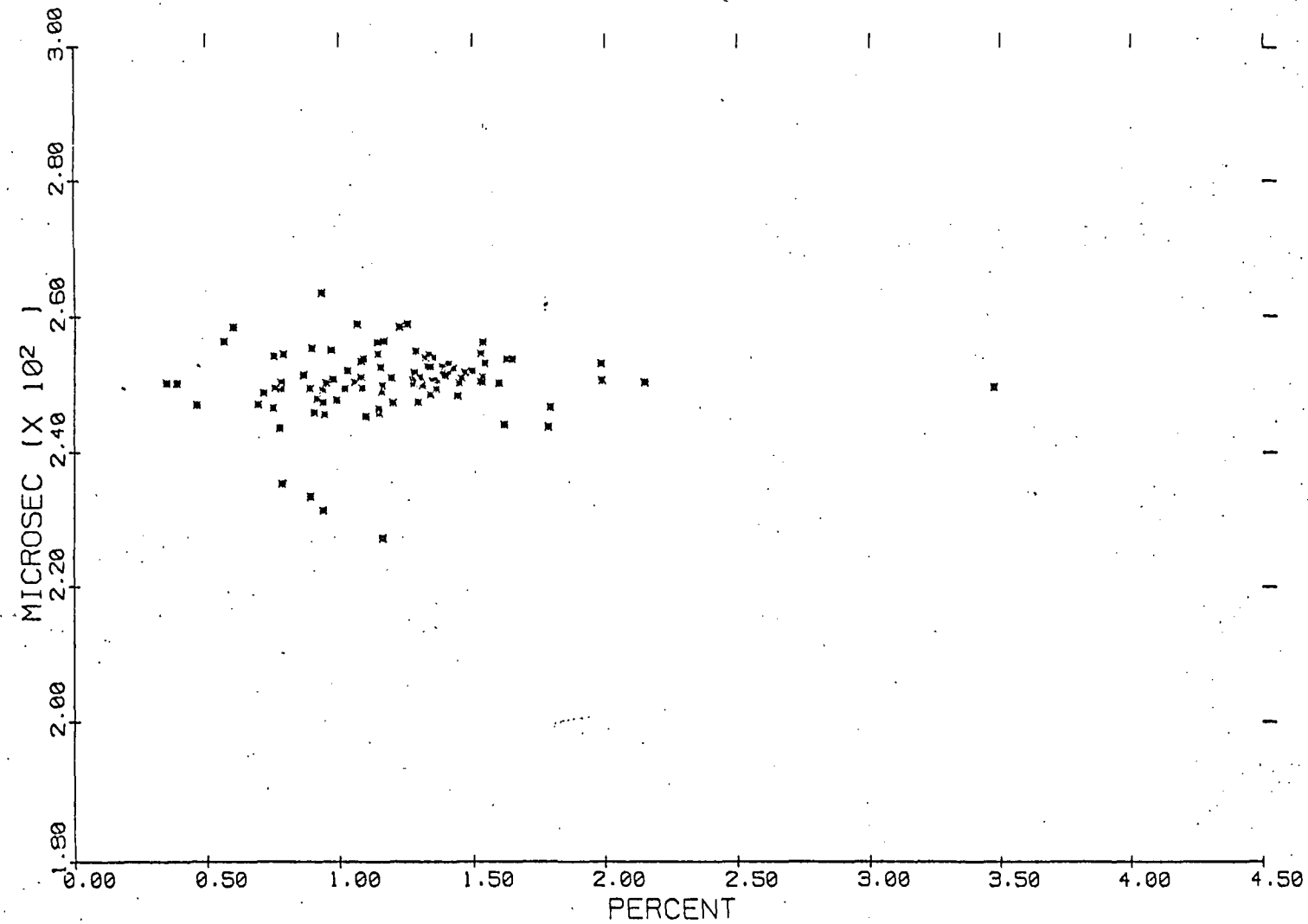

C/T 2 FIGURE 6.15

AT 6601.00 - 6799.00 FEET, 2012.0-2072.3 METERS
2.00 DEPTH UNIT INTERVALS, .61 m INTERVALS

4. Density-Velocity Cross Plots. The lack of transmitter and receiver separation again precludes construction of standard cross plots. However, the DA bulk density data are plotted versus the Schl. travel time data for the same three intervals used above. The plots are show in Figures 6.16, 6.17 and 6.18. Greater correlation exists between the travel time and the density than observed between the neutron and travel time data. The common rock property affecting both logs is probably density and density is principally related to the mafic mineral content. The density and velocity (reciprocal of travel time) are both higher in the granodiorite than in the quartz monzonite.

5. MN, AK and Z Plots. MN and Z plots are special data cross plots advocated by Schlumberger (1972, 1974) and the former is a registered trademark of that company. Dresser Atlas (1979) proposes the use of the MN plot and the AK plot which has similar properties to the MN plot.

The MN and AK plots are constructed from the neutron, density and velocity log data as follows:

$$M = \frac{\Delta t_f - \Delta t}{\rho_b - \rho_f} \times 0.01 \qquad (6\text{-}11)$$

$$N = \frac{\phi_{Nf} - \phi_N}{\rho_b - \rho_f} \qquad (6\text{-}12)$$

and

$$A = \frac{\rho_b - \rho_f}{1 - \phi_N} \qquad (6\text{-}13)$$

$$K = 0.01 \times \frac{\Delta t_f - \Delta t}{\phi_{Nf} - \phi_N} \qquad (6\text{-}14)$$

These equations are developed from the basic log response equations

TRAVEL TIME VS BULK DENSITY

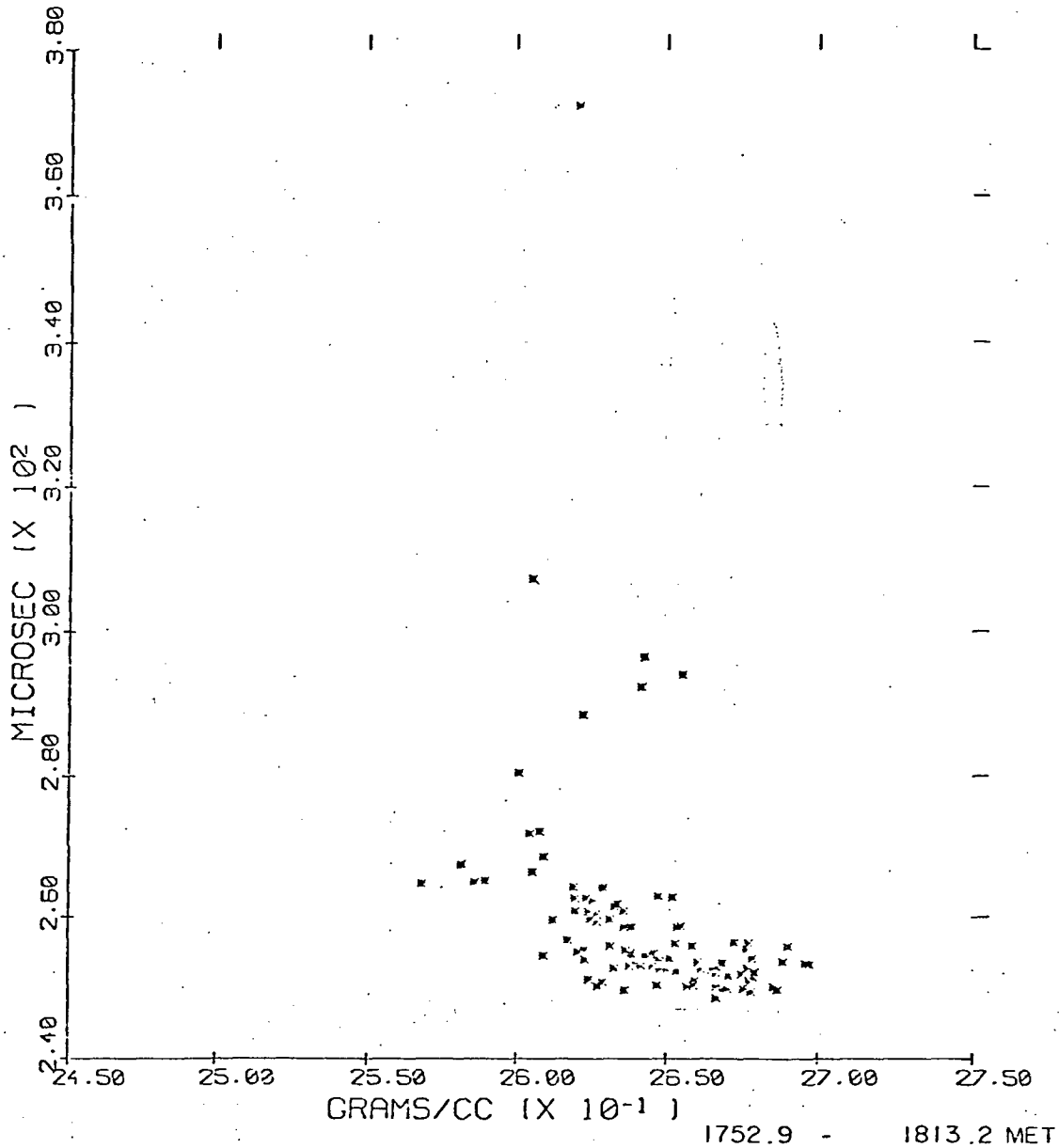

C/T 2 FIGURE 6.16

1752.9 - 1813.2 METERS
5751.00 - 5949.00 FEET
AT 2.00 DEPTH UNIT INTERVALS
.61 m. INTERVALS

TRAVEL TIME VS BULK DENSITY

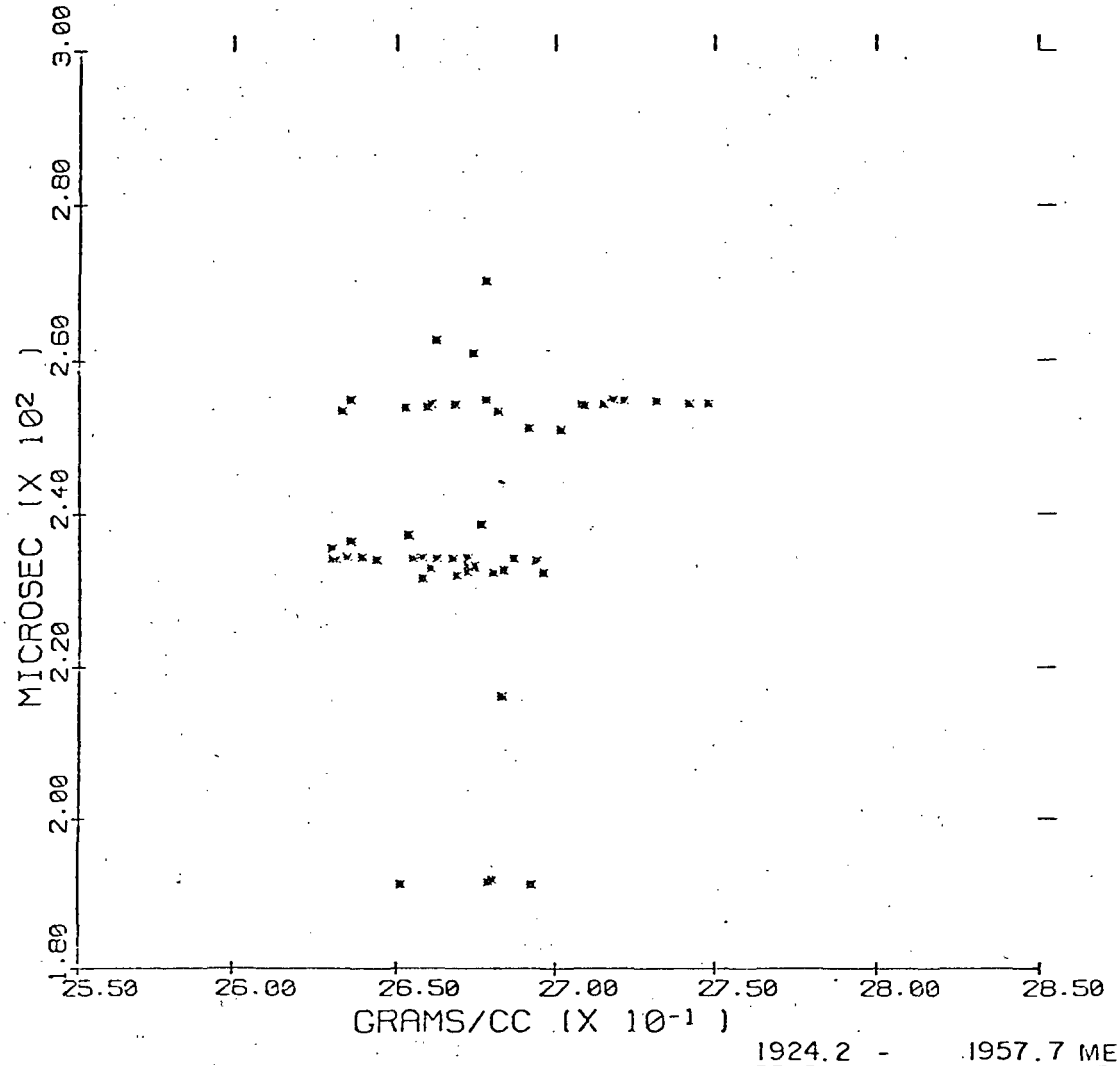

1924.2 - 1957.7 METERS
6313.00 - 6423.00 FEET
AT 2.00 DEPTH UNIT INTERVALS
.61m DEPTH UNIT INTERVALS

C/T 2 FIGURE 6.17

TRAVEL TIME VS BULK DENSITY

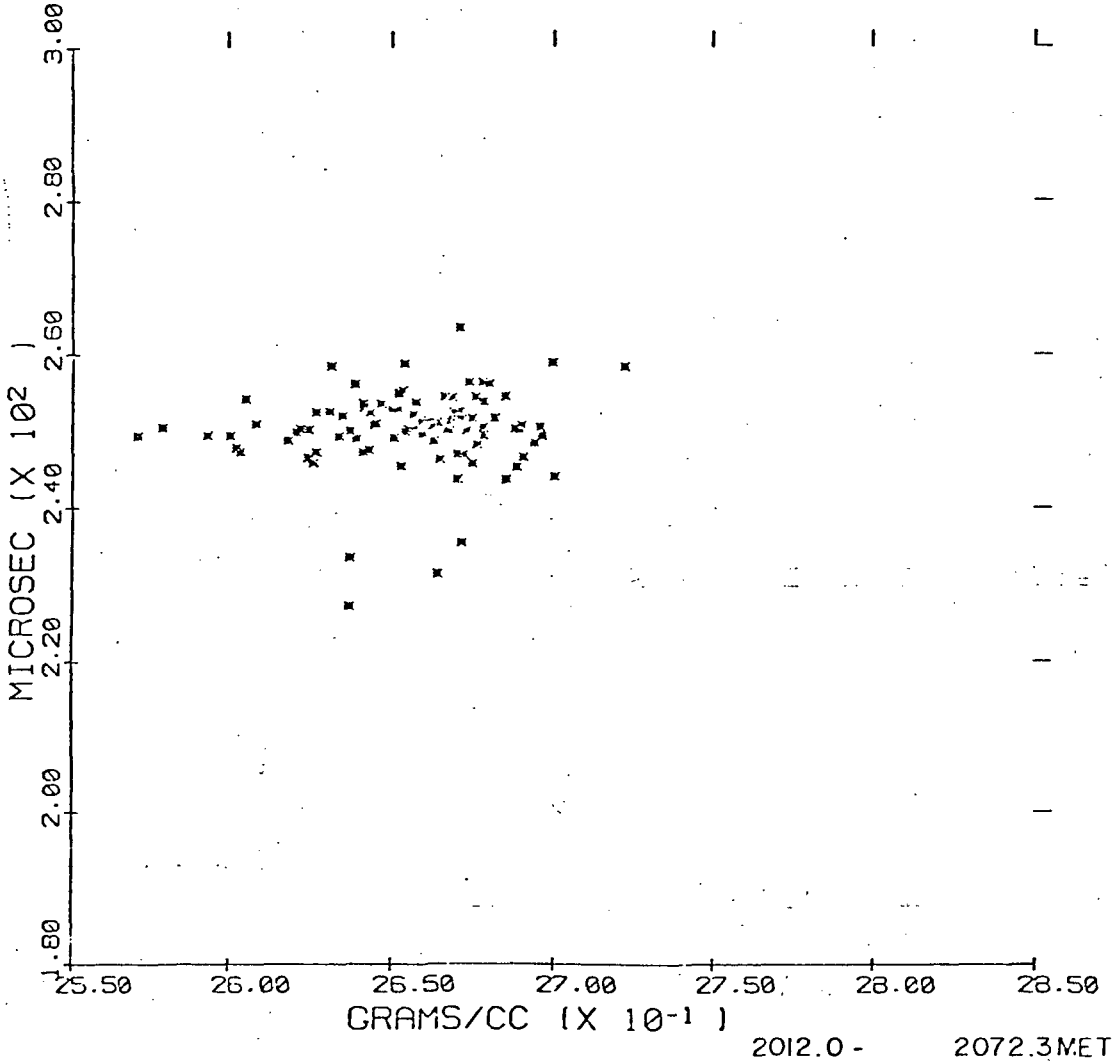

2012.0 - 2072.3 METERS
6601.00 - 6799.00 FEET
AT 2.00 DEPTH UNIT INTERVALS
.61m DEPTH UNIT INTERVALS

C/T 2 FIGURE 6.18

whereby primary porosity has been eliminated. Hence these quantities are viewed to be primarily lithology dependent. Particular rock types have characteristic pairs of MN and AK values. We did not plot either the MN or AK plot since they require interval travel time data.

The Z-plot is simply a presentation which incorporates a third set of log data into a standard cross plot. The third set of log data is plotted as a scaled value at the corresponding plot point of the other two log values. A common log plotted as the Z variable is the gamma-ray log.

The Z-plots, using the DA gamma-ray log for Z and the neutron and density cross plot, for the intervals discussed above, are shown in Figures 6.19, 6.20 and 6.21. Only the interval 1753 to 1813m (5751 to 5949 ft) exhibits any particular pattern. Highest neutron porosities correlate with gamma-ray counts between 100 and 120 API units and represented by a 4 in Figure 6.19. These data probably indicate the presence of clay minerals which contain both potassium and bound water. Clay minerals also have a range in densities consistent with the wide distribution of points indicated in Figure 6.19.

6. Gamma-ray Cross Plots. The DA gamma-ray data have been plotted versus both density and neutron data for all three intervals and the plots are shown in Figures 6.22, 6.23 and 6.24.

In the 1752.9-1813.2m (5751-5949 ft) interval the gamma-ray and bulk density data appear to be better correlated than the neutron and gamma-ray data (Figures 6.22a and 6.22b). The only neutron and gamma-ray correlation is the one at higher neutron porosities previously noted on the Z-plot (Figure 6.19). Remember that this interval crosses the quartz monzonite and granodiorite contact. The higher gamma-ray and lower density values reflect

BULK DENSITY VS NEUTRON POROSITY

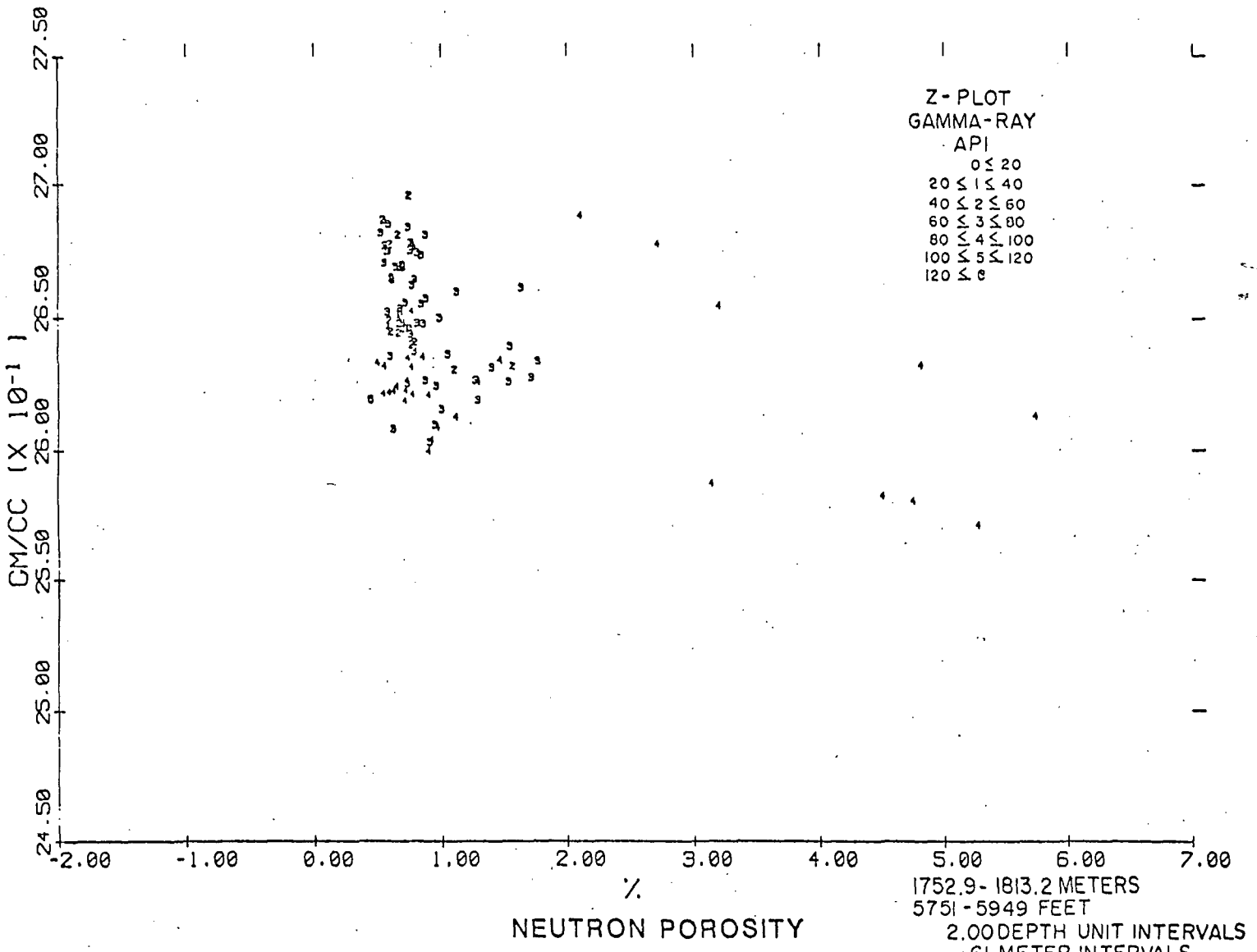

C/T-2 FIGURE 6.19

BULK DENSITY VS NEUTRON POROSITY

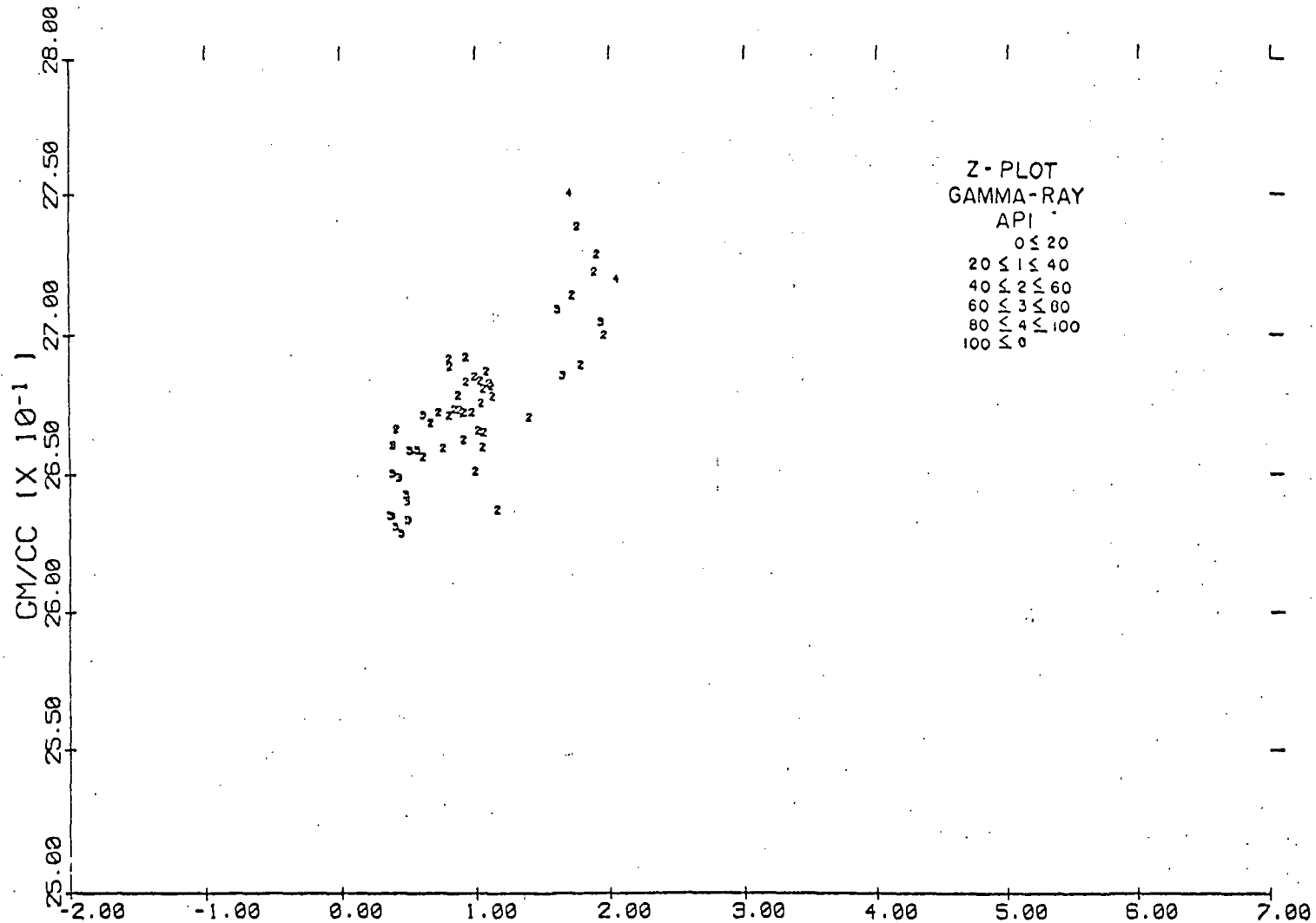

CT/2 FIGURE 6.20

BULK DENSITY VS NEUTRON POROSITY

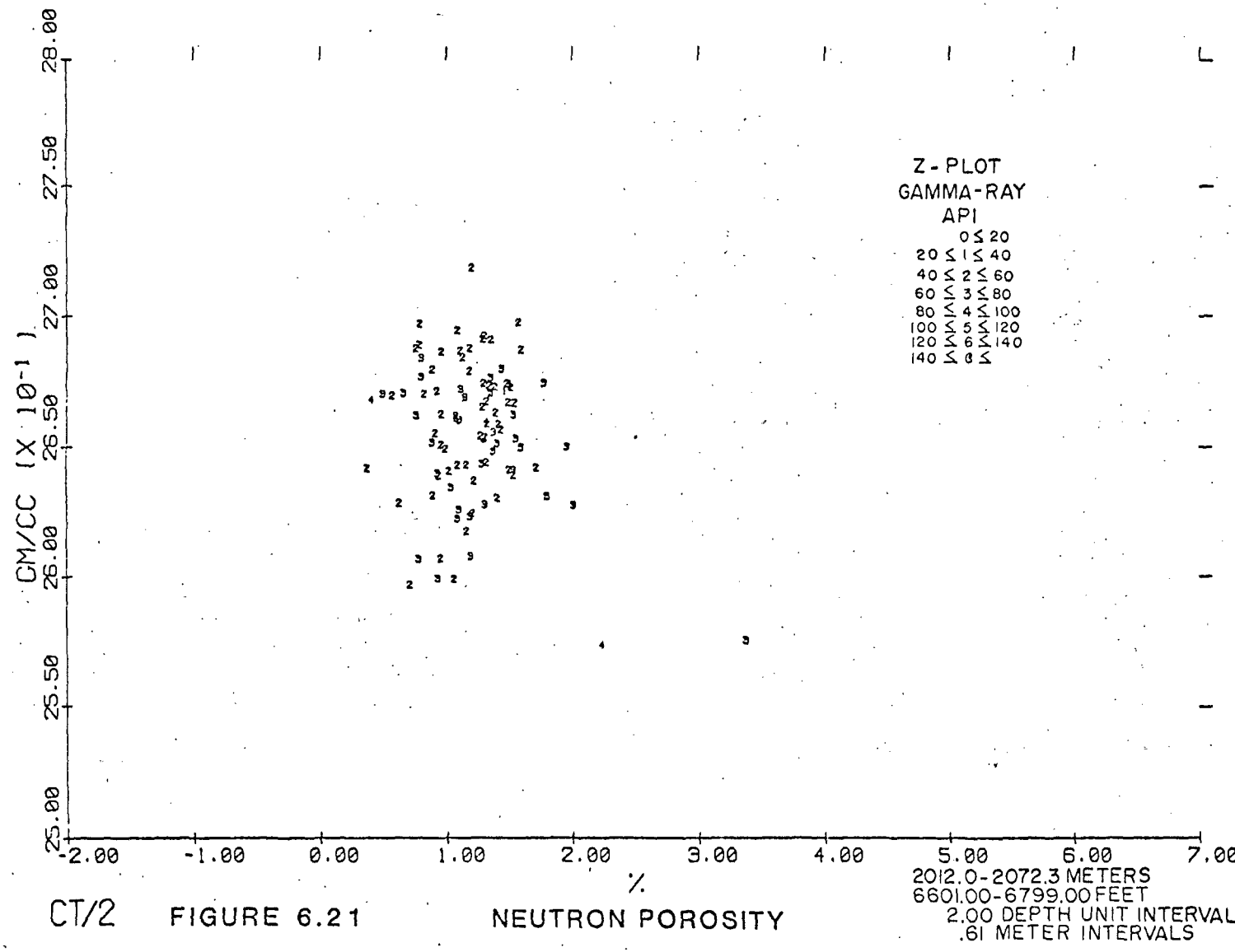

CT/2 FIGURE 6.21

GAMMA RAY VS NEUTRON POROSITY

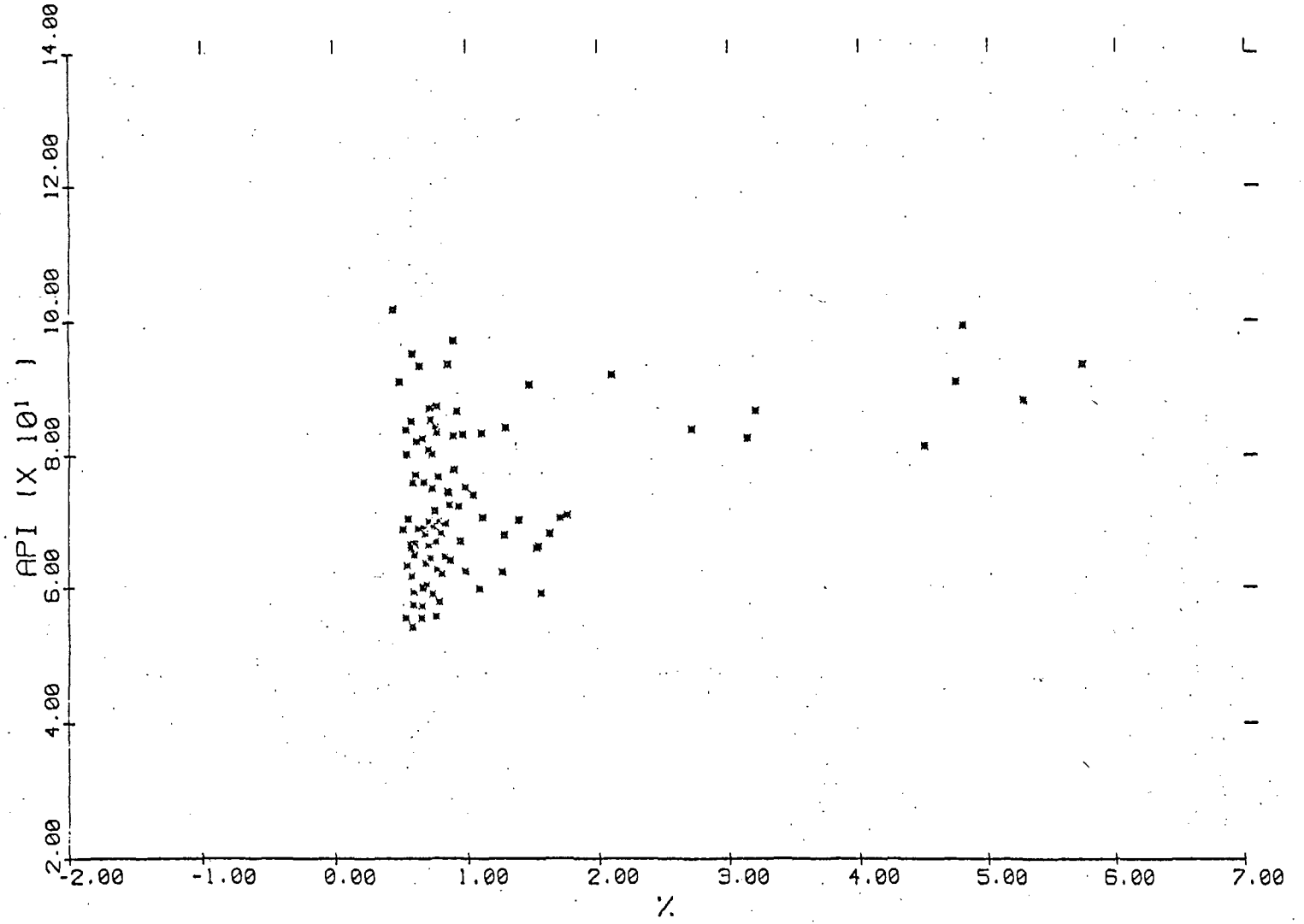

C/T-2 FIGURE 6.22a

5751.00 — 5949.00 FEET, 1753.9 - 1813.3 METERS
AT 2.00 DEPTH UNIT INTERVALS, .61 METER INTERVALS

GAMMA RAY VS. BULK DENSITY

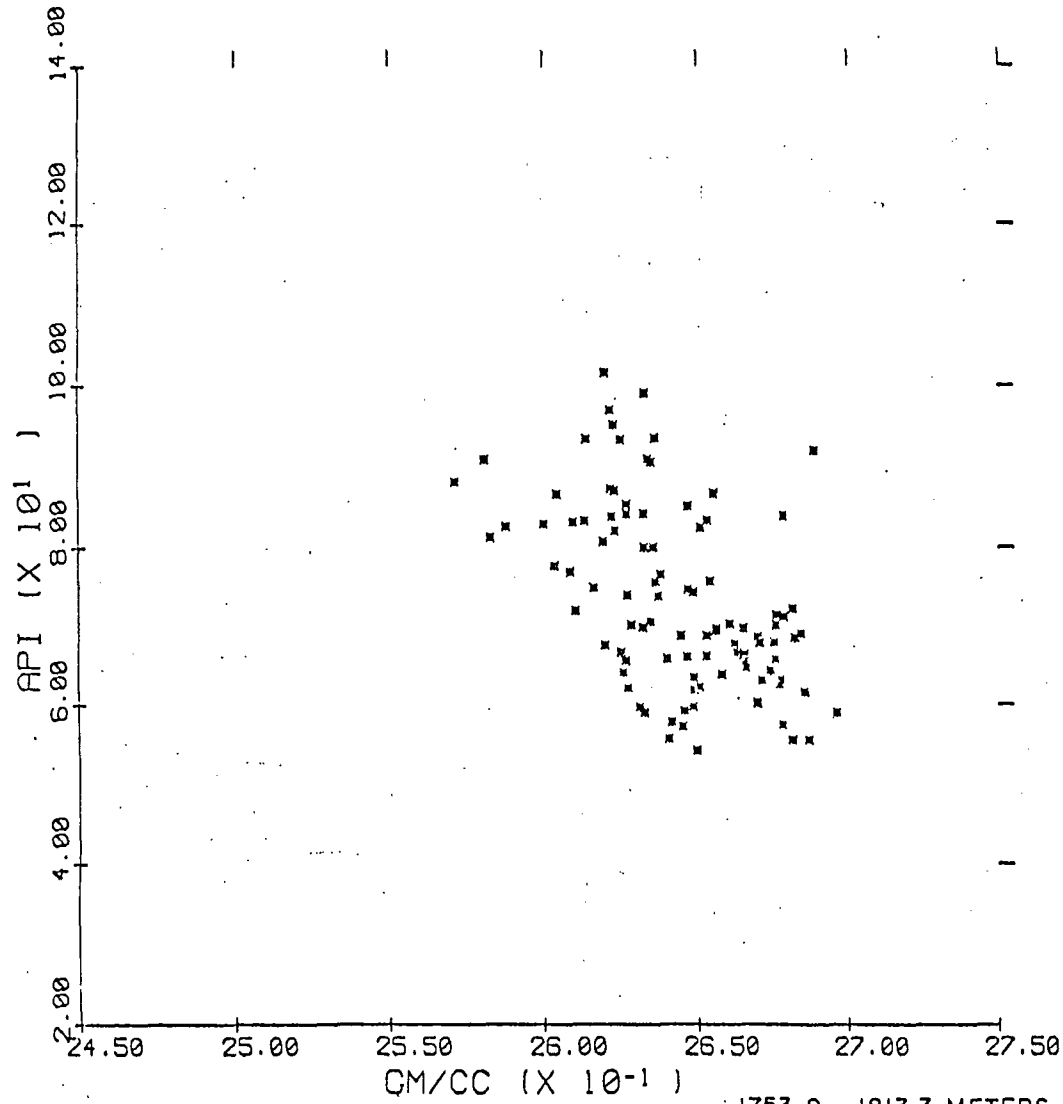

1753.9 - 1813.3 METERS
5751.00 - 5949.00 FEET
AT 2.00 DEPTH UNIT INTERVALS
.61 METER INTERVALS

C/T-2 FIGURE 6.22b

GAMMA-RAY VS. NEUTRON POROSITY

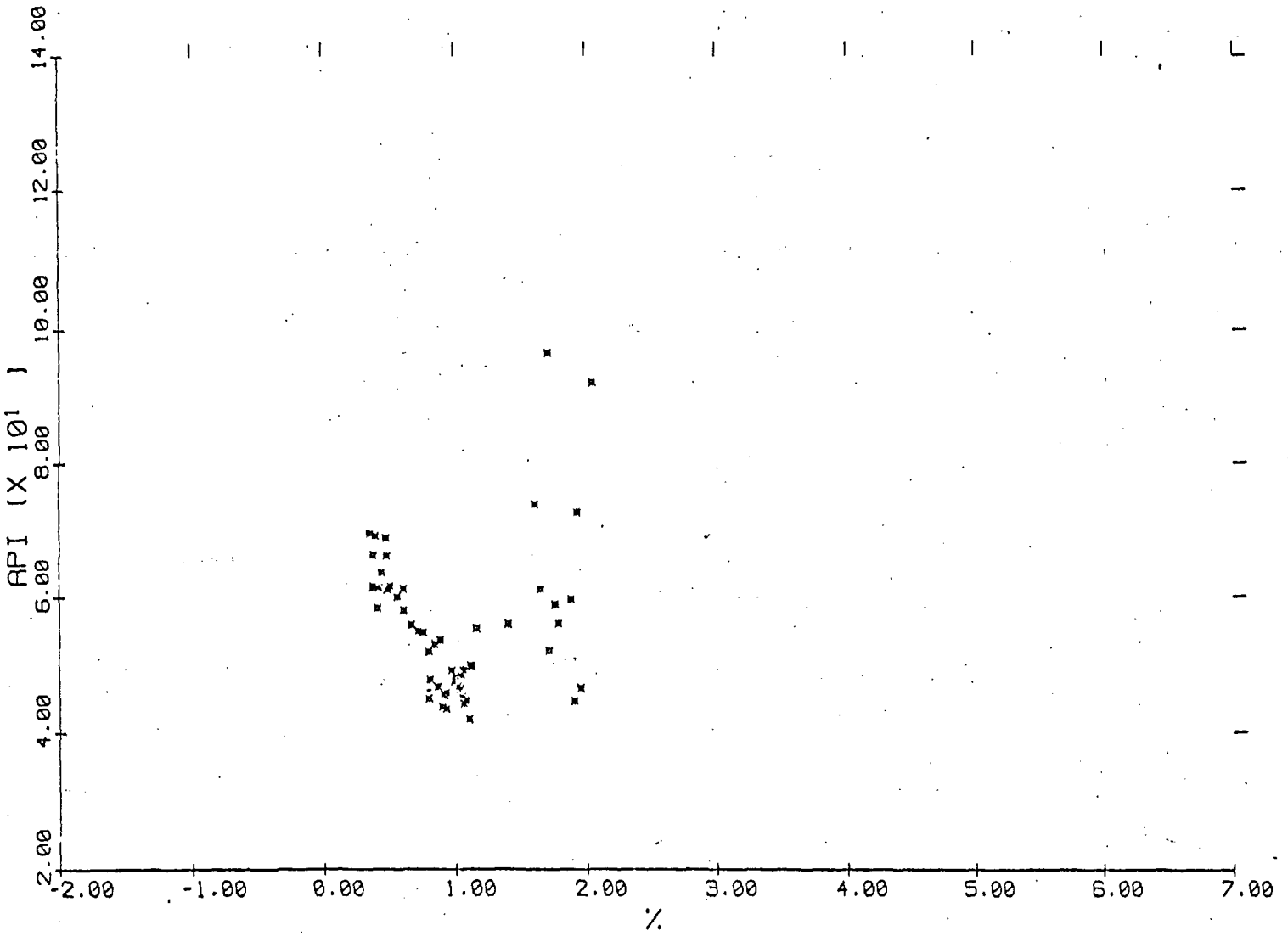

1924.2 - 1957.7 METERS
6313.00 - 6423.00 FEET
AT 2.00 DEPTH UNIT INTERVALS
.61 METER INTERVALS

C/T-2 FIGURE 6.23a

GAMMA-RAY VS BULK DENSITY

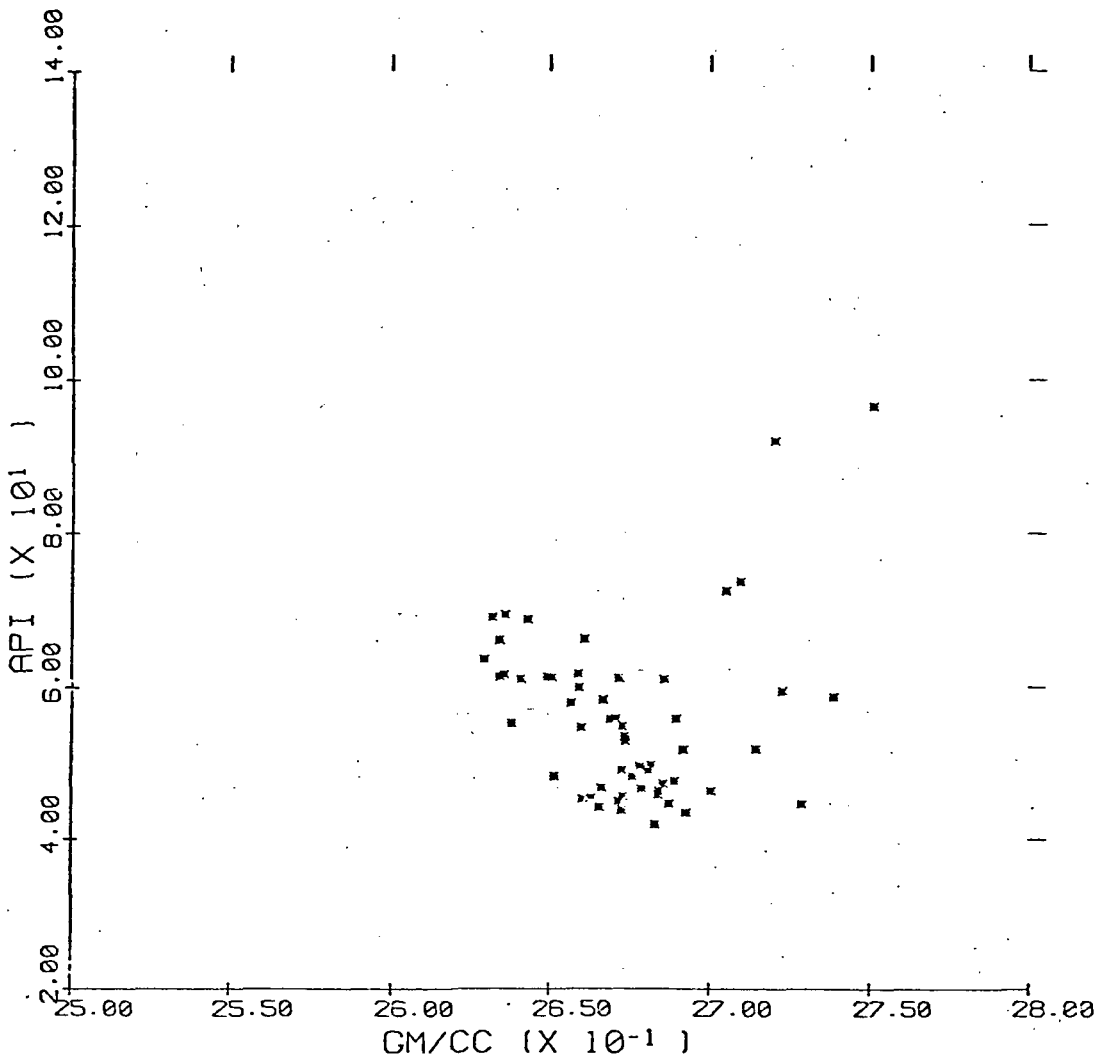

C/T-2 FIGURE 6.23b

1924.2 - 1957.7 METERS
6313.00 - 6423.00 FEET
AT 2.00 DEPTH UNIT INTERVALS
.61 METER INTERVALS

GAMMA RAY VS NEUTRON POROSITY

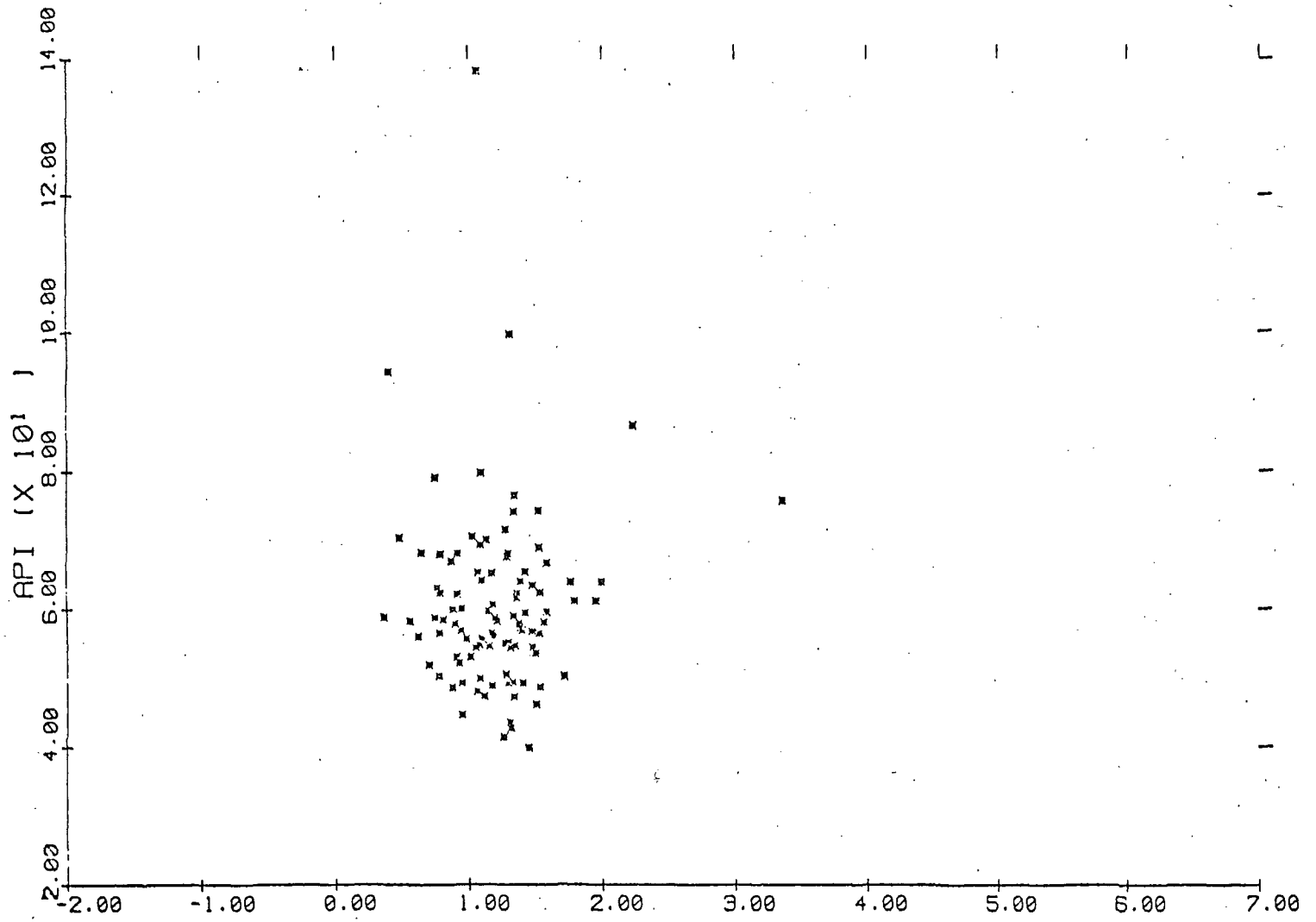

2012.0 - 2072.3 METERS
6601.00 - 6799.00 FEET
AT 2.00 DEPTH UNIT INTERVALS
.61 METER INTERVALS

C/T-2 FIGURE 6.24a

BULK DENSITY VS GAMMA RAY

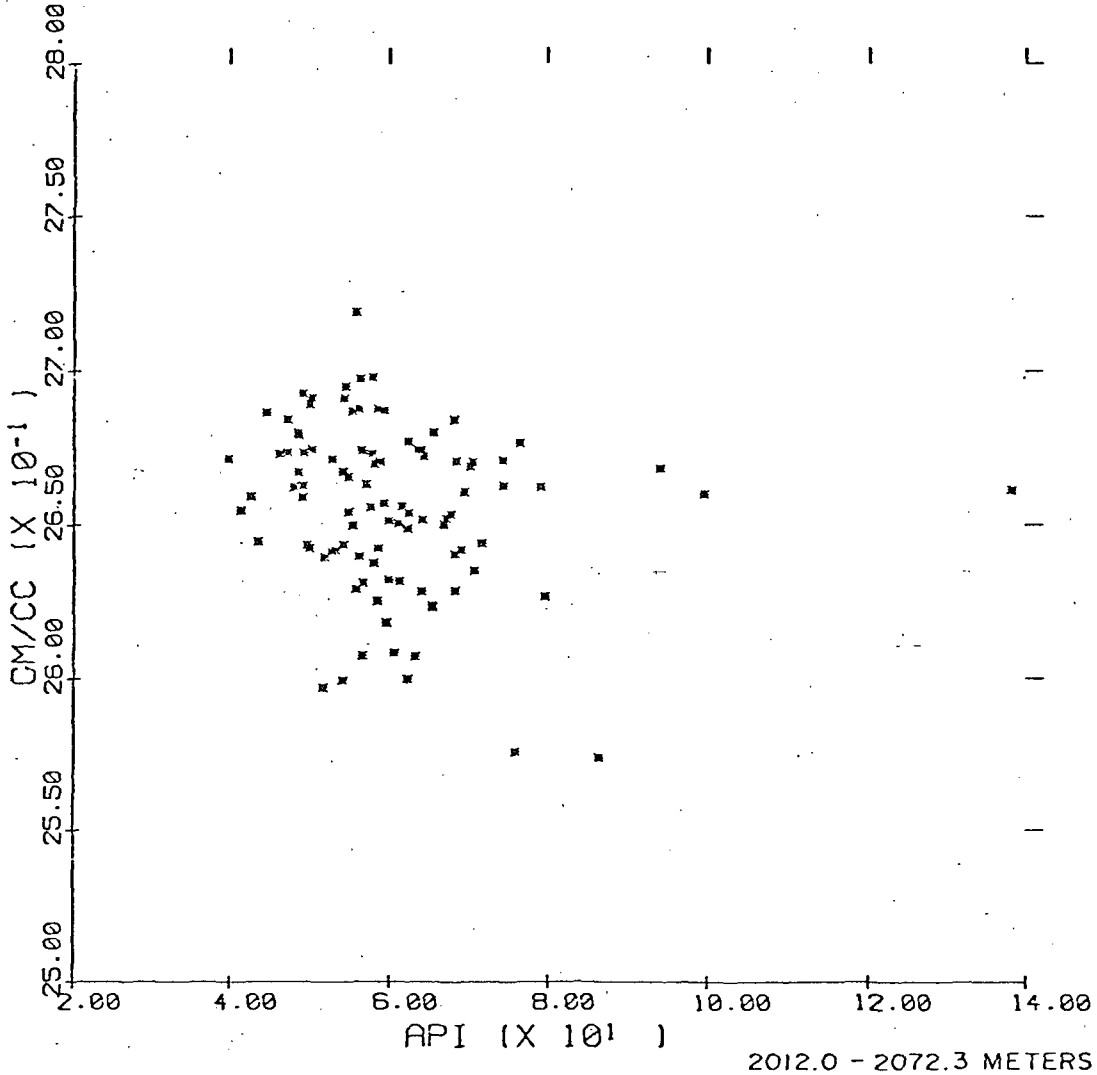

C/T-2 FIGURE 6.24b

2012.0 - 2072.3 METERS
AT 6601.00 - 6799.00 FEET
2.00 DEPTH UNIT INTERVALS
.61 METER INTERVALS

the greater amount of potassium feldspar and lower amount of heavier mafics in the quartz monzonite.

In the 1924.2-1957.7m (6313-6423 ft) interval the gamma-ray data are highly correlated to both bulk density and neutron porosity data. Increasing gamma-ray counts (API units) correspond to lower neutron porosity and lower bulk density. This result is consistent with the conclusions made for the 1752.9-1813.2m (5751-5949 ft) interval. The potassium variation (gamma-ray log) is due primarily to potassium feldspar variations. Potassium feldspar has a density between 2.55 and 2.62 gm/cc and is non-hydrous. The higher neutron porosity, higher density and lower gamma-ray reflect the decreasing K-feldspar content and increasing amounts of hydrous, lower potassium minerals, the mafic minerals.

The third interval, 2012.0-2072.3m (6601-6799 ft), exhibits similar, although less compact, trends to the above interval. The relationships are those already described.

7. Log Data-Chemical Data Cross Plots. Various cross plots were constructed between density, neutron and gamma-ray logs and K_2O, Fe_2O_3, MgO, Li and Loss data where Loss is assumed to be water lost during fusion of the sample. The most interesting plots are presented here. The same three intervals studied above are used except only those portions of the intervals that have chemical data are plotted. The log data were averaged on 3.1m (10 ft) intervals to correspond to the chip sample length used for the chemical analyses.

The three interval plots of K_2O versus gamma-ray data are shown in Figures 6.25, 6.26 and 6.27. With few exceptions, mostly in the deepest

K2 O VS GAMMA

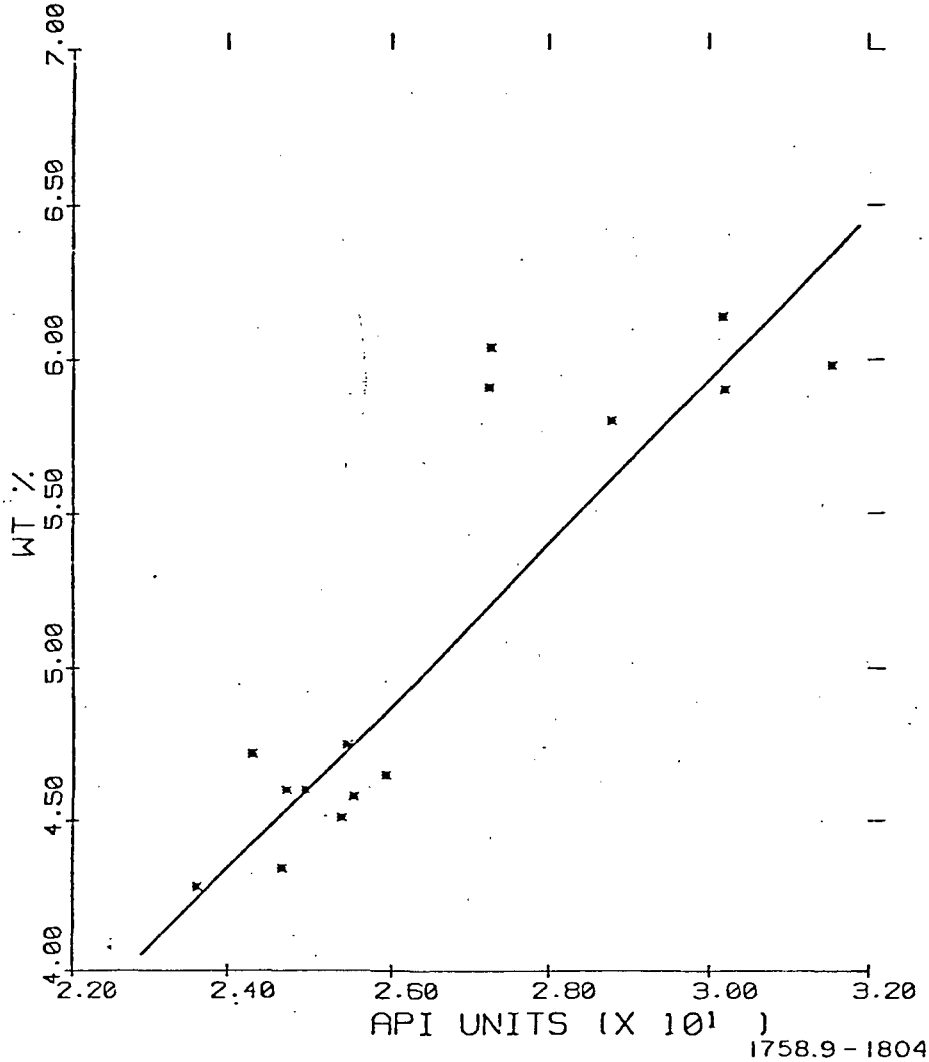

1758.9 - 1804.4 METERS
5770.00 - 5920.00 FEET
AT 10.00 DEPTH UNIT INTERVALS
3.1 METER INTERVALS

C/T 2 FIGURE 6.25

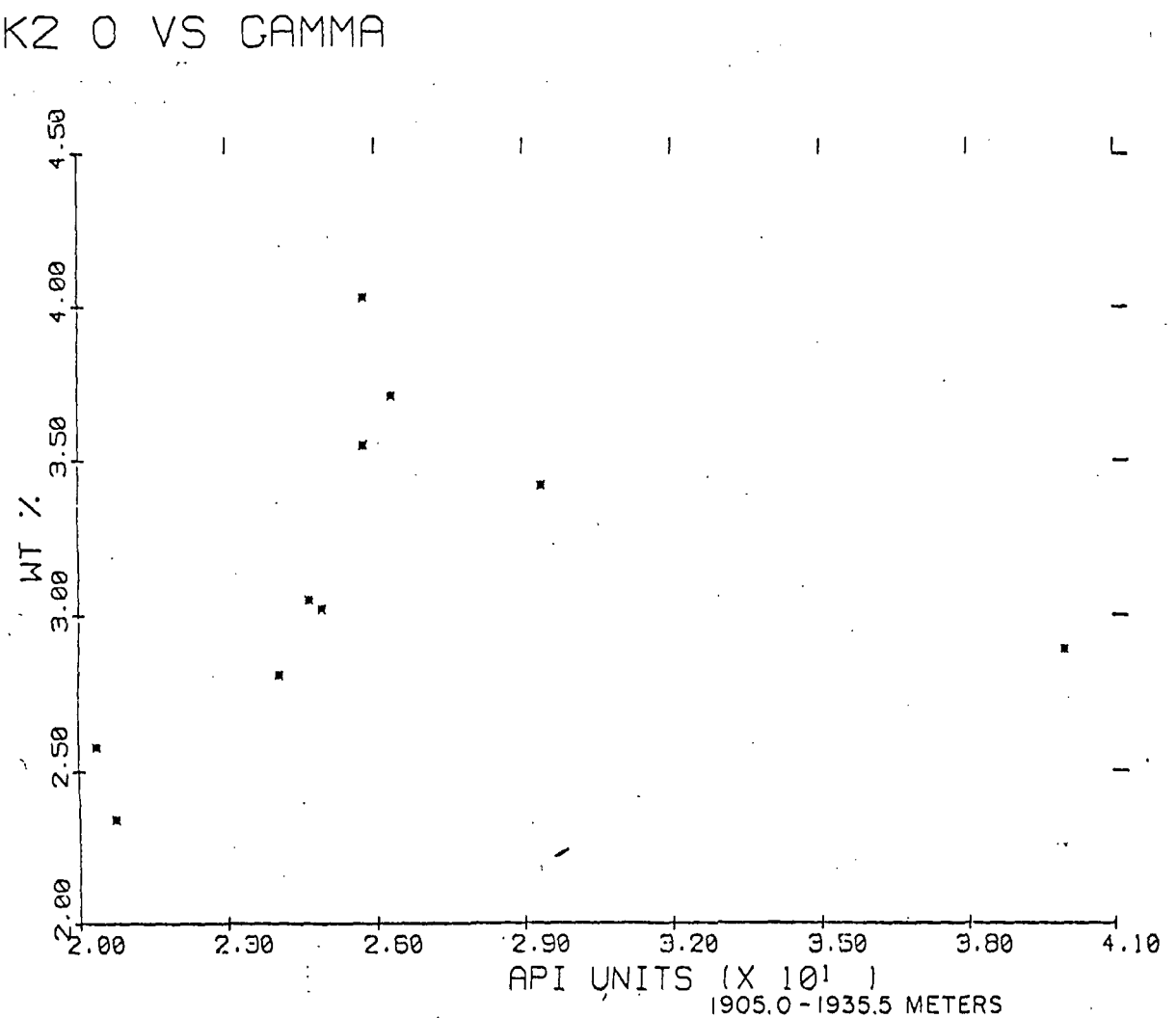

1905.0 - 1935.5 METERS
6250.00 - 6350.00 FEET
AT 10.00 DEPTH UNIT INTERVALS
3.1 METER INTERVALS

C/T 2 FIGURE 6.26

K2 O VS GAMMA

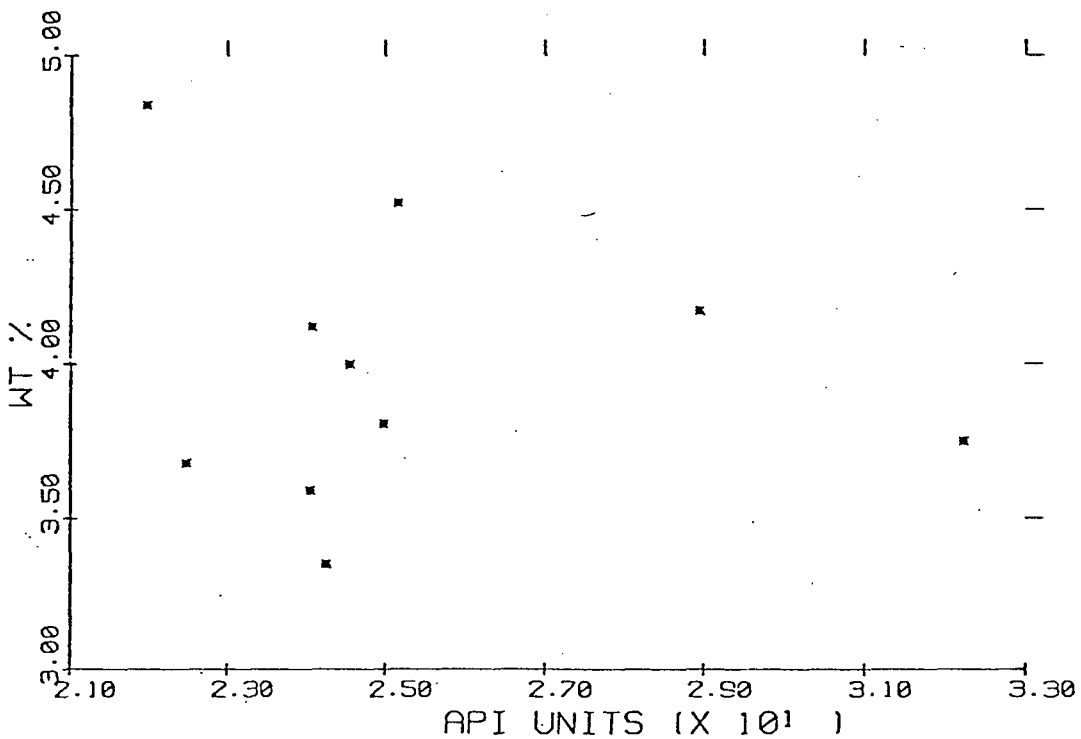

2023.8 - 2057.4 METERS
6640.00 - 6750.20 FEET
AT 10.00 DEPTH UNIT INTERVALS
3.1 METER INTERVALS

C/T 2 FIGURE 6.27

interval, the gamma-ray and K_2O data correlate quite well. This correlation has been used for lithologic identification in mineralized igneous rocks using well logs (Glenn and Nelson, 1977). We will show later that in three short intervals, believed to be fracture or fault intercepts, the gamma-ray response is partly due to uranium and thorium and/or their daughters.

The bulk density log data were plotted versus Fe_2O_3 and MgO data and good correlation was evident between the log data and both substances. Therefore plots were made between the logs and a sum of Fe_2O and MgO. These plots are shown in Figures 6.28, 6.29 and 6.30. Both Fe_2O_3 and MgO are largely in the mafic minerals. Some iron, although reported as Fe_2O_3, is in magnetite as Fe_3O_4. In either case, the correlation between density and Fe_2O_3 and MgO is expected.

Lithium was also plotted versus the gamma-ray data and exhibits a good correlation which suggests the lithium is in the potassium feldspar. It can also occur in the mica lepidolite.

Neutron porosity data were plotted versus the Loss observed in the chemical analyses (Figures 6.31, and 6.32). The Loss is assumed to be largely water, both pore and bound. Since the analyses were done on chips, the water loss is primarily bound water. Although the correlation is not particularly good, the level of loss indicates enough bound water is present to explain most of the neutron response.

Two plots of chemical data are shown in Plates III and IV at 12m/cm (100 ft/in). These plots enable one to make a direct comparison of the chemical data to the log data in Plate II. Only data that have demonstrated some correlation have been included in the plots.

FE2 03 + MG 0 VS BULK DENSITY

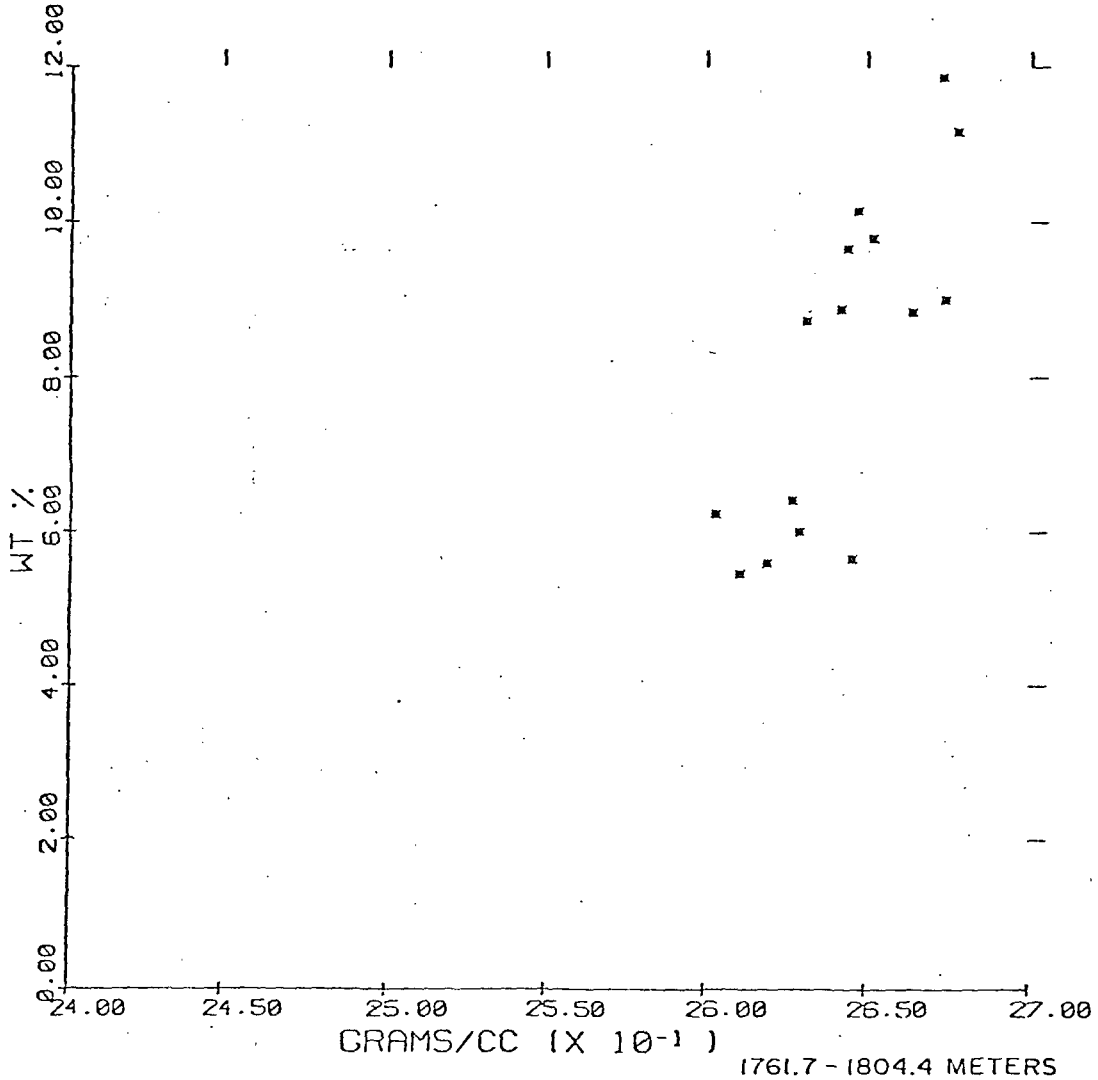

C/T 2 FIGURE 6.28

AT 1761.7 - 1804.4 METERS
5780.00 - 5920.00 FEET
10.00 DEPTH UNIT INTERVALS
3.1 METER INTERVALS

FE2 03 + MG O VS BULK DENSITY

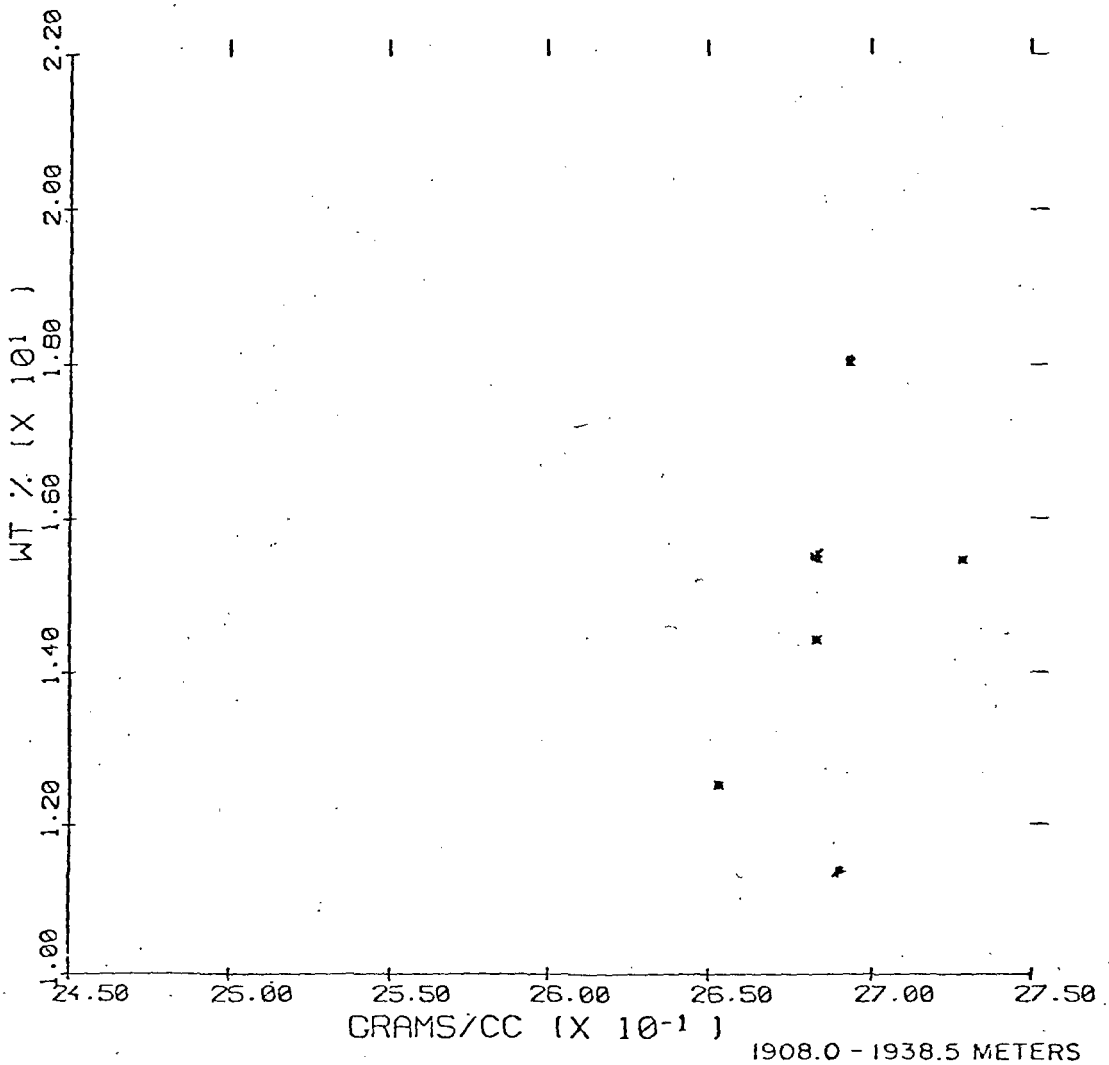

C/T 2 FIGURE 6.29

AT 1908.0 - 1938.5 METERS
6260.00 - 6360.00 FEET
10.00 DEPTH UNIT INTERVALS
3.1 METER INTERVALS

FE2 03 + MG O VS BULK DENSITY

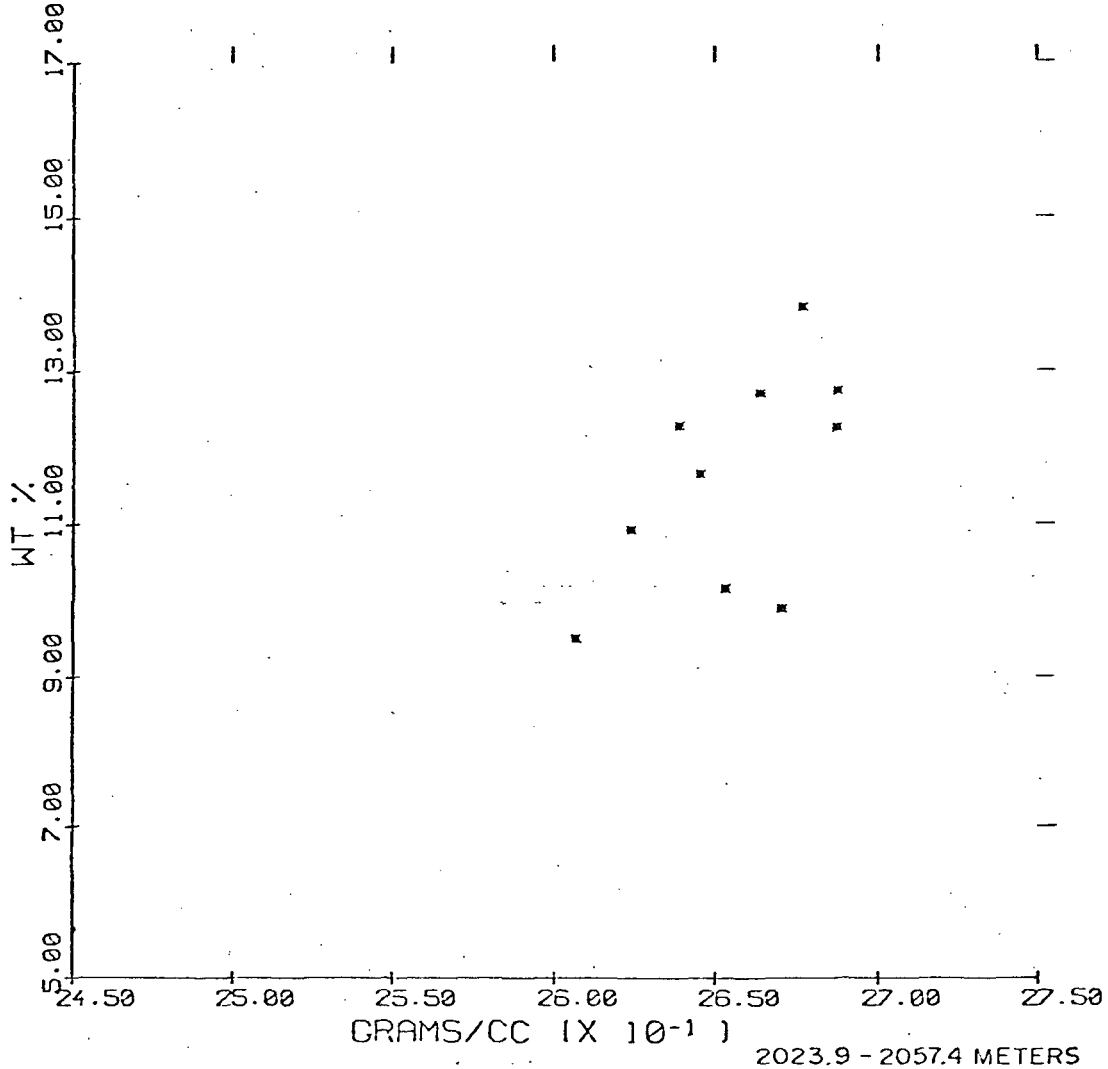

C/T 2 FIGURE 6.30

AT 2023.9 - 2057.4 METERS
6540.00 - 6750.20 FEET
10.00 DEPTH UNIT INTERVALS
3.1 METER INTERVALS

LOSS VS NEUTRON POROSITY

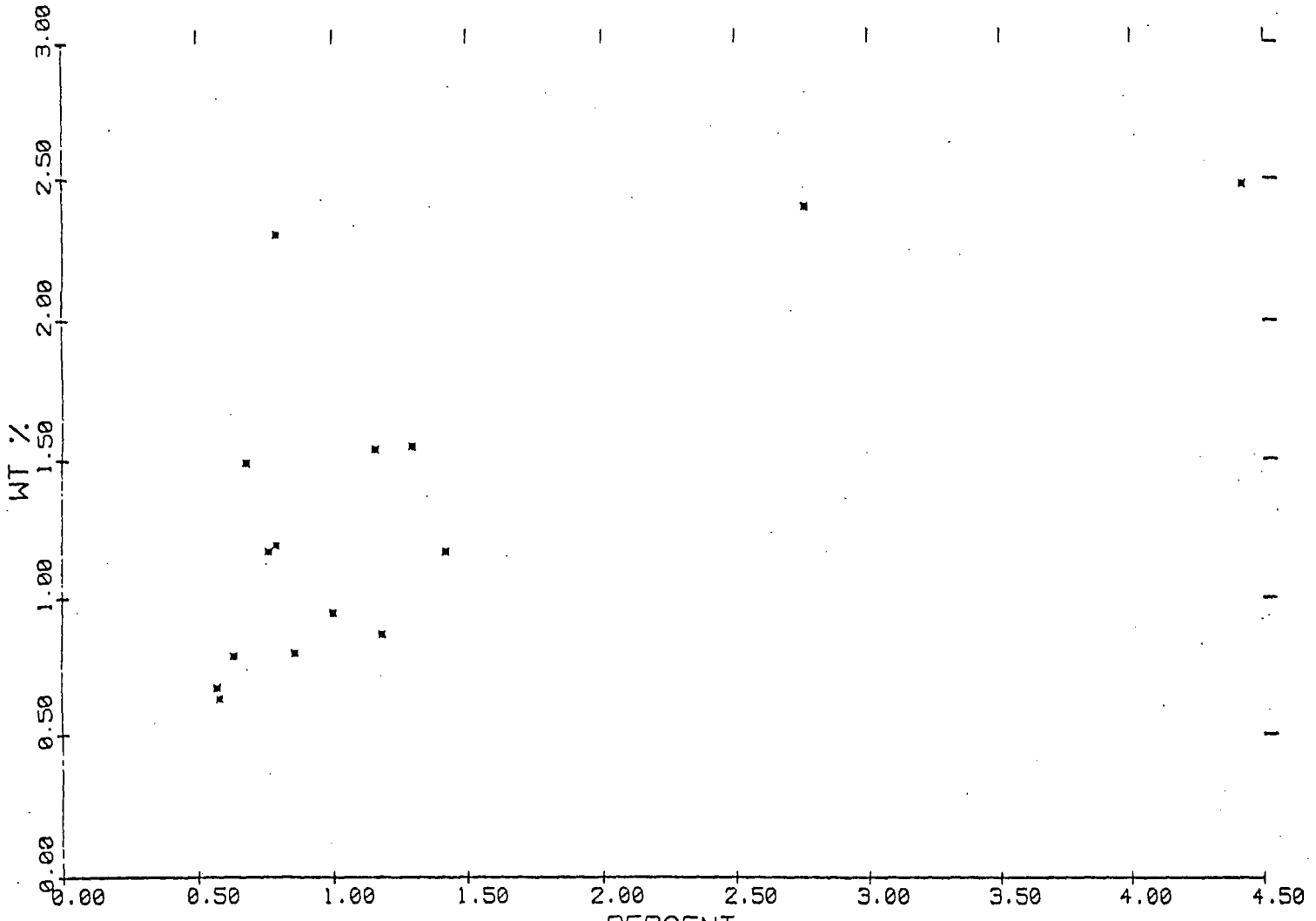

1761.7 - 1804.4 METERS
5780.00 - 5920.00 FEET
AT 10.00 DEPTH UNIT INTERVALS
3.1 METER INTERVALS

C/T 2 FIGURE 6.31

LOSS VS NEUTRON POROSITY

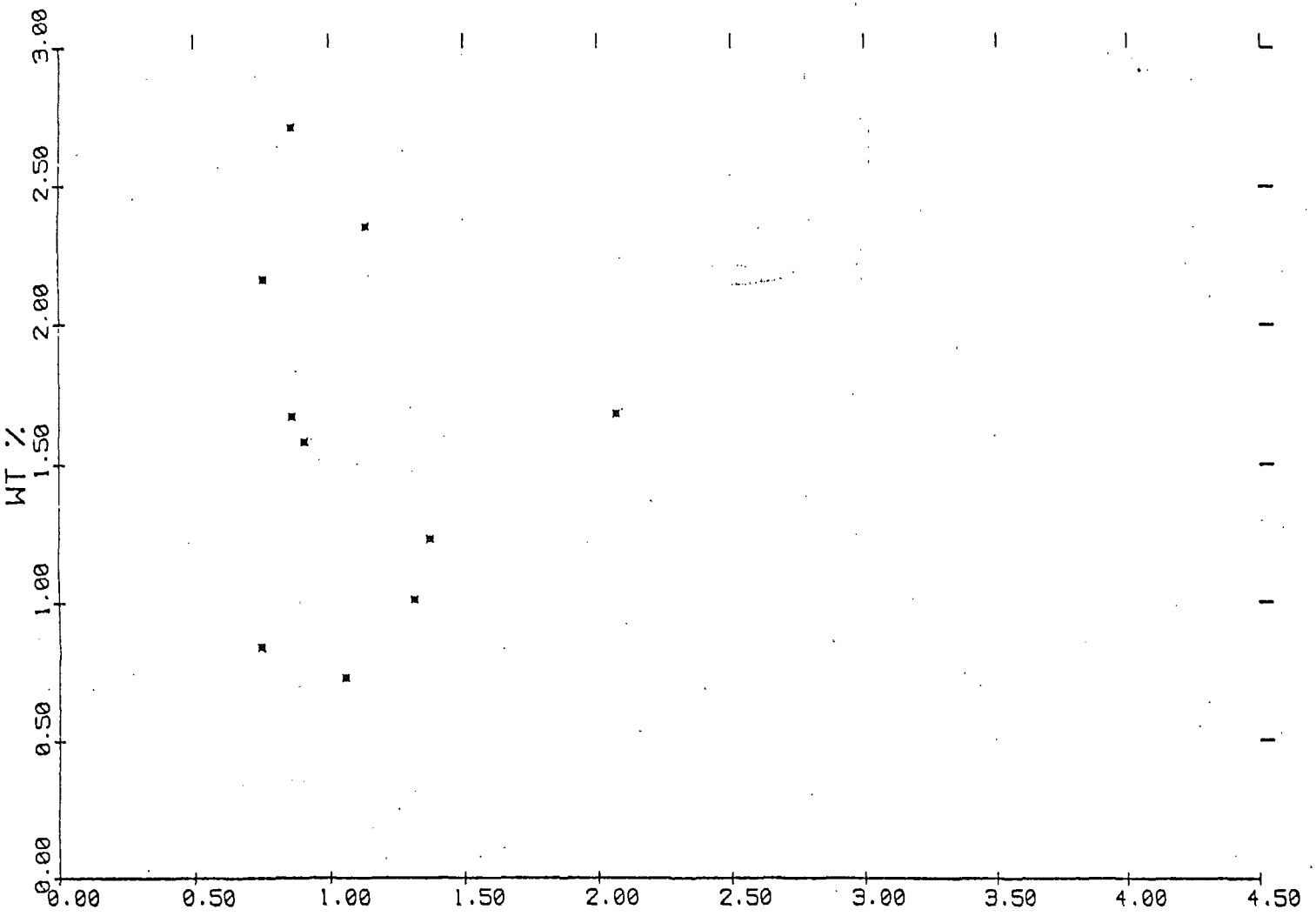

2023.9 - 2057.4 METERS
6640.00 - 6750.00 FEET
AT 10.00 DEPTH UNIT INTERVALS
3.1 METER INTERVALS

C/T 2 FIGURE 6.32

The chemical data clearly mark the rock contact at 1917.2m (6290 ft) and the several interpreted fracture or fault intercepts at 1453.9m (4770 ft), 1767.8m (5800 ft) and 1920.2m (6300 ft). Uranium and thorium and/or their daughters, in addition to potassium, are concentrated in these intervals. These elements may be mostly in alteration minerals, primarily clay minerals.

D. Summary of Log Interpretations.

Various standard well log data interpretation cross plots were constructed from the LASL C/T-2 neutron, density, acoustic and gamma-ray well logs. Cross plots of log data versus selected chemical data were plotted.

Neutron and density log cross plots were interpreted in terms of both porosity and dense, hydrous mineral variations. In typical, low porosity igneous and metamorphic rocks, these two logs' response is principally due to mineralogic variations in the rocks. The logs obtained in C/T-2 further illustrate this characteristic.

The two rock types, quartz monzonite and granodiorite, occurring in the open hole interval of C/T-2 exhibit distinct responses on several logs. The quartz monzonite has a higher gamma-ray, lower density, lower neutron porosity and a lower velocity than the granodiorite. The rock contact at 1917.2m (6290 ft) is clearly defined by each log. Average and range of log values for each rock type are listed in Table 6.5.

TABLE 6.5: Average and range of log values for the two rock types in the open hole interval of C/T-2. The data are for the Dresser Atlas logs.

	Neutron Porosity %	Bulk Density gm/cc	Gamma-Ray API
Quartz Monzonite	.5 (0-1)	2.62 (2.64-2.73)	90 (70-100)
Granodiorite	1.5 (1-3)	2.68 (2.64-2.73)	50 (30-70)

The resistivity and SP logs, in addition to the above logs mark three possible fracture or fault intercepts in the open hole interval centered at 1453.9m (4770 ft), 1767.8m (5800 ft) and 1920.2m (6300 ft). The first two are clearly identified by analyses of chip samples.

The resistivity log indicates the rocks have a resistivity of 100 ohm-m or greater. The log was obtained with a decentralized induction tool and the data are probably inaccurate. Induction logs in other Roosevelt holes exhibited similar limitations (Glenn and Hulen, 1979). In these holes resistivity log saturation occurred at 1500 to 2000 ohm-m.

Acoustic velocities for the two rock types were not computed since no transmitter receiver separation was recorded on the log. However, for the separation used the quartz monzonite generated a 10 μsecond faster travel time than did the granodiorite.

ACKNOWLEDGEMENTS

Completion of this study would have been impossible without valuable contributions from many of our associates at the Earth Science Laboratory and the University of Utah Department of Geology and Geophysics. H. Crecraft, J. M. Ballantyne and S. H. Evans facilitated obtaining and interpreting microprobe analyses of selected rock-forming and alteration minerals. We thank F. Brown and J. Mason for chemical analyses by X-ray fluorescence. Mason also prepared clay separates of selected samples and analyzed them by X-ray diffraction. R. Kroneman completed arsenic analyses by colorimetry and all analyses by plasma spectrometry. Mercury analyses were done by B. Cerling. Carbon and oxygen isotopic analyses were completed by D. Rohrs and interpreted by D. Cole, who also wrote most of Section IV of this report. Chemical and Mineralogical Services, Salt Lake City, provided potassium, uranium and thorium analyses by closed-can gamma-ray spectrometry and uranium analyses by fluorometry. T. Dustman measured magnetic susceptibilities and densities. W. Wilson and D. Chapman provided thermal conductivity measurements. J. Atwood, M. Diely and M. Hyland contributed to digitizing, checking and plotting the well log data. Illustrations were prepared by D. Cullen and D. Bolaris. The manuscript was typed by L. Stout with assistance from H. Baker.

REFERENCES

Ballantyne, J. M., "Hydrothermal alteration at the Roosevelt Hot Springs thermal area, Utah: modal mineralogy, and geochemistry of sericite, chlorite and feldspar from altered rocks, Thermal Power Co. well Utah State 14-2", Salt Lake City, Univ. of Utah Dept. of Geology and Geophysics Rept., 42 p. (1978).

Ballantyne, J. M., and Parry, W. T., "Hydrothermal alteration at the Roosevelt Hot Springs thermal area, Utah: petrographic characterization to 2 kilometers' depth", Salt Lake City, Univ. of Utah Dept. of Geology and Geophysics Rept., 21 p. (1978).

Ballantyne, G. H., "Hydrothermal alteration at the Roosevelt Hot Springs thermal area, Utah: characterization of rock types and alteration in Getty Oil Company well Utah State 52-21", Salt Lake City, Univ. of Utah Dept. of Geology and Geophysics Rept., 24 p. (1978).

Bamford, R. W., "Geochemistry of solid materials from two U. S. geothermal systems and its application to exploration", Univ. of Utah Research Inst., Earth Science Laboratory, Rept. 6, Salt Lake City, 196 p. (1978).

Bamford, R. W., Christensen, O. D., and Capuano, R. M., "Multielement geochemistry of solid materials in geothermal systems and its applications Part 1: The hot-water system at the Roosevelt Hot Springs KGRA, Utah", Univ. of Utah Research Inst., Earth Science Laboratory Rept. 30, Salt Lake City, (1980).

Bence, A. E., and Albee, A. L., "Empirical correction factors for the electron microanalysis of silicates and oxides", Jour. Geol. v. 76, p. 382-403 (1968).

Bethke, P. M., and Rye, R. O., "Environment of ore depostion in the Creede mining district, San Juan Mountains, Colorado: Part IV. Source of fluids from oxygen, hydrogen and carbon isotope studies": Econ. Geology, v. 74, p. 1832-1851, (1979).

Bottinga, Y., "Calculation of fractionation factors for carbon and oxygen isotopic exchange in the system calcite-carbon dioxide-water": J. Phys. Chem., v. 72, p. 800-808, (1968).

Bryant, N. L., and Parry, W. T., "Hydrothermal alteration at Roosevelt Hot Springs KGRA--DDH 1976-1", Salt Lake City, Univ. of Utah Dept. of Geology and Geophysics Rept., 87 p. (1977).

Burke, J. A., Schmidt, A. W., and Campbell, Jr., R. L., "The litho-porosity crossplot"; The Log Analyst, Nov.-Dec., also in SPWLA Reprint v. Gamma Ray, Neutron and Density Logging, March (1978).

Casadevall, T., and Ohmoto, H., "Sunnyside mine, Eureka mining district, San Juan County, Colorado: Geochemistry of gold and base metal ore formation in the volcanic environment": Econ. Geology, v. 72, p. 1285-1320, (1977).

Craig, H., "Isotopic standards for carbon and oxygen and correction factors for mass-spectrometric analysis of carbon dioxide": Geochim. Cosmochim. Acta, v. 12, p. 133-149, (1957).

Craig, H., "Standard for reporting concentrations of deuterium and oxygen-18 in natural waters": Science, v. 133, no. 3467, p. 1833-1834 (1961).

Dresser Atlas, "Log Interpretation Charts", Dresser Industries, Inc., Houston Texas, p. 107, (1979).

Dresser Atlas, "personal communication", (1980).

Edmundson, H., and Raymer, L. L., "Radioactive logging parameters for common minerals": SPWLA Twentieth Annual Logging Symposium Transactions, Paper O, (June, 1979).

Elders, W. A., Hoagland, J. R., and Olson, E. R., "Hydrothermal mineralogy and isotope chemistry in the Cerro Prieto Field, Mexico, III, Practical applications", Trans. Geotherm. Res. Council, v. 2, p. 177-180. (1978).

Ewers, G. R., and Keays, R. R., "Volatile and precious metal zoning in the Broadlands geothermal field, New Zealand", Econ. Geology, v. 72, p. 1337-1354, (1977).

Fournier, R. O., "Geochemical and hydrologic considerations and the use of enthalpy-chloride diagrams in the prediction of undergound conditions in hot-spring systems": J. Volcanol. Geotherm. Res., v. 5, p. 1-16 (1979).

Friedman, I., and O'Neill, J. R., "Compilation of stable isotope fractionation factors of geochemical interest", U. S. Geol. Survey Prof. Paper 440-KK, (1976).

Glenn, W. E., and Hulen, J. B., "Interpretation of well log data from four drill holes at Roosevelt Hot Springs KGRA", Univ. of Utah Res. Inst., Earth Sience Laboratory Rept. 28, Salt Lake City, 74 p. (1979a).

Glenn, W. E., and Nelson, P. H., "Borehole logging techniques applied to base metal ore deposits": Exploration 77 Symposium, Ottawa, Canada (1977) and in Geol. Surv. of Canada Economic Geology Rept. 31, p. 273-294 (1979).

Hulen, J. B., "Stratigraphy and alteration, 15 shallow thermal gradient holes, Roosevelt Hot Springs KGRA and vicinity, Millard and Beaver Counties, Utah": Univ. of Utah Res. Inst., Earth Science Laboratory Rept. 9, 14 p. (1978).

Jack, R. N., and Carmichael, I. S. E., "The chemical "fingerprinting" of acid volcanic rocks", in short contributions to Califronia geology, Calif. Div. Mines and Geology Spec. Rept. 100, p. 17-32, (1969).

James, G. W., "Parts-per-million determinations of uranium and thorium in geologic samples by x-ray spectrometry", Analytical Chem., v. 49, p. 967-968.

Kendall, C., "Petrology and stable isotope geochemistry of three wells in the Buttes area of the Salton Sea geothermal field, Imperial Valley, California, U.S.A.", Univ. of Calif., Riverside, Inst. of Geophys. and Planet. Phys. Rept. UCR/IGPP-76/17, 211 p., (1976).

Lipman, P. W., Rowley, P. D., Mehnert, H. H., Evans, S. H., Nash, W. P., and Brown, F. H., "Pleistocene rhyolite of the Mineral Mountains, Utah--geothermal and archaeological significance": Jour. Res., U. S. Geol. Surv. 6, p. 133-147, (1978).

Mathews, M., "Log responses from the Geothermal Calibration Test Well C/T-2": SPWLA Twentieth Annual Logging Symposium Transactions, v. II, Paper SS (1979).

McCrea, J. M., "The isotopic chemistry of carbonates and a paleotemperature scale": J. Chem. Phys., v. 18, p. 849, (1950).

Newman, K. L., "Calibration/Test well management", Geothermal Log Interpretation Program. First yearly topical report (1979).

Nielson, D. L., Sibbett, B. S., McKinney, D. B., Hulen, J. B., Moore, J. N., and Samberg, S. M., "Geology of Roosevelt Hot Springs KGRA, Beaver County, Utah", Univ. of Utah Res. Inst., Earth Science Laboratory Rept. 12, Salt Lake City, 121 p. (1978).

Norrish, K., and Hutton, J. T., "An accurate X-ray spectrographic method for the analysis of a wide range of geologic samples": Geochim. et Cosmochim. Acta, 33, no. 4, p. 431-454, (1969).

Ohmoto, H., and Rye, R. O., "Isotopes of sulfur and carbon", in Geochemistry of Hydrothermal ore deposits, (Barnes, H. L., ed.), 2nd ed.; New York, Wiley, p. 509-567. (1979)

Parry, W. T., "Mineralogy of the clay fraction from cuttings, Thermal Power Co. well Utah State 14-2", Salt Lake City, Univ. of Utah Dept. of Geology and Geophysics Rept., 8 p (1978).

Parry, W. T., Ballantyne, J. M., Bryant, N. L., and Dedolph, R. E., "Geochemistry of hydrothermal alteration at the Roosevelt Hot Springs thermal area, Utah", Geochim. Cosmochim. Acta, 44, p. 95-102 (1980).

Parry, W. T., Bryant, N. L., Dedolph, R. E., Ballantyne, J. M., Ballantyne, G. H., Rohrs, D. T., and Mason, J. L., "Hydrothermal alteration at the Roosevelt Hot Springs thermal area, Utah", Salt Lake City, Univ. of Utah Dept. of Geology and Geophysics Rept., 29 p. (1978).

Parry, W. T., Benson, N. L., and Miller, C. D., "Geochemistry and hydrothermal alteration at selected Utah Hot Springs", Univ. of Utah Dept. of Geology and Geophysics Rept., Salt Lake City, 131 p, (1976).

Pickett, G. R., "Pattern recognition as a means of formation evaluation"; SPWLA Fourteenth Annual Logging Symposium. Trans., Paper A. (1973).

Plewa, S., "Correlation between therma conductivity and other physical parameters of rocks", in KAPG Geophysical Monograph, A., Adam, editor, Akademcai Kidao, Budapest, (1976).

Poupon, A., Hoyle, W. R., and Schmidt, A. W., "Log analysis of sand-shale sequences--a systematic approach"; J.P.T., July, (1970).

Ratcliffe, E. H., "Thermal conductivities of fused and crystalline quartz," British Jour. Applied Physics, v. 10, p. 22-25, (1958).

Robinson, B. W., "The origin of mineralization at the Tui mine, Te Aroha, New Zealand, in the light of stable isotope studies": Econ. Geology, v. 69, p. 910-925, (1974).

Rohrs, D., and Parry, W. T., "Hydrothermal alteration at the Roosevelt Hot Springs Thermal Area, Utah: Thermal Power Co. well Utah State 72-16", Salt Lake City, University of Utah Dept. of Geology and Geophysics Rept., 23 p. (1978).

Sass, J. H., Lachenbruch, A. H., and Monroe, R. J., "Thermal conductivity of rocks from measurements on fragments and its application to heat-flow determinations", Jour. Geophys. Res., v. 76, no. 14, p. 3391-3401, (1971).

Savre, W. C., "Determination of more accurate porosity and mineral composition in complex lithologies with the use of sonic, neutron, and density surveys";, J.P.T., Sept., (1963).

Schlumberger, "Log Interpretation Charts", Schlumberger Limited, New York, p. 92, (1972).

Schlumberger, "Log interpretation, Volume II--Applications," Schlumberger Limited, New York, p. 116, (1974).

Sibbett, B. S., and Nielson, D. L., "Geology of the central Mineral Mountains, Beaver County, Utah", Univ. of Utah Res. Inst., Earth Science Laboratory Rept. (1980; in final review).

Suhr, N. H., and Ingamells, C. O., "Solution technique for analysis of silicates," Anal. Chem., 38, p. 730-734., (1966).

Taylor, H. P., "Oxygen and hydrogen isotope relationships in hydrothermal mineral deposits", in Geochemistry of hydrothermal ore deposits, (Barnes, H. L., (ed)), 2nd ed.: New York, Wiley, p. 236-277, (1979).

Ward, S. H., Parry, W. T., Nash, W. P., Sill, W. R., and Cook, K. L., Smith, R. B., Chapman, D. S., Brown, F. H., Whelan, J. A., and Bowman, J. R., "A summary of the geology, geochemistry and geophysics of the Roosevelt Hot Springs thermal area, Utah", Geophysics, 43, no. 7, p. 1515-1542, (1978).

Wilson, W. R., and Chapman, D. S., "Thermal studies at Roosevelt Hot Springs, Utah", Univ. of Utah Tech. Rept., DOE/DGE, Contract DE-AC07-78ET28392, (1980).

Zen, E., and Thompson, A. B., "Low-grade regional metamorphism: Mineral equilibrium relations", Ann. Review Earth and Planetary Sciences, 2, p. 179-212, (1974).